Structural Integrity Analysis of Marine Dynamic Cables

Nicholas Fagan 201924476

Robbie McCormick 201914748

Tom Marwood 201917152

Greg Stewart 201919528

Supervisor: Dr. Zhiyuan Li

zhiyuan.li@chamlers.se

Project Advisor: Dr. Jonas Ringsberg

jonas.ringsberg@chalmers.se

Word count: 30,454

A report submitted in partial fulfilment of the requirements of the MEng in Aero / Mechanical Engineering

Acknowledgements

Firstly, the team would like to express its sincere gratitude towards Dr Zhiyuan Li and Dr. Jonas Ringsberg in their capacity as project supervisors. The successful completion of the project would not have been possible without their expertise and time devoted, despite their extremely busy schedules. We would also like to thank our supervisors for providing the opportunity to publish a conference paper based on this thesis, which will be presented at the ASME 2024 43rd International OMAE Conference in Singapore.

Secondly, the team would also like to extend thanks to Dr. Andrew McLaren who granted the team this fantastic opportunity and provided support throughout the semester when required.

Finally, we would also like to thank Chalmers University of Technology as a whole, and especially the Division of Marine Technology who truly welcomed us and provided us with excellent facilities.

Abstract

Over the last two decades, there has been a global emphasis on renewable energy due to the climate change crisis. This has been a catalyst for tapping into offshore renewable energy sources such as wave energy convertors and offshore wind farms. This has resulted in the need for durable marine dynamic power cables, with long fatigue life, to utilise theses sources. Offshore power cables are typically designed to have a service life of around twenty-five years however, a pattern is emerging where these cables are only lasting ten years or even as low as two. The main consensus as to why the fatigue life is so short is due a combination of global and local fatigue, and a phenomenon called water treeing. The global fatigue is due to the harsh oceanic sea states that the cables will endure, fretting and wear are the main contributors to local fatigue of the cables. Water treeing is the development of a crack in the insulating material of the cable, these cracks grow due to the mechanical and Maxwell stresses acting on the crack whilst the cable is in operation. The purpose of this paper is to develop numerical simulation methods to analyse the structural integrity of marine dynamic power cables and estimate their fatigue life. To perform a comprehensive global analysis of the cable, SIMA and MATLAB are used to identify critical regions along the cable's length. This serves as a basis for subsequent local models where Abaqus and Python can be implemented to calculate the maximum wear depth and accumulated damage due to fretting. To conduct analysis of water tree crack propagation COMSOL and MATLAB will be implemented to analyse the effects of both mechanical and Maxwell stresses on the water tree crack, leading to an estimate of the overall fatigue life.

Key Words: Renewable energy, marine dynamic power cable, fatigue life, Maxwell stresses, water tree, fretting, numerical simulation.

Contents

List of Figures

List of Tables

Acronyms

AC	Alternating Current
COF	Coefficient of Friction
DOF	Degree of Freedom
EPFM	Elastic Plastic Fracture Mechanics
FDA	Fatigue Damage Accumulation
FEA	Finite Element Analysis
JONSWAP	Joint North Sea Wave Project
LEFM	Linear Elastic Fracture Mechanics
MCE	Multipoint Constraint Equation
MDC	Marine Dynamic Cable
PTO	Power Take-off
SWT	Smith-Watson-Topper
UK	United Kingdom
UTS	Ultimate Tensile Strength
W4P	Waves 4 Power
WAFO	Wave Analysis for Fatigue and Oceanography
WEC	Wave Energy Converter
XLPE	Cross Linked Polyethylene

Nomenclature

Symbol	Definition	Units
θ	Angle	°
P	Applied Load	N
A	Area of Plate	m^2
σ_b	Bending Stress	MPa
C	Capacitance	F
C	Capacitance	F
μ	Coefficient of Friction	-
Y	Configuration Factor	-
A	Contact Area	m^2
b	Contact Half Width	m
$p(x)$	Contact Pressure	N/m^2
da/dN	Crack Growth Rate	$m/cycle$
a	Crack Length	m
N	Current Cycle	-
N_f	Cycles Until Failure	-
κ_l	Dimensional Local Wear Coefficient	-
δ_E	Displacement Amplitude	m
x	Distance in x-direction	m
E	Electric Field Strength	Vm^{-1}
W	Energy Accumulation	Joules
n	Factor of Safety	-
ε_f'	Fatigue Ductility Coefficient	-
c_f	Fatigue Ductility Exponent	-
σ_w	Fatigue Limit	MPa
σ_f'	Fatigue Strength Coefficient	-
b_f	Fatigue Strength Exponent	-
K_{Ic}	Fracture Toughness	$MPa\sqrt{m}$
Q	Frictional Force	N

ε_e	Independent Elastic Strain	-
ε_p	Independent Plastic Strain Amplitude	-
L	Length	m
p_{max}	Maximum Contact Pressure	N/m^2
σ_{max}	Maximum Normal Stress	N/m^2
F	Maxwell Stress	Pa
σ_m	Mean Stress	MPa
D, d	Miner-Palmgren Damage	-
ΔN	No. of Cycle Jumps	-
$\Delta\varepsilon_a$	Normal Cyclic Strain Range	-
ε_{11}, ε_{22}	Normal Principal Strains	-
σ_{11}, σ_{22}	Normal Principal Stresses	N/m^2
N_i	No. of cycles to failure	-
K	No. of stress amplitudes	-
C	Paris Law Co-efficient	-
m	Paris Law Co-efficient	-
ε_o	Permittivity in Vacuum	Fm^{-1}
Y, y	Positions in the y-direction	-
$N_{f,i}$	Predicted Failure Cycle	-
τ_{12}	Principal Shear Stress	N/m^2
R	Radius	m
ε_r	Relative Permittivity of XLPE	Fm^{-1}
$q(x)$	Shear Stress	N/m^2
Hs	Significant Wave Height	m
S	Sliding Distance	m
c	Stick Half Width	m
σ_a	Stress Amplitude	N/m^2
σ_a	Stress Amplitude	MPa
n_i	Subjected number of cycles	-
σ_t	Tensile Stress	MPa

K_{th}	Threshold Stress Intensity Factor	$MPa\sqrt{m}$
σ_{UTS}	Ultimate Tensile Stress	MPa
H	Vickers Hardness	F/m^2
V	Voltage	V
V_0	Volume of Insulation	m^3
γ	Wave Gamma Factor	-
Ts	Wave Period	s
K	Wear Coefficient	-
h	Wear Depth	m
V	Wear Volume	m^3
σ_{yield}	Yield Strength	MPa
E	Young's Modulus	N/m^2

Executive Summary

Introduction

In order for sustainable energy production methods to compete with the more traditional techniques, they must be equally, if not more, reliable and robust. In recent years there has been a substantial amount of research into green offshore energy technologies such as floating wind turbines and wave energy convertors (WEC's). These systems both require subsea dynamic cables in order to transport the electricity generated from the system to a central hub where it is then transported onshore. However, as these cables are suspended in the water, they are subjected to the harsh and unpredictable movement of the sea which can reduce their service life from the expected 25 years to as little as 2. Marine dynamic power cables fail due to a number of reasons. However, this paper will focus on the global fatigue damage accumulation, local fretting fatigue and well as a phenomenon known as water trees which arise in the insulation layer of the power cable.

Global Analysis

The purpose of a global analysis in this application is to identify critical regions along the dynamic powers cable's length. In order to achieve robust results, a multitude of different of environmental conditions were simulated in order to capture the true behaviour of the cable. These environmental parameters were derived from the wave scatter diagram associated with where the WEC is situated, Runde, Norway.

Utilising the software, DNV SIMA an accurate 3D model of the WEC, mooring lines, conditions and dynamic power cable was created. All cases were simulated and verified, from here the raw results could be extracted and post-processed through an in-house MATLAB code.

The first post-processing phase deals with the fatigue damage accumulation aspect of the study. From SIMA, the respective moments and forces for the cable were extracted and inputted into the MATLAB code. The MATLAB code utilises cycle counting methods and damage accumulation laws to predict stress ranges, fatigue damage, fatigue life and hence allowing for critical regions along the cable to be identified,

The second phase of the post-processing involves extracting elemental global displacements directly from SIIMA and converting them into more practical relative elemental displacements. Relative displacements were calculated for two locations, that were deemed of importance, across the power cable's length. Applying beam theory, these relative displacements could be integrated into a local FEA model, enabling a more thorough examination of the cable's behaviour.

The results from the global study aligned well with previous literature. The main findings revealed that the greatest fatigue dagame manifests at the beginning of the cable (near the WEC) for calm sea states. However, under harsher conditions, there is a notable shift in the greatest fatigue damage towards the centre of the cable's length and accompanied by a substantial spike. As anticipated, the cable's predicted fatigue life decreases significantly as conditions become harsher. It was found that the cable's predicted fatigue life decreases from 6.05e+21 years to 3.858e+10 years as we move from Case 1 to Case 3, a calm sea state to a harsh sea state.

Fretting Study

Fretting is the small-scale relative oscillatory motion between two surfaces in contact in the range of a few microns up to roughly 300 μm. Fretting can occur in every tribology system and usually exists between two surfaces that are assumed to be stationary relative to one another. In the context of marine dynamic cables, this fretting problem usually occurs between the wires within the conductor layer. Although this fatigue phenomenon is often not considered in design, studies show it can reduce the life of a system by 30%[1] at loads even below the fatigue limit. The stress concentration and surface damage induced by this movement can cause cracks to initiate and propagate leading to failure of the system. It was for this reason it was chosen to be studied for this project and compared to the other failure mechanisms to determine how it will affect the overall life of the cable.

The original objective for this section was to build from the existing 2D fretting model and create a 3D model to determine if this yielded more favourable results. A 3D FEA model was created using Abaqus, however, in order to extract the relevant data and process the results a Fortran and Python script would also have to be developed. Running the 3D model with the default solver for only 4 fretting cycles also took over 48 hours to run. As there was only one student working on this section where there had previously been two, it was determined that there was not sufficient time to complete this task.

The scope of this section was then changed to further develop the existing model and conduct a sensitivity analysis on different parameters. The parameters chosen to study was the loading force, sliding distance and coefficient of friction (COF).

The results from this study showed good similarity to the literature and theory and it was found that the loading force had the biggest influence on the fatigue life of the wires. It was also discovered that the life due to fretting was much lower than that of the global fatigue damage which is also true in practical applications.

Water Trees

Water treeing is a degradation phenomenon that occurs within the insulation of marine power cables due to water droplets entering the material during manufacturing. A water tree consists of micro voids that are linked together by micro channels giving a tree like structure, hence the name. Water trees are commonly separated into two distinct categories: vented water trees and bow-tie water trees. This investigation focuses solely on vented water trees as they frequently cause the dielectric breakdown of marine dynamic power cables.

When examining marine dynamic cables, water treeing develops within the XLPE insulation material. As the power cable being investigated is submerged there is a higher likelihood that water droplets will find their way into the XLPE material. Subsequently, water treeing has become one of the major reasons for the reduced service life of power cables attached to WECs. Water treeing can be described as the development of a crack in the insulating material of the cable, these cracks grow due to the mechanical and electrical induced stresses acting on the crack whilst the cable is in operation.

The mechanical induced stresses arise from the harsh environment the cable operates within, the environment will produce axial tensile stress on the XLPE insulation layer of the cable. In order to determine this axial tensile stress, the displacements found within the global analysis had to be utilised. A local model of the cable was developed on ANSYS with the displacements being incorporated and the axial tensile stresses within the insulation calculated. The stress

values given from the local model could be used to analyse the crack growth with a single edge crack model that was developed on COMSOL Multiphysics.

The electrical induced stresses are a result of the electric field produced when current flows through the power cable during electricity generation. A concentrated electric field is observable at the tip of the water tree crack, this electric field causes the water droplets to cyclically micro-jet against the tip of the micro-void. The field produces a Maxwell force at the same position and when this Maxwell force occurs the XLPE insulation will be subjected to cyclic mechanical stress as the cable is an AC system. Again, using COMSOL the crack growth of a water tree crack due to electrical stress was investigated and the kinetic theory of fatigue was utilised to determine a service life.

The objective of this analysis was to combine both mechanical and electrical loading conditions acting on the water tree crack to determine the fatigue life of the marine dynamic cable. To achieve this, an incremental case study was initiated with the goal of examining water tree growth in finer detail. The study focuses on observing water tree growth within a specified increment range for both mechanical and electrical stresses.

The results of the water tree analysis showed notable consistency with the existing literature on the topic. It was concluded that the electrical induced stress will steadily propagate the crack over time, increasing moderately as the crack grows toward the centre of the cable. Also, the investigation found that an edge crack in finitely extended plate was the most conservative case, when analysing mechanical stress, and was utilised to predict a service life of the cable. Once both electrical and mechanical stress fatigue were combined it was found the cable had a fatigue life of 31.6 years.

Groupwork Reflections

For the duration of this exchange period, the group worked well as a team and implemented relevant project management techniques to ensure the success of the project.

The team utilised tools such as a Gantt chart and a risk matrix to have a clear understanding of the goals and timeline as well as the potential risks involved and how to mitigate them. This meant work was completed in a timely manner and ensured enough time was left to complete the other deliverables.

Regular meetings with the supervisor also gave the team the opportunity to ask any questions they had related to the work. This was especially helpful in the initial stages of the project as the subject, and some of the software, had not been previously studied by any of the team members. Having an additional advisor was also beneficial as it allowed knowledge to be drawn from different areas of expertise and often lead to tackling problems in an alternative way.

The team also has shared accommodation and office space for the duration of the exchange period. This allowed for effective and frequent communication between the group which was crucial to the project’s success.

1 Introduction

1.1 Background and Motivation

Today, the negative impacts of fossil fuels are well established, and energy production methods are changing in order to decrease the world's dependency on these methods. In recent years, there has been a large push to further develop renewable energy sources and infrastructure to help the global problem of climate change.

In December of 2015, at COP 21, 196 countries signed the Paris agreement. The goal of this, set by the United Nations Framework Convention on Climate Change (UNFCCC), was to limit the average global temperature to below 2℃, ideally below 1.5℃, compared to pre-industrial levels [2]. As bold as this target is, many experts believe it is not ambitious enough. The global temperature has already risen 1.1 ℃ above pre-industrial levels and the current goals are not enough to stop it reaching 1.5℃ within the next two decades [3]. The significant rise in global temperature is primarily attributable to human activities, including the burning and utilisation of fossil fuels. Climate change, driven by these factors, has a detrimental impact on life worldwide, and in some cases, it renders certain locations uninhabitable. Notably, rising sea levels pose a substantial risk to coastal areas, increasing the likelihood of devastating floods which can make rebuilding or growing food in these locations impossible. Furthermore, the heightened frequency of extreme heatwaves and droughts in already arid regions will reduce crop yield, as will the increase of storms and flash floods in wetter areas. These reasons highlight the importance of further research and development into green energy infrastructure. With the goal of being net zero by 2050, energy produced by renewable sources must double by 2030 [4].

With these issues in mind, governments have been required to look for more sustainable energy production methods than the traditional technique of burning fossil fuels. In the UK, the main focus has been into the development of wind and nuclear energy, with them making up 26.8% and 15.5%, respectively, of the total energy produced in the UK as of 2022 [5]. Despite this, hydro power only makes up 1.8% of the total energy produced, this includes all hydro production methods and not just wave energy. This demonstrates that wave energy and Wave Energy Converters (WECs) are potentially areas of great expansion as relatively little infrastructure is in place at the moment. Having a diverse range of sustainable energy production methods also has other benefits. As methods, such as wind and solar, rely on the weather, they can only produce energy intermittently when conditions are right. Furthermore, as the power grid was created around large, controllable methods, it has very little storage capacity. This means that if the UK were to solely rely on these intermittent methods, there could be regular black outs when the weather is not suitable to produce energy. To deal with this the grid could be improved to increase its storage capacity, or alternatively, more consistent energy production is required. WECs are ideal for this as they can produce power around the clock, as there is always some level of oceanic movement to convert to energy. Having a mix of green energy methods will help countries reach climate goals while avoiding issues such as black outs.

The ocean holds an immense amount of untapped energy, with estimates ranging from 20,000 TWh to 80,000 TWh of electricity generation per year. That represents 100% to 400% of the current global demands [6]. This highlights the importance of the development of robust and reliable WEC systems. It is for this reason that an investigation on the fatigue analysis of marine dynamic cables, used in these systems, is presented.

There are many different types of WECs with one study claiming to have found over 7,400 different patents for their designs[7]. The most common, and the one included in this study, is

known as a point absorber. These are tall floating structures that capitalise on the heave motion of the waves and convert this to electrical energy. They typically do this by fixing one end of the absorber to the seabed while the other end moves with the waves. The subsequent cyclic motion is converted to electrical energy using a series of generators.

The design chosen in this study is created by Waves4Power, a Swedish company, with their WEC located in Runde, Norway. This design consists of two main sections, the buoy body which floats above the surface and a vertical acceleration tube below. The buoy is held in place by a series of ties and is joined by a low voltage cable to a connection hub. This connection hub transforms the electricity to high voltage and sends it onshore via a fixed sea cable. The Figure 1 shows a cross section of this system including the internal hydraulic system used to convert the motion into electrical power.

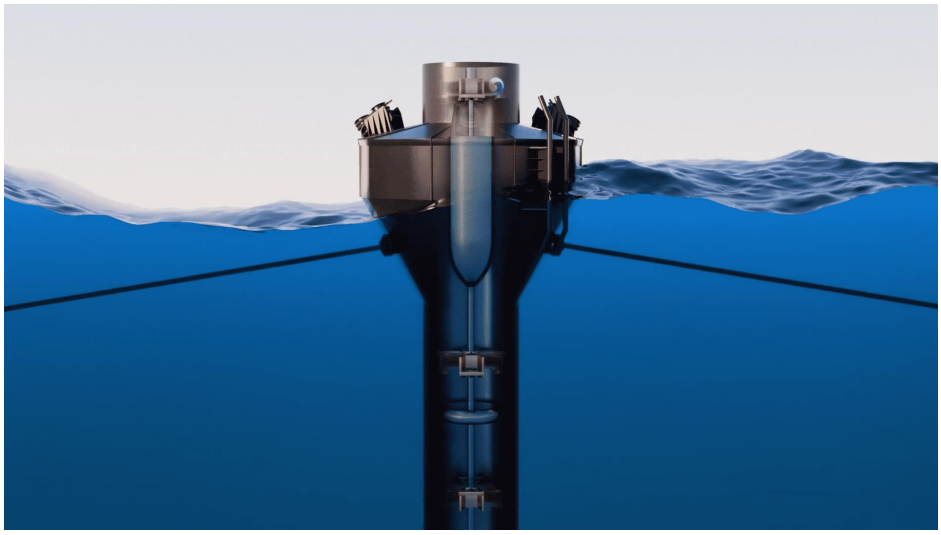

Figure 1: Waves4power WaveEL 4.0 buoy [8]

Each cluster of around 6 buoys is estimated to produce enough energy to power 250 to 300 homes [8]. These systems have great potential for creating consistent energy with zero emissions, however, if an issue does arise, maintenance would be very costly and time consuming. Therefore, each component must be able to withstand the consistent cyclic loading and severe storm conditions.

Offshore energy generation such as WECs hold great promise, as they offer a substantial reduction in land usage for electricity production and have minimal impact on human life due to their strategic locations. Whilst this solution has potential the transportation of electricity from WECs remains a pivotal factor [9]. This study analyses the structural integrity of this low voltage cable between the buoy and the connection hub, which can be categorised as a subsea dynamic cable. As this cable cannot be fixed, it must move with the ocean which subjects it to adverse loads and motion. The subsea environment has many challenges that dynamic power cables can encounter; bird caging, buckling problems, corrosion, cable rupture, global fatigue, fretting, over-stressing, over-bending, tension, sheath damage, wear, and water treeing.

The current cable design is intended to endure stresses for 20-25 years. However, cable failures have been observed to occur earlier, in the region of 2-5 years, due to the various factors discussed above. Maintaining and repairing offshore WEC facilities incur high costs attributed to the environmental challenges faced, advanced equipment requirements, and the skilled personnel essential for task completion. The majority of maintenance pertains to the dynamic subsea cables attached to the WECs. Repair work on offshore wind projects in the

UK has accumulated a cost of nearly £12.5 million and repair times can range from three to five months which would put the WECs out of production for a significant amount of time [10].

This study analyses the structural integrity of this low voltage dynamic cable, between the buoy and the connection hub, which due to its environment and operating conditions can cause premature failure of the cable. This report will demonstrate the effect water trees, fretting and global fatigue have on the cable's deterioration and the subsequent effect on its fatigue life.

1.2 Aims and Objectives

This investigation aims to contribute to the existing research on the fatigue life of subsea dynamic power cables for WEC facilities. To achieve this a global model was developed to assess fatigue across the entire length of the cable as shown in Figure 2 (the umbilical like cable). Additionally, a fretting local model was assessed to determine the impact of different parameters on the fatigue life of the conductor wires, shown in Figure 3. To analyse the fatigue life due to water tree propagation in the conductor insulation, demonstrated in Figure 3, two models were created. One which assesses water tree propagation as a result of mechanical stress acting on the insulator and another that analyses water tree propagation due to electrical stress on the crack tip during operation. The main objective of this project is to develop numerical solution methods to analyse the structural integrity of a marine dynamic cable.

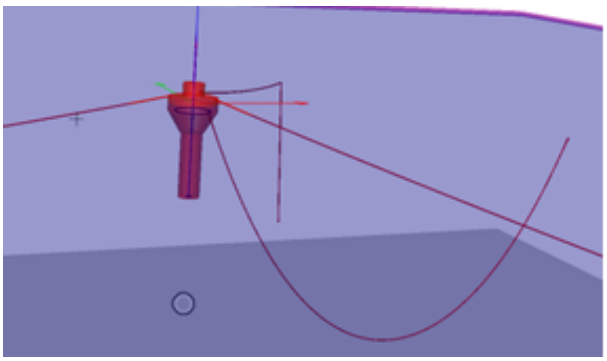

Figure 2: Global SIMA Model

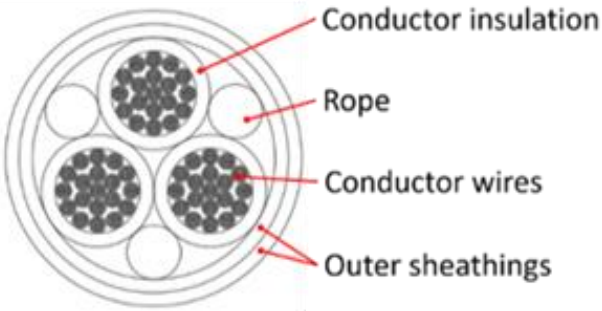

Figure 3: Marine Dynamic Cable Cross Section

1.2.1 Global Analysis Objectives

1. Conduct a literature review to understand the purpose of a global model, global failure modes, theories of damage accumulation and the respective software required.
2. To conduct a global analysis of the 1kV dynamic power cable and utilise post processing tools to identify critical regions along the cable.
3. To utilise post-processing tools to calculate relative displacements along the cable to allow further and more detailed local analysis.

1.2.2 Local Fretting Fatigue Objectives

1. Conduct literature review to outline fretting mechanics and the various mathematical models involved in calculating the damage and wear depth.
2. Conduct sensitivity analysis using a 2D fretting model on the following parameters: loading force, sliding distance and COF.
3. Compare these results to determine which has the biggest impact. Also compare results to global model to conclude if the cable fails prematurely due to fretting.
4. Compare different conductor materials fretting fatigue life and assess their suitability for marine dynamic cable application.

1.2.3 Water Tree Fatigue Objectives

1. Understanding water tree phenomena through an examination of existing literature and pinpointing the constraints and underlying assumptions for the thesis.
2. Develop simulations of water tree cracks to analyse mechanical and electrical stresses on crack propagation.
3. Combine both mechanical and electrical loading conditions acting on the water tree crack to determine the fatigue life of the marine dynamic cables.

1.3 Assumptions and Limitations of the Study

This section lays out the main assumptions and limitations of the investigation. In order for a comprehensive study to be carried out limitations and assumptions had to be assessed prior to initiating the research, ensuring a clear understanding of the study's scope.

1.3.1 Global Analysis Assumptions

In the 3D SIMA global model, the super node linked to the end of the dynamic cable (furthest away from WEC) has been set to operate as a spatially fixed node. This is a realistic assumption as the hub connected to the cable is generally stationary.

In this analysis, to conserve computational time, both wind and current have been neglected in the Global Model simulations.

The temperature of the environment in the SIMA simulations was assumed to be constant. Furthering this, Biofouling was also neglected as it is very complex to model accurately.

It is also assumed that the entire analysis is based on linear elastic mechanics. This is an accepted assumption as the system involve high cycle fatigue.

For the purpose of this analysis, it is assumed that the greatest fatigue damage will occur on the main segment of the cable *i.e.,* Segment 8. This segment excludes the bending stiffeners and hence segments near the WEC and hub are not analysed.
To simplify the task, the global model assumes that the cable has a homogeneous cross section with fixed properties *i.e.,* no property degradation over time. The global model does not include insulators, Kevlar ropes or sheathing as is treated instead as a thick-walled cylinder.

1.3.2 Fretting Analysis Assumptions

The interwire contact model in this section is assumed to be that of a half cylinder on a rectangle. This is a valid assumption and is used extensively in literature.

The contact and fretting were also modelled as 2D which assumes that the layup angle between the wires is 90 degrees. This is not often the case is helically wound conductors.

As explained later in the report, the damage accumulation was assumed to be linear after the number of cycles simulated had been reached. This was done to save on computational time and did not result in much discrepancy in the results.

1.3.3 Water Tree Analysis Assumptions

XLPE material data is extremely uncertain and unknown. Material properties had to be gathered from other fields of research such as the medical field. A comprehensive methodology was developed to predict the service life of marine dynamic cables due to water treeing. However, due to ambiguity in XLPE material data the fatigue lives calculated cannot be applied to real world marine dynamic cables at this time.

An assumption was made that a water tree crack will not propagate from mechanical stresses until K_{th} has been reached, which meant assuming LEFM was only applicable in this study. EPFM was not incorporated, again due to the extreme unknown and uncertain material properties of XLPE.

It is assumed that only tensile stress will contribute to the fatigue life of the marine dynamic cable in this study. When the cable is suspended between two points axial tension is of the utmost importance. This assumption is also relevant as it has been found that compressive stress and strains can retard the propagation of water trees.

This investigation operates under the assumption that within the insulation cross-section only a single water tree crack will be present. This can be considered a valid assumption as [10] states the length of the water tree plays a significant role in the electrical breakdown of the marine dynamic cable, whilst it is unaffected by the density of water trees within the same cross-section.

When investigating cable degradation because of water trees present in XLPE insulation, this project solely analyses vented water trees with bow-tie water trees ignored. This is because vented water trees are the structurally critical water tree geometry.

The study also does not account for micro-jetting of water molecules within water trees under an electric field. Instead, the propagation of water trees is regarded solely as a consequence of the Maxwell stress resulting from electric field distortions and the mechanical stresses occurring from the dynamic environment.

The marine dynamic cable is also assumed to be operating at full capacity 100% of the cables service life.

1.4 Report Organisation

This short section outlines the contents of each chapter in the report.

In chapter 2, an overview is provided on the current body of literature concerning global, fretting and water tree analysis on marine dynamic cables. It also expands to the current methods of determining fatigue due to these phenomena. The background of WECs and subsea dynamic cables is also covered in this section.

Chapter 3 introduces the methods and models developed and used for structural integrity analyses. The section describes the process of the SIMA global model and how a fatigue assessment and relative displacements can be found using the methodology. Furthermore, the chapter outlines the method for calculating fatigue damage and service life of the cable when considering the fretting and water tree phenomena.

The results from each numerical simulation and a discussion of the findings are illustrated in Chapter 4, these are followed by the investigations key findings in Chapter 5. Chapter 6 then goes on to outline several suggestions for future work within each section of the structural analysis.

2 Literature Review

This section outlines the main theories and assumptions applied to enhance the understanding of the subject. A comprehensive literature review of the global and local scale has been conducted to gain a better understanding of the failure modes that are associated with marine dynamic power cables. Wave Energy Converters are introduced, followed by the details of the dynamic cable including both the mechanical and electrical properties, global and local failure mechanisms, and finally concluding with the phenomena of Water Trees.

2.1 WEC

The entire procedure of transforming wave energy into electricity can be segmented into three separate phases [9] as shown in Figure 4.

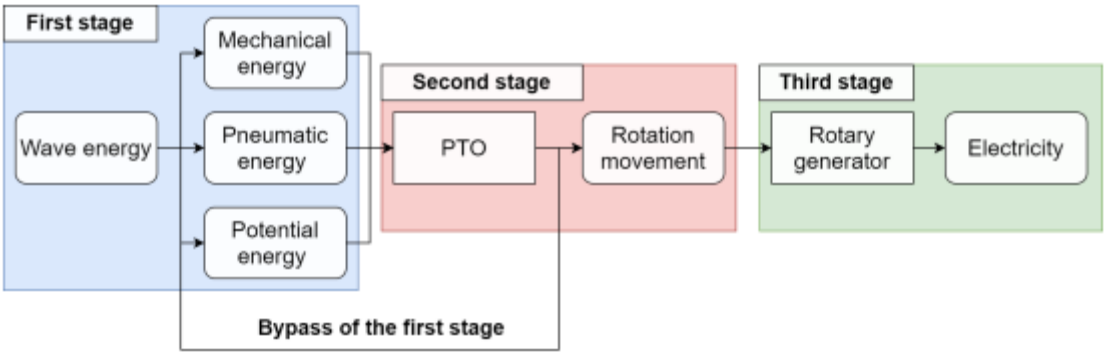

Figure 4: Wave to Electrical Energy Flow Chart

The initial phase involves the conversion of wave energy into potential, pneumatic or mechanical energy employing various WEC technologies to accomplish this transition. These technologies can be categorised into four distinct groups: point absorbers, oscillating bodies, oscillating water column, and overtopping [9]. This investigation focuses on a point absorber WEC, these are the WECs that are currently installed at Runde, Norway. A point absorber is a floating structure that operates in close proximity to the water's surface, capturing energy from waves in all directions. The setup of displacers and reactors allows for flexibility in implementing different power take-off systems however, they typically do this by fixing one end of the absorber to the seabed while the other end moves with the waves. The reciprocating motion can drive either a fluid pump or a linear generator, thereby producing practical power. This type of WEC will harness wave motion at a specific location and have a constrained horizontal scale relative to their vertical size. The majority of configurations for point absorbers are similar to that of a typical buoy as depicted in Figure 5 [11].

Figure 5: WEC Typical Buoy Structure

In the next phase of generation, the energy generated in the initial stage is transformed into practical mechanical energy. The significance of this mechanical energy lies in its potential conversion into electrical energy. This transformation is accomplished through a power take-off (PTO) system, the initial stage energy is converted into a mechanical rotational movement. The final phase harnesses the rotational motion to generate electricity through a rotary generator. Bypassing of the initial stage is possible, only if direct conversion of wave energy into practical mechanical energy is achievable.

2.2 Subsea Dynamic Cables

To transport the energy produced offshore back to land, WECs and other offshore energy production methods require very long subsea cables which are fixed to the seabed. These static cables are well understood as they have been used for many years in industry, however, due to the rise in floating production facilities there has been an increased need for dynamic power cables. In the context of WECs, these cables are used to connect the buoys to the central hub which then converts the energy to high voltage and sends it onshore via the fixed power cable. These subsea dynamic cables must be able to endure the dynamic stresses resulting from greater water depths and the motion of the floating vessel it is connected to [12].

Many designs exist for these cables, however, a typical configuration, shown in Figure 6, consists of seven separate layers[13].

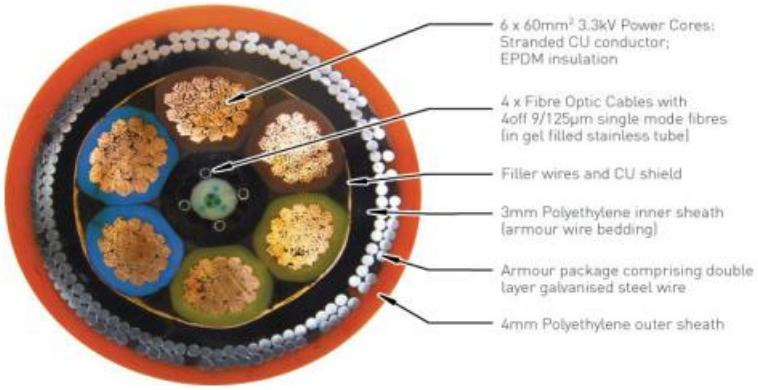

Figure 6: Detailed Cable Cross Section

These layers are:

1. Conductor core
2. Electrical insulator
3. Screen
4. Sheath
5. Armature
6. Optical fibre
7. Protecting sheath

Many of the layers, such as the screen, sheath, armature and protecting sheath, are there to serve protection to the cable from mechanical or electrical induced stresses. The conductor is typically made from copper and is comprised of many wires wrapped helically around a central core wire. The separate elements of the cable are also wound helically to reduce the induced stresses when the cable undergoes bending. This study mainly focuses on the different local fatigue phenomena in these conductor wires and the electrical insulators, typically made from XLPE.

During the life of these power cables, they will experience serve weather conditions which cause high levels of oscillatory movement and forces. Particularly in WEC applications as they are typically located in deep waters due to the larger waves. Although this leads to higher potential energy production it also results in harsher operating conditions, so precautions must be taken to ensure these cables can survive in such conditions.

It was concluded by Thies *et al* [10] that the most critical region of the cable is at the point it is attached to the WEC. Due to the relative differential motion between the waves and the WEC, this point experiences the highest bending curvatures and axial force through the wire. Shown below is how the power cable is typically attached to the WEC [14].

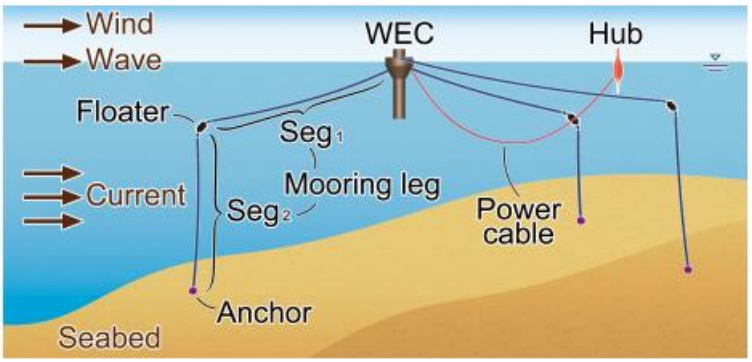

Figure 7: WEC and Power Cable Diagram

Improvements have been made to the subsea dynamic power cables, however, most of the development is focused on improving life when subjected to bending, torsional and tension loading. This report aims to explore the impact of local phenomena such as inter-wire fretting and water tree propagation to see how this compares to the global fatigue life of the cable.

2.3 Properties and Parameters

This investigation will be focused on low voltage 1kV subsea dynamic power cables, these alternating current (AC) cables are standard cables used in wave energy generation. NKT are responsible for the development and manufacturing of the cables [15]. As the basis of this project required an extensive range of software to investigate a multitude of components, there was a diverse array of material properties used. The following section accentuates a detailed cross section of the 1kV subsea dynamic cable used in this project. Furthermore, the mechanical material properties used for the global simulation using SIMA, water tree local model in ANSYS, fretting analysis in ABAQUS and fracture mechanics analysis in COMSOL Multiphysics are presented. Finally, the electrical material properties required to assess water tree propagation due to Maxwell stresses in COMSOL Multiphysics are illustrated.

2.3.1 Geometry

The total length of the dynamic cable being studied is 135m and has a parabolic geometry with an umbilical like shape, as shown above in Figure 7. Figure 8 showcases a cross section representation and the schematics of the subsea dynamic cable.

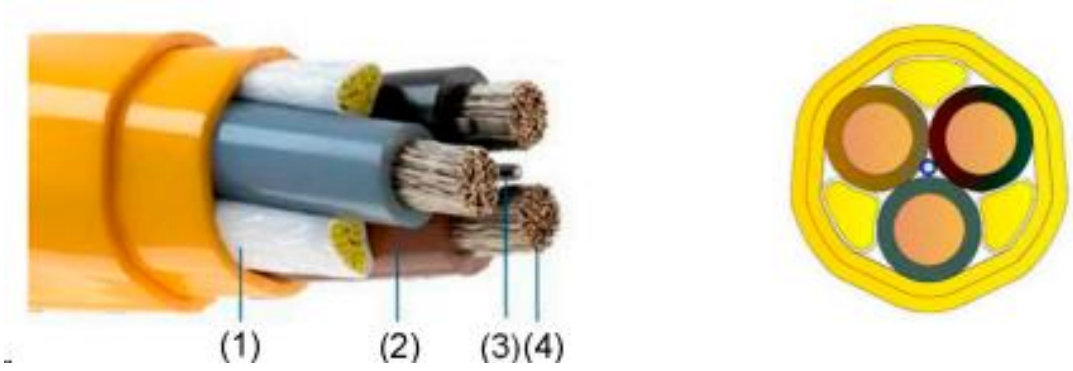

Figure 8: Real Life Depiction of Cable (1) Kevlar Ropes, (2) XLPE Insulation, (3) Fiber Optic Cable, (4) Conductor Wires

Normal designs for WEC dynamic cables include armour wire layers as illustrated in Figure 8. The flexibility of the cable being studied has been enhanced by removing these armoured layers. This process will lower the bending stiffness enabling it to adapt to the movements of devices like a WEC heaving point absorber without adverse effects on its motion. Additionally, removing the armour simplifies the cable's handling during installation and maintenance.

For the study the cable cross-section has been simplified to reduce computational times, this cross-section is shown in Figure 3. The fundamental dimensions of the cables are outlined in Table 1 [16].

Table 1: Cable Component Dimensions

Cable Component	Length (mm)
Outer Diameter of Cable	38
Conductor Diameter	9.3
Insulation Thickness (XLPE)	2
Outer Sheathing Thickness	3.4
Rope Diameter	6.5

2.3.2 Global Properties

The properties illustrated in Table 2 list the parameters used in the Global SIMA analysis. The properties are based on a 1kV dynamic power cable that would be likely used by W4P at the Runde site and were obtained from Yang 2018 [17].

Table 2: Global Model SIMA Properties [17]

Property	Magnitude	Unit
Cable Length	135	m
Mass	2.3	Kg/m
Cable Diameter	0.038	m
Axial Stiffness	4.7e06	MN
Bending Stiffness	5	Nm^2
Torsional Stiffness	3	Nm^2/rad

2.3.3 Mechanical Properties

To conduct precise analysis of the dynamic cable using finite element and COMSOL Multiphysics reliable material data of the cables cross section was imperative to know. The materials comprising the cross section of the cable are as follows; cross linked polyethylene, XLPE, for the conductor insulation, the copper conductor, Kevlar ropes and polyethylene outer sheaths. All materials within COMSOL, ANSYS and ABAQUS were assumed to be isotropic, i.e., material properties are irrespective of direction. Table 3 depicts the mechanical material properties from Young [10] used for this work.

Table 3: Mechanical Material Properties

Material	Density [$\boldsymbol{kgm^{-3}}$]	Youngs Modulus [MPa]	Poisson's Ratio
Copper	8600	1.17×10^{11}	0.33
XLPE	924	350	0.40
Kevlar Ropes	N/A	7.05×10^{9}	0.40
Polyethylene	N/A	30	0.49

2.3.4 Electrical Properties

The properties illustrated in Tables 4 and 5 are the electrical parameters used in the COMSOL models that analyse Maxwell stress acting on water tree cracks in the conductor insulation. These properties are taken from bodies of work already conducted on this area [9].

Table 4: Electrical Properties (1)

Property	Magnitude	Unit
Frequency	50	Hz
Cable Voltage	1000	V

Table 5: Electrical Properties (2)

Material	Electrical Conductivity [S/m]	Relative Permittivity
Copper	9.33e6	1
XLPE	1e-17	2.3
Water	1e-8	10
Air	0	1

2.4 Global Analysis

As a result of the power cable being a sub-sea free hanging dynamic cable, it is known that they are subjected to a range of mechanical loads. Due to the complexity of the interwire arrangement, the global analysis focuses solely on the stresses induced by the wave oscillations. Focussing on this, it enables for critical regions along the cable to be identified and allows for intricate local analysis to be conducted.

2.4.1 Failure Modes

Marine dynamic cables exhibit flexibility in both bending and torsion, due to their low material stiffnesses. However, simultaneously have a high tensile strength as a result of their high axial stiffness. Marine dynamic power cables are subjected to a variety of different forces during their operational lifetime. These stresses are dependent on many factors:

1. Wave height, direction, and period
2. Wind speed and direction
3. Current strength and direction

As a result of these oceanic conditions, different global and local failure modes arise. In a global sense, the most dominant effects are characterised as bending, tension, and torsional effects – this loading arises from the heave, surge and pitch of the cable [18]. From these effects, a number of different failure modes are introduced.

Simple axial tension experienced by the cable is a consequence of the prevailing oceanic conditions present. These conditions cause the cable to either compress, seeking to “shorten” or “elongate” due to tension. Axial tension is of importance especially when the dynamic cable is suspended between two points – in this paper’s context this would relate to the linkage between the Wave Energy Converter and the hub. This type of configuration is commonly referred to as an “umbilical” cable.

As a result of the harsh oceanic conditions, bending of the cable plays a major role in the calculation of the fatigue life of the dynamic cable. From previous studies, and simple simulations using SIMA, it is evident that the greatest bending moments occur within areas of high curvature – these areas of high curvature are present at the connection points between the dynamic cable and the Wave Energy Converter or the hub. As a result of these areas of high bending moments, bending stiffeners are often implemented to increase the structural integrity of the cable at these points. Bending stiffeners also prohibit the cable having direct contact with the Wave Energy Converter. A typical bending stiffener is presented in Figure 9:

Figure 9: Typical Bending Stiffener Used by Balmoral Offshore[72]

Birdcaging is a unique phenomenon which occurs when a cable experiences negative axial stress (compression) and causes the individual strands of the cable to separate and rendering the cable non-functional [19]. This phenomenon occurs primarily within the armouring of a cable, in this thesis the armouring has been intentionally removed to reduce the cable's bending stiffness. As a result, this enables the cable to conform more flexibly to the dynamic movements of the oceanic environment. Birdcaging induces a separation between the outer strands and the inner core and causes permanent deformation. This provides another rationale for excluding this phenomenon from the scope of this thesis. Figure 10 below provides a schematic representation of Birdcaging:

Figure 10: Birdcaging Phenomenon on a Wire Cable[19]

An additional failure mode can arise from the extreme pressures induced by the depth of the ocean. In this thesis, to mitigate this concern, the depth of the seabed will be constrained to approximately 90 metres. By imposing this limit, the cable will not experience extreme pressures and as a result this failure mode can be neglected.

2.4.2 Environmental Conditions

A marine dynamic power, over a lifetime, must be able to withstand a diverse range of sea-state conditions. The fatigue life of the cable may hinge upon sea states and other phenomena known as biofouling. Sea states consists of many factors such as waves, winds and currents and differ from location to location. This thesis focusses on a WEC that is found in Runde. Runde is an island off the west coast of Norway, illustrated with a red arror below in Figure 11 [20]:

Figure 11: Location of Runde Norway on map

Figure 12 illustrates the potential sea-state conditions that are found in Runde, with significant wave height, Hs [m] against wave period, Tp [s] with probability of occurrence being displayed in each cell [21]:

H_s [m]	T_z [s]														Sum
	2.5	3.5	4.5	5.5	6.5	7.5	8.5	9.5	10.5	11.5	12.5	13.5	14.5	15.5	
12.5	0	0	0	0	0	0	0	1	2	3	0	0	0	0	6
11.5	0	0	0	0	0	0	0	2	7	0	0	0	0	0	9
10.5	0	0	0	0	0	0	0	11	10	0	0	0	0	0	21
9.5	0	0	0	0	0	0	6	42	10	0	0	0	0	0	58
8.5	0	0	0	0	0	2	29	87	2	0	0	0	0	0	120
7.5	0	0	0	0	0	14	107	103	2	0	0	0	0	0	226
6.5	0	0	0	0	0	44	267	33	5	1	0	0	0	0	350
5.5	0	0	0	0	7	166	337	37	7	2	0	1	0	0	557
4.5	0	0	0	0	43	558	136	32	14	5	1	1	0	0	790
3.5	0	0	0	1	371	563	123	48	19	6	2	1	0	0	1134
2.5	0	0	4	179	877	303	130	71	33	16	7	2	0	0	1622
1.5	0	0	221	1014	501	220	146	110	66	36	16	3	1	0	2334
0.5	644	367	684	248	107	142	162	192	117	64	19	22	3	4	2775
Sum	644	367	909	1442	1906	2012	1443	769	294	133	45	30	4	4	10002

Figure 12: Sea state scatter diagram

2.4.3 Global Fatigue Life Calculation

Within the global model, a common S-N approach has been utilised alongside a rain-flow counting method and Palmgren-Miner's rule – a recognised damage accumulation rule. Through these methods, the fatigue damage accumulation can be calculated along the full length of the cable and can be converted into a fatigue life.

For a Wave Energy Converter, and consequently a dynamic power cable, the non-uniform loading arising from harsh oceanic conditions is evident. As a result of this, to calculate the fatigue life, a straightforward S-N curve cannot be implemented directly. S-N curves illustrate the relationship between Stress (s) and the Number of Cycles to failure (N), however this relationship relies on the assumption that material properties and loading is constant with a mean cycle stress of 0 – which is not applicable in the dynamic and unpredictable ocean environment. Another limitation of the S-N approach is that it does not account for the frequency of the loading. Frequency of loading can impact the fatigue life of a system significantly, especially if it aligns closely with the resonance frequency of the system [22]. In our study, it is reasonable to assume that high cycle fatigue is incurred and consequently all fatigue transpires in the elastic region.

2.4.4 Rainflow Counting Method

For irregular sea-states, it is imperative that a Rainflow counting system is implemented in order to achieve accurate stress-time histories of the cable.

Through the implementation of a Rainflow counting method and a stress history of a system, fatigue analysis can be carried out. A widely used, and extremely important, approach for converting complex non-uniform cycles into simpler cycles, is the Rainflow counting system. The "Rainflow Counting" system is a method employed to quantify the fatigue cycles in a load time history [23]. The Rainflow counting algorithm was initially proposed by Matsuishi and Endo in 1968. There are different types of methods some including, the Pagoda method or the 3- or 4-point counting method, which give similar results and follow a common procedure. In this thesis, a 4-point method is described to understand the fundamentals of the concept.

Both methods initially involve the removal of small cycles and non-turning points from the cycle. This is justified by acknowledging that the most significant fatigue damage arises from the cycle's maxima and minima and as a result these small cycles can be neglected – this process is known as Hysteresis Filtering.

Following this, Peak-Valley Filtering is introduced and aims to only preserve the pivotal turning points in the cycle. The strategy stems from the realisation that the maxima and minima represent the critical points where the greatest fatigue damage accumulation occurs. Consequently, these intermediate points are systematically eliminated from the cycle and hence further streamlining and simplifying the overall cycle [24].

From here, a discretisation process, commonly known as "binning". This process effectively decomposes a stress cycle into pre-defined stress ranges to reduce the number of y-axis values and aiding the counting of cycles. Figure 13 below aids the understanding of the "binning" process:

Figure 13: An Example Cycle Where "binning" has taken place[73]

In Figure 13, the orange dots represent where the actual value is located, and the green line represents the adjusted values. These new values all lie precisely on a whole integer simplifying the counting process. It is worth noting that the greater number of bins enhances accuracy of the results however concurrently extended computation time.

The penultimate stage of the process involves the counting of the cycles. Different counting methods utilise different conditions in which qualifies as a cycle, however all methods, to maintain accuracy, must account for the amplitude and mean of the cycles. For reference, the conditions for a cycle include that if the stress range of the inner cycle is bounded by the stress range of the outer cycle, the cycle is counted. The process is repeated until all closed cycles have been counted. Typically, at the end of the process, a 'residue' of unclosed cycles is left – these are preserved and presented. A graphical representation is presented below in Figure 14:

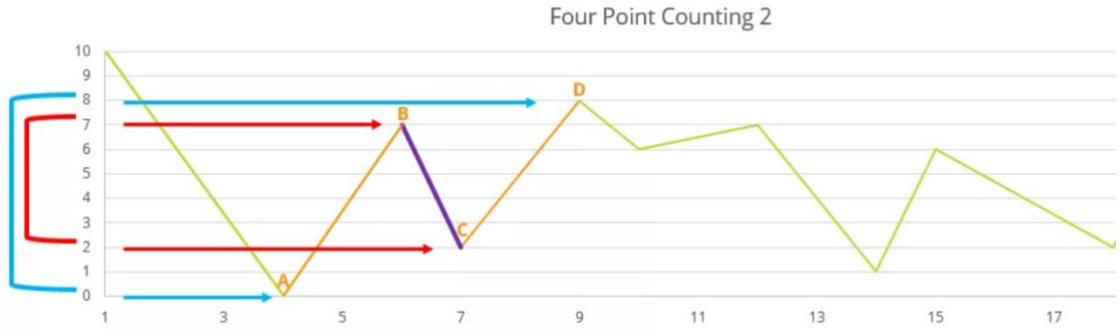

Figure 14: Figure Illustrating Points B and C Being Bounded Within A and D [73]

Finally, through the counting process, the data is converted into a Rainflow matrix which is a user-friendly graphical representation highlighting the most and least damaging cycles and the compressive and tensile cycles. A typical Rainflow Matrix is illustrated below in Figure 15.

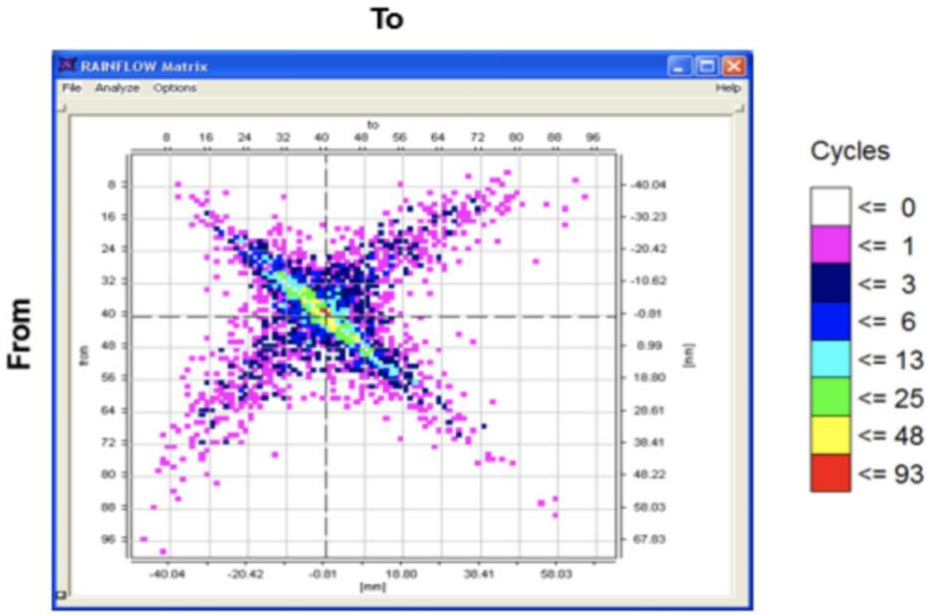

Figure 15: Typical Rainflow Matrix [23]

Examining Figure 15, it can be found that the most damaging cycles occur in the top right and bottom left portions of the graph while the least damaging align along a diagonal from the top-left to bottom-right. Cycles situated below this diagonal, specifically in the bottom-right quadrant and cycles found to be in tension while those in the upper-left quadrant are experiencing compression. In our study, it is the tensile stresses that are more concerning as these dominate the fatigue damage.

2.4.5 Palmgren-Miner's Damage Accumulation Rule

For uniform stress cycles, Palmgrem Miner's Rule can be implemented alongside the S-N curve in order to capture an accurate estimation of the fatigue damage of a system. Miner's rule is a simple expression which calculates total damage from the time history and S-N curves of a specific system. Miner's rule is denoted in Equation 1 [25]:

$$D = \sum_{i=1}^{k} \frac{n_i}{N_i} \tag{1}$$

Where, D = Total Damage

n_i = Number of cycles, of a given amplitude, that the system is subjected to.

N_i = Number of cycles, of a given amplitude, that the system can survive (calculated through laboratory testing)

K = The number of different stress amplitudes a system experiences.

For context, when the Total Damage, D, of a system reaches 1, the system is considered to have failed. Conversely, a system with a Total Damage of 0, is considered to be a system that is pristine and has not experienced any stress. In the context of a dynamic cable, the stress cycles are non-uniform and have a complex load history. As a result, the non-uniform cycles must be converted into a series of uniform stress cycles, this can be done through the use of a cycle counting method explained in section 2.4.4.

2.4.6 Goodman/Gerber Relations

The Gerber and Goodman relations are mathematical models that allow for the maximum number of cycles to be calculated before failure for a given system [26]. The two relations are mathematically similar; however, the Goodman is a liner approximation derived from the Gerber relations and is deemed a more conservative approach. The Gerber relation is defined as:

$$\left(\frac{n\sigma_m}{\sigma_{UTS}}\right)^2 + \frac{n\sigma_a}{\sigma_w} = 1 \quad (2)$$

The Goodman relation is highlighted in Equation 3:

$$\frac{\sigma_m}{\sigma_{UTS}} + \frac{\sigma_a}{\sigma_w} = \frac{1}{n} \quad (3)$$

Where n = Factor of safety, σ_m= mean stress, σ_a = stress amplitude, σ_{UTS} = ultimate tensile stress, σ_w = fatigue limit. The Goodman is a more conservative approach than the Gerber and lies within the Gerber parabola. Figure 16 illustrates a plot highlights the relations [27]:

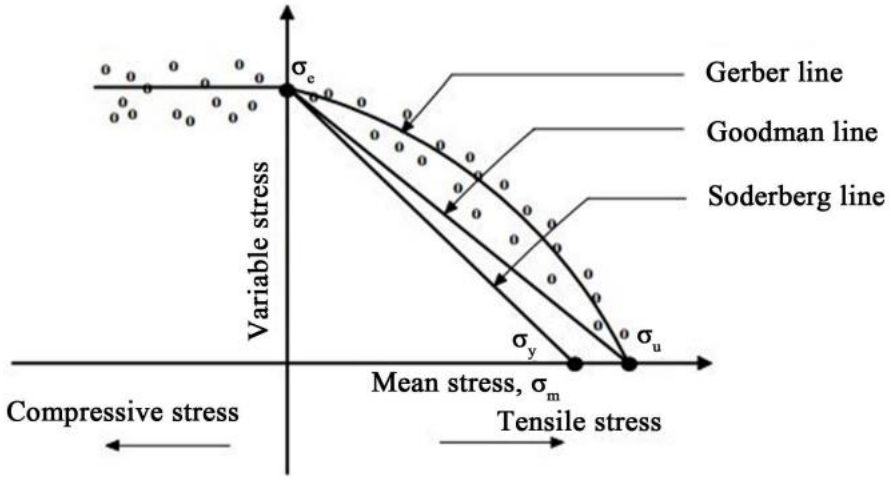

Figure 16: Illustration of Gerber and Goodman Relation

2.5 Fretting

In engineering systems, it is standard practice that sliding contacts are properly lubricated which typically leads to minimal damage to the system. However, when two contacts are assumed to be stationary relative to one another, oscillatory loads or vibrations can lead to small scale differential movement. This is known as fretting. Fretting is a form of fatigue, which as stated previously, is induced by small relative oscillatory motion between two surfaces in contact in the range of a few microns up to roughly 300 μm. The damage develops at the asperities of the material and occurs when the contacting bodies are under load. Based on the relative motion at the contact face, fretting is categorised into three types; stick regime is when there is no movement at the interface, partial slip regime is when there is sticking at the centre of the interface with sliding near contact edges, and gross sliding regime when sliding

occurs along the entire contact interface [28]. The fretting process is often characterised by three main steps that take place regardless of the fretting type [29]:

1. The initial stage is the damage and disintegration of the asperities protruding from the material surface.
2. The second stage is the generation of wear debris by oxidation. Due to the gap between the two bodies and the oscillation amplitude being very small, the debris cannot escape and subsequently acts as an abrasive.
3. The third stage is the initiation of cracks at the edges of the loaded areas due to the cyclic loading.

Fretting wear significantly degrades the material properties and reduces the life of a system. Fretting can cause many unfavourable outcomes, such as, connected parts may become loose, sliding parts may stick together or the stress concentration and generation of cracks may cause early failure of the system.

Fretting can be further categorised by the application of the load. Figure 17 outlines the four most common types:

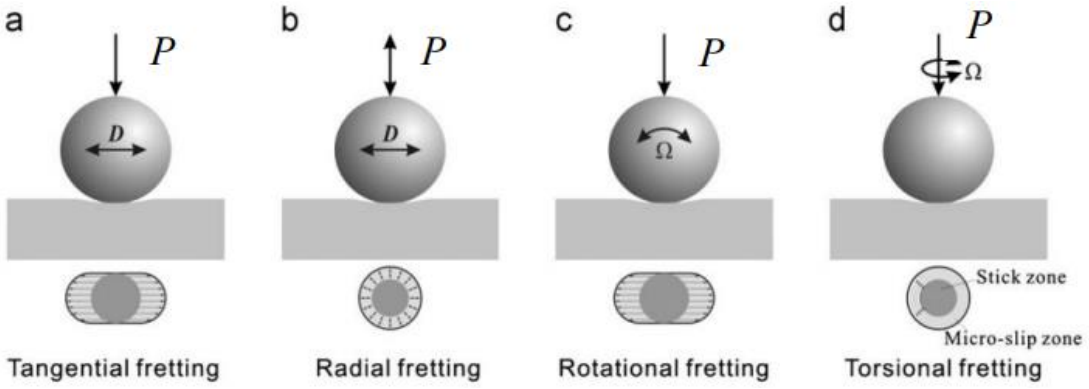

Figure 17: Fretting Types [30]

Tangential fretting is the most common form and is the dominant type occurring within the conductor of the marine dynamic cables. For this reason, it will be the form investigated in this project. Radial fretting can is usually induced by a variable normal load or sometimes by thermal cycling. As the two surfaces always remain in contact, the slip occurs due to the two materials having different elastic constants. The other two forms are induced by vibration causing either rotational or torsional motion.

Fretting occurs in every tribosystem but is often not considered in the design process. However, studies show that it can reduce the life of a system by up to 30%[1]. It is essential that further investigation is done in this area to develop a better understanding of how to mitigate these issues and allow the manufacture of more robust systems.

The factors which influence fretting are the applied normal load and the tangential displacement amplitude. Therefore, a theory has been produced to combine these parameters.

The first method, proposed by Vingsbo *et al* [31], plotted the frictional force Q against the displacement amplitude δ_E which creates a hysteresis or fretting loop. From the shape of this fretting loop, shown in Figure 18, the fretting regime can be determined.

a) Stick Regime: The $Q - \delta_E$ curve is closed suggesting that the slip is accounted for by the elastic deformation and there is no energy dissipation.

b) Partial Slip Regime: In this instance $Q - \delta_E$ has an elliptical shape. In this regime the shear-strain relation changes from elastic to plastic. In this regime the center of the contact is stuck, and slip is occurring at the edges. The amount of energy dissipated can be calculated from the area of the elliptical shape.
c) Gross sliding regime: The $Q - \delta_E$ shows a rectangular shape.

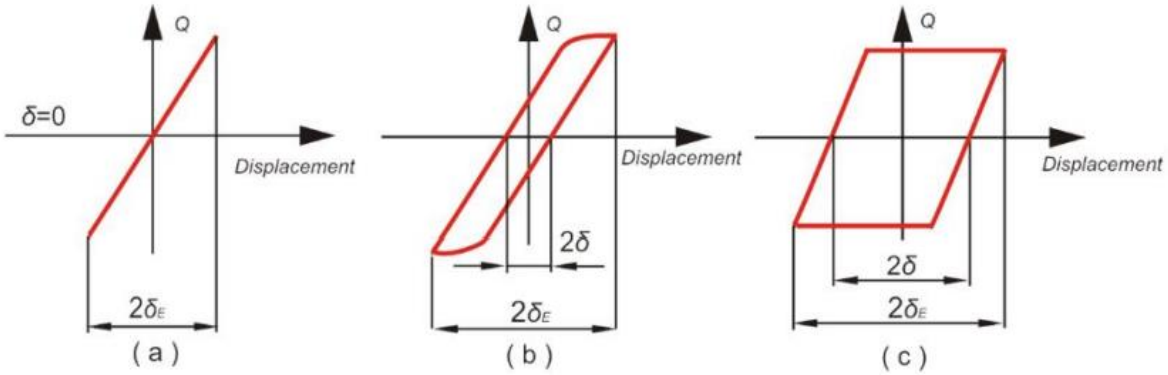

Figure 18: Fretting Loops in Different Regimes

2.5.1 Fretting Damage

Further categorisation can be done on the fretting damage, which can be divided into three sub-categories [32].

Fretting Wear: This phenomenon can occur in partial slip and gross sliding regimes but is the dominant damage in the gross sliding condition. From the surface which has undergone fretting wear, it is possible to determine whether the system was in partial or gross sliding conditions. The partial slip example will have two distinct areas of the stick and slip zone, whereas the gross sliding example will only have one as the entire contact is sliding. This is illustrated in Figure 19.

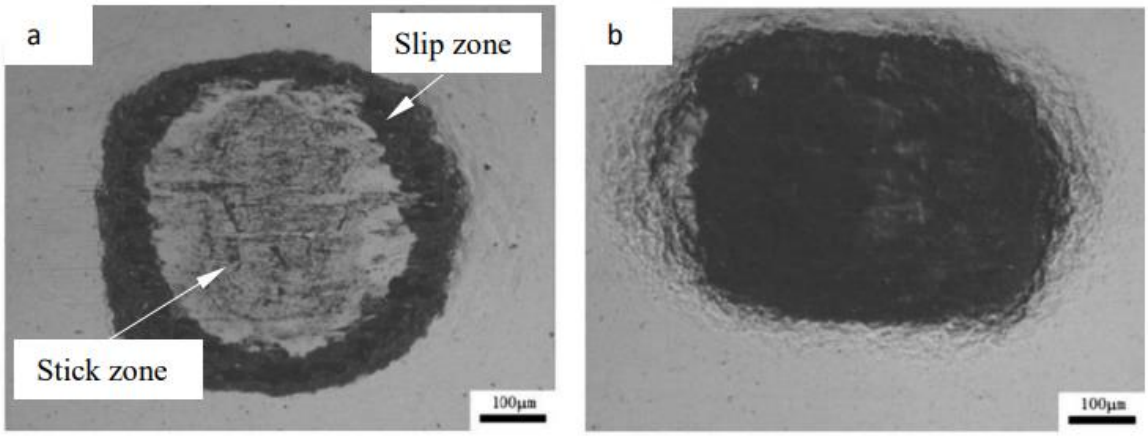

Figure 19: Fretting Wear; Partial Slip vs Gross Sliding

Fretting Fatigue: As suggested, this is when a body experiences fatigue due to the effects of fretting. Similar to standard fatigue, this can cause cracks to propagate and lead to total failure of a system at stress levels well below yield stress. However, fretting fatigue can even occur below the fatigue failure limit. The damage mechanism is likely to occur in the partial slip regime. This is because there is less material being removed than in gross sliding regime giving cracks the chance to propagate through the material.

Fretting Corrosion: Similarly, this is the disintegration or corrosion of the material due to the fretting process.

2.5.2 Contact Mechanics

Contact mechanics is a complex issue that has been studied for many years. The high stresses that develop at the contact surfaces can cause significant damage that can take on many forms, such as fracture, yielding or surface fatigue [28]. To avoid these issues, an effective way of modelling the stresses is required. But due to complex geometry and surface roughness this is very challenging. However, with the use of certain approximations, some theories have been developed, the most commonly used being Hertzian contact theory created in 1882 by Heinrich Hertz.

2.5.3 Hertzian contact

The Hertzian contact theory has been utilised in engineering applications since its creation to calculate contact variables. This theory makes the following assumptions:

1. Contact surfaces are continuous and non-conforming (e.g., initial contact is a line or point).
2. Strains due to contact are small.
3. Each contact body can be considered as in perfectly elastic half-space.
4. The surfaces of contact are frictionless.

This implies that the contact radius, a, is much smaller than the effective radius of curvature of the two bodies, R.

$$\frac{1}{R} = \frac{1}{R_1} + \frac{1}{R_2} \tag{4}$$

Where R_1 and R_2 are the radii of the two bodies in contact, respectively.

The Hertzian theory can be broken down into different sections depending on the type of contact occurring. These include point and line contact. Point contact is typical when two spheres are in contact, and therefore is not very applicable when modelling wire contact. However, line contact is as a typical configuration is two cylinders with parallel axes. Henceforth, literature covering line contact will be further reviewed in this section.

Figure 20 below shows two cylinders of the same length (L) and radii (R_1, R_2), in contact under load (P).

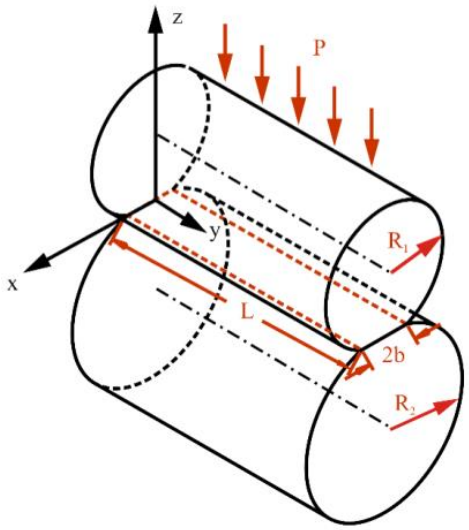

Figure 20: Line Contact Configuration

As the contact area in the x-direction is much smaller in comparison to the length of the cylinders, this is considered a plane strain problem. The stresses are formed in the shape of an elongated rectangle which runs the length of the cylinders. The area of this rectangle is equal to $2bL$ where b is the half width and is given by:

$$b = \sqrt{\frac{4PR}{\pi E^* L}}$$

(5)

Where E^* is defined by the Young's Modulus (E_1, E_2) and Poisson's ratio (ν_1, ν_2) of the contacting bodies:

$$\frac{1}{E^*} = \frac{1-\nu_1^2}{E_1} - \frac{1-\nu_2^2}{E_2}$$

(6)

From this the contact pressure can be determined by:

$$p(x) = \frac{2P}{\pi L b^2}(b^2 - x^2)^{1/2}$$

(7)

From the equation above, it can be seen that the maximum pressure will occur when $x = 0$, or at the center of the contact area. The pressure will also reduce to zero at the contact edges. The equation for maximum pressure is derived by combining equations 5 and 7 and is given below:

$$p_{max} = \left(\frac{PE^*}{\pi LR}\right)^{1/2}$$

(8)

2.5.4 Sliding Mechanics

To capture the effects of fretting, the Hertzian solution must be modified to include the tangential force and motion. In the basic form of the Hertzian solution, the coefficient of friction (CoF) is not considered yet it has a significant effect on the stress distribution and relative. This section will outline how these can be considered.

First, the following additional assumptions must be introduced:

1. The deformation due to the normal load and the tangential force are independent.
2. Coulomb's friction law is applied to the contact surfaces.

Coulomb's friction law relates the tangential and normal forces with a linear relationship using a coefficient of friction (μ). The CoF is dependent on many variables, such as material hardness, surface roughness and lubrication. The equation of Coulomb's friction law is given below:

$$Q = \mu P \tag{9}$$

Where Q is the tangential force and P is the applied normal load. This equation implies that if the tangential force is less than the product of the CoF and the applied load then the sliding will not occur [33]. If the tangential force is greater than this product, the system will enter the gross sliding regime where all parts of the two bodies are moving relative to one another.

The shear stress can then be calculated using Coulomb's friction law as:

$$q(x) = \mp \frac{2\mu P}{\pi L b^2}(b^2 - x^2)^{1/2} \tag{10}$$

If the tangential load is less than the product of the normal force and the CoF, the system may enter the partial slip regime. This is when part of the contact surfaces slides relative to one another while other parts remain stationary.

Solved by Cattaneo in 1938, the tangential force, at the point of slipping, is given by:

$$q'(x) = \mp \frac{2\mu P}{\pi L b^2}(b^2 - x^2)^{1/2} \tag{11}$$

When the tangential force does not reach the limiting force, a stick area exists with half width c. The distribution of the tangential stress in this area is given by:

$$q''(x) = \mp \frac{c}{b}\frac{2\mu P}{\pi L b^2}(b^2 - x^2)^{1/2} \tag{12}$$

The total tangential stress is given by the super position of the previous two equations. Figure 21 shows the relative motion of the two bodies. A small-scale relative motion appears at the edge of the contact and the centre is in the stick regime.

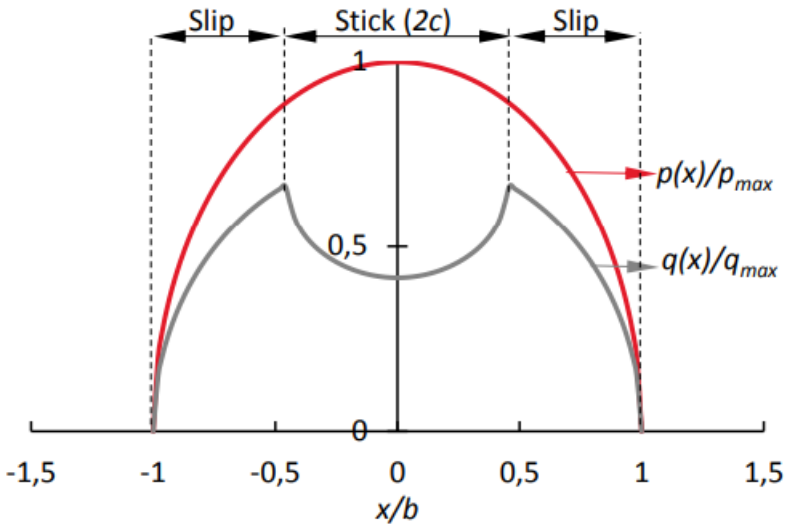

Figure 21: Contact Pressure and Shear Stress Distribution

The half width of the previously stated stick area is given by:

$$\frac{c}{b} = (1 - \frac{Q}{\mu P})^{1/2} \quad (13)$$

This shows that the tangential motion and the normal force have a strong effect on the tangential motion at the contact interface.

2.5.5 Coefficient of Friction

It is key to understand the evolution of friction in fretting to properly model its behaviour. Friction is not an inherent property of a material or part; it can change due to many factors. These variables were listed by Blau [34] and include contact geometry, fluid properties and flow, lubricant chemistry, relative motion, applied forces, third-bodies, temperature, stiffness and vibrations.

The evolution of the CoF during the fretting process is often categorised into three sections. In the initial stage the CoF starts off small as the materials have an oxide layer acting as a film and causing less adhesion at the contact surfaces. The second stage is when the CoF steadily increases. This is due to the oxide film being removed and causing more adhesion at the surfaces. The debris generated also acts as an abrasive and mostly cannot escape as the gap between the surfaces and the oscillations are very small. The CoF beings to level off in the final stage once the volume of debris being generated and ejected is equal. This is demonstrated in figure 22 [35]:

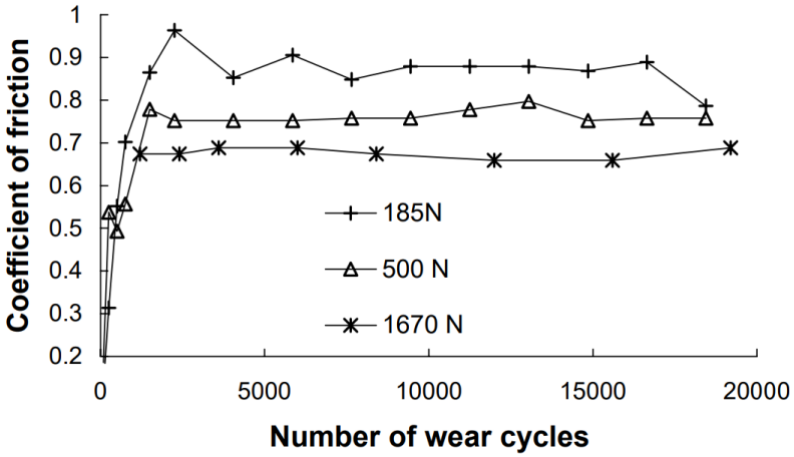

Figure 22: CoF vs Wear Cycles

The value of the CoF is also highly dependent on the applied load and the tangential displacement amplitude. In a paper written by Yan Shen *et al.* [36], this relationship of the displacement amplitude on the CoF is investigated. It was found that the CoF increased with the displacement in both lubricated and non-lubricated regimes. This can be explained by the increased displacement causing a rise in the amount of interface contact and subsequently more friction and fretting. Figure 23 illustrates this phenomenon.

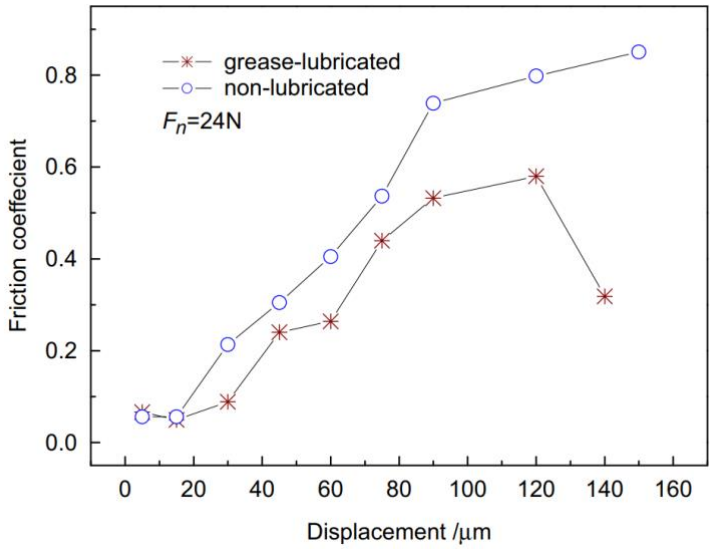

Figure 23: CoF vs Tangential Amplitude Displacement

The effect of the normal load on the CoF was investigated by Zhang *et al.*[37] and is shown in Figure 8. In this paper, it is shown that as the applied load increases, the CoF decreases. It is suggested that the reasons this relationship occurs is because at low applied loads, the asperities of the two surfaces inter-lock causing a high value of CoF. However, when the load is increased, the asperities are flattened causing the surfaces to appear smoother and the CoF decreases.

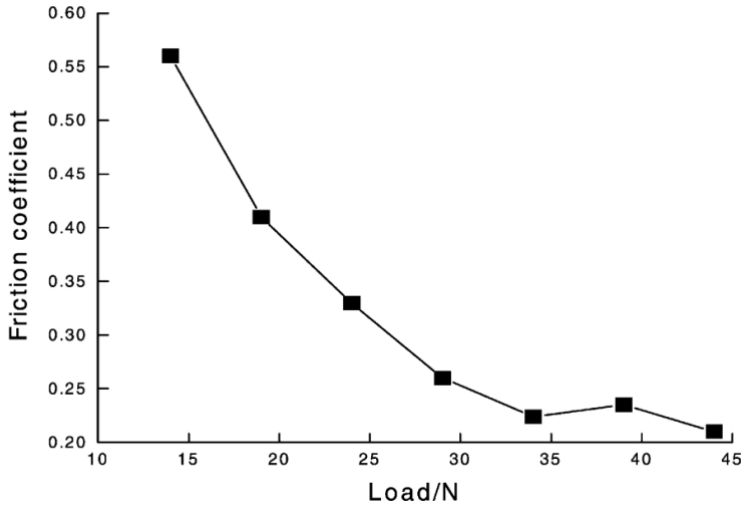

Figure 24: Normal Load vs CoF, Constant Displacement Amplitude of 75 μm

These findings show that the evolution of the CoF is complex as it varies with many different parameters. This makes it challenging and computationally expensive to model the variation of the CoF in fretting problems. It can be found in most of the literature modelling fretting problems a constant CoF is used. This is an appropriate assumption if the number of cycles is sufficiently high, as the CoF levels out after the first few thousand cycles. Also, if the applied load and displacement amplitude are constant, the CoF will remain constant. The assumption can be verified by Tongyan Yue's research paper titled: Finite Element Analysis of Fretting Wear [34]. In this study, the scar width and depth of the fretting scar are compared when using a constant or variable CoF. The results are shown in Figure 25:

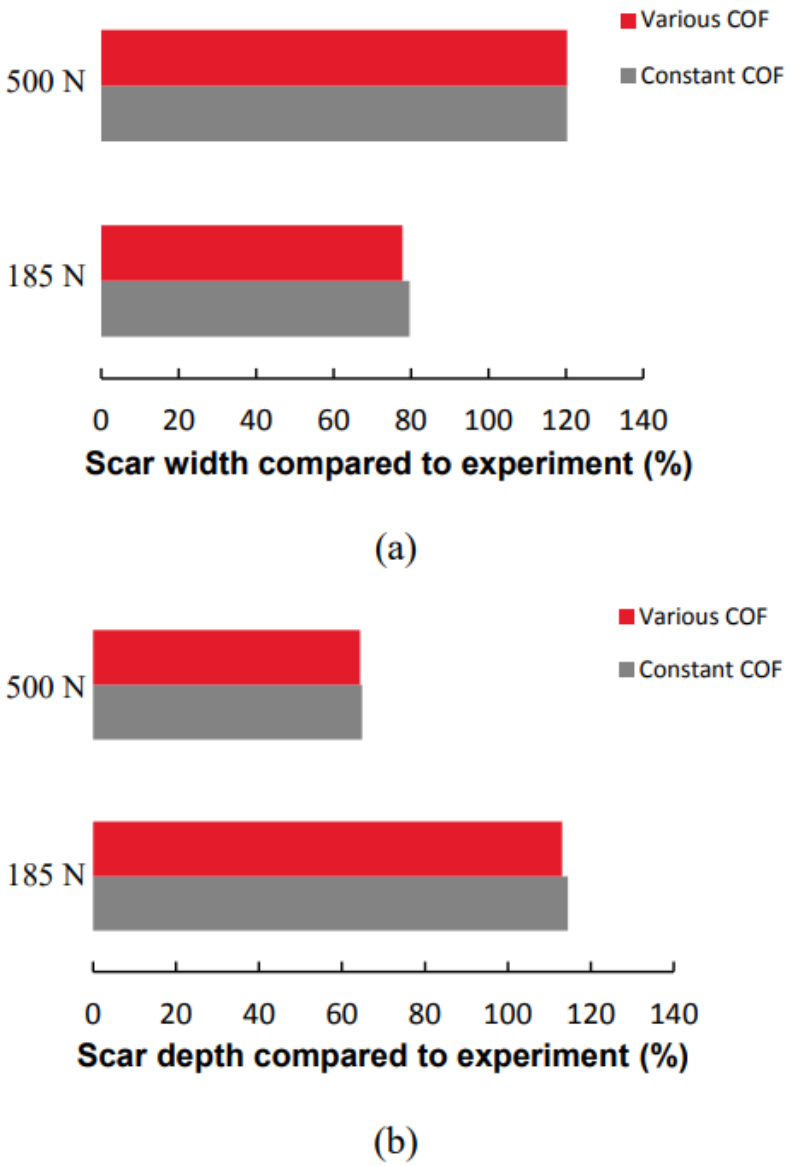

Figure 25: Fretting Scar Width and Depth and Using Variable or Constant CoF ((a) scar width, (b) scar depth)

As shown in the figure above, there is very little variation in the accumulated fretting damage when using a variable or constant CoF.

2.5.6 Friction Model

The most used friction model is the relatively simple Coulomb's Law, previously mentioned in section 2.5.4, which states that maximum shear force which can be exerted by a contact is proportional to the normal load applied:

$$Q \leq \mu P \tag{9}$$

Where Q is the tangential force, μ is the CoF and P is the normal force.

This implies that if the tangential force is less than the product of the CoF and the normal force, no contact will remain stationary. This law can be applied to the individual nodes to model the effects of friction at a local section [38]. However, even using this simple equation, due to the discontinuities involved with friction, a relatively complex solution is required for

FEA applications. For Abaqus, the FEA software used in this study, there are two available methods:

1. The penalty method
2. Lagrange multiplier method

Both methods perform well and display similar results in most cases. However, in some situations the Lagrange multiplier method displays higher accuracy [39]. The penalty method allows for small elastic slip at surface points when the shear stress is less than the critical value for sliding which improves the convergence of the model, especially in mixed-slip cases. On the other hand, the Lagrange method enforces exact sticking and shows much smaller sensitivities for the forces and better estimates the gap between the bodies. It is therefore more stable and is more applicable to complex geometries but is more computationally expensive. Despite it is the chosen method for the fretting problem due to the improved accuracy.

2.5.7 Debris Model

Another important consideration when modelling the effects of fretting, is whether to include the effects of the debris layer. As mentioned in Section 2.5.5 the debris layer, plays an important role in the fretting process as it acts as an abrasive and can lead to a higher CoF and subsequently more fretting damage.

Contrasting findings have been reported when simulating the effect of the debris layer in the fretting process. In Tongyan Yue's research paper titled: Finite Element Analysis of Fretting Wear [34], it is found that during the running in stage the model without a debris layer experiences more damage due to fretting.

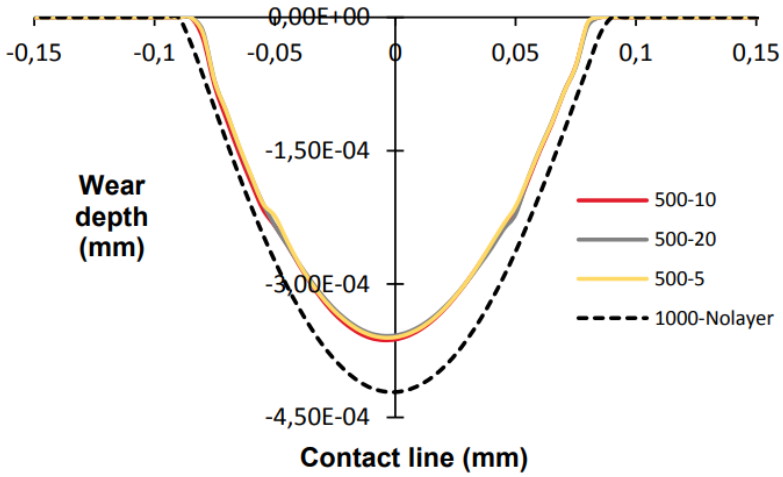

Figure 26: Wear Scar After 1,000 Cycles with Debris Layer Thickness of 5 μm, 10 μm, 20 μm

Figure 26 demonstrates there is very little variation in the wear scar when the debris layer thickness is increased. At this stage, the effect of the boundary layer reduces the scar width and depth by 5% and 15% respectively.

Later on in the process, this paper finds that the debris layer has the opposite effect and increases the amount of wear on the specimen.

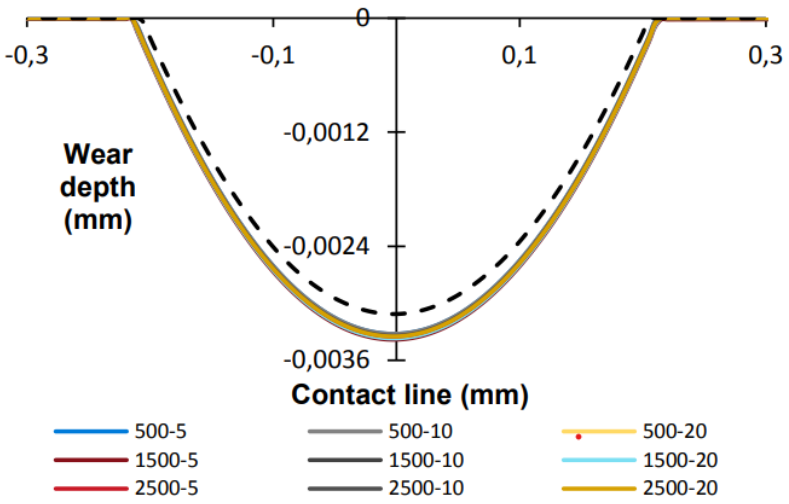

Figure 27: Wear Scar After 18,000 Cycles with Debris Layer Thickness of 5 µm, 10 µm, 20 µm

As illustrated in Figure 27, the models which include a debris layer have a larger scar width and depth of 10% and 13.6% respectively. The thickness of the debris layer still has very little impact on the overall wear. The reason for this reversal in effect as the number of cycles increases could be explained by the following. In the running in stages, the debris layer acts as a protective layer and reduces the amount of damage caused by fretting. However, as the number of cycles increases, the wear volume on the debris layer model develops faster due to the larger contact area.

In another study, by J. Ding *et al.* [40], it was concluded that the debris layer caused a smaller scar width and only a slightly deeper scar depth. This shows that the problem of the debris layer is a complex one and should be an area of future research. Despite this, both studies found that the differences when including the debris layer to the simulation only made a slight difference to the final wear scar. For this reason, a debris model will not be included in the following work.

2.6 Water Tree

Water treeing is a degradation mechanism present in the insulation layer of subsea marine dynamic cables, as shown below in Figure 28. Dendritic pathways, known as water trees, emerge within the insulation layers of XLPE in marine dynamic cables as a result of exposure to mechanical stress, electrical stress and immersion in water. A frequent method in which water ingresses into the polyethylene is during the steam curing process employed to create the crosslinked structure of XLPE [9]. Also, throughout the installation and operational phases the sheath of XLPE cables may incur damage due to the impacts of chemical erosion and mechanical stresses. Consequently, moisture may penetrate the insulation layer, initiating the formation of water trees [41]. Water trees are a structurally critical phenomenon since they are incredibly hard to detect, leading to premature failure and consequent service life of a subsea cable. Young [10] estimates the existence of water trees can decrease a cables service life by five-fold, from 25 years to approximately 5 years.

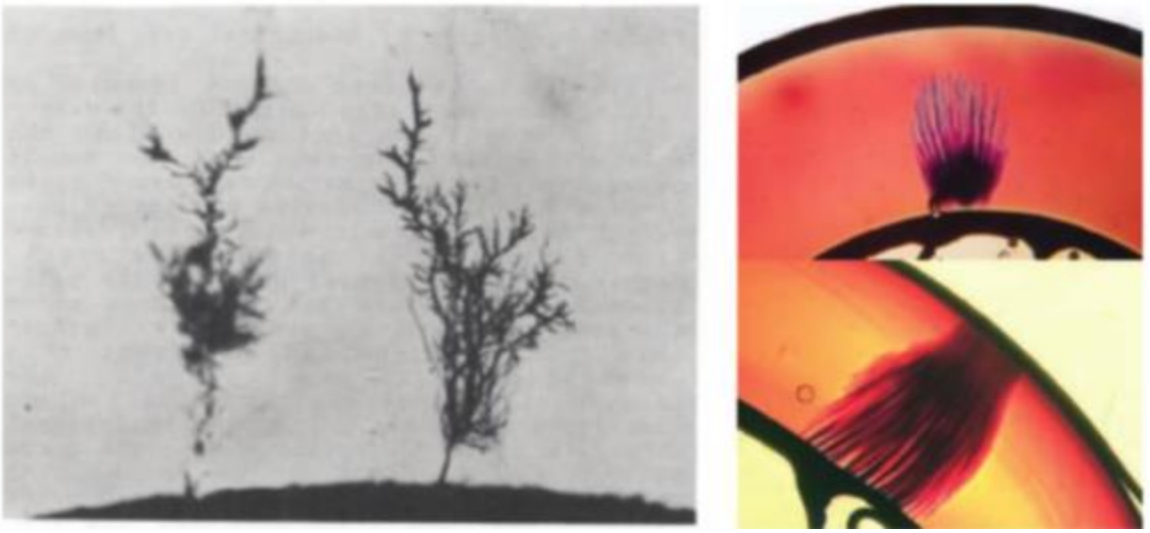

Figure 28: Water Tree Present in XLPE Insulation

2.6.1 Water Tree Geometry

In the early 1960s, XLPE insulation cables were introduced for 3-6 kV applications. Subsequently, during the 1980s, the use of XLPE insulation expanded to cover voltage ranges of 11-33 kV. In recent years, there has been further extension, with XLPE insulation being employed for voltages as high as 275-500 kV. This is due to the fact XLPE insulation significantly outperforms the majority of other insulation materials in terms of electrical, thermal, and mechanical properties. One major factor leading to cable system failures is the deterioration of the XLPE electrical insulation. Operational stresses experienced by cable insulation, such as mechanical, thermal, and electrical effects, fluctuate over time and can induce degradation through consequential physical and chemical alterations in cable properties. These alterations lead to the generation of partial discharges at the areas of degradation, partial discharges are minor electrical discharges occurring as a result of localised intensification of electrical stress at the defect. The discharge within the XLPE insulation is due to the high electric fields produced, triggered by the presence of defects or voids. Water treeing is linked to these discharges and occur at the tips of a void within the insulating material [42].

When characterising water trees, they can commonly be separated into two distinct classifications: vented water trees and bow-tie water trees. Vented water trees are specified as those which are present at the boundary between two materials from an initial defect existing. In the context of subsea dynamic cables, vented water trees initiate at the edges of the XLPE insulation layer, where they can develop at the conductor-insulator medium and propagate through the thickness of the insulator. Similarly, they can occur at the outer interface of the XLPE insulator and propagate towards the inner core of the wire. [43] state water trees which initiate at the conductor-insulator medium are defects created from manufacturing whereas vented trees present at the XLPE insulator outer surface are related to external damage and age. Hence, for older marine dynamic cables this is the predominant water tree form. Contrary to vented trees, bow-tie water trees grow within the XLPE layer due to impurities and grow in unsystematic directions throughout the XLPE insulator. Figure 29 highlights a pictorial representation of vented and bow-tie water trees present in a cable's insulation cross-section.

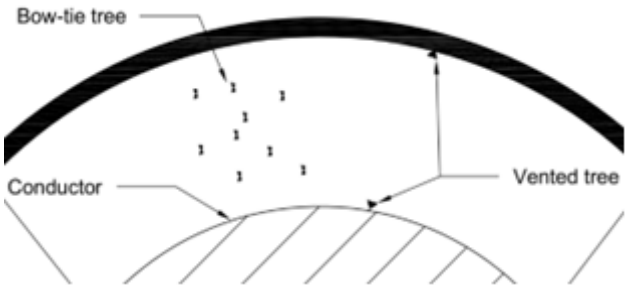

Figure 29: Vented & Bow-tie Water Trees

Radu et al [44] describe the dangers of water tree defects increase as they grow in size. Not only due to their size but also because of the increase in average permittivity. Radu et al [44] state this is significantly more marked by vented water trees making them the structurally critical water tree geometry. J. Ringbergs et al [45] define a critical vented water tree length of 60% of insulator thickness, beyond 60% of insulator thickness the specimen is categorised as having failed. Therefore, the vented water tree is integral to the structural integrity of the XLPE insulator and will be used as the geometry for this project.

Dielectric breakdown of the cable related to water tree growth is more intricately connected to the length of a water tree crack than the density of water treeing within the insulation. The formation of bow-tie water tree within the insulating material is attributed to impurities and following their initiation they expand bidirectionally until they reach 60% of the insulator thickness. Both vented and bow-tie water trees are categorised as electric trees once their length reaches the 60% mark and critical rupture occurs [9]. This stage of the water tree growth is out with the scope of this investigation with the propagation stage being the primary focus.

The configuration of the water tree is influenced by various factors, including the applied voltage of the marine cable, the voltage frequency water content and electrical stress. All of the factors culminate together and give the water tree crack a string and pearl structure as shown in Figure 30. This geometry consists of micro voids that are linked together by micro channels, Figure 31 depicts two micro voids connected by a channel [9]. Figure 31 gives

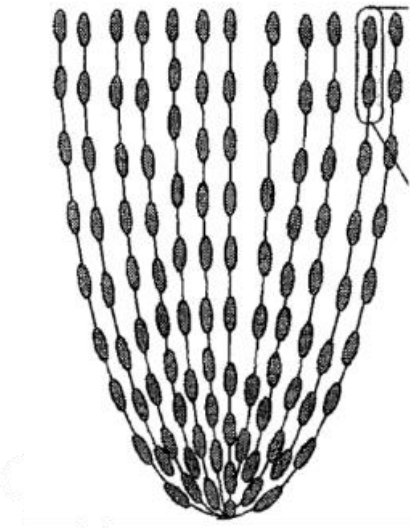

Figure 30: String and Pearl Geometry

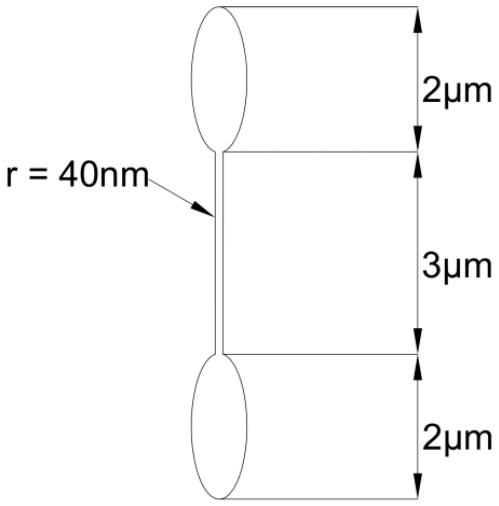

Figure 31: Micro-voids Connected to Channel

dimensions of the micro voids, however micro void lengths can range from 0.1µm to 5µm [46].

The growth of water trees is primarily influenced by the strength of the electric field at the water tree branch tips, with a more robust electrical field leading to the extension of tree branches. When a high enough voltage is applied the electrical field produced induces micro-jets, propelling water droplets within the void. These micro-jets have the potential to initiate the propagation of the water tree as they open up channels, enabling deeper penetration of water into the insulation [10]. This is shown in Figure 32.

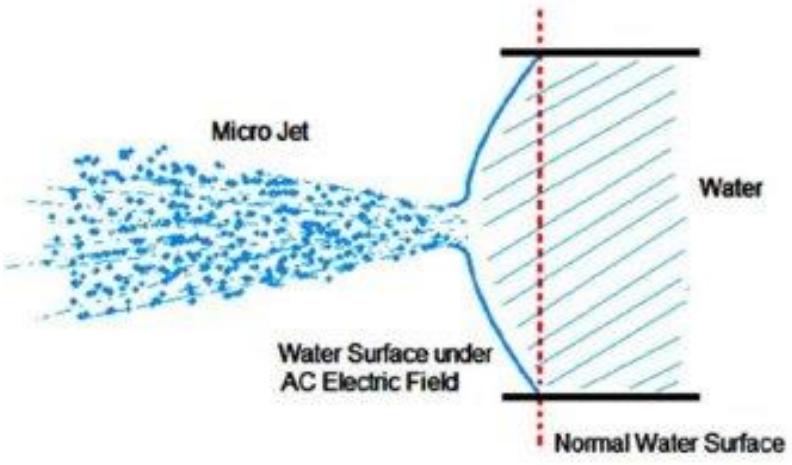

Figure 32: Water Tree Micro Jets

2.6.2 Stages of Water Tree Growth

The initial stage of water tree growth in known as the initiation, this stage begins with the development of micro voids within the XLPE insulation layer. Water ingresses into the polyethylene during the steam curing process causing these voids to appear, they are also created during the installation process of the cables. This stage of water tree growth is out with the scope of this investigation.

The second stage of water tree growth is the propagation of the water tree crack. In this stage the crack will propagate due to the mechanical and electrical stresses acting on the water tree crack. The mechanical stresses occur due to the harsh dynamic working environment the cable operates within, and the electrical stresses occur due to the electrical current that flows through the cable. The propagation stage will be studied throughout this investigation.

Critical failure is the final stage of water tree growth. This stage occurs once the water tree crack has reached a length at which it can no longer sustain the mechanical and electrical stresses. Again, this stage is out with the scope of the investigation as it has been deemed appropriate to study the crack until 60% of the thickness has been reached [47].

2.7 Water Tree Propagation

The most current and up to date research on water tree development suggests that water tree propagation is mainly facilitated by the presence of mechanical and electrical stresses generated in the operating environment [9].

2.7.1 Mechanical Stresses

During the lifespan of the cable, it is subject to various loading conditions as a direct result of sea state conditions. A. Abideeen et al [48] state there is a considerable connection between static axial tensile loading and the growth of water trees. E. IIdstad et al [49] discovered axial tensile strains enhances the growth of water trees, believed because they increase the

magnitude of elongated micro voids in the XLPE insulation. E. IIdstad et al [49] unearthed the opposite for compressive strains, acknowledging they retard the propagation of vented water trees. Figure 33 demonstrates a cross section representation of the cable and how it would experience tension and compression.

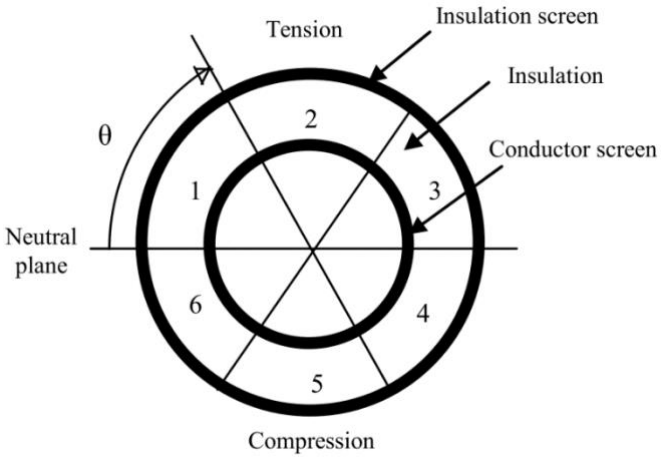

Figure 33: Tension & Compression in Cable Cross Section

Consequently, the analysis within this body of work will neglect compressive strains and stresses, only focussing on tensile interactions. Additionally, H. Bardsen [50] state a water tree crack will not propagate unless the crack tip is stressed in a tensile manor. Consequently, despite the cable experiencing an array of stress states, e.g. axial and bending, only axial tensile stress will be investigated in this body of work because it is classed as the dominant stress. Young [10] and Bardsen [50] conclude that the majority of vented water trees initiate in the mechanically stressed zones of the XLPE insulation, suggesting mechanical stress is vital for the initiation of water trees but not as influential in their propagation.

2.7.2 Electrical Stresses

Extensive investigations into potential mechanisms underlying water tree growth found that the growth of water trees is predominantly influenced by the strength of the electric field within the XLPE insulation. The current flowing through the conductor wires produces this electric field, however, when a micro void or water tree is present there is an alteration of the electric field distribution throughout the cross-section of the XLPE insulation. The concentration of the electric field is observable at the tip of the water tree crack or micro void, especially the area nearest to the conductor [10]. The electric field at the boundary between the crack tip and insulation will intensify as the water tree crack propagates. This intensification results in the polymer chains breaking down and the subsequent formation of a microstructure of cracks. These microstructures, filled with moisture, gradually increase in length drawing closer to the cable's conductor. In the case of the vented water trees originating from the outer surface of the insulation, which are being investigated, the rate of water tree growth escalates as the crack grows in length [45]. It is important to know that there is no overall electric field present within the void of the water tree.

When subjected to the electric field, water molecules within the void, undergo micro-jets propulsion. In an AC system, the water molecules align their dipoles in sync with the voltage frequency, resulting in continuous rotation and propulsion upon the XLPE insulation. This motion imparts a force upon the polymer chains of the XLPE. This provides insight into the

correlation between elevating the frequency of the marine dynamic cable and the increase in crack length. Also, when subjected to the alternating electric field, the XLPE material experiences a Maxwell stress at the tip of the crack, resulting in the fracture of molecular chains. When this Maxwell force occurs the XLPE insulation will be subjected to cyclic mechanical stress as the cable is an AC system. At present, it remains uncertain whether the increase in water tree length is attributed to water micro-jetting or the induced Maxwell stress. The extent of water micro-jetting has not been taken into account, nevertheless, it is anticipated to be addressed in future studies[10]

Vulnerable points within the XLPE polymer chain are potential sites at which alternating Maxwell stress can induce rupture or fracture, as shown in Figure 34**.**

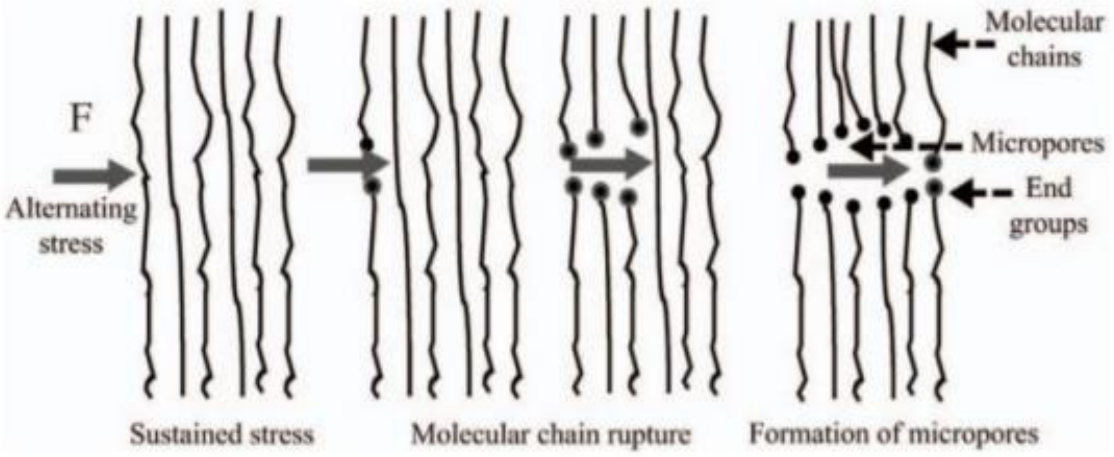

Figure 34: Maxwell Stress within XLPE Polymer Chains

While advancing toward the cable core, the Maxwell stress value at the water tree crack tip will increase. The Maxwell stress value can be calculated using Equation 14 which demonstrates why electric field value is a dominating factor in water tree growth [10].

$$F = \frac{\varepsilon_0}{2}(\varepsilon_r - 1)E^2 \qquad (14)$$

Where ε_0 is the permittivity in a vacuum (Fm^{-1}), F is the Maxwell stress (Pa), E is the electric field strength (Vm^{-1}) and ε_r is the relative permittivity of XLPE (Fm^{-1}).

The Maxwell forces at the tips of the void tips induce plastic deformation, ultimately resulting in the creation of channels between the micro voids[51]. Figure 35 illustrates the overall phenomenon.

STEP 1:

- Water molecules enter into voids because of humidity
- Electric field influences voids present inside the insulator.

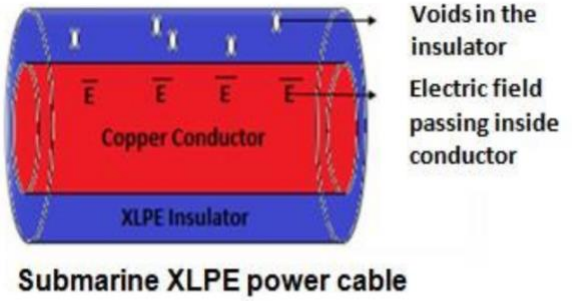

Submarine XLPE power cable

STEP 2:

- Electric field causes plastic deformation Of voids
- Relative distance between voids influences Plastic deformation

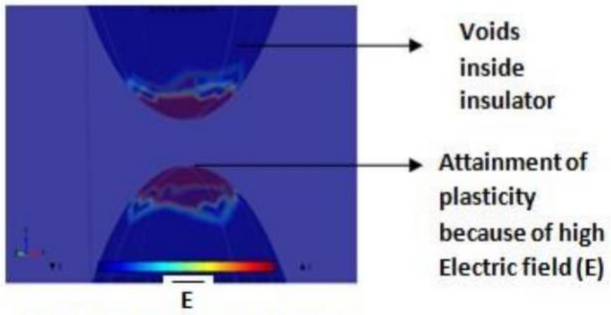

Magnified image of voids

STEP 3:

- Formation of channel between voids
- Voids merge with each other forming a Water tree

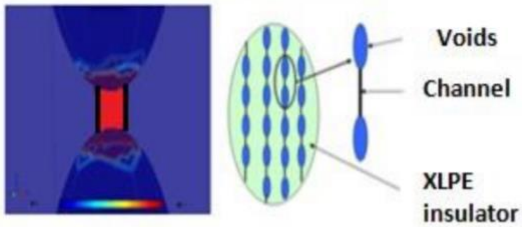

Channels interconnecting Voids

STEP 4 :

- Propagation of water tree towards the conductor
- Corrosion of conductor
- Degradation of cable

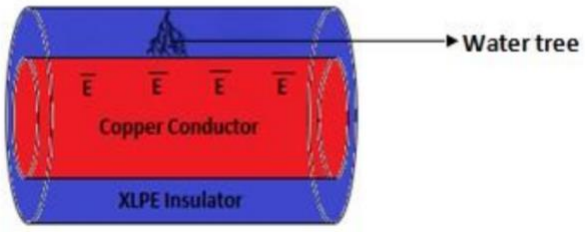

Water tree growing towards conductor

Figure 35: Water Tree Phenomenon Process

2.8 Water Tree Fatigue

This section describes the approaches that can be taken to determine the fatigue life of a marine dynamic cable due to water treeing.

2.8.1 Linear Elastic Fracture Mechanics

Regarding many structural components, the thickness of such component is commonly considerably smaller than any in-plane characteristic dimension. The consequence of this scenario is when a specimen is subject to a multitude of loading conditions, the 3D stress state it experiences is generally significantly small in relation to the overall volume of the component. However, when a geometric discontinuity is involved, in this case a crack, the stress concentrations at this region are critical and commonly initiate failure.

When investigating the influence of cracks in the structural integrity of engineering components, fracture mechanics is the predominant approach. Fracture mechanics acknowledges the presence of cracks, moreover, it facilitates the safe operation of flawed structural components up to some critical defect size. Fracture mechanics analysis incorporates both static and cyclic loading to investigate the potential failure of a component. Static loading can be uniaxial or multiaxial but remains consistent and does not change as a function of time. On the contrary, cyclic loading is the application of repeated or alternating mechanical loads, where the loading conditions can have constant or fluctuating amplitudes. Crack growth due to cyclic loading is called ‘fatigue crack growth’ and can cause a structure to fail once the crack grows to a critical size.

Linear elastic fracture mechanics (LEFM) is the bedrock of fracture mechanics. The theory is built upon the understanding of an extremely localised infinite stress concentration at the tip of the crack. However, no structure can endure infinite stress without plastic deformation occurring. Therefore, LEFM assumes the plastic zone where the stress concentration originates is essentially a singularity. Such assumption is anchored on the belief that this plastic zone is significantly smaller than the volume of the structural component, owing to the structure respectively [52].

George Irwin [53] concluded that the stress concentration patterns extremely close to the crack tip are identical for all discontinuity shapes, with the exception of one condition. The condition being the applied load must have the same orientation relative to the crack plane. Irwin established a classification for load orientations which he referred to as ‘modes’. Figure 36 depicts the three most common fracture modes. Mode I, opening mode, resembles when the stress field is symmetric with respect to the crack plane. In this case there is no shear and slip throughout the displacement or along the face of the crack. This project deems axial tensile stress the dominant stressor, hence, Mode I is the only investigated mode.

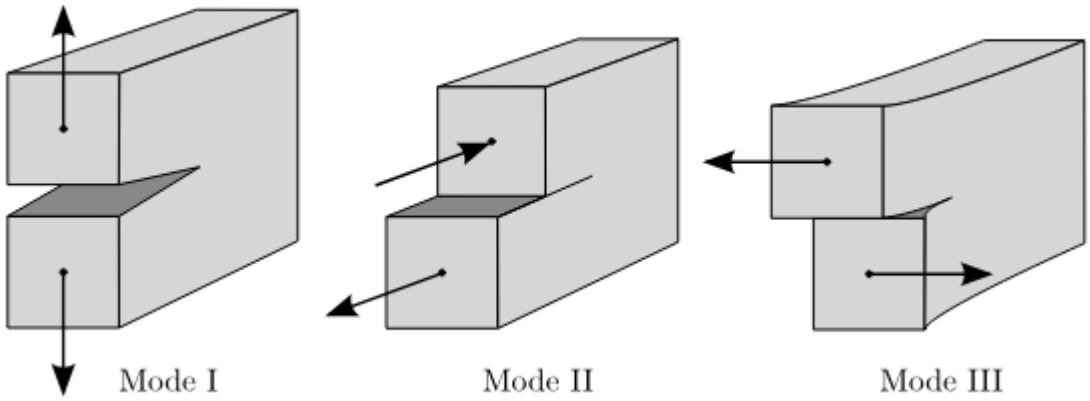

Figure 36: Fracture Modes

[54] Factor, K, and the remotely applied stress, σ, for a Model I crack. The relationship in its simplest term can be represented by Equation 15.

$$K = Y\sigma\sqrt{\pi a}$$

(15)

Where, Y, is a configuration factor for the geometry. For most crack geometries the value of Y can be looked up or calculated from technical handbooks.

A crack present within a structure will not grow under an applied load until the stress concentration, intensity, at the crack tip reaches a specific threshold value. This value is known as the threshold stress intensity and is denoted as Kth in Equation 16.

$$K \geq K_{th}$$

(16)

Beyond the threshold stress intensity, a crack can exist and propagate in a stable manner without occurring failure. From Figure 37, region 2 refers to the region when the value of Kth is met and then exceeded. During this region LEFM is applicable, enabling the application of the Paris Law. Based on LEFM theory, Paris et al [55] devised a solution to utilise Irwin's stress intensity factor to symbolise the rate of crack growth per load cycle. The Paris Law is only valid for uniaxial loading and LEFM conditions. Equation 17 depicts the Paris Law equation.

$$\frac{da}{dN} = C(\Delta K)^m$$

(17)

Where,

$$\Delta K = K_{max} - K_{min}$$

Where, C and m are material constants that can be determined experimentally, $\frac{da}{dN}$ is the crack growth rate per load cycle, and ΔK is the change in SIF.

A crack will grow stably until the fracture toughness, KIc, of the material is met. Once K = KIc, LEFM and the Paris Law are no longer applicable. On Figure 37, KIc refers to region 3. Beyond such critical quantity, the crack will grow unstably and hence failure will occur.

2.8.2 Elastic Plastic Fracture Mechanics

When the stress intensity factor is applied to long fatigue crack propagation in the high cycle regime the following figure is applicable, denoting a crack propagation rate – cyclic stress intensity factor curve.

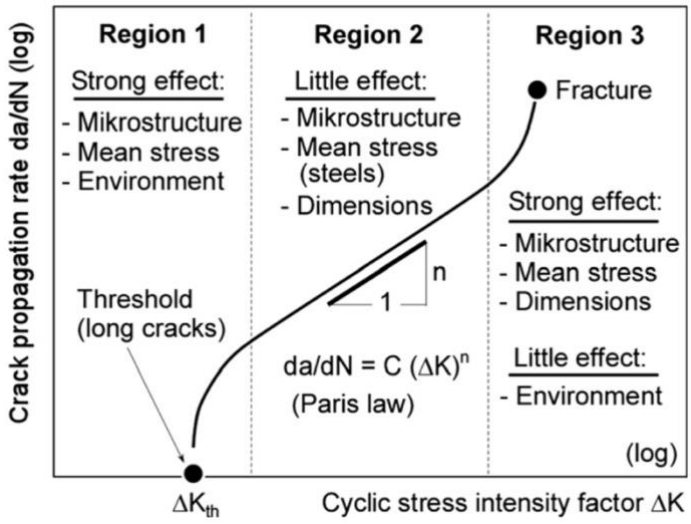

Figure 37: Crack Growth Regions

[56]The issue is when dealing with short cracks and the concept of ΔK is applied, it is found that the cracks will still grow at ΔK values less than ΔK_{th}. In other words, the long crack curve $\frac{da}{dN} - \Delta K$ cannot be used to describe short crack propagation. This is because the assumption of small-scale yielding cannot be applied to short cracks. The reason for this is the plastic zone encompassing the crack tip will be a greater portion of the overall crack length when compared to long cracks. Consequently, although the crack tip does not yield entirely, elastic-plastic fracture mechanics (EPFM) may have to be employed.

The validity of EPFM when dealing with short crack theory is bolstered when the defect is present is Polymers. Polymers are extremely complex materials that exhibit a wide range of stress-strain behaviours [57].

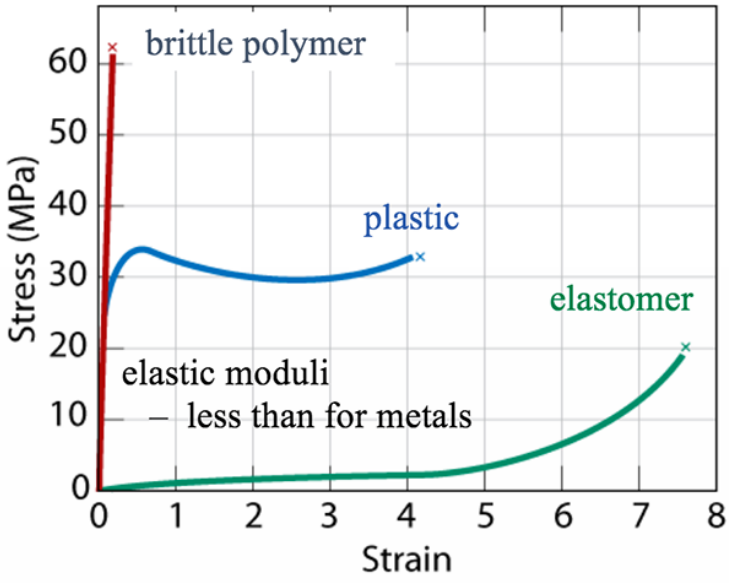

Figure 38: Stress vs Strain for Varying Materials

The brittle polymer denoted by the red curve in Figure 38, will experience considerable elastic deformation and fracture before the onset of plastic deformation. The blue curve highlights a plastic polymer with a recognizable curve that somewhat mimics a metal whilst the green curve illustrates a hyperelastic polymer that will behave wholly elastic until the material reaches its fracture toughness. If a polymer is subject to low temperature and high strain rates the material is likely to behave linear elasticity and become more brittle, making the argument for LEFM commendable. However, such operating parameters are not absolute, necessitating the argument for additional fracture mechanics analysis for polymers.

When implementing EPFM for fatigue analysis the predominant approach is the cyclic J-Integral concept. The J-Integral first proposed by J.R. Rice [58] is the most prominent crack tip parameter to define the stress strain field intensity in the crack tip deformation zone. For elastic plastic material behaviour, the J-Integral corresponds to the energy release rate within the crack. In the realms of this project, for two-dimensional plane problems, the J-integral is path independent. For cyclic loading, Rice proposed the cyclic J-Integral as a suitable variable of crack driving force to depict fatigue crack growth.

2.8.3 Kinetic Theory of Fatigue

Using the kinetic theory of fatigue, the assumption is made that the propagation of water trees under electrical stresses is driven by the breakdown of interatomic bonds due to electric field energy, ultimately resulting in polymer fracture. Kinetic theory of fracture states that the breaking of a polymer monomer chain requires the accumulation of electric energy over multiple cycles [45]. In the context of the kinetic theory, fracture is viewed as a progressive process evolving within a body under loading, rather than an event triggered when a critical stress is reached. In the case of a polymer such as XLPE, the bonds are both intermolecular and chemical connections. The successive rupture of the bonds results in the eventual macroscopic failure of the insulation, it is also the reason water tree cracks form their string and pearl geometry [10].

Under the assumption that a single cycle of electrical stress corresponds to one unit of energy accumulation, the cumulative energy over multiple cycles may surpass the yield strength of XLPE required for the breaking of the monomer chain. W defines the energy accumulation as shown in Equation 18:

$$W = 0.5V_0\varepsilon_0(\varepsilon_r - 1)E^2$$

(18)

Equation 18 resembles the Maxwell stress equation in section 2.7.2, except V_0 has been integrated into the equation. V_0 represents the volume of the insulation material where the energy imparted by the electrical stress is accumulated. [45]

The diameter of a polymer monomer is required to calculate the rate at which crack propagation occurs. The diameter of a XLPE polymer monomer is considered to be 3.9×10^{-10} m. Compared to typical chemical bonds this is marginally larger due to the cross-linking of the polymer chains. [10]

Equation 19 below is the energy accumulation equation:

$$0.5V_0\varepsilon_0(\varepsilon_r - 1)E^2 > \sigma_{yield}V_0$$

(19)

Where σ_{yield} is the yield strength of XLPE (Pa).

This equation can be used to determine how many cycles are needed for a monomer chain to be broken. After one cycle's energy accumulation is calculated, the number of cycles necessary to break a monomer chain can be determined utilising the yield strength of XLPE. Therefore, since the frequency of the cable and diameter of a polymer is known, the crack growth rate and ultimately the service of the marine dynamic cable can be calculated due to electrical stress [9].

3 Methodology

This section outlines the different methodologies utilised in this project to study the structural integrity of subsea dynamic cables. Each section outlines the approach utilised to arrive at the final results gained in this thesis. In this thesis, there are four independent multiscale and multi-physics approaches that analyse the cable to best capture the full behaviour.

3.1 Global Model

The overall purpose of the global analysis phase is to model the entire system – encompassing the WEC, mooring lines and cable – on a global scale. This approach aims to capture the complete behaviour of the system and its impact on the power cable. The primary aim of this analysis is to identify critical regions along the length of the dynamic power cable across the selected sea states.

To conduct a thorough global analysis of the dynamic power cable, SIMA and MATLAB were used in conjunction to ensure an accurate and comprehensive representation of the cable's behaviour. The global analysis results are subsequently integrated into the local modelling phase to provide a more accurate representation of the fatigue life of the cable.

3.1.1 SIMA Global Model

SIMA is a "simulation and analysis tool for marine operation and floating systems" [59]. SIMA enabled a complete 3D depiction of the WEC, mooring lines and power cable. In addition to this, it allowed for different environments to be implemented to offer a better representation of the conditions that could be experienced. Figure 39 illustrates the approach used in the global analysis:

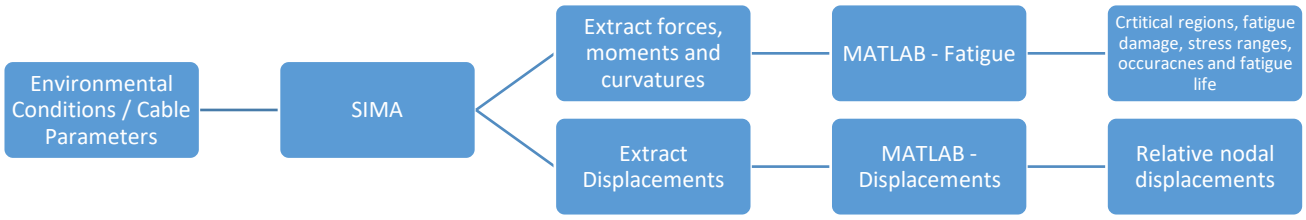

Figure 39: Global Analysis Flowchart

3.1.2 Environmental Conditions

The initial step in the global analysis is to select environmental conditions that accurately capture the potential sea-states that take place at Runde. For this thesis, three potential sea-states were selected: a calm sea-state, a very probable sea-state and a harsh sea-state. A

diverse spectrum of sea-states enables a more robust comparison and increased overall accuracy. Table 6 displays specific sea-states chosen for analysis.

Table 6: Sea States

	Wave Height, Hs [m]	Wave Period [m]	Wave Direction [∘]	Current velocity [m/s]	Wind velocity [m/s]	Wave Gamma Factor, γ	Simulation Time (s)
Case 1	0.5	4.5	0	0	0	3.3	1200
Case 2	2.5	6.5	0	0	0	3.3	1200
Case 3	5.5	8.5	0	0	0	3.3	1200

The above chosen sea-states aim to encompass a range of highly probable environments to extreme conditions and were derived from the wave scatter diagram from Runde in Figure 12. Case 1 represents a notably calm sea-state, with a probability of 6.84%. Case 2 portrays a highly probable sea-state, standing at an 8.77% likelihood. Case 3 depicts an extreme condition, registering a probability of 3.37%. It's noteworthy that wind and current factors were omitted in this study to streamline computational processes and minimise complexity. The wave direction is also kept constant and can be visualised in Figure 40.

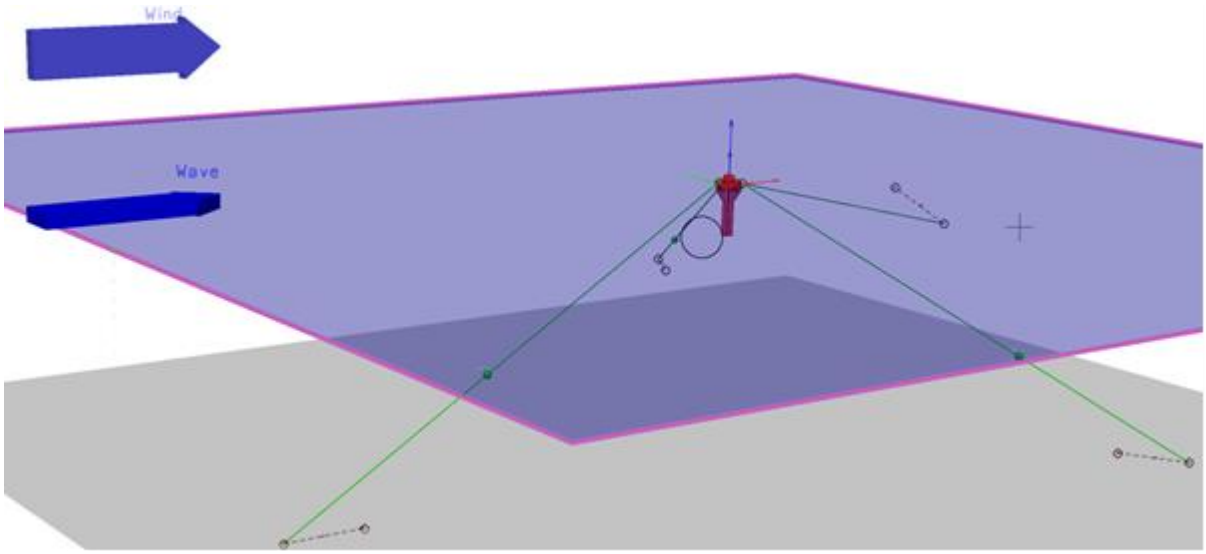

Figure 40: Wave Direction Illustration

The wave gamma factor remains constant for all three state states and is a major part of the JONSWAP spectrum. The JONSWAP (Joint North Sea Wave Project) spectra is a mathematical model used in oceanography and marine engineering to best describe the distribution of wave energy in the ocean. For this thesis, the JONSWAP – 3 parameter is utilised which contains three primary parameters. Significant wave height, Hs, Peak wave period, Tp, and the Wave Gamma Factor, Υ. The Wave Gamma Factor plays an important role in the shaping of wave energy across different wave frequencies [2]. The JONSWAP – 3 parameter is enabled in SIMA to better represent the irregular waves found in Runde. A wave

gamma factor of 3.3 is a typical value used to represent open sea conditions, similar to the ones found in Runde.

3.1.3 3D SIMA Model

The 3D model under examination in this thesis is a combination of two previous models. This ultimate model comprises of a 1kV dynamic power cable and a WEC (designed for Runde) and its respective mooring lines. Figure 41 highlights the approach used in SIMA to model the system.

Figure 41: Approach used in the 3D SIMA Model

Once the environmental conditions and cable / mooring lines parameters had been carefully selected, it was then imperative to check that the WEC and cables were behaving correctly. To achieve this, regular wave conditions were integrated to observe the motions of the WEC, cable and mooring lines, ensuring they exhibited consistent sinusoidal behaviour. Once verified, the irregular JONSWAP – 3 environmental conditions were applied. Figure 40 illustrates a comprehensive overview of the entire system highlighting all components. Within this illustration, it is evident that mooring anchors are not solely situated on the seabed (86.6m below sea level). They are positioned at specific depths: -86.6m, -66.6m and -54.1m, aligning with the geographical features found at Runde [18].

Following this, boundary conditions were applied to the system to increase accuracy. All mooring line anchors were spatially fixed in their predefined location. The end of the power cable (furthest from the WEC) was also spatially fixed to represent how it would be attached to the fixed hub at Runde. The beginning of the cable (close to the WEC) has a super node in which acted as a slave to a fixed point on the WEC, this ensured the cable followed the WECs motions. The above cases outlined in Table 6 were simulated over a duration of 1200s, each with their respective properties. This timeframe was selected to effectively capture the predominant behaviour of the power cable while optimising the computational process.

3.1.4 MATLAB Fatigue Assessment

Once all cases were simulated, post-processing could begin in MATLAB. The purpose of this post-processing is to identify critical regions along the cable to allow for a smaller scale analysis. To do so, the MATLAB code utilised a combination of theories to arrive at an accumulated fatigue damage of each element of the cable. A brief description of the code is presented below (the full scripts are shown in Appendix A):

- The first script 'Parameter_input.m' is where the important parameters of the system are inputted *e.g.,* cable diameter, simulation time/time step and ramp up periods. This script calls in the 'WAFO' toolbox (rain flow counting system) along with the other main scripts.
- The second script 'main_program_read.m' reads the dynamic elmfor.bin (element forces) file that is extracted directly from SIMA.
- The third script 'main_program_calculation.m' is where the main calculations take place. This script calculates the stress ranges and fatigue damage for each time step and for each of the 12 hotspots on the cross-section. Through the use of damage accumulation laws, the MATLAB code is able to calculate a predicted fatigue life through the length of the cable.
- The fourth script 'main_program_output_save.m' saves and displays the numerical results. These results include the maximum stress ranges, stress amplitudes, fatigue damage. The location along cable length, location on cross section and times of where these maxima occur is also identified.
- The fifth script 'main_program_figure' plots all results in a more user-friendly manner and allows for trends to be easily identified.

3.1.5 MATLAB Relative Displacements

In order to achieve displacements that could be integrated into a local FEA model, the displacements outputted in SIMA had to be converted into relative nodal displacements. The displacements in SIMA are essentially global positional displacement for each node along the cable's length for the entire time series. To apply beam theory, relative displacements for neighbouring nodes had to be calculated.

In this analysis, since the SIMA model only records every third element/node, to streamline the computational process, the beam is made up of three elements. In the 3D global model, Segment 8 (main portion of the power cable) was divided up into 184 elements each having a length of 0.7m. As a result of only recording every third element, the neighbouring nodes in this instance are 2.1m apart.

A brief description of the MATLAB displacement code is given below (the full script is shown in appendix B):

- The global displacement are extracted directly from SIMA and converted into an array in MATLAB for all x,y and z-axis displacements. This was completed for nodes 1 and 4 and nodes 91 and 94 for all three cases as these were areas of interest. nodes 1 and 4 lie at the beginning of segment 8 (near the WEC) nodes 91 and 94 are found at the centre of segment 8 (middle of the dynamic cable).
- Since the neighbouring nodes have an initial distance that they are separated, this need to be accounted for. In order to do this, the difference in displacements at the first-time step was calculated. This initial separation is highlighted in Figure 42.

- Once this distance was calculated, this distance was implemented, and the relative displacements could then be calculated for all time steps.
- The total displacement was calculated for the entire time series and the mean total displacement was found. Examining the plot, time steps that aligned with the mean total displacement were pinpointed. Using this same time step, the new relative displacements were accessed and the respective displacement for that specified time step was noted.
- These relative displacements were scaled respectively and utilised in the local FEA model.

Figure 42 illustrates the initial displacement between the neighbouring nodes:

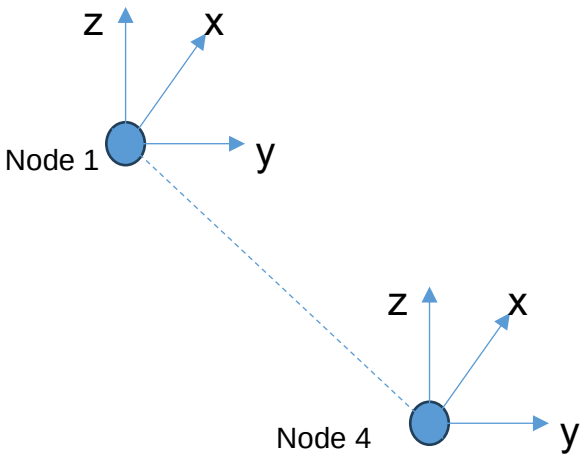

Figure 42: An example illustrating the initial distance the nodes are separated.

The dotted line in Figure 42 is the 'Total Displacement', this displacement does not get used in calculations however is the basis of gaining the relative x,y and z-axis displacements for both sets of nodes.

A total-displacement graph has been illustrated in figure 43 for Case 2 nodes 91 and 94 to better understand the process involved:

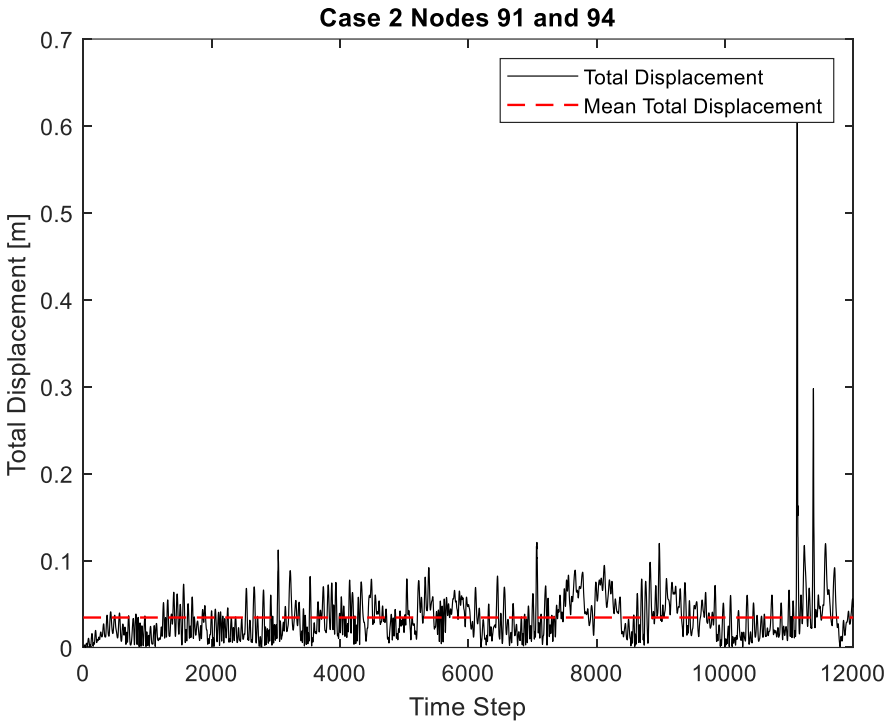

Figure 43: Case 2 Total Relative Displacement Nodes 91 and 94

For this specific case, it was found that time step 1282 lay on the mean total displacement and hence is now the governing time step to gain access to the relative x,y and z-axis displacements. Figure 44 illustrates the relative x,y and z-axis displacements for the given time series for Case 2 nodes 91 and 94:

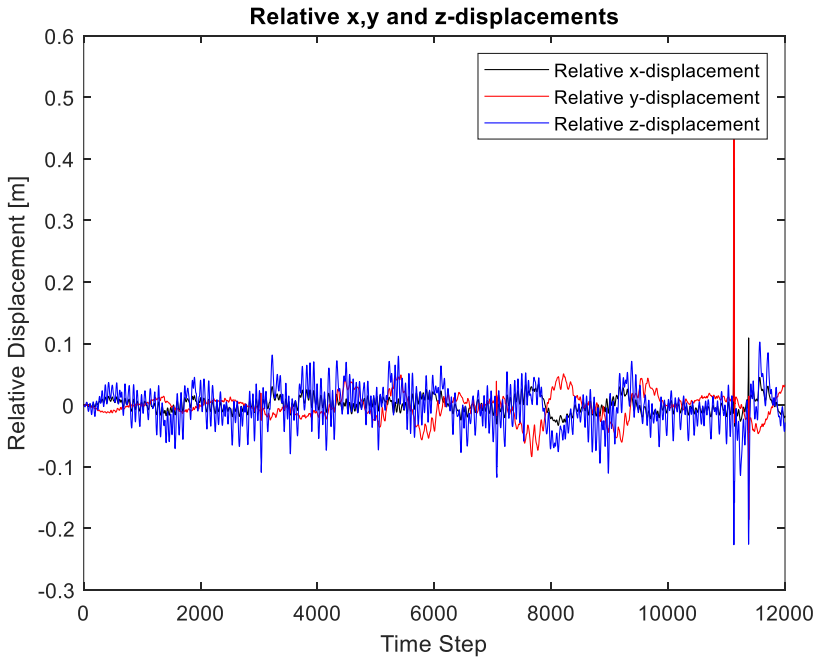

Figure 44: Relative Displacements vs Time Step for x,y and z-displacements

In MATLAB, indexing can then take place to extract the relative displacements for the respective time step chosen. The displacement is then scaled to match the elemental length used in the local model and then integrated into the local FEA model.

3.2 Fretting Model

3.2.1 Archard Wear Model

To capture the extent of the sliding wear damage due to the evolution of the stress and strain cycles, the Archard wear equation is used [38] and is given in Equation 20.

$$\frac{V}{S} = K\frac{P}{H} \tag{20}$$

Where V is the wear volume, S is the sliding distance, K is the wear coefficient, P is the normal load and H is the hardness of the material.

To apply the formula to a given point on one of the contact surfaces, the differential formula for the Archard Model is given as:

$$\frac{dh}{dS} = k_l p \tag{21}$$

Where h is the wear depth, k_l is the dimensional local wear coefficient and p is the contact pressure.

Using Equation 21, McColl *et al* [60] developed a numerical approach to simulate the fretting wear. For this method the contact geometry, pressure distribution and relative slip are calculated using FEA. However, to accurately capture the contact surface, it is essential to model the local wear depth at a given horizontal position, x, at every node of the model. This means that for an infinitesimally small contact area, dA, the change in wear depth, dh, is calculated caused by the appropriate sliding distance, dS. This allows the development of a new geometry of the model which has overgone fretting wear. The updated Archard equation used is shown in Equation 22:

$$dh = k_l p(x) dS \Delta N \tag{22}$$

The parameter ΔN or cycle jumps are introduced to improve computational efficiency. This assumes that the wear is constant over a small number of cycles rather than modelling each cycle explicitly.

The dimensional wear coefficient, k_l, can be expressed as $k_l = \frac{K}{H}$ or dimensionless wear coefficient divided by hardness. For metals, this value is in the range of 10^{-2} to 10^{-5}.

At the end of each time step, the wear at each node on the contact surface is determined and the node is displaced by this calculated amount perpendicular to the local surface. Through repeating this process for each increment, wear simulation is achieved.

The change in position of these nodes can be calculated using a subroutine built in Fortran called UMESHMOTION.

3.2.2 Fatigue Mechanics of Fretting

As fretting is a complex problem, it requires a more sophisticated method to analyse the fatigue than an S-N curve. To accurately model the fretting fatigue, multi-axial fatigue analysis must be used and additional parameters, not just stress and strain, must be considered.

A crucial parameter, used extensively in literature of fretting fatigue, is the Smith-Watson-Topper (SWT) fatigue damage parameter. This parameter is based on strain-life analysis which relates the total strain to fatigue life from the two strain-based fatigue equations [61]. For high cycle or stress-controlled fatigue where the dominant factor is the elastic strain or the stress level, the Basquin equation is used. This relationship is as follows:

$$\sigma_a = \sigma_f'(2N_f)^{b_f} \tag{23}$$

Where σ_a is the stress amplitude, σ_f' is the fatigue strength coefficient, b_f is the fatigue strength exponent and N_f is the cycles to failure.

For low cycle fatigue, the Coffin-Manson equation is utilised:

$$\varepsilon_p = \varepsilon_f'(2N_f)^{c_f} \tag{24}$$

Where ε_p is the independent plastic strain amplitude, ε_f' is the fatigue ductility coefficient and c_f is the fatigue ductility exponent.

In situations where both elastic (ε_e) and plastic (ε_p) strains play a significant role, the strain-life equation can be expressed as a sum of the previous two equations, Equation 23 and 24:

$$\varepsilon_a = \varepsilon_e + \varepsilon_p = \frac{\sigma_a}{E} + \varepsilon_p = \frac{\sigma_f'}{E}(2N_f)^{b_f} + \varepsilon_f'(2N_f)^{c_f} \tag{25}$$

The Smith-Watson-Topper parameter modifies the total cyclic strain amplitude to account for mean stress and is given by Equation 26 [62]:

$$SWT = \sigma_{max}\Delta\varepsilon_a = \frac{\sigma_f'^2}{E}(2N_f)^{2b_f} + \varepsilon_f'(2N_f)^{b_f+c_f} \tag{26}$$

Where σ_{max} is the maximum normal stress in a cycle and $\Delta\varepsilon_a$ is the normal cyclic strain range. The maximum normal stress and cyclic strain range are chosen as they represent the stress-strain conditions occurring at the critical plane.

Fatigue life predictions for multiaxial scenarios are generally more accurate when they consider the concept of the critical plane. This theory is based on the fact that cracks initiate and propagate on a specific plane of the material. First proposed by Findley *et al* [63], the critical plane was determined by maximising a linear combination of the shear stress amplitude and maximum value of normal stress. The critical plane can be calculated by applying the stress and strain transformation equations through a number of angles:

$$\sigma_{11}' = \frac{\sigma_{11} + \sigma_{22}}{2} + \frac{\sigma_{11} - \sigma_{22}}{2}\cos(2\theta) + \tau_{12}\sin(2\theta)$$

(27)

$$\varepsilon'_{11} = \frac{\varepsilon_{11} + \varepsilon_{22}}{2} + \frac{\varepsilon_{11} - \varepsilon_{22}}{2}\cos(2\theta) + \varepsilon_{12}\sin(2\theta)$$

(28)

Where σ_{11} and σ_{22} are the normal stresses and τ_{12} is the shear stress. σ'_{11}, is the new normal stress when transformed through an angle of θ. Likewise, ε_{11} and ε_{22} are the normal strains and ε_{12} which results in a new normal strain ε'_{11} when transformed by the angle θ. To calculate the cycles to failure, firstly one must maximize σ'_{11} over a cycle to find σ_{max}, then ε'_{11} must be maximised and minimised to find $\Delta\varepsilon_a$. Next, the angle θ which maximises the SWT parameter must be selected and the product of σ_{max} and $\Delta\varepsilon_a$ is found, which is the SWT parameter.

A flow chart, Figure 45, is provided below to show the steps involved in calculating the critical plane fatigue damage induced by the fretting wear.

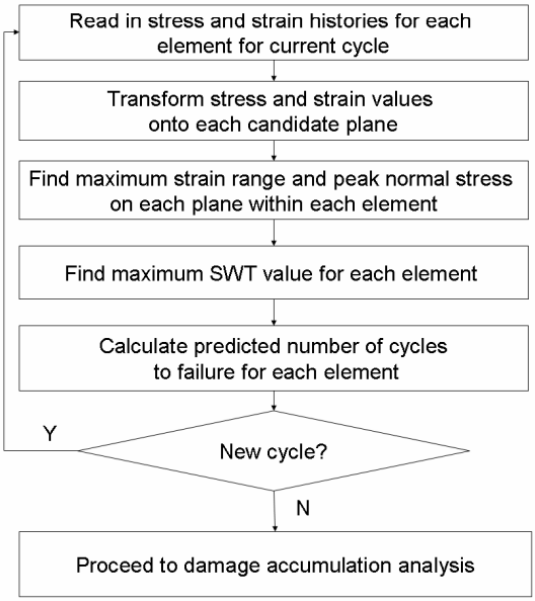

Figure 45: Critical Plane SWT Value Calculation Process Flowchart [38]

3.2.3 Damage Accumulation

After performing the critical plane fatigue damage, the fatigue damage at the specified elements is known for each cycle included in the wear simulation. However, as material is removed, the geometry changes and subsequently the stresses differ from one cycle to the next. The SWT value only provides a measure of the rate of fatigue for that point in time. Using only the SWT parameter to calculate the cycles until failure would not give an accurate result for this problem. Since the SWT is a function of the stress field, and the process of wear changes this field, a damage accumulation methodology needs to be utilised to predict fatigue life.

The linear Miner-Palmgren model was chosen to model the damage accumulation due to fretting. This is because it does not require any further material data than what is already provided for the SWT parameter. The Miner-Palmgren equation is given as:

$$D = \sum_{i=1}^{\frac{N}{\Delta N}} \frac{\Delta N}{N_{f,i}}$$

(29)

Where ΔN is the cycle jump, N is the current cycle and $N_{f,i}$ is the predicted failure at the i[th] step.

The formula works by summing the contribution of each cycle towards failure, which occurs when $D = 1$. This value can also be adjusted to include a factor of safety, however, a value of 1 is used in this study. In this version of the formula, the cycle jumps technique is included. This is done for the same reasons as previously stated, as it saves on computational time by assuming linearity over a small number of cycles. Despite this assumption, it still gives accurate results.

A methodology used to apply the accumulative damage law to the fretting problem was proposed by Cruzado *et al* [64]. First, the cyclic damage D is calculated (using Eq. 29) due to the initial fretting cycle at the centroid point Y_n of each element. Due to material being removed during each cycle, the damage at the centroid point of the first cycle will not remain constant as the centroid has moved to a new position, y_n. This paper, by Cruzado *et al,* assumes fretting only occurs in the first three layers of the mesh, so two equations are generated to show the damage evolution between the first and second layer then the second and third layer.

$$D_1(Y) = \frac{D_2 - D_1}{Y_2 - Y_1}(Y - Y_1) + D_1$$

(30)

$$D_2(Y) = \frac{D_3 - D_2}{Y_3 - Y_2}(Y - Y_2) + D_2$$

(31)

A more general set of equations can be produced to allow for an unknown number of layers by replacing the integer subscripts with variables (i.e. $i, j, i+1, j+1$).

The damage due to the second fretting cycle is determined at the new centroid location for each element. This is done by using the Miner-Palmgren law and is given as follows:

$$d_n = \frac{\Delta N}{N_{i,l+1,n}}$$

(32)

The damage from the first cycle is then interpolated to the new position at the new centroid location, y_n. This is done using equations 33, 34 and 35:

$$d_1' = \frac{D_2 - D_1}{Y_2 - Y_1}(y_1 - Y_1) + D_1$$

(33)

$$d_2' = \frac{D_3 - D_2}{Y_3 - Y_2}(y_2 - Y_2) + D_2$$

(34)

$$d'_3 = \frac{D_3 - D_2}{Y_3 - Y_2}(y_3 - Y_2) + D_2$$

(35)

The fretting damage from both the first (d'_n) and second cycle (d_n) is then accumulated by summing them together. This process is then repeated for the desired number of cycles or until the damage value equals 1.

The flowchart below, Figure 46, outlines the processes used within the fretting methodology:

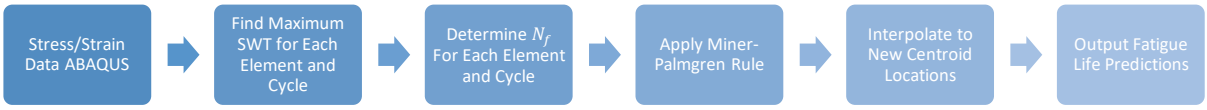

Figure 46: Fretting Theory Flowchart

First the stress and strain data is taken from Abaqus and used to find the maximum SWT for each element and cycle. Next the number of cycles until failure is calculated for each cycle and element. Then the Miner-Palmgren rule is applied, and damage data is interpolated to find new centroid locations. Once the damage value D=1 is reached the system has failed and the number of cycles is the fatigue life.

3.3 Mechanical Stress Models

This section illustrates the process into determining a fatigue life from mechanically stressed water trees. To analyse the crack growth of vented water trees through the XLPE insulation layer due to mechanical stress the theory of fracture mechanics was employed. Figure 47 highlights the methodology behind predicting a water tree fatigue life due to mechanical stress.

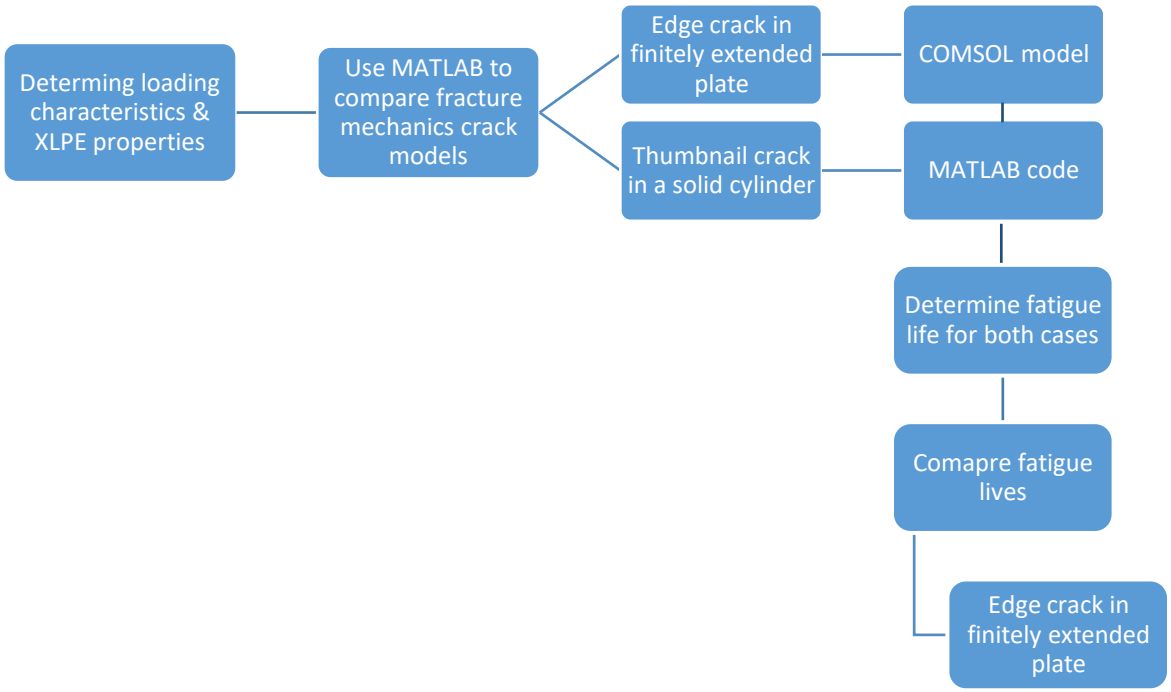

Figure 47: Mechanical Stress Flow Chart

Before utilizing COMSOL Multiphysics and MATLAB to conduct fracture mechanics analysis it was imperative to determine which crack case model would be most applicable in the investigation of vented water tree propagation. To reiterate the following assumptions have been made for the water tree propagation analysis.

- Only one vented water tree is present per cross section and is only capable of growing in one plane,
- Therefore, for computational efficiency, a 2D model is valid,
- Axial tensile stress is the critical axial stress. Compressive axial stress has a negligible effect on the structural integrity of the cable.
- Bending stresses can be examined, but alike compressive stresses, have no detrimental effect on the structural integrity of the cable.

Utilizing MATLAB, an in-house code was developed for five crack case models of varying geometric intricacy. The MATLAB code determines the minimum axial tensile and/or bending stress to cause crack propagation for a predetermined defect length. An Engineering Selection Matrix was created to determine the most applicable crack case model.

To conduct the analysis LEFM was assumed, and the Paris Law was employed. As previously mentioned in Section 2.8.1. Therefore, a threshold stress intensity factor, Kth, had to be predetermined. K_{th} is the minimum stress intensity factor required to cause propagation of a preexisting crack defect. Once this threshold value is met it is scientifically accurate to assume the material exhibits linear elastic behaviour and the Paris Law can be applied. Li et al [45] resourcefully defined material parameters for XLPE, including a threshold stress intensity factor Kth.

Table 7: Paris Law Co-efficients

Parameter	Symbol	Magnitude	Unit
Threshold Stress Intensity Factor	K_{th}	0.60	$MPa * m^{0.5}$
Fracture Toughness	K_{Ic}	3.94	$MPa * m^{0.5}$
Paris Law Co-efficient	m	3.63	
Paris Law Co-efficient	c	1.71e-4	

3.3.1 Case 1

The first crack case model considered for further analysis was the single edge crack in a finitely extended plate.

The case solely considers axial tensile stress. Additionally, the geometry is 2D with the crack depth considered to be negligible. Such geometry typically takes on the convectional form of a semi-infinite plate, depicted on the left in Figure 48.

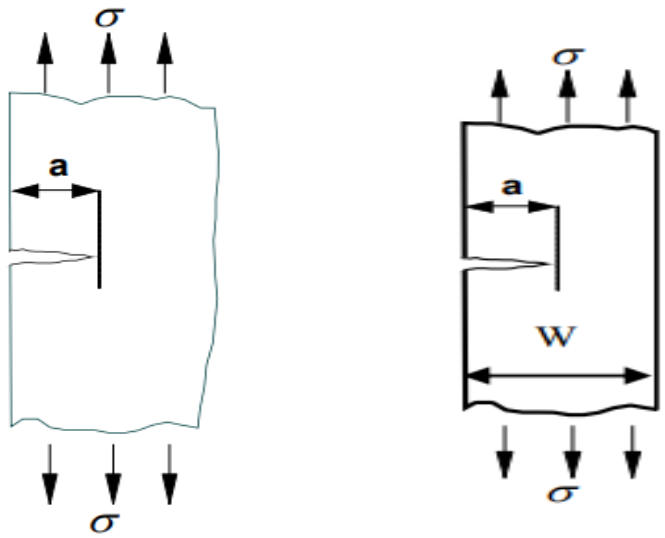

Figure 48: Edge Crack in Semi-Infinite Plate vs Finitely Extended Plate [74]

When a semi-infinite plate is assumed the following stress intensity equation applies as shown in Equation 15.

$$K = Y\sigma\sqrt{\pi a} \tag{15}$$

Where, Y is the geometry configuration factor,

$$Y = 1.12$$

This variation of the edge crack geometry assumes a constant Y magnitude, not considering the thickness of the plate. When dealing with marine dynamic cables this would be an oversimplification since the insulator thickness is fixed. This is why a single edge crack in a finitely extended plate has been employed.

Y is no longer constant and becomes a function of the crack length. Equation 36 highlights the geometry configuration function.

$$f\left(\frac{a}{w}\right) = \frac{\sqrt{\frac{2w}{\pi a}\tan\frac{\pi a}{2w}}\left(0.752 + 2.02\frac{a}{w} + 0.37\left(1 - \sin\frac{\pi a}{2w}\right)^3\right)}{\cos\frac{\pi a}{2w}} \tag{36}$$

Where, a, is the crack length and, w, is the finite width of the plate, depicted as 'W' in Figure 48. Hence, the stress intensity factor, K, is calculated using Equation 37.

$$K = f\left(\frac{a}{w}\right)\sigma\sqrt{\pi a} \tag{37}$$

Subjectively speaking, the model accurately resembles the manner in which a vented water tree would propagate through the insulator thickness, beginning at the conductor-insulator boundary and stretching through the thickness of the insulator. Additionally, it highlights that the water tree will only grow in one plane. However, the geometry fails to capture the cylindrical shape of the cable, and consequently the insulator.

3.3.2 Case 2

The second crack case model considered for further analysis was the Centre Through Crack in Plate (Figure 49). The model assumes an initial defect in the centre of the geometry. Additionally, the crack experiences combined loading stemming from axial tensile and bending stresses. Lastly, unlike Crack Case #1, the model incorporates a thickness, t.

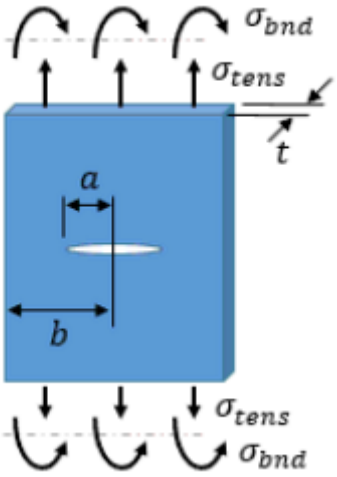

Figure 49: Centre Through Crack in Plate [75]

The stress intensity factor for Crack Case #2 is defined by Equation 38.

$$K = (Y_t\sigma_t + Y_b\sigma_b)\sqrt{\pi a} \tag{38}$$

Where $Y_t and\ Y_b$ are geometric configuration coefficients related to axial stress, σ_t,and bending stress, σ_b, respectively. Each configuration factor is calculated independently using Equation 39 and Equation 40**.**

$$Y_t = \sqrt{\sec\left(\frac{\pi a}{2b}\right)} \tag{39}$$

$$Y_b = \frac{Y_t}{2} \tag{40}$$

The MATLAB code's objective was to determine the most stress critical geometry. Therefore, the axial and bending stresses were not superimposed. Instead, the consequent stress to cause crack propagation for both axial and bending stress was calculated independently. It is assumed the influence of bending stress is insignificant. However, if it is deemed greater than

the axial stress for Crack Case #2 then it will be taken as the driving stress for the engineering selection matrix.

Crack Case #2 is advantageous as it captures more realistic loading conditions, with axial and bending stress. However, the centre crack closer resembles a bow-tie water tree rather than a vented tree. Additionally, even with a relatively small assumed initial crack length the crack could still breach sixty percent of the insulator thickness since the crack initiates at the middle of the insulator.

3.3.3 Case 3

The third crack case model considered for further analysis was the Single Edge Through Crack in Plate (Figure 50). Crack Case #3 is identical to Crack Case #1 besides the fact it involves plate thickness.

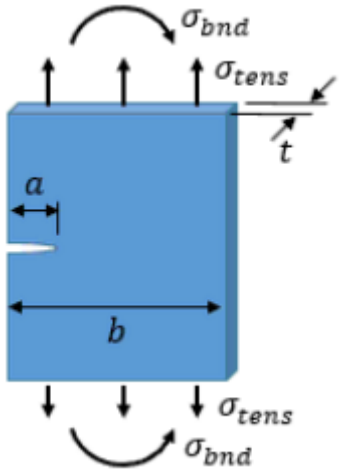

Figure 50: Edge Through Crack in Plate [75]

Due to plate thickness a bending stress can now be applied to the geometry, contrary to Crack Case #1. The stress intensity factor for Crack Case #3 is defined by Equation 38**.**

$$K = (Y_t\sigma_t + Y_b\sigma_b)\sqrt{\pi a} \tag{38}$$

Where $Y_t and\ Y_b$ are geometric configuration coefficients related to axial stress, σ_t,and bending stress, σ_b, respectively. Each configuration factor is calculated independently using Equation 41 and Equation 42.

$$Y_t = 0.265(1-\propto)^4 + \frac{0.857 + 0.265 \propto}{(1-\propto)^{\frac{3}{2}}} \tag{41}$$

$$Y_b = \sqrt{\frac{2}{\pi \propto} tan\frac{\pi \propto}{2}}\left[\frac{0.923 + 0.199\left(1 - sin\frac{\pi \propto}{2}\right)^4}{cos\frac{\pi \propto}{2}}\right] \tag{42}$$

Where,

$$\propto = \frac{a}{b}$$

This model exhibits identical advantages and drawbacks to that of Crack Case #1.

3.3.4 Case 4

The fourth crack case model considered for further analysis was the Elliptical Surface Crack in Plate (Figure 51).

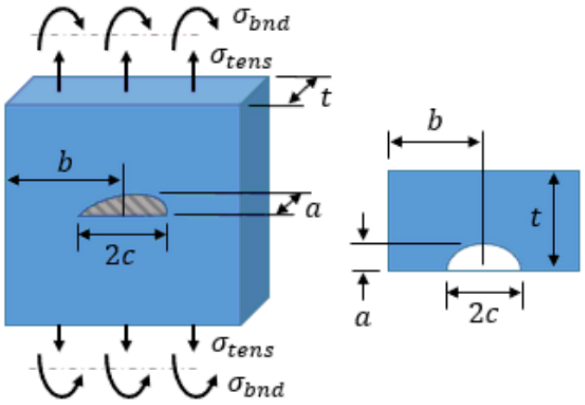

Figure 51: Elliptical Surface Crack in Plate[75]

The crack case assumes the crack is present on the surface of the geometry, propagating along the length of geometry along with through its thickness. This is represented with the additional variable of crack width, denoted as 'a'. The focus is on the crack's propagation through thickness, where crack growth along the geometry's width can be deemed negligible. The stress intensity factor for Crack Case #4 is defined by Equation 38**.**

$$K = (Y_t\sigma_t + Y_b\sigma_b)\sqrt{\pi a}$$

(38)

Where $Y_t and\ Y_b$ are geometric configuration coefficients related to axial stress, σ_t,and bending stress, σ_b, respectively. Each configuration factor is calculated independently using Equation 43 and Equation 44**.**

$$Y_t = F\sqrt{\frac{1}{Q}}$$

(43)

$$Y_b = H * Y_t$$

(44)

F, Q and H are dependent variables which rely on numerous variables. Hence, further explanation of their determination will not be explained here. Refer to Section 8, Appendix F to sight how each variable is calculated.

Crack Case #4 accurately captures the finite width of the insulator with the variable 't'. Furthermore, it illustrates the crack originates at the edge of the insulator and grows inwards through the thickness. However, the necessity to define a crack width, c, is insignificant since

water trees have a width of approximately 3μm. Finally, the model does not represent the cylindrical shape of the cable like many of the other cases.

3.3.5 Case 5

The fifth and final crack case model considered for further analysis was the Thumbnail Crack in Solid Cylinder (Figure 52).

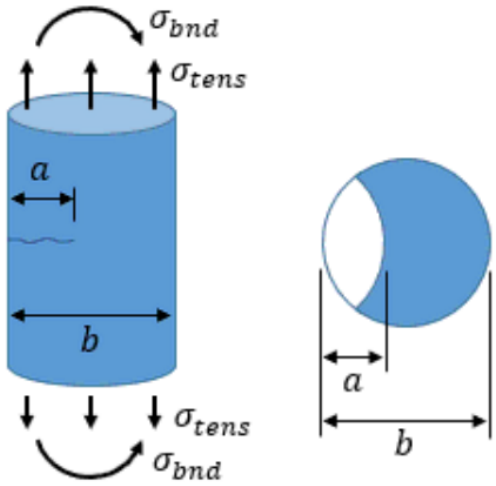

Figure 52: Thumbnail Crack in Solid Cylinder[75]

Both axial and bending stress is applied to the solid cylinder, with the crack present on the surface of the cylinder and propagating through the cylinder's thickness, b. The stress intensity factor for Crack Case #5 is defined by Equation 38**.**

$$K = (Y_t\sigma_t + Y_b\sigma_b)\sqrt{\pi a} \tag{38}$$

Where $Y_t \; and \; Y_b$ are geometric configuration coefficients related to axial stress, σ_t, and bending stress, σ_b, respectively. Each configuration factor is calculated independently using Equation 45 and Equation 46.

$$Y_t = G(0.752 + 1.286\beta + 0.37H^3) \tag{45}$$

$$Y_b = G(0.923 + 0.199H^4) \tag{46}$$

G, H and β are dependent variables which rely on numerous equations. Hence, further explanation of their determination will not be explained here. Refer to Section 8, Appendix G to sight how each variable is calculated.

Crack Case #5 represents the overall geometry of the marine dynamic cable more than any other crack case since it captures the cylindrical shape of the XLPE insulator. Even with the insulator being a hollow cylinder, the representation of a solid cylinder still greatly increases the validity of the model. However, since the model is 3D it is believed the crack can grow in more than one plane. This deviates from the initial assumptions of a 2D geometry that can only grow in one direction.

3.3.6 Comparison of Crack Case Models

The final criteria, and potentially the most impactful, of the engineering selection matrix is the conservativity of each crack case. When analysing the structural integrity of any engineering component it is imperative to observe each scenario and determine the structurally critical case. Hence, an in-house MATLAB code was developed to calculate the minimum axial and bending stress required to cause crack propagation for each crack case demonstrated in Sections 3.3.1 to 3.3.5. The code utilizes the equations for each crack case model to calculate the axial and bending stresses to cause propagation for a range of initial crack lengths. The MATALB code establishes ten different initial crack lengths for which the minimum axial and bending stress to cause crack propagation is calculated individually. The first initial crack length step is equal to 0.01 mm, such value stems from Drissi-Habti et al [51] where they define the length of a typical void radii. The final initial crack length is equal to 1.2 mm which is the value related to 60% of the insulator thickness. This is because once 60% of the insulator thickness has been reached there is a dielectric breakdown within the insulator and the cables short circuits.

Table 8 shows the minimum axial and bending stress to cause crack propagation for each crack case model when the crack length equals the initial crack length (0.01 mm).

Table 8: Minimum Stress to Cause Crack Propagation for 0.01mm

	Case #1	Case #2	Case #3	Case #4	Case #5
Minimum Axial Stress	95.28	107.05	95.19	N/A	162.68
Minimum Bending Stress	N/A	87.40	47.96	N/A	163.79

Table 8 depicts the extremely large stresses to propagate the crack at such small crack lengths. Crack case #4 does not generate any results since the length of the crack through thickness, a, is not greater than the length of the crack across the geometries length, 2c. From Table 8 it is apparent crack case #1 and #3 yield the most conservative stress results. Even though crack case #3 yields minutely smaller stresses compared to crack case #1, it is a 3D geometry. Therefore, crack case #1 is still favoured. The entirety of the stresses presented in Table 8 are of severely high magnitude in relation to the stresses that are thought to be subject to the insulator. Hence, a larger crack size was to be assumed.

Table 9 shows the minimum axial and bending stress to cause crack propagation for each crack case model when the crack length equals 0.671 mm.

Table 9: Minimum Stress to Cause Crack Propagation for 0.671mm

	Case #1	Case #2	Case #3	Case #4	Case #5
Minimum Axial Stress	7.28	13.10	7.27	10.46	12.44

Minimum Bending Stress	N/A	25.77	3.28	9.31	19.62

With a significant increase in initial crack length, the axial and bending stresses to cause propagation for each crack case substantially decreased. Like the results in Table 8**,** for an initial crack length of 0.671 mm crack case #3 produces the most conservative axial and bending stresses. Also, crack case #1 and #3 show identical axial tensile stress required to cause propagation. It is already clear that unless crack case #2 and #5 drastically outperform in other criteria of the engineering matrix neither will be selected for further analysis due to their ostentatious stresses.

Table 10 shows the minimum axial and bending stress to cause crack propagation for each crack case model when the crack length equals the final crack length (1.20 mm).

Table 10: Minimum Stress to Cause Crack Propagation for 1.2mm

	Case #1	Case #2	Case #3	Case #4	Case #5
Minimum Axial Stress	2.41	9.76	2.43	5.87	4.12
Minimum Bending Stress	N/A	19.58	-1.35	5.18	8.79

Table 10 illustrates the axial and bending stresses related to when the initial crack length equals the final crack length, 60% of the insulator thickness. Although this is the most critical case, it captures if the axial stresses determined from the local model in ABAQUS in Section 4.3.2 are of great enough magnitude to influence the crack propagation before structural failure of the insulation layer and subsequent cable. From Table 10 crack case #3 has a negative bending stress. This can be ignored and taken as 0 MPa since compressive stresses are assumed to be negligible.

3.3.7 Determination of Crack Case Model

Figure 53 shows the engineering selection matrix used to determine the most appropriate crack case model. The matrix considered four decisive criterion which were scored from one to five. One relating to the crack case poorly reflecting the criterion, and 5 relating to the crack case fully representing the criterion.

	Crack Case Selection Matrix					
	Crack Case Models	Geometric Resemblance	Vented Tree Resemblance	Loading Conditions	Conservativity	Total
Case #1	Edge Crack in Finitely Extended Plate	3	5	5	5	18
Case #2	Center Through Crack in Plate	2	1	3	2	8
Case #3	Edge Through Crack in Plate	3	5	3	4	15
Case #4	Elliptical Surface Crack in Plate	2	2	3	4	11
Case #5	Thumbnail Crack in Solid Cylinder	5	5	3	3	16

Figure 53: Crack Case Engineering Selection Matrix

It was concluded that crack case #5, thumbnail crack in solid cylinder, best captured the geometry of the cable, describing its cylindrical shape and water tree propagation through the insulator layer. On the other hand, the centre crack and elliptical surface crack did not do an accurate job in simulating a vented water tree. Vented water trees originate at the conductor-insulator boundary or exterior boundary of the insulator, and propagate towards the middle of the insulator, the centre and elliptical surface crack did not replicate such phenomena. Moving on, all crack cases scored relatively high in 'Loading Conditions', all accurately encapsulating axial and/or bending stresses. Finally, crack case #1 scored the highest for conservativity.

The goal of any engineering selection matrix is to determine a clear outcome that can progress to the next stage, or in this case for further analysis. The outcome is determined by the case that totalled the greatest number of points. Therefore, in accordance with Figure 53, the Edge Crack in Finitely Extended Plate (Crack Case #1) will be used for further analysis using COMSOL Multiphysics.

However, to ensure an accurate prediction of the fatigue life of the marine dynamic cable due to mechanical stress a second crack case geometry was chosen. In accordance with Figure 53, crack case #5 'Thumbnail Crack in a Solid Cylinder' was selected. Crack case #5 will allow for investigation of a crack growing in a thin body with a cylindrical geometry. Using MATLAB an in-house code was developed to determine the fatigue life of crack case #5 for a series of loading condition. Three integration methods were developed to calculate the fatigue life. Ultimately the most conservative integration method will be used as the service life of the model.

3.3.8 Fracture Mechanics COMSOL Model

To model the Edge Crack in a Finitely Extended Plate geometry and investigate its resemblance to a water tree propagating in the XLPE insulating layer of a marine dynamic cable COMSOL Multiphysics was used. The model deals with the stability of a plate with an edge crack that is subjected to an axial tensile load. To analyse the stability of exciting cracks, structural mechanics analysis was performed on COMSOL. This enables the use of COMSOL's built in fracture mechanics analysis.

Firstly, the geometry was modelled as 2D since it is assumed a vented water tree is only capable of growing in one plane. Furthermore, a single edge crack is present since it is assumed only one water tree is present per cross section. Moving on, to model the geometry a symmetry condition was implemented as the geometry is perfectly symmetrical about its mid plane. An applied tensile load was applied to the upper and lower horizontal edge as depicted in Figure 54. The applied tensile stress to both upper and lower horizontal edges of the geometry was used to fulfil the physics of a Mode I fracture, where the crack opens, and its

faces move away from one another. The inputted axial tensile stress is determined via the local FE model mentioned in Section 4.3.2.

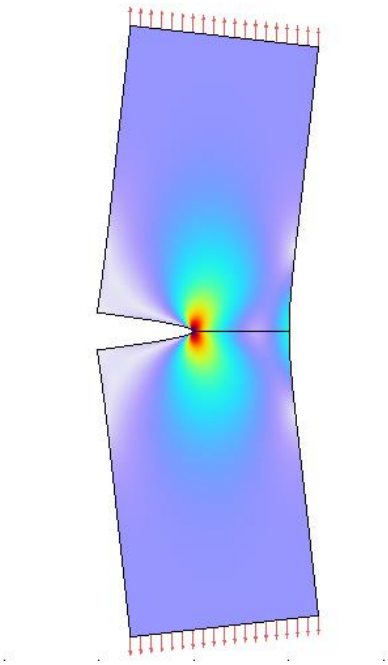

Figure 54: COMSOL Edge Crack Model

As the geometry in Figure 54 replicates a vented water tree crack in XLPE the width of plate was fixed to the thickness of the insulator layer, 2 mm. COMSOL then uses a numerical solution to determine the configuration factor as a function of the crack length as noted in Section 3.3.1, Equation 36. Implementing this function will yield more accurate stress intensity values at the crack tip.

The model was analysed using linear elastic fracture mechanics with the material properties defined in Section 3.3, Table 7.

3.3.9 Plasticity COMSOL Model

Furthermore, employing the identical model outlined in section 3.3.8, COSMOL was then used to attempt to simulate elastic-plastic fracture mechanics (EPFM). Previously mentioned in Section 2.8.2 when dealing with short cracks it is valuable to investigate the plastic stress-strain field at the crack tip since the crack may grow at stress intensity values less than the threshold value, K_{th}, of XLPE. COMSOL's fracture mechanics tool was altered to include a plasticity model, specifying a yield strength and tangent modulus, which was added to the existing material data. The aim of involving EPFM was for a J-Integral value to be calculated for each crack length before the crack length corresponding to K_{th} was reached. However, the simulation failed to converge with J-Integral magnitudes computing as zero. Attempts were made to refine the mesh encompassing the crack tip with the assumption that the plastic strains were extremely small thus requiring an exceptionally refined mesh. However, the solution still did not converge.

Consequently, the scope of the project focussed solely on LEFM with EPFM not included in fatigue life calculations. The use of elastic-plastic material behaviour was included in section 6.3 'Future Work, Water tree', where it is encouraged that analysing the plastic zone encompassing the crack tip may promote more accurate cable service life predictions.

3.4 Local Model

To estimate local mechanical stresses subjected to the XLPE insulator layer a local model was developed. The local model geometry was initially modelled based on Segment 8, nodes 1 and 4 and nodes 91 and 94 of the main segment of the cable. Segment 8 excludes bending stiffeners and has a homogenous cross section. From SIMA the distance between nodes 1 and 4 and nodes 91 and 94 in Segment 8 is 2.1 meters. Such length was not computationally efficient for FEA on ANSYS and consequently the local model cable length was shortened to 10% of the overall length of Segment 8 nodes 1 and 4 / 91 and 94. To ensure the decrease in length did not impact the magnitude of stress within the insulator layer a verification method was employed. Identical arbitrary displacements were applied to the original full-length cable and 10% length cable with the stresses arising in the insulator recorded. Indistinguishable stress values occurred in both models confirming under linear elastic material behaviour the stress per unit length is consistent. From here on the local model had a length of 10% its original length.

Furthermore, the local model was modelled with all components within Segment 8 of the cable: including Kevlar ropes, XLPE insulator layer, copper conductors and outer sheathing. The modelling of the copper conductors was simplified to a solid cylinder as shown in Figures 55 and 57. Modelling approximately all 30 wires that comprise the conductor drastically decreases computational efficiency and implies complex interactions between each wire strand that is not in the scope of this project. Furthermore, the outer sheath layers of Polyurethane have been modelled as one singular layer due to not considering friction coefficients. Modelling the outer sheathing as one single layer has no effect of the local stresses present in the insulator. Section 2.3.2 Table 1 highlights the dimensions of the cable components.

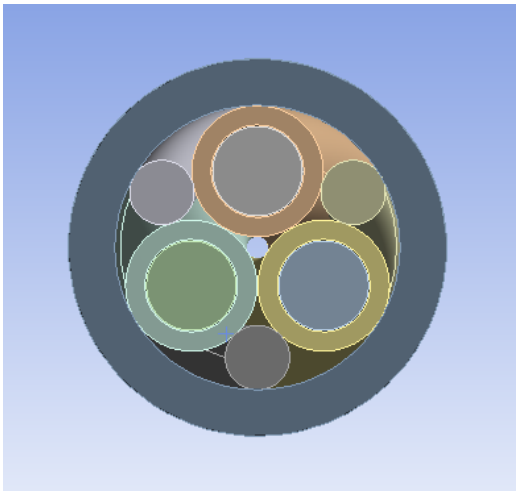

Figure 55: ANSYS Local Model Cross Section

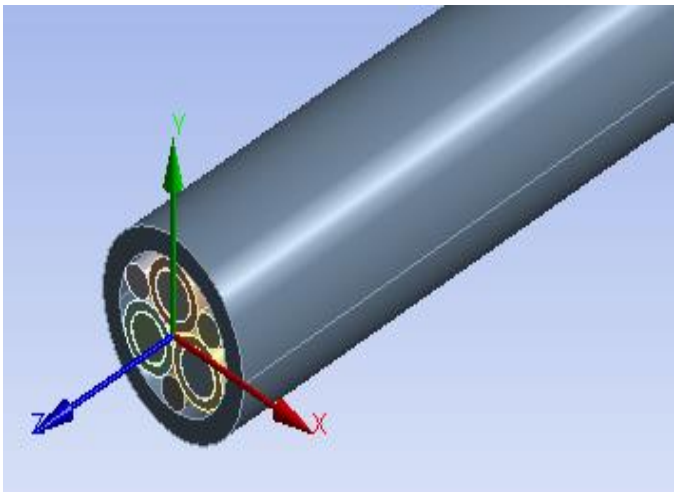

Figure 56: ANSYS Local Model Coordinate System

Finally, the model was developed on SolidWorks using the sweep Method. The sweep method allows for accurate manipulation of the number of revolutions the wire takes about the centre axis of the cables length, resulting in the local model accurately depicting its helical real-life orientation as depicted in Figure 57.

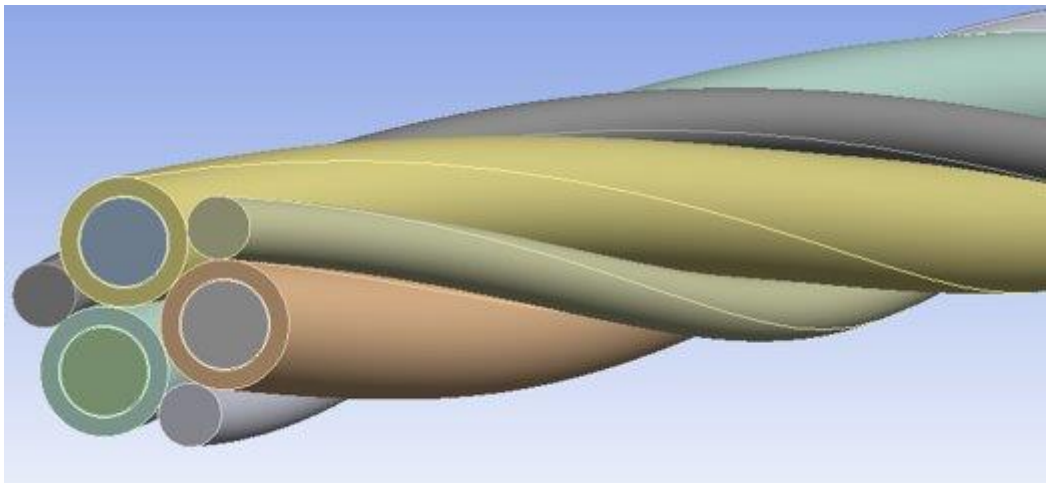

Figure 57: Helical Geometry of Local Model Components

3.4.1 Local Model Boundary Conditions

The model was then imported to ANSYS as a .IGS file for finite element analysis. Importing as such allows for each component of the cable to be characterized as its own part and behave independently. Each component comprising the local model is assumed to follow the full stick condition. Therefore, each contact region in ANSYS was set to bonded. When contact regions are bonded there is no sliding or separation between the faces or edges is contact. This assumption allows for a linear solver, and hence solution since the contact area will not change with loading [65].

Moving forward, it was necessary to conduct a mesh convergence study of the insulator layer. It was imperative to refine all components incorporated in the local model to ensure each component was responding correctly in relation to its material characteristics. A mesh convergence study was imperative to ensure the solution was mesh independent and of the greatest accuracy. Figure 58 demonstrates the mesh independence study for the local model as a plot of percentage convergence versus the number of elements. Percentage convergence was determined by Equation 47.

$$Percentage\ Convergence = \left(1 - \left(\frac{Final\ Normal\ Stress - Current\ Normal\ Stress}{Final\ Normal\ Stress}\right)\right) * 100 \quad (47)$$

With the independent mesh result having a percentage convergence of 100. During the mesh convergence study, it was concluded the maximum stress arises at the exterior face of the cable, where the cable is free to move. However, there was still a focus on refining all components of the model so the material characteristics of each component is simulated as accurately as possible. The final mesh had 9728295 and 2222366 nodes and elements respectively. The final mesh refinement did include a greater number of nodes and elements but since it yielded an equal stress to the pre-requisite mesh refinement, the pre-requisite

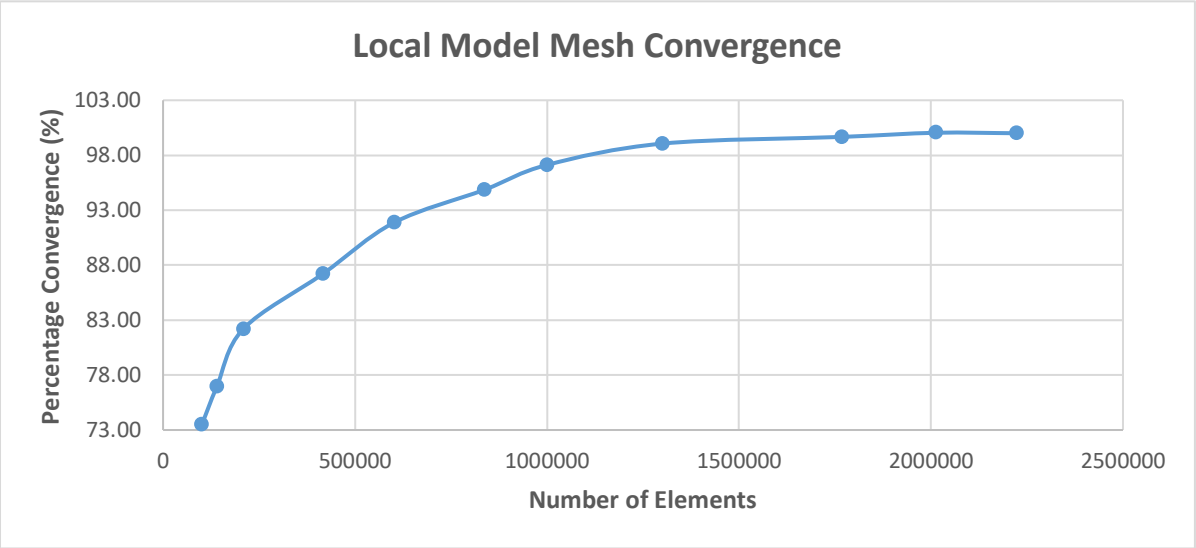

Figure 58: Local Model Mesh Convergence

mesh was used for computational efficiency. Figure 59 shows a refined mesh for all components comprising the Local Model.

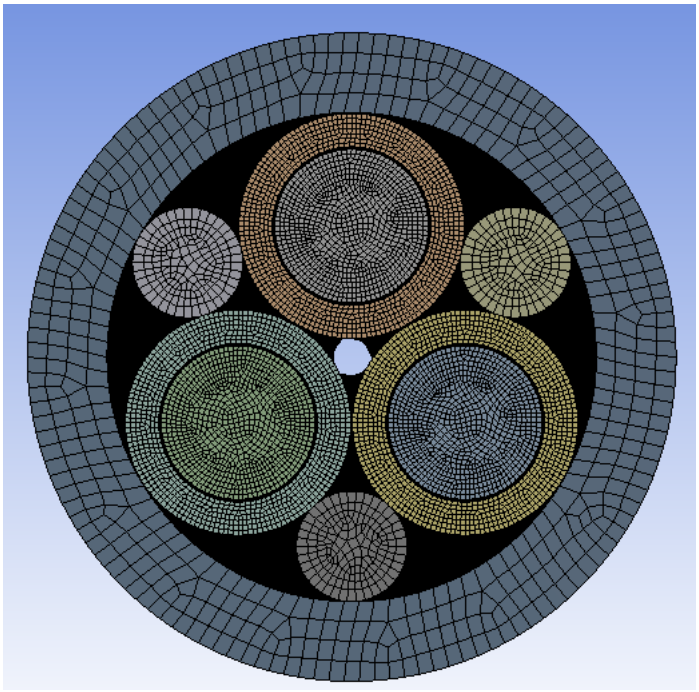

Figure 59: Local Model Mesh

Furthermore, the local stress within the insulator was calculated by applying the relative displacement between nodes 1 and 4. Referring to Section 4.1.3 Tables 13 to 18 displacement scenarios were analysed, reflecting 3 different sea states. To implement the relative displacements one end of the cable was fixed by applying a 'fixed support' boundary condition to all faces on the cross section. To apply the relative displacements between nodes 1 and 4 a remote point was implemented. A remote point was used to replicate the behaviour and kinematics of the desired portion of the geometry. A remote point is represented by a Pilot Node which is connected to the geometry via Multipoint Constraint Equations (MPCs). To scope the remote point to the free to move faces of the cable a nodal selection was created. This allows for each node, on each face of the free to move end of the cable, to be scoped with the remote point. The scoped nodes are solid nodes with 3 DOFs where the remote point is a single point that represents the kinematics of the scoped nodes. Hence, a remote point has 6 DOFs 3 translational and 3 rotational. The remote point was defined to an arbitrary location, constrained to zero in the x and y axis and 0.5 meters in the z. Lastly, the behaviour of the remote point was set to 'coupled'. This allows the nodes scoped to the remote point to all move simultaneously with the same displacement in the x, y and z-axis directions [66].

To conduct the linear elastic analysis the isotropic elasticity material model was incorporated, requiring the Youngs Modulus, E, and Poisson's Ratio, v, of each component's material. Refer to Section 2.3.3, Table 3. Isotropic elasticity allows for a solution to be developed irrespective of direction, i.e., material properties do not vary with direction. Once mesh independence was guaranteed and the model was accurately constrained the normal stress within the insulator in the z direction was calculated for all three sea states. The normal stress in the z direction is the stress through the cross section of the cable, see Figure 56, and accurately represents the axial tensile stress subject to the single edge crack in a finitely extended plate.

3.5 Electrical Stress Models

This section illustrates the process of determining a fatigue life from electrically stressed water trees. To analyse the crack growth of vented water trees through the XLPE insulation layer multiple electrical models were developed on COMSOL Multiphysics. COMSOL Multiphysics functions as a versatile finite element analysis solver, enabling the execution of complex multi-physics simulations. It is able to provide simulations that spans applications in mechanical, electrical, and fluid flow domains. Every physics tool within the software offered on this platform is fully equipped for multi-physics simulations. The software encompasses diverse study capabilities, incorporating time-dependent, stationery, parametric studies, and frequency response. As the marine dynamic cable being investigated operates within an AC system at 50Hz a frequency domain study was chosen for the models. In the final model developed, to analyse a water tree micro void, a coupled multi-physics approach that integrates both electrical and mechanical phenomena was used.

The models, created using COMSOL, were utilised to simulate the electric field strength at the tip of a water tree crack. The software accurately depicts the electric field distortion resulting from the presence of a water tree. [9] An iterative method of analysing the electric field value was utilised, because, as the water tree increases in length the electric field strength at the tip of the crack will also increase. This iterative method was performed for various propagation lengths across the insulation thickness.

Each model undertook an incremental study with an initial water tree crack length of 0.01mm, taken from [10] as the initial vented crack length to meet a micro void, increasing by 0.045mm until 60% of the insulation thickness was reached. This stage of propagation is when water trees have been documented to instigate cable failure through the occurrence of shortcut. This

shortcut is an arc fault, this occurs between two conductors, in this case the conductor wires and the crack tip, when they have different voltages[10].

Once electric field values are determined for each stage of the study, the Maxwell stress can be calculated using Equation 14 as discussed in Section 2.7.2:

$$F = \frac{\varepsilon_0}{2}(\varepsilon_r - 1)E^2 \tag{14}$$

The fatigue life of the cable due to electrical stress can then be calculated, using the method described in Section 2.8.3, the time taken for each for each crack increment can be determined. This can be calculated using Equation 19:

$$0.5V_0\varepsilon_0(\varepsilon_r - 1)E^2 > \sigma_{yield}V_0 \tag{19}$$

Operating conditions and parameters of the 1kV dynamic were found and were incorporated into the models developed. A 2D and 3D model were created in order to analyse the growth of a water tree and both undertook the incremental study previous discussed. Once Maxwell stress values were determined for each crack length a fatigue life was calculated for each model. A comparison between the models concluded that for the combination of both electrical and mechanical stress the 3D model results would be utilised as this was the most conservative option. This methodology is illustrated below in Figure 60.

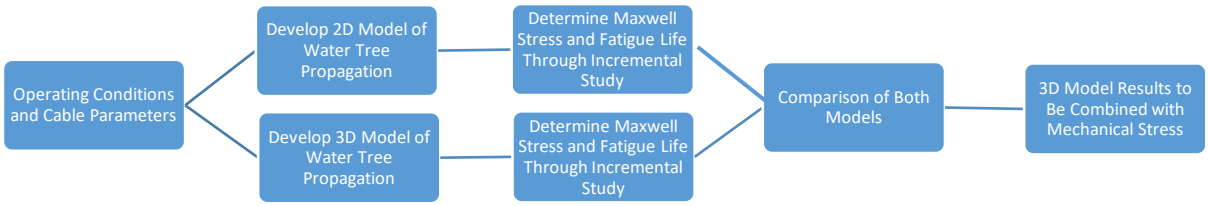

Figure 60: Electrical Stress Methodology Flow Chart

A separate methodology was also developed to achieve the combination of both electrical and mechanical stresses with one COMSOL model, using the discovered conditions and parameters. This model utilised the multi-physics function within COMSOL, not only analysing the electric field at the tip of a void but also analysing how axial stress will affect the crack propagation. This methodology is shown below in Figure 61. The red sections of the flow chat are possible areas of future work for this methodology.

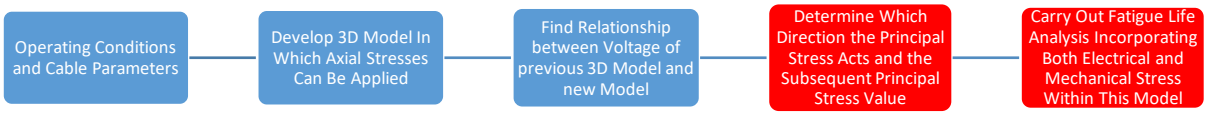

Figure 61: Combination of Electrical and Mechanical Methodology Flow Chart

Despite extensive research efforts, there is currently no standard methodology for simulating and analysing electrical stress effects on water treeing even with substantial contributions from both experimental and numerical investigations in this field [45].

3.5.1 2D Electrical Stress Model

A 2D cross-section of the 1kV cable was modelled, the ropes and outer sheathings are removed as they are not essential and do not interfere with the electric field results. The properties of the cable are taken from Section 2.3.1, Table 1**.** Each section of the model is assigned a material in accordance with the real-life cable, these materials are set up with the properties discussed in Section 2.3.4, Tables 4 & 5. The conductor is modelled as a homogenous solid in order to reduce computational time.

A water tree crack is then modelled at the outer edge of the insulation, simulating a vented water tree as shown in Figure 62. The water tree is assigned the material properties of water in order to correctly analyse the crack tip. The conductor is assigned as the terminal and the outer edge of the insulation is grounded to capture the electric field within the insulation.

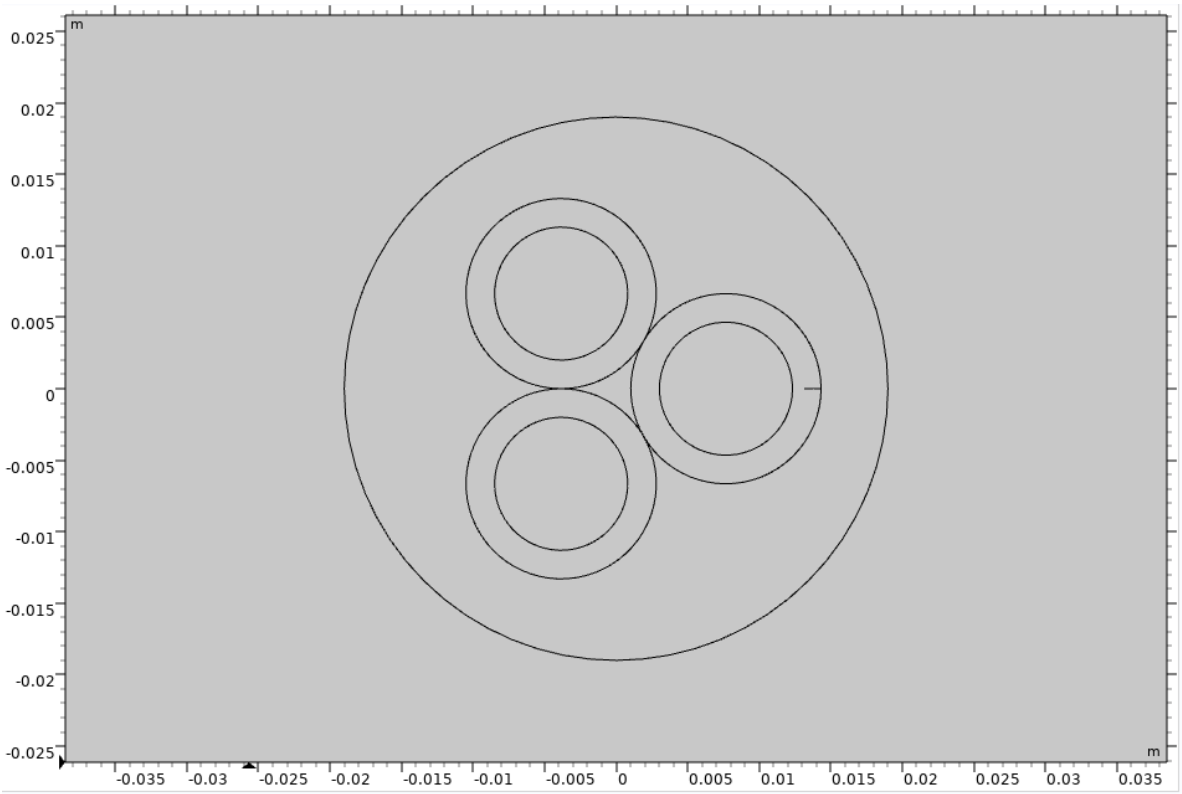

Figure 62: Electrical COMSOL Cross Section

Moving forward, it was necessary to complete a mesh convergence of the 2D electrical model. The mesh convergence study had to be completed to confirm the solution was mesh independent. The mesh convergence study was focused on the void tip as this is the area of interest within the investigation. Figure 63 demonstrates the mesh independence study for the 2D electrical model as a plot of percentage convergence versus the number of elements. Percentage convergence was determined by Equation 47.

$$Percentage\ Convergence = \left(1 - \left(\frac{Final\ Maxwell\ Stress - Current\ Maxwell\ Stress}{Final\ Maxwell\ Stress}\right)\right) * 100 \quad (47)$$

With the independent mesh having a percentage convergence result of 100. The final mesh had 174566 elements.

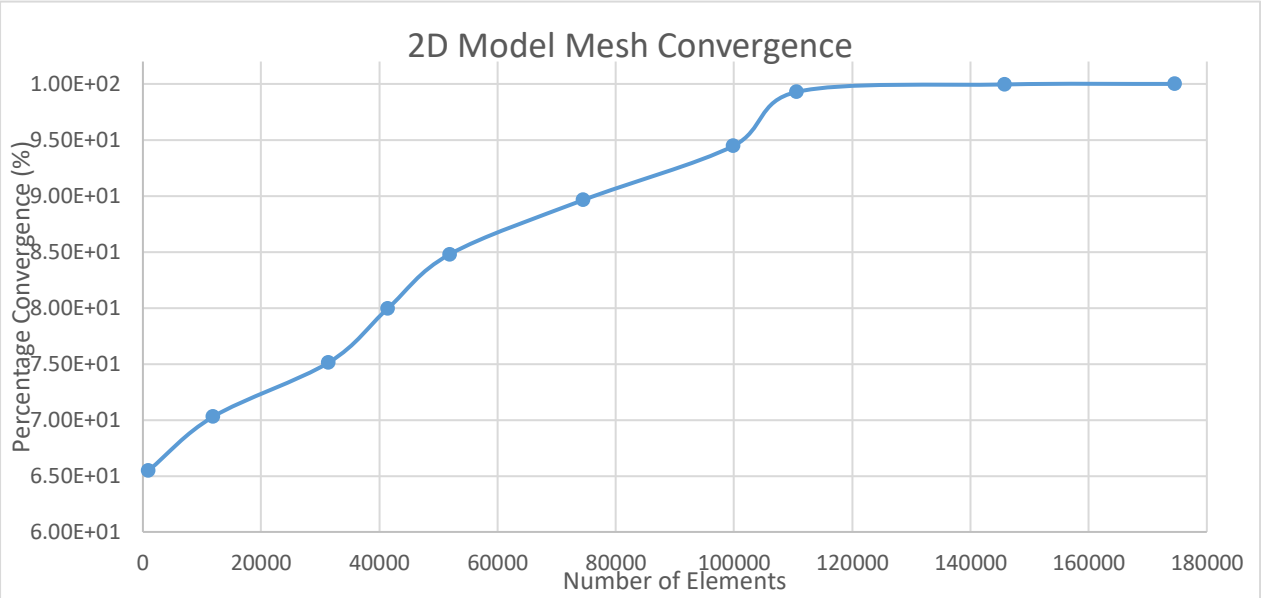

Figure 63: 2D Model Mesh Convergence

Figure 64 illustrates the final mesh of the 2D electrical model at the micro void. From literature it was found that water tree micro voids can range in their dimensions from 0.1μm to 5μm. Therefore, it was imperative that a dimensional void comparative study was carried out. From the study it was concluded that the water tree void dimensions that would be implemented in the incremental study were a length of 3μm and width of 1.5μm as this was the most conservative approach. Below Table 11 shows the comparative study.

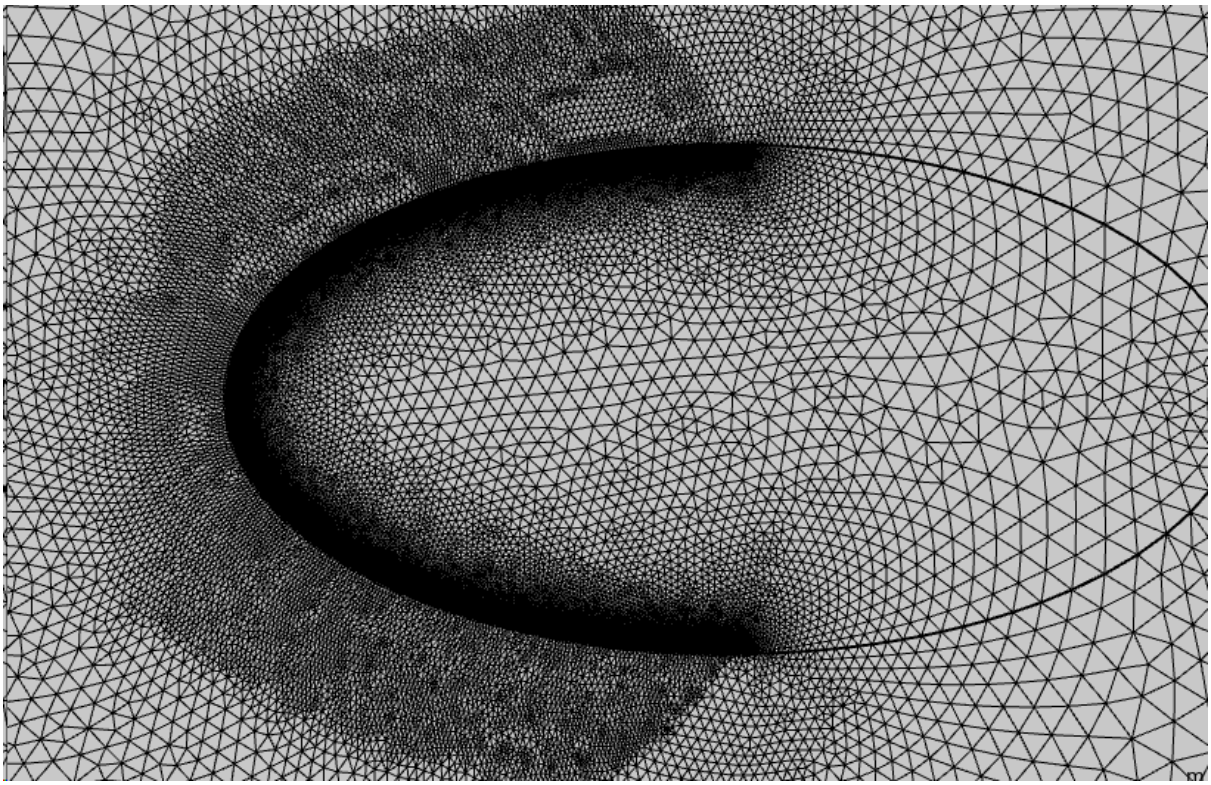

Figure 64: 2D Electrical COMSOL Model Mesh

Table 11: 2D Model Comparative Study

Water Tree Void Length (um)	Water Tree Void Width(um)	Electric Field (V/m)
0.2	0.1	1.08×10^6
0.5	0.25	1.25×10^6
1	0.5	1.41×10^6
1.5	0.75	1.25×10^6
2	1	1.29×10^6
2.5	1.25	1.34×10^6
3	1.5	1.58×10^6
3.5	1.75	1.56×10^6
4	2	1.29×10^6
4.5	2.25	1.31×10^6
5	2.5	1.29×10^6

3.5.2 3D Electrical Stress Model

A 3D model was also developed to analyse water tree propagation due to electrical stress. This model simply expands the previous 2D model into a 3D geometry, it also simulates a vented water tree with the same parameters discussed in the previous model. The 3D model is illustrated in Figure 65, it also demonstrates the how the electric field is generated throughout the insulation.

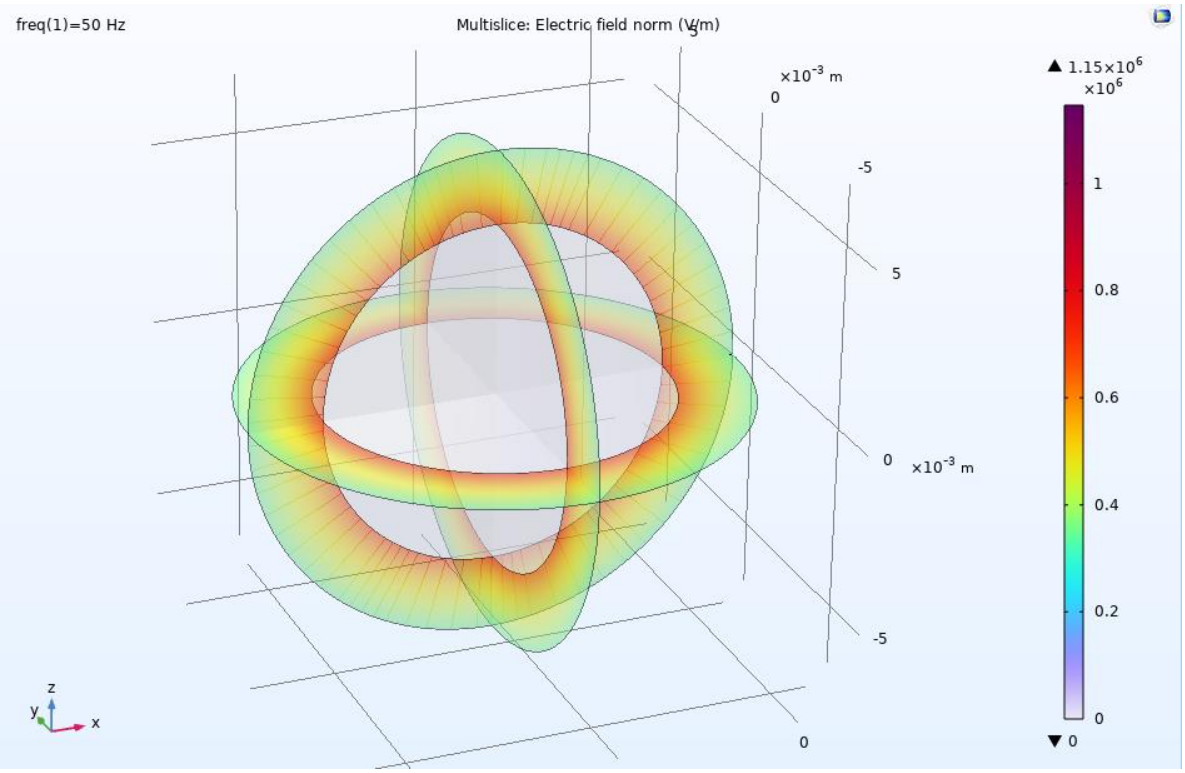

Figure 65: 3D Electrical Water Tree Model

Again, it was necessary to complete a mesh convergence of the 3D electrical model. Similarly, to the 2D mesh convergence, the study was fixated around the void tip as this is the area of interest within the investigation. Figure 66 demonstrates the mesh independence study for the 3D electrical model as a plot of percentage convergence versus the number of elements. The independent mesh result reached a percentage convergence of 100. The final mesh had 4141341 elements.

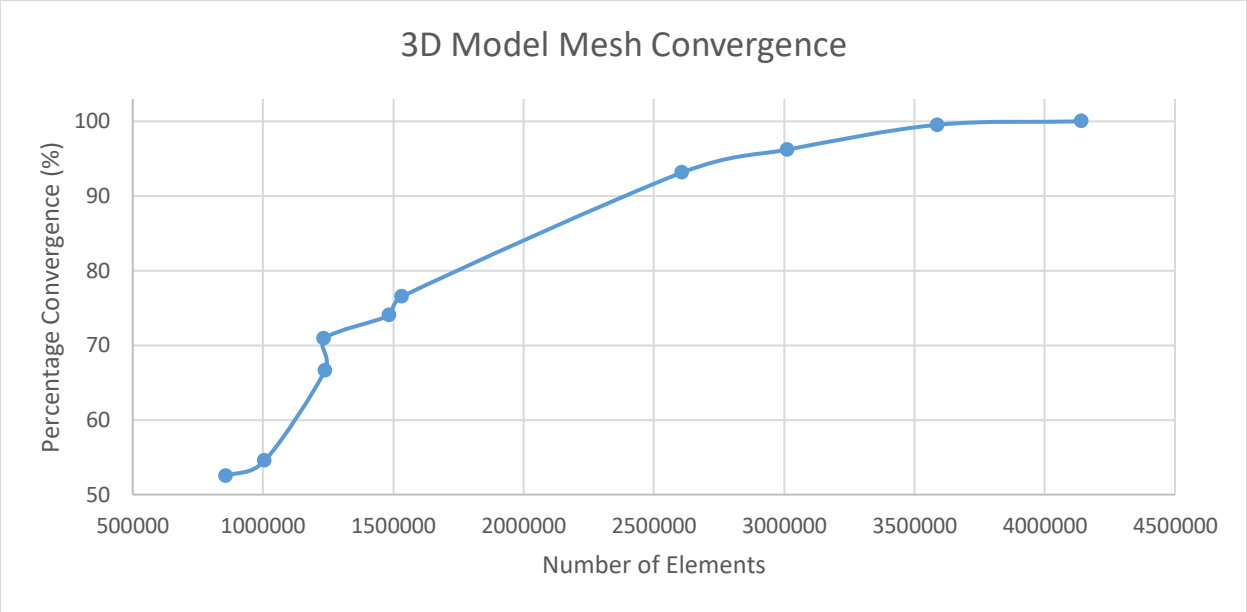

Figure 66: 3D Model Mesh Convergence

Figure 67 illustrates the final mesh of the 3D electrical model at the micro void.

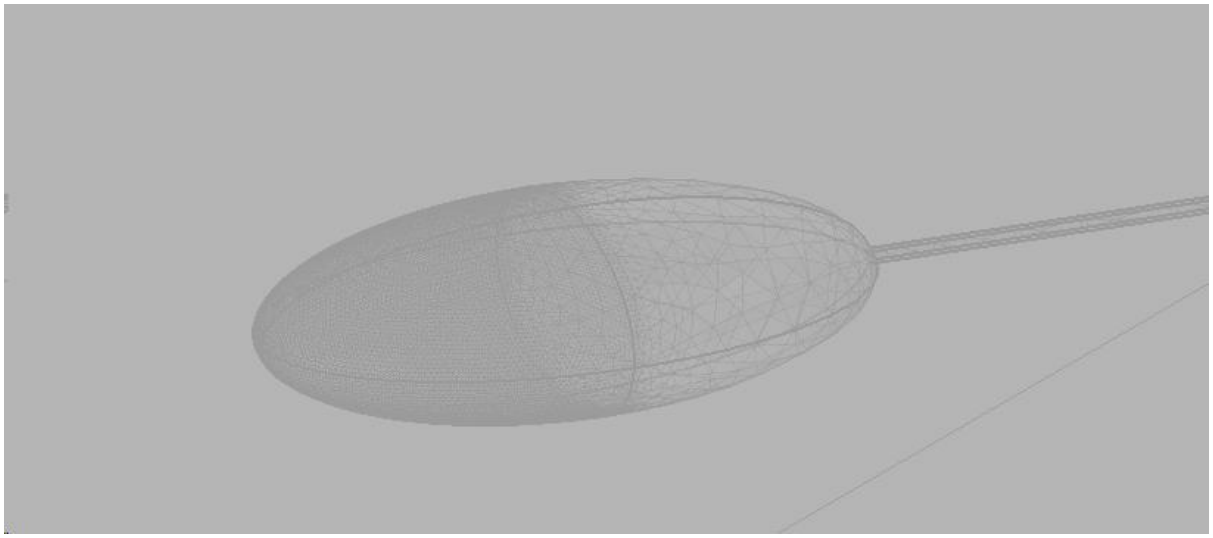

Figure 67: 3D Electrical COMSOL Model Mesh

The same dimensional void comparative study was carried out to determine the most conservative void dimensions that would be used in the 3D electrical model. This comparative study, shown in Table 12, agreed with the previous 2D study and therefore the water tree void dimensions that would be implemented in the incremental study were a length of 3µm and width of 1.5µm.

Table 12: 3D Model Comparative Study

Water Tree Void Length (um)	Water Tree Void Width(um)	Electric Field (V/m)
0.2	0.1	1584826.2035924671
0.5	0.25	1558567.9718268719
1	0.5	1668389.6509475824
1.5	0.75	1570257.2006266639
2	1	1538471.9166822997
2.5	1.25	1716240.8523369746
3	1.5	1795586.8759452351
3.5	1.75	1792811.7278029432
4	2	1619709.87699041
4.5	2.25	1578160.8384770928
5	2.5	1749855.1609728483

3.5.3 Multiphysics 3D Electrical Stress Model

A multi-physics electrical model was developed to incorporate both electrical and mechanical stresses within one model, the multi-physics tool can simulate static structural mechanics with

electrostatics. The same material properties from the previous models were used in this model and the void dimensions are that of the previous 3D model. The multi-physics function within COMSOL is extremely computationally intensive. Therefore, for COMSOL to compute a Multiphysics model of this complex phenomena an extreme scaled down version had to be created to just a small section of the insulator, 10μm x 10μm x 10μm. The micro void is modelled at the centre of this model, the model is depicted in Figure 68 below.

The highlighted boundaries in Figure 68 are the boundaries at which axial stress is applied, this axial stress can be taken from the local model developed. As there is no conductor in this model, the terminal is applied to the lower boundary of the model and the top boundary is grounded. The model allows electric field, displacement, and principal stress values at tip of the void to be analysed. The stress due to the electric field and the stress due to the boundary load are combined within the principal stress value.

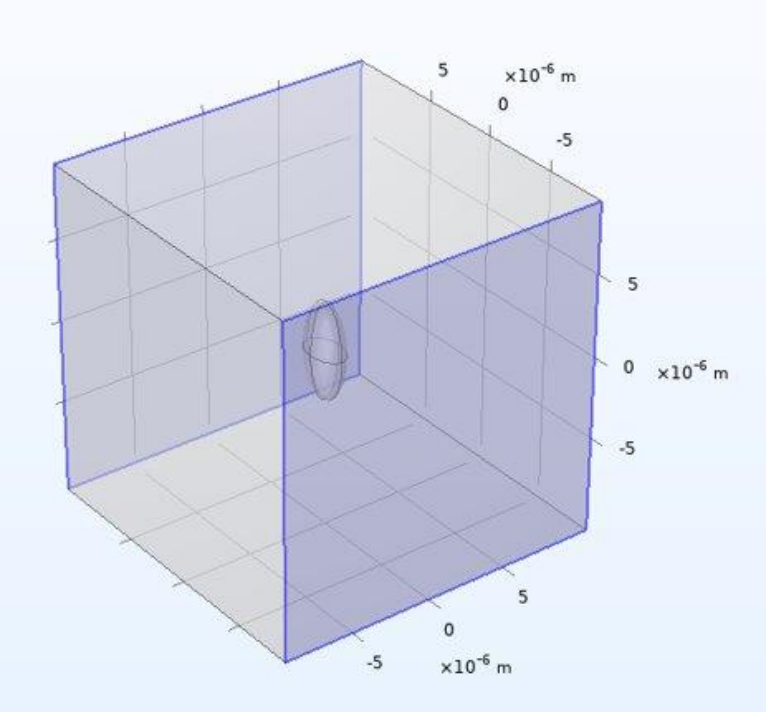

Figure 68: 3D Micro Void Geometry

A final mesh convergence was carried out for the multi-physics model to confirm the solution was mesh independent and of good accuracy. Even though this model has been scaled down the mesh convergence is still conducted at the micro void tip. Figure 69 demonstrates the mesh independence study for the multi-physics model as a plot of percentage convergence versus the number of elements. The independent mesh result reached a percentage convergence of 100. The final mesh has 745265 elements.

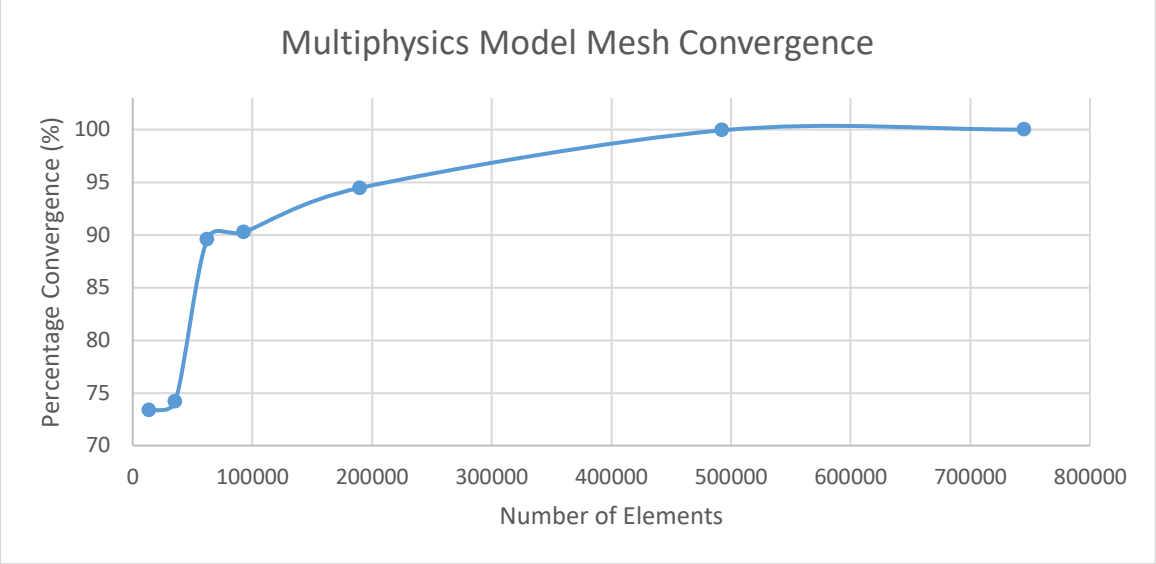

Figure 69: Multiphysics Model Mesh Convergence

Figure 70 illustrates the final mesh of the multi-physics model at the micro void.

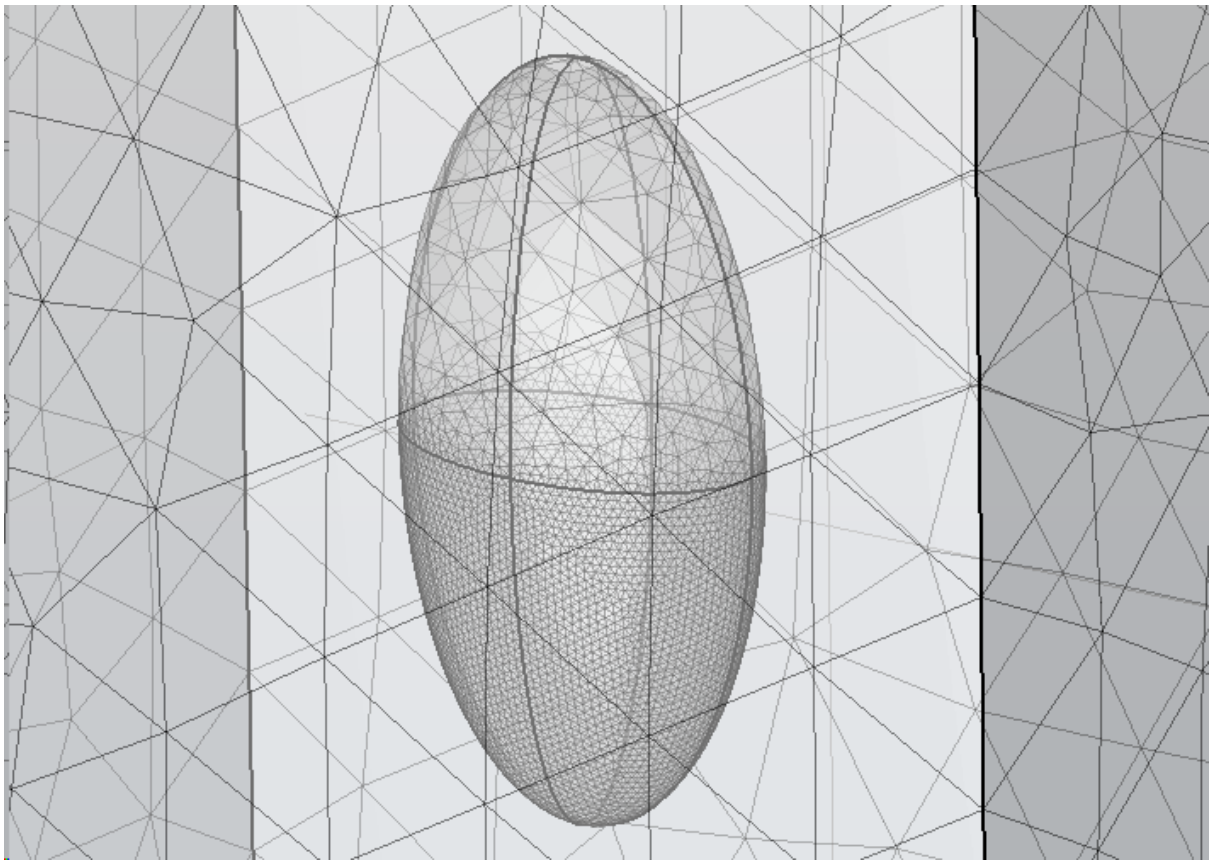

Figure 70: Multi-physics Mesh

For this model to correlate with the 1kV cable being studied, a method had to be developed in order to determine the terminal voltage that should be applied. The graph, in Figure 70, illustrates the electric field values from the original 3D model as it progressively passes through the insulation thickness.

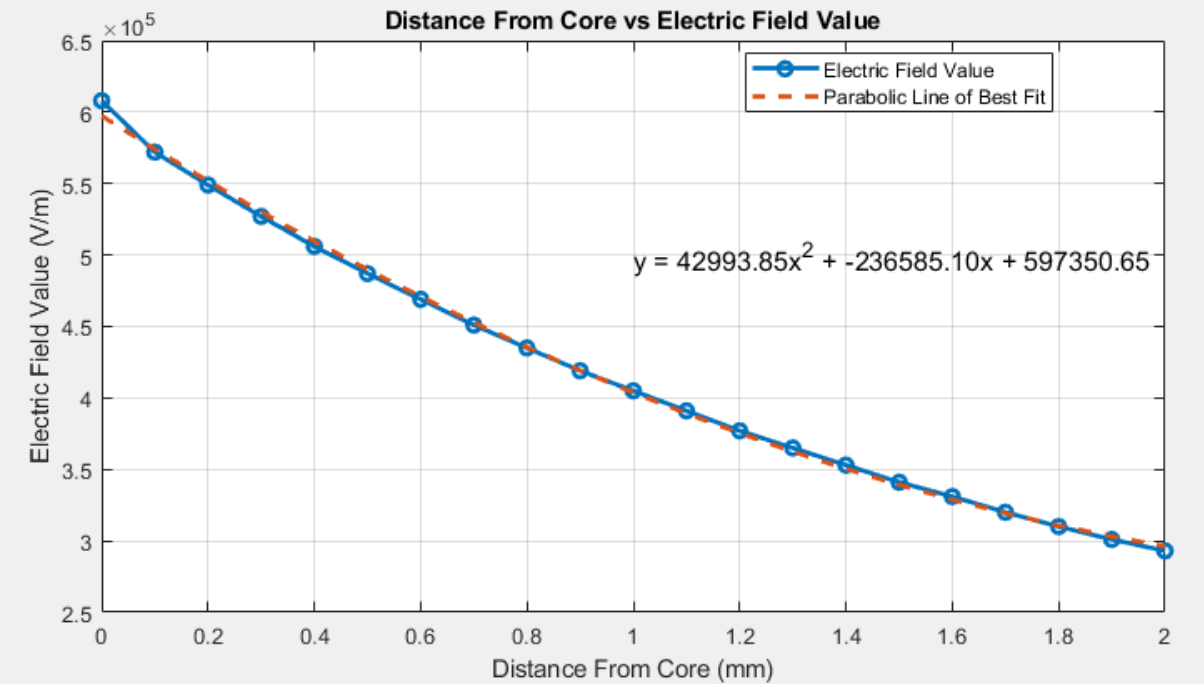

Figure 71: Distance from Core vs Electrical Field Value

To determine the voltage that would need to be applied to the model so that a 1kV cable insulation can be simulated the multi-physics model was treated as a capacitor. The voltage which needs to be applied depends on the distance at which you want to analyse the void. Using the graph in Figure 70 an equation has been found for the line of best fit, the distance (x) can be inserted into the equation shown in Figure 71 which gives the approximate electric filed value at that distance through the insulator.

Assuming the model is a capacitor, as when XLPE insulation is fully wrapped around the cable core the electric field that distributes throughout the insulation will decrease as the it gets further from the core [10]. The electric field will also be equal throughout the circumference of the insulation, this assumption is valid as the previous models have proven both phenomena. Capacitance can be calculated from Equation 48:

$$C = \varepsilon_0 \varepsilon_r \frac{A}{d}$$

(48)

Where C is capacitance (F), A is the area of the plates (m^2) in this case the top and bottom boundaries of the model, d is the distance between the two plates (m^2), ε_0 is the permittivity in a vacuum (Fm^{-1}) and ε_r is the relative permittivity of XLPE (Fm^{-1}).

However, capacitance can also be calculated as a ratio of charge to voltage as shown in Equation 49:

$$C = \frac{Q}{V}$$

(49)

Where V is voltage (V) and Q is charge (C).

Coulombs law can be used to calculate electric field strength and can integrate both of these equations, Coulombs law is shown below:

$$E = \frac{Q}{4\pi\varepsilon_0\varepsilon_r r^2}$$

(50)

Where E is electric field (V/m) and r is the radius (m), however, in this case r is the distance through the insulation that the void will be analyse in the multi-physics model.

After inserting Equations 48 and 49 into Equation 50 and rearranging an equation can be used to calculate the voltage for the scaled model with Equation 51 shown below:

$$V = 4\pi E r^2 \frac{d}{A}$$

(51)

3.6 Combining Mechanical and Electrical Stresses

To complete the objective of the water tree analysis a superposition method had to be developed for this multi-physics problem. A factor that contributes to the challenge of combining stresses is the discrepancy in frequencies; the mechanical stresses induced by WEC and cable motion fall within the seconds range, whereas the electrical stress frequency in this investigation is 50 Hz. Therefore, a direct superposition of these stresses is not possible even though the stresses have comparable magnitudes.

Also, the water tree crack propagation related to mechanical and electrical stresses are not directly related. For mechanical loading, the water tree grows on the theory of linear elastic fracture mechanics. For electrical stresses, the water tree grows on the kinetic theory of fatigue.

One incremental crack growth due to mechanical induced stress is known as $\Delta a_{mechanical}$, and can be correlated with "time" through the wave period, which represents the loading frequency derived from a specific sea state. Conversely, the propagation of the crack under electrical induced stress results from the accumulation of electric energy causing the rupture of the polymer monomer chain. $\Delta a_{electric}$ is defined as the length of polymer chains breaking during the time equivalent to one load cycle of the mechanically induced stress. Its correlation with "time" is established through the operational current frequency of 50 Hz.

The superposition method is shown in equation (52).

$$\Delta a = \Delta a_{\text{mechanical}} + \Delta a_{\text{electrical}}$$

(52)

With each progression of crack growth induced by mechanical stresses, an additional increment of crack growth arising from electrical stress is incorporated into the cumulative crack growth. As the water tree crack advances, the growth increment Δa is accordingly updated in Equation 17.

The service life of the cable due to both induced stresses can then be calculated by finding the time until 60% insulation crack length is reached.

Under the project assumptions in Section 1.3, the maxwell stresses will solely drive the water tree growth until the initiation of the Paris Law for each designated sea state. The water tree length at which the mechanical stresses, and consequently the Paris Law, become influential

is proportional to the mechanical stresses that originate from each sea state. Once fracture mechanics theory is active the incremental crack case study will involve both mechanical and electrical stress involvement.

4 Results

This section provides the results developed from the methodologies created for each section and goes on to discuss the implications of these results.

4.1 Global Results

This section outlines the effect of different environmental conditions on the fatigue life of the dynamic power cable. The cable properties associated with these results are denoted in table 2. All cases were simulated, in SIMA, for 1200s with a 300s inclusive ramp up period to negate any unwanted transient behaviour and to allow the wave spectrum to fully develop.

4.1.1 Global SIMA Raw results

All sea states were simulated for 1200s (300s ramp up) with a storage time step of 0.1s and hence 12000-time steps were recorded. For each case, the results were recorded for all 15 segments of the power cable. For this study, segment 8 is of interest as it is deemed to be unaffected by the bending stiffeners which are located at either end of the cable. Segment 8 comprises of 184 elements (each with a length of 0.7m) and is considered the main section of the cable. Figure 72 depicts the axial force [N] for Case 1 Segment 8 Element 1 against time [s] and has a maximum axial force of 900.52 N:

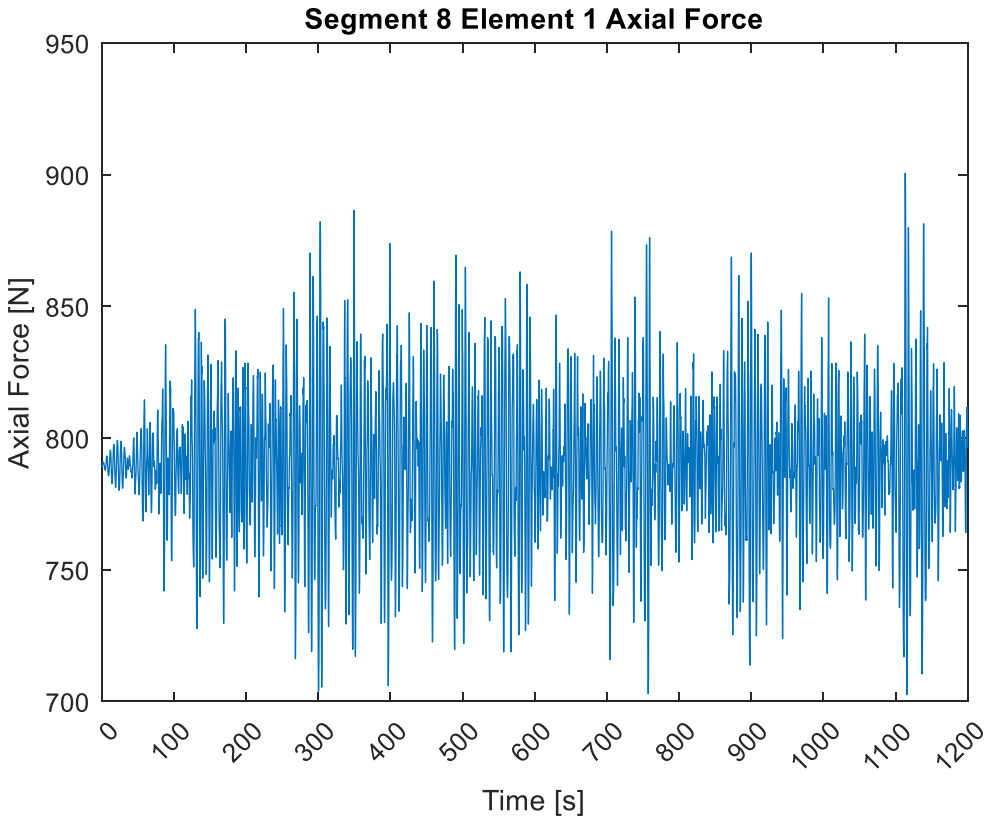

Figure 72: Axial Force [N] vs Time [s] – Segment 8 Element 1

Figure 73 presents the Moment about the local y-axis of the beam element over the entire time series and contain a maximum absolute bending moment of 0.0839 Nm:

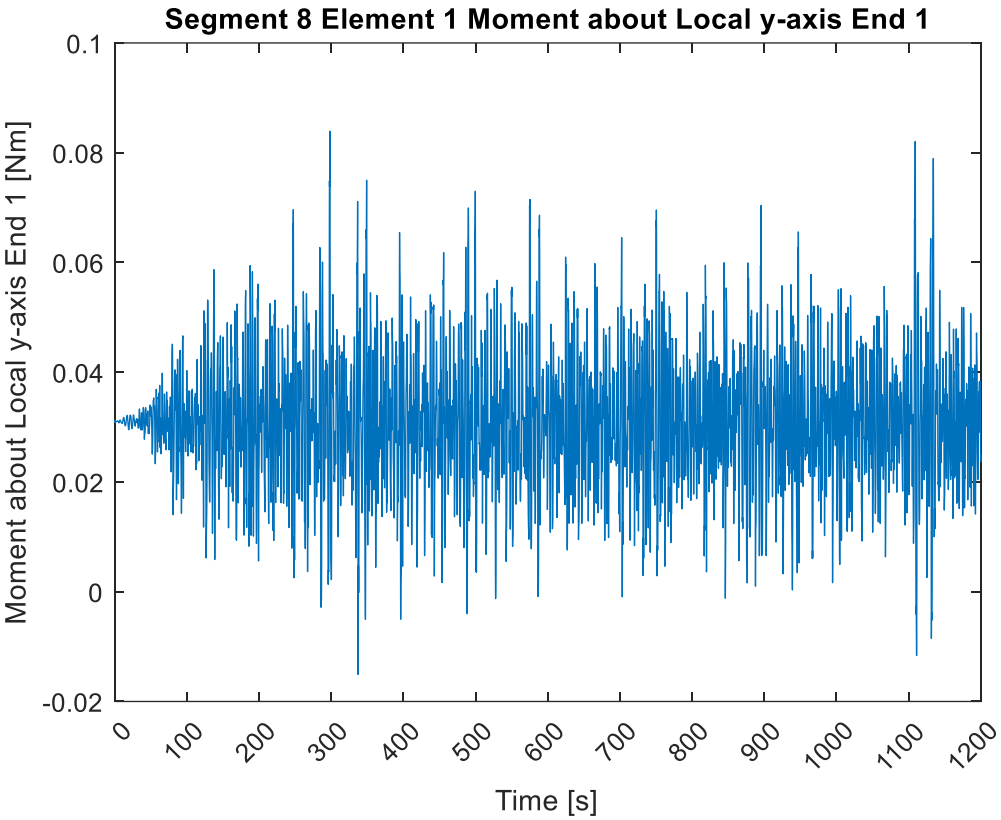

Figure 73: Moment about Local y-axis End 1 [Nm] vs Time [s] – Segment 8 Element 1

Figure 74 highlights the Moment about the local z-axis for the beam element over the entire time series and is found to be significantly lower than the y-axis bending moment with an absolute maximum bending stress of 0.0178 Nm:

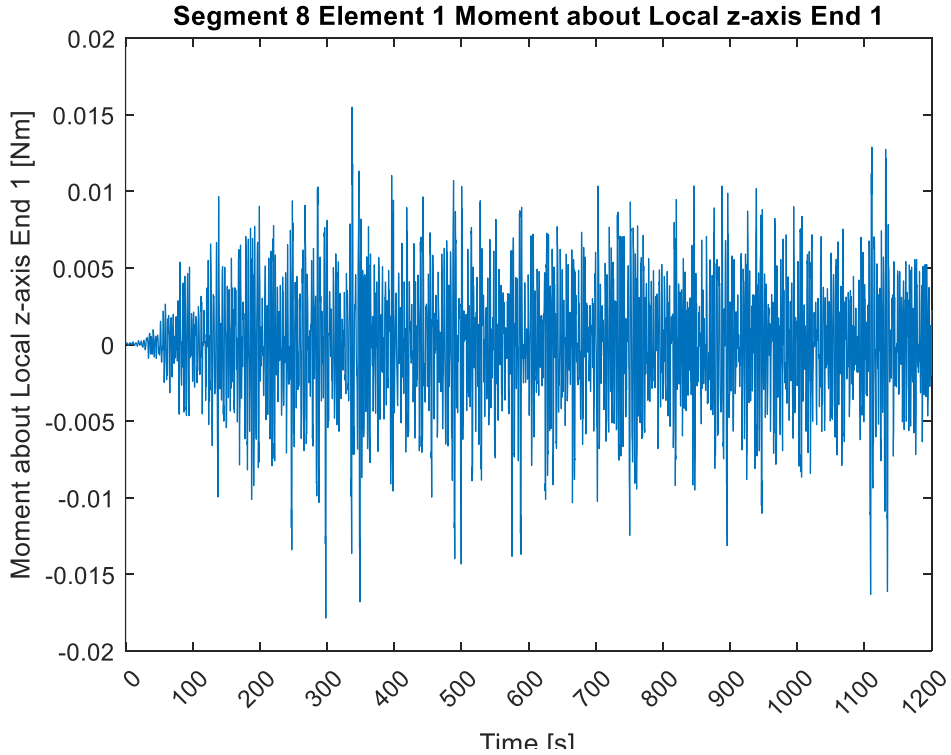

Figure 74: Moment about Local z-axis End 1 [Nm] vs Time [s] - Segment 8 Element 1

4.1.2 MATLAB Fatigue Damage

For all three cases, the raw element forces were extracted from SIMA and post processes through the MATLAB fatigue analysis code. Along the length of the dynamic power cable, in the main segment, there are a total of 184 elements. In order to streamline computational time, only 1 out of 3 elemental forces are processed by the MATLAB code. This approach viable as the location of the greatest fatigue damage is of importance while maintaining accuracy. Since SIMA only stores the results of 1 in 3 elements, the plots produced in this section represent the length of the entire power cable and hence only 61 elements are plotted.

Case 1 - Hs = 0.5m Tp = 4.5s

Figure 75 highlights the how the stress range (utilising the goodman relation) varies along the length of the cable. It can be found that the greatest stress range occurs at the beginning of the cable (near the WEC) and decreases along the length. From the way MATLAB results it can be accurately found that the greatest stress range reaches 0.18335 MPa and located at the first element. From Figure 75 it is evident that this maximum stress range is recorded at 90º through the cross-section.

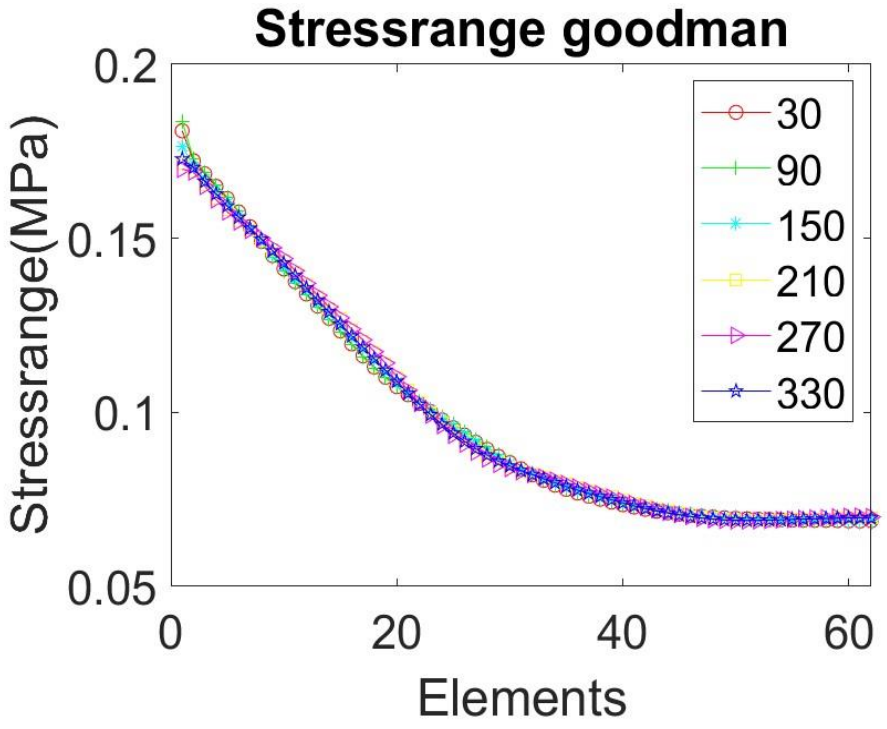

Figure 75: Case 1 Stress Range Goodman (MPa) vs Length (Elements)

Figure 76 represents the respective Total Fatigue damage along the cable's length. The greatest fatigue damage is found at element 1 and occurring again at 90º through the cable's cross-section with a maximum fatigue damage of 2.4333e-24.

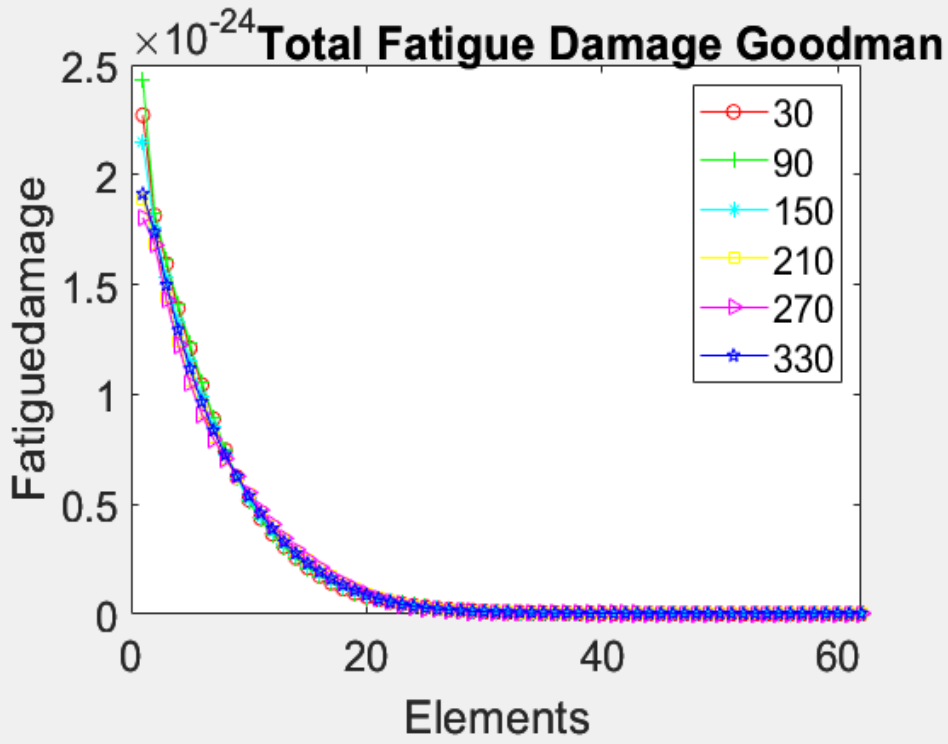

Figure 76: Case 1 Total Fatigue Damage vs Length (Elements)

Figure 77 highlights the cable's predicted fatigue life for a calm sea state (Case 1) and agrees with the predicted fatigue damage results. From Figure 77, it is found that the minimum fatigue life of the cable is approximately 6.05e+21 years and a maximum fatigue life of 1.509e+22 years.

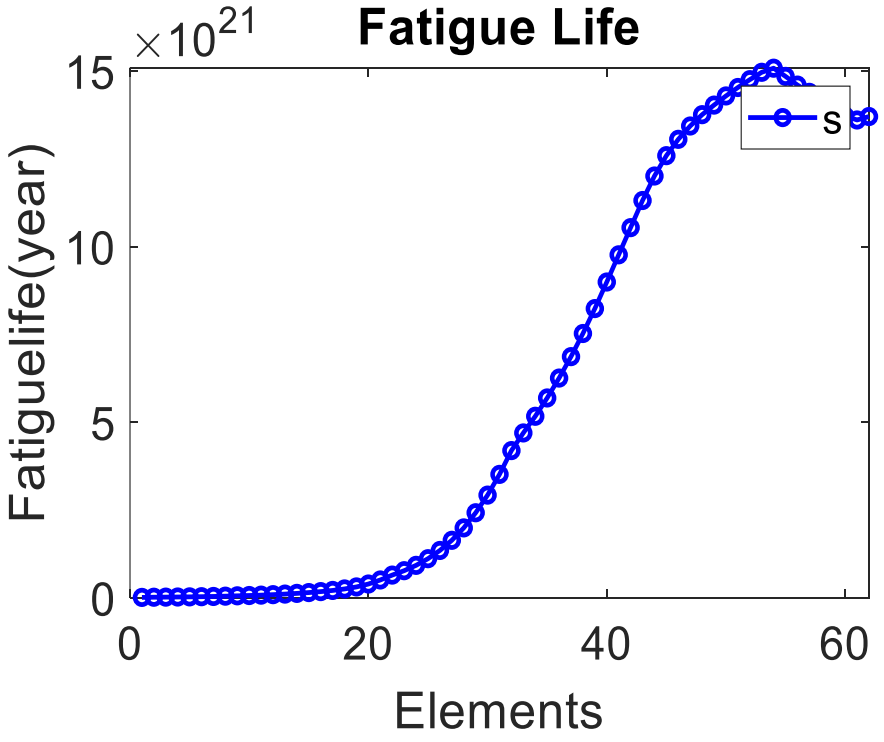

Figure 77: Case 1 Fatigue life (years) vs Length (Elements)

Case 2 – Hs = 2.5m Tp = 6.5s

Figure 78 depicts the stress range along the cable's length utilising the conservative Goodman approach:

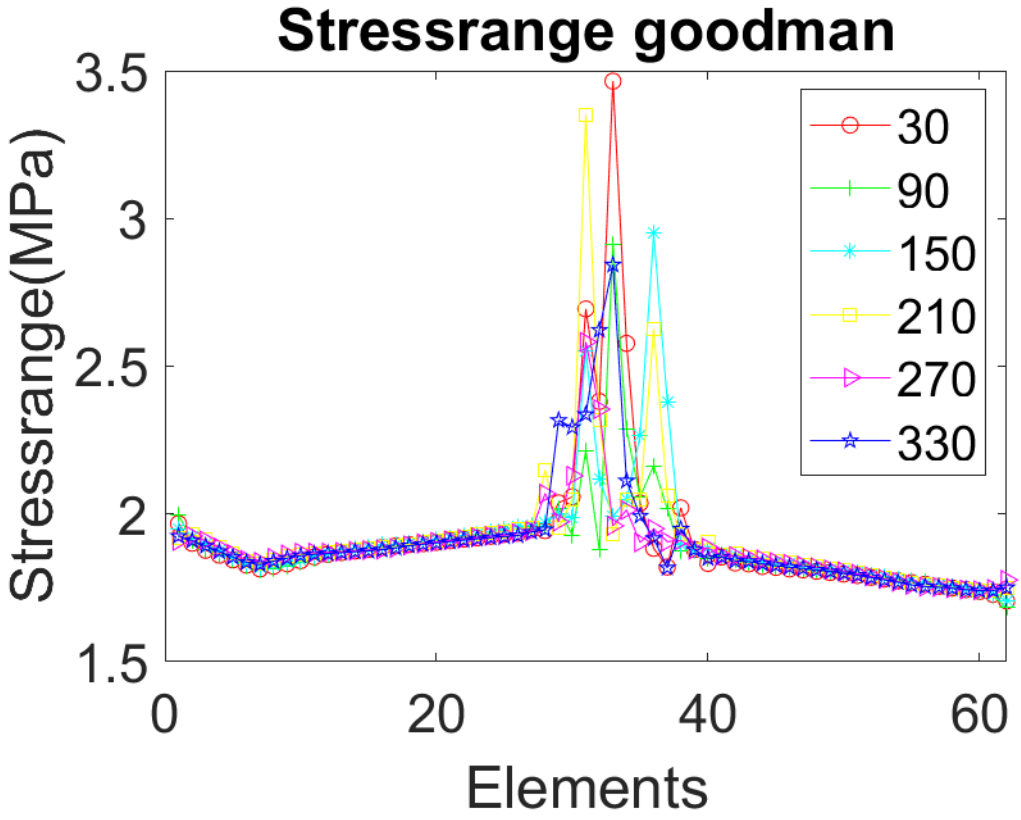

Figure 78: Stress Range Goodman (MPa) vs Length (Elements)

From Figure 78 the maximum stress range is located at element 33 (approximately the middle of segment 8) at 30º through the cross-section. At this location the maximum stress range is 3.46461 MPa, notably greater than the stress ranges found for case 1.

Agreeing with the stress range for case 2, the greatest fatigue damage can also be found at element 33 at 30º with the greatest total fatigue damage (Goodman) of 5.3711e-17 shown in Figure 79.

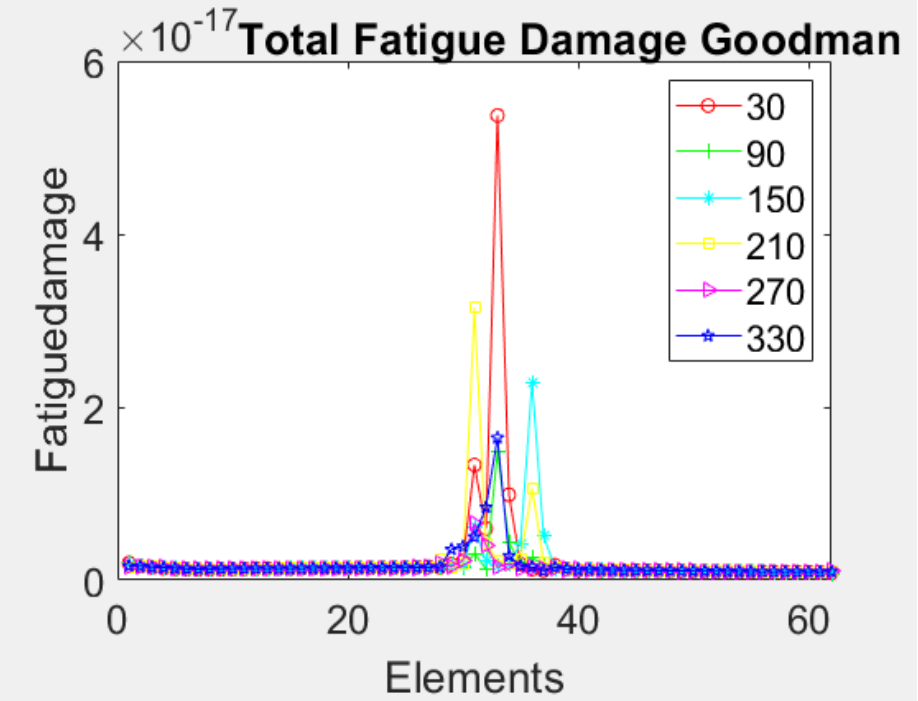

Figure 79: Case 2 Total Fatigue Damage vs Length (Elements)

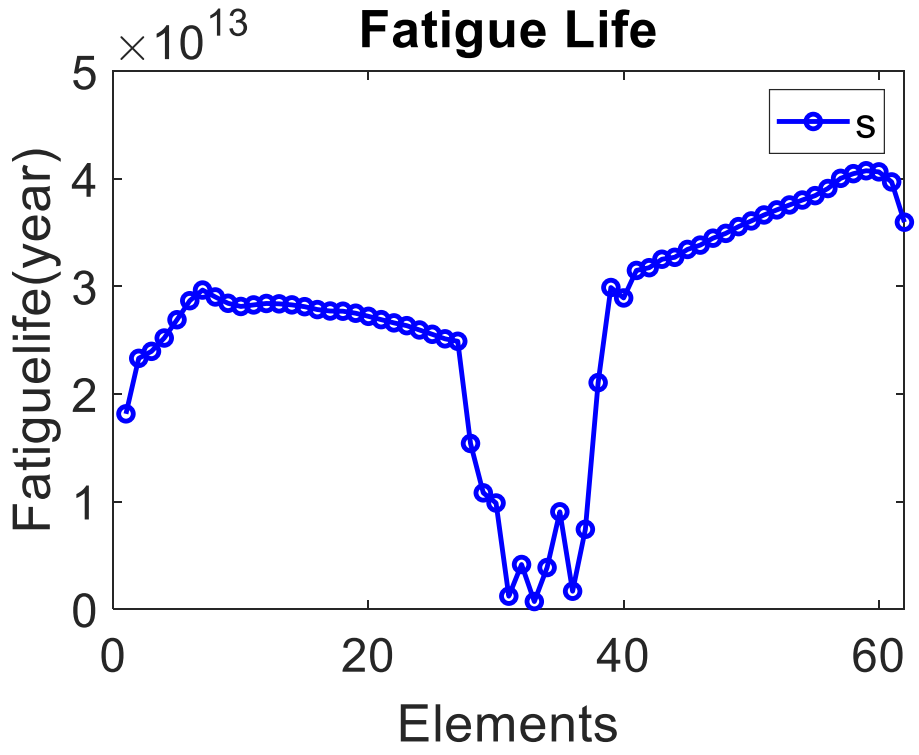

Figure 80: Case 2 Fatigue Life (years) vs Length (Elements)

The most conservative fatigue life for Case 2 is found in element 33 and has a conservative fatigue life of approximately 7.096e+11 years. The maximum fatigue life of the cable in case 2 is 4.076e+13 year and this is found in element 59 (end of cable near hub).

Case 3 – Hs = 5.5m Tp = 8.5s

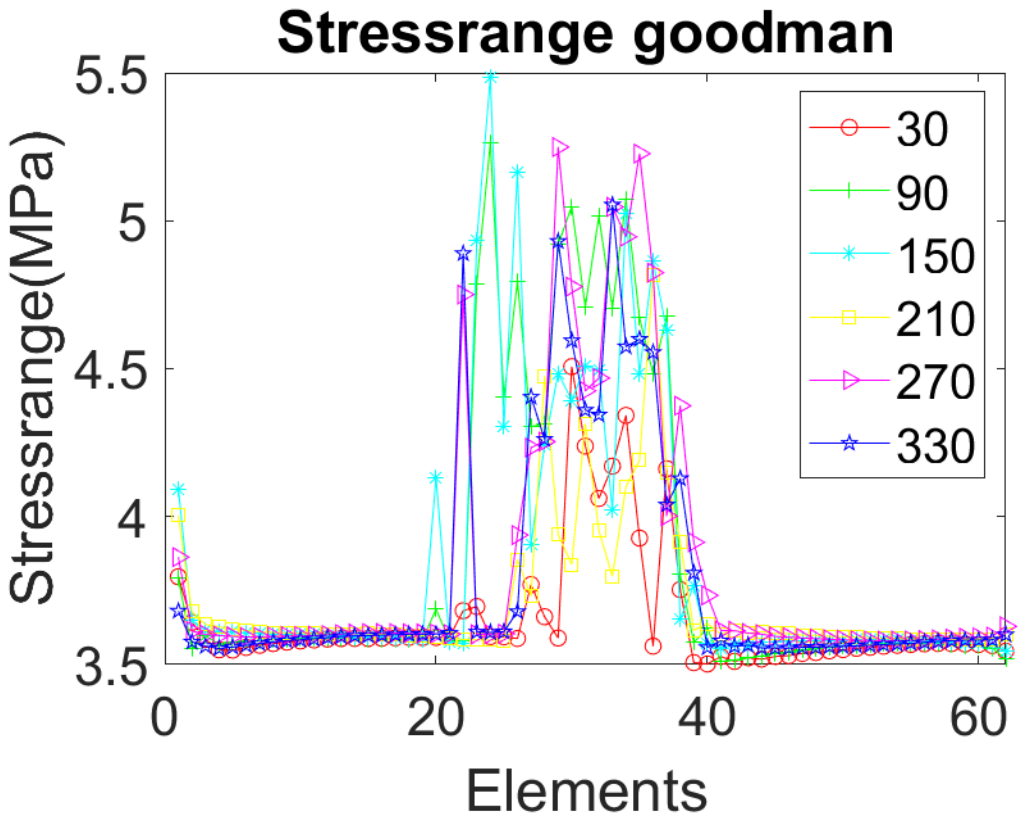

Figure 81: Case 3 Stress Range Goodman (MPa) vs Length (Elements)

Figure 81 highlights the maximum stress range and that it occurs at element 24 (approximately 1/3 of the cables length from the WEC). From MATLAB, the maximum stress range is 5.48346 MPa and is located at 150º on the cross-section of the cable.

The total fatigue damage (Goodman) for case 3 is illustrated in Figure 82:

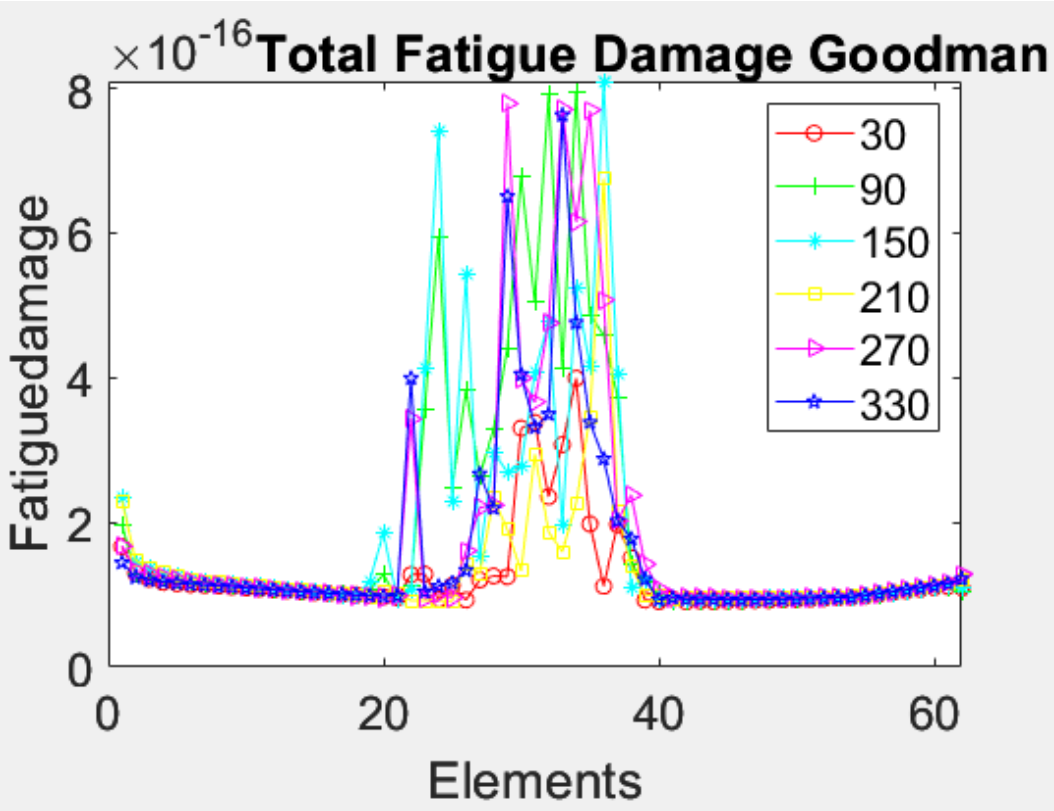

Figure 82: Case 3 Total Fatigue Damage vs Elements (Elements)

Analysing Figure 82 it can be found that the greatest fatigue damage occurs approximately in the centre, the maximum fatigue damage is located on element 36. Element 36 has a calculated fatigue damage of 8.09492e-16 and is found at 150º on the cable's cross-section.

Figure 83 illustrates the fatigue life through the cable's length for case 3:

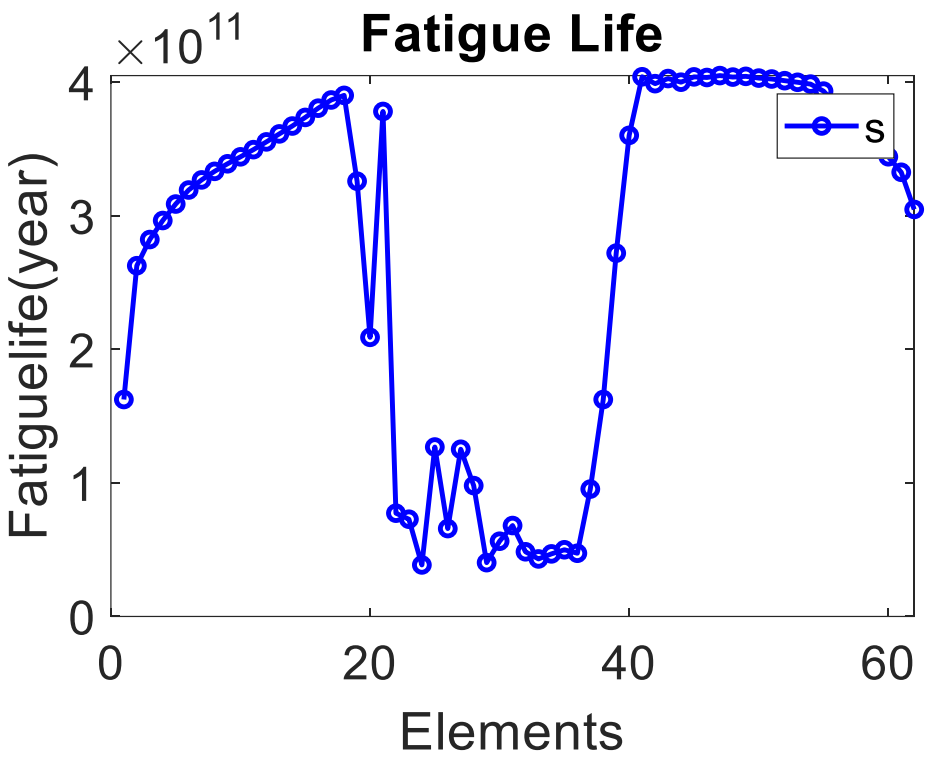

Figure 83: Case 3 Fatigue Life (years) vs Length (Elements)

From Figure 83, it can be found that the minimum fatigue life lies throughout the centre of the cable with the minimum fatigue life calculated at element 24. The respective element has a fatigue life of 3.858e+10 years.

4.1.3 MATLAB Relative Displacements

The global positions were extracted from SIMA and post-processed through MATLAB to provide more useful relative displacements. Relative displacements were calculated for all three sea states and for two separate locations. The locations of interest were chosen based off the MATLAB fatigue analysis. From the fatigue post-processing analysis, it was common that the beginning of segment 8 (main portion of dynamic power cable excluding bending stiffeners) and the centre of the cable had the greatest accumulative fatigue damage. As a result of this, elements 1 and 4 and elements 91 and 94 were chosen to best capture these areas of interest and to calculate relative displacements. These displacements are valid for a cable element having a length of 2.1m. The relative displacements align with the global coordinate system illustrated in section 4.1.5.

Tables 13 and 14 represent the relative displacements for both nodes 1 and 4 and nodes 91 and 94 for case 1. For case 1 both sets of displacements were taken at the same time step of 2352, this was selected from the mean total displacement plot as described in section 4.1.5.

Table 13: Case 1 Relative Displacements Nodes 1 and 4

Nodes 1 & 4	Displacement [m]
x-displacement (time step 2352)	-0.0102
y-displacement (time step 2352)	-1.36E-04
z-displacement (time step 2352)	-0.0044

Table 14: Case 1 Relative Displacements Nodes 91 and 94

Nodes 91 & 94	Displacement [m]
x-displacement (time step 2352)	-3.47E-04
y-displacement (time step 2352)	2.20E-03
z-displacement (time step 2352)	0.0012

Tables 15 and 16 represent the relative displacements for both nodes 1 and 4 and nodes 91 and 94 for case 2. For case 2, to separate time steps were chosen as the total displacement at these time steps better aligned with the mean total displacement.

Table 15: Case 2 Relative Displacements Nodes 1 and 4

Nodes 1 & 4	Displacement [m]
x-displacement (time step 8047)	-0.0438
y-displacement (time step 8047)	0.1186
z-displacement (time step 8047)	-0.0068

Table 16: Case 2 Relative Displacements Nodes 91 and 94

Nodes 91 & 94	Displacement [m]
x-displacement (time step 1282)	-0.0251
y-displacement (time step 1282)	2.43E-02
z-displacement (time step 1282)	-0.0689

Tables 17 and 18 represent the relative displacements for both nodes 1 and 4 and nodes 91 and 94 for case 3. For case 3, the same time step for both locations were also used and was derived following the same process described in section 4.1.5.

Table 17: Case 3 Relative Displacements Nodes 1 and 4

Nodes 1 & 4	Displacement [m]
x-displacement (time step 5110)	-0.3806
y-displacement (time step 5110)	-0.1463
z-displacement (time step 5110)	-0.1978

Table 18: Case 3 Relative Displacements Nodes 91 and 94

Nodes 91 & 94	Displacement [m]
x-displacement (time step 5110)	2.78E-04
y-displacement (time step 5110)	1.69E-01
z-displacement (time step 5110)	0.1417

4.1.4 Global Analysis Results Discussion

When comparing the results obtained from the Global Analysis SN approach, it can be found that they agree well with previous literature. In a paper recently written in 2021 [67] although not the exact same model was used, accumulated fatigue damages of a similar magnitude were found for the power cable and hence a similar fatigue life. Although different approaches were used to calculate displacements, it is found that if the two different models were scaled to the same size, similar displacements would be obtained.

Overall, it was observed that from the results it can be found that there are two locations of interest. From figures 25, 28 and 31 it can be found that the fatigue damage accumulation peak shifts for different sea states. For case 1, figure 25 highlights that the greatest fatigue damage occurs near the beginning of the cable. In contrast to this, figures 25 and 28 illustrate that the greatest fatigue damage has shifted toward the middle of the cable. As a result of this observation, two elements that would represent these locations well were selected, these elements consisted of nodes 1 and 4 and nodes 91 and 94. These nodes were selected to allow a further analysis utilising a local FEA model of these respective locations.

The main finding, and as expected, was that for harsher sea states the fatigue damage accumulation increases and hence the overall predicted fatigue life of the cable significantly decreases. It was found that as conditions become harsher *i.e.,* moving from Case 1 to Case 3, the conservative fatigue life reduced from 6.05e+21 years to 3.858e+10 years. This significant decrease in fatigue life is due to a harsh increase in accumulated fatigue damage, Figure 84 below highlights such.Upon further post-processing, relative displacements for two sections along the power cable were achieved. The two areas of interest were located at

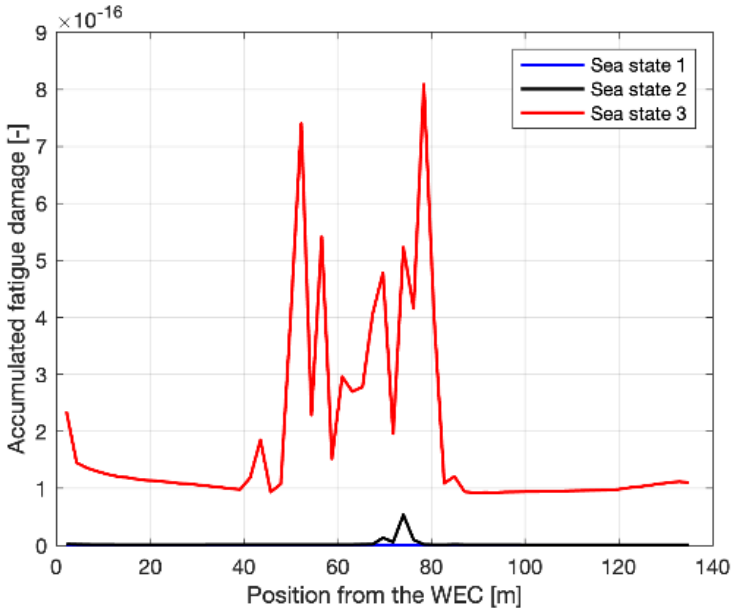

Figure 84: Accumulated Fatigue Damage vs Position from WEC [m] for all sea states

nodes 1 and 4 (near the WEC) and nodes 91 and 94 (middle of cables length), these were chosen from the fatigue damage post processing. From the displacement results, it was found that as harsher sea conditions are introduced, the relative displacements increase significantly. Expressing the relative displacements as strains more effectively highlights the nature of the displacements for each sea state. For sea state 1,2 and 3 for nodes 91 and 94 (centre of cable), the average strain over the time series was 0.3078%, 1.641% and 5.475% respectively and hence highlights the significant increase in relative displacements as sea states become harsher.

Overall, these results highlight that the accumulated fatigue damage associated with the conductors, calculated using the SN approach, are very small and produce a predicted fatigue life significantly larger than the target design life of 25 years.

4.2 Fretting Results

This section will outline the effect the loading force and sliding distance has on the life and wear depth on the copper wire within an MDC. The initial simulations were conducted with the following material properties shown in Table 19

Table 19: Conductor Material Properties

Material	Young's Modulus (GPa)	Poisson's Ratio	Vickers Hardness (MPa)	Dimensional Wear Coefficient (MPa^{-1})
Class 2 Copper	97	0.34	50	2×10^{-7}

These values were taken from an inter-wire fretting paper for subsea power cables by Poon *et al* [68]. These were chosen as it is a realistic material model for the fretting case studied in this project.

The geometry of the wire was also determined from the same paper written by Poon *et al*.

Table 20: Wire Geometry

Radius (mm)	1.25
Width (Flat) (mm)	2.5
Length (Flat) (mm)	1.25
Width (Contact Area) (mm)	0.5
Length (Contact Area) (mm)	0.35

4.2.1 Model Verification

The first step was to verify the current model with the existing 2D model. This was done by running the fretting simulation with the same input parameters shown in Table 21.

Table 21: Fretting Parameters

Material	Class 2 Copper
Loading Force (F_N)	0.194 N
Sliding Distance	200 μm
COF	0.8
Number of Sliding Steps	180
Cycle jump	100

The value of $F_N = 0.194N$ was also used from the paper produced by Poon *et al* [68]. Without being able to model the inter-wire contact due to the global motion of the MDC, this value was chosen as a realistic value to occur in the fretting process.

The results, using this applied load are provided in Figure 85.

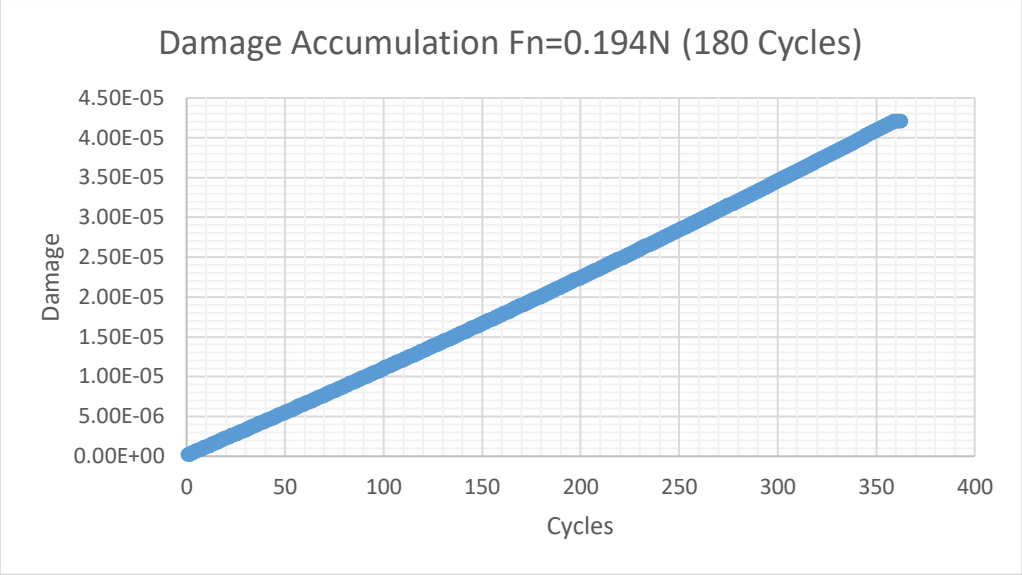

Figure 85: Damage Accumulation Fn=0.194 N (180 Cycles)

This shows that the damage increases linearly with the number of cycles. This means the data can simply be extrapolated to D=1 to estimate the life of the wire. This value is reached after 8558696 cycles. As the data varies exponentially linearly, this allows for the simulations to be run with fewer cycles without much reduction in accuracy. This was done as it significantly reduces the computational time of the simulation.

The same simulation was run again with 50 sliding cycles to reduce the computational cost. This will result in a very small maximum wear depth, however, it still allows for adequate comparison between the different fretting results. These new results are given in Figure 86.

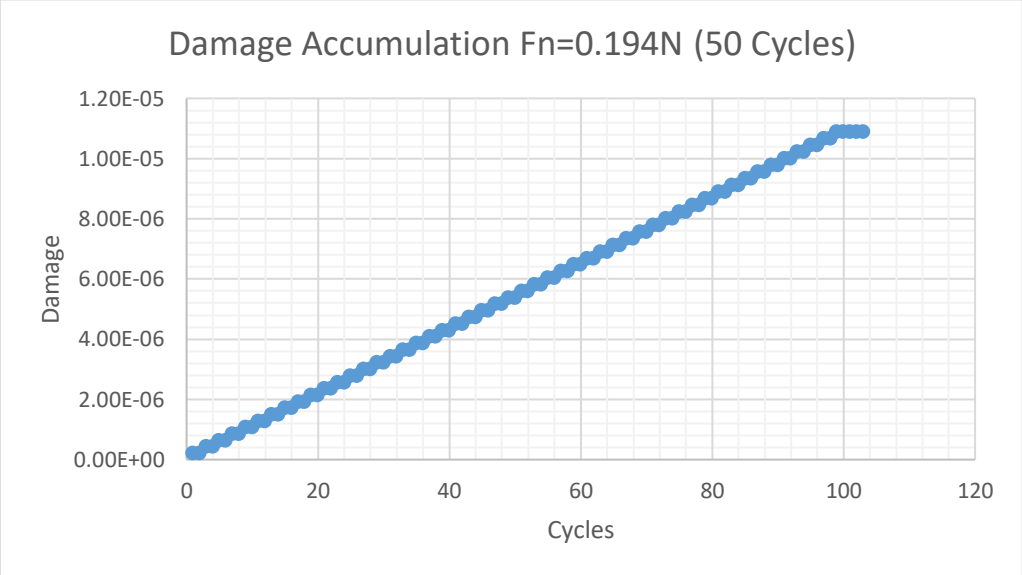

Figure 86: Damage Accumulation Fn=0.194 N (50 Cycles)

From this simulation, the fatigue life is estimated as 9185840 cycles. This is a 7.3% increase from the previous simulation, however, as the purpose of this fretting study is to conduct a sensitivity analysis, this small discrepancy in the fatigue life is deemed acceptable.

4.2.2 Variable Force Results

The simulation was run again with different applied loads to study its impact on the predicted life of the wire.

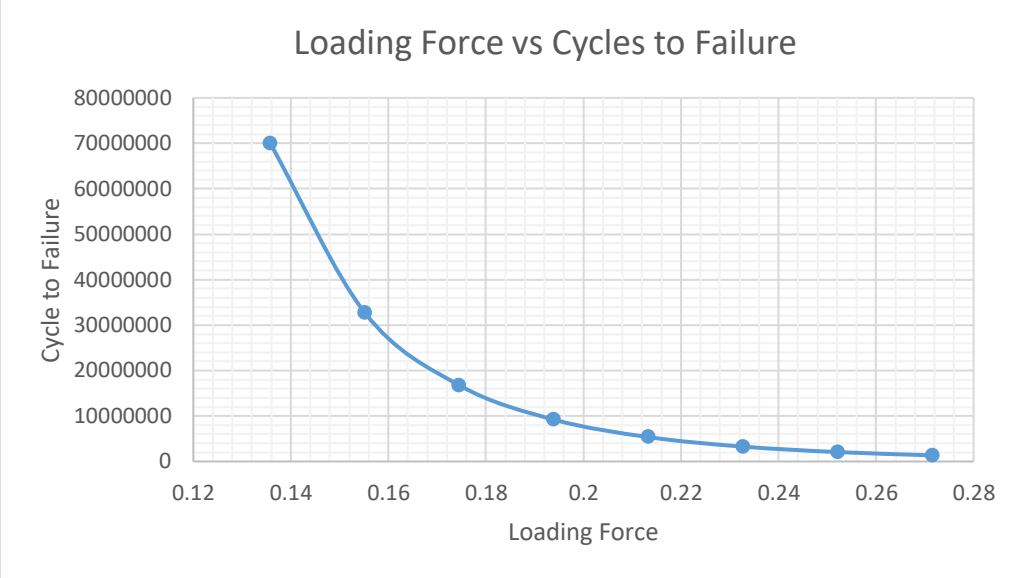

Figure 87: Loading Force vs Fatigue Life

Figure 87 shows a relationship of exponential decay between cycles to failure and increasing loading force. This implies that at fatigue life of the cable reduces significantly with each incremental increase when the force is low and begins to plateau as the force continues to increase. The difference between the first two points is 53.2% whereas the difference between the last two points is 34.5%.

The wear depth is found by plotting the motion in the y-direction of the central node on the lower contact surface. The maximum wear depth will occur in the centre of the contact so the displacement of this node can be assumed to be the maximum wear depth.

The maximum wear depth for each case is also given in Figure 88.

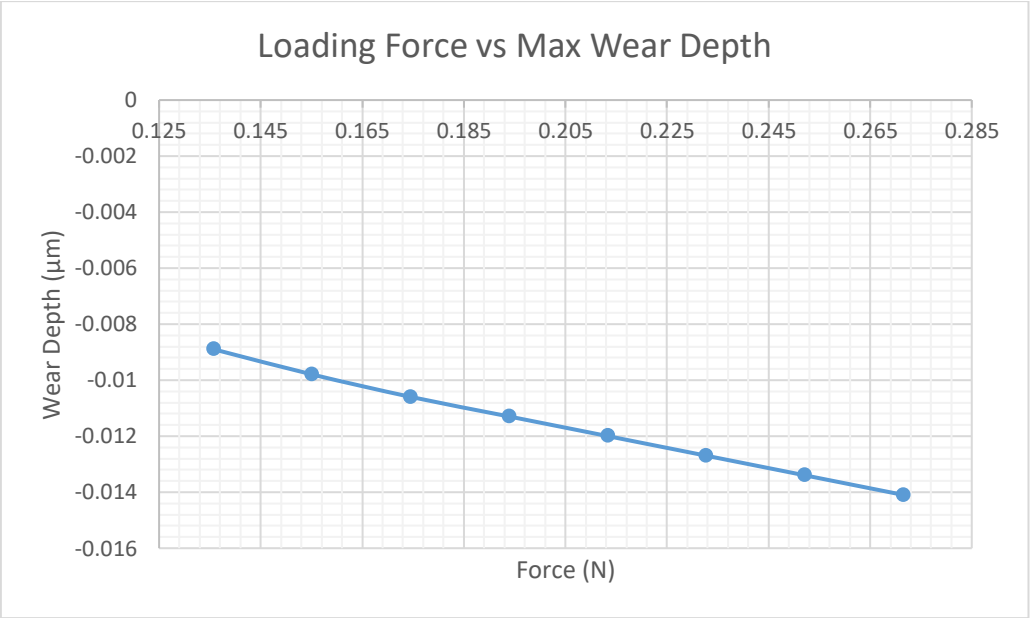

Figure 88: Loading Force vs Max Wear Depth

Unlike the fatigue life, the maximum wear depth varies linearly with the applied loading force. With each incremental increase of 10% to the applied load, the wear depth only increased by on average 6.8%. This demonstrates that the applied load has a much greater effect of the fatigue life of the cable compared to the maximum wear depth.

4.2.3 Variable Sliding Distance Results

The simulations were also run again using a varied sliding distance. Again, without an accurate inter-wire local model or experimental data, it is difficult to determine the magnitude of the sliding distance. It is for this reason that a sensitivity analysis will be conducted to determine its effect on the maximum wear depth and fatigue life of the cable.

From incrementally increasing and decreasing the sliding distance, the fatigue life results are given:

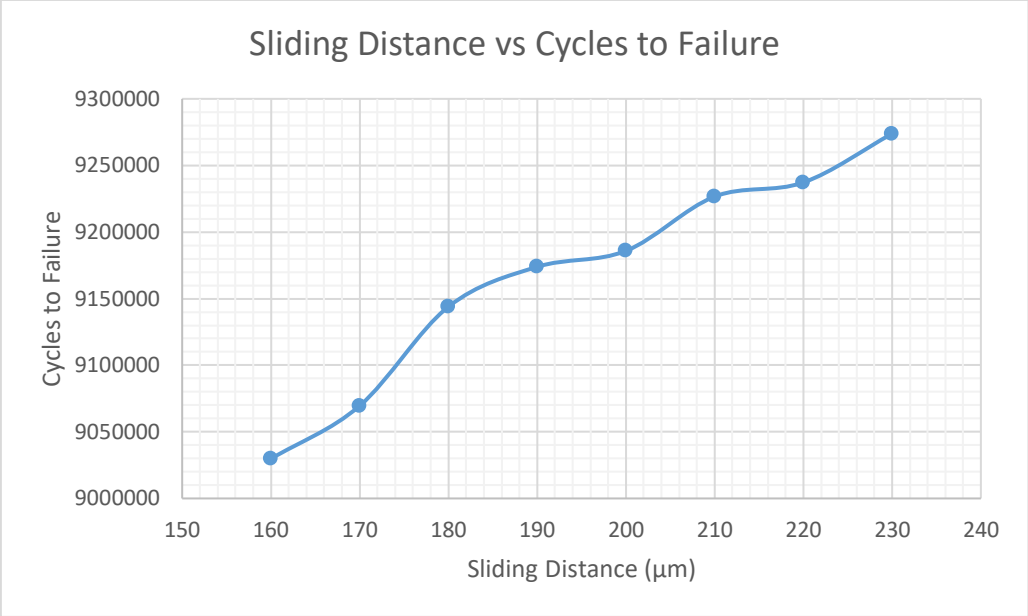

Figure 89: Sliding Distance vs Cycles to Failure

Figure 89 shows that the sliding distance also influences the fatigue life of the cable. It demonstrates that the number of cycles until failure increases with the fretting sliding distance. This behaviour is likely due to the fact that for a smaller sliding distance, the wear is concentrated into a smaller area and causes cracks to initiate sooner. However, the effect of the sliding distance on the fatigue life is much weaker than that of the loading force. A decrease of the sliding distance by 10% only resulted in a reduction of 0.46%.

The effect on the wear depth is also given in Figure 90.

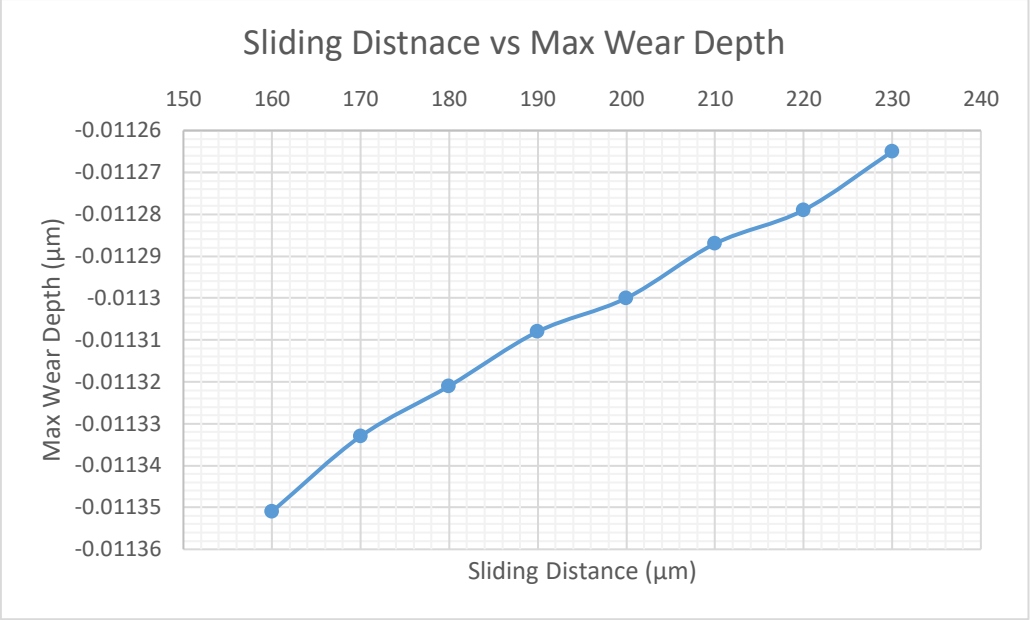

Figure 90: Sliding Distance vs Max Wear Depth

This further demonstrates that as the sliding distance decreases the damage due to fretting increases. As the sliding distance increases, the width of the fretting scar will obviously increase but this will also result in a shallower scar.

4.2.4 Varied COF Results

The simulations were then run with a number of different COF values. As the COF is not an inherent property of a part or material, it is also challenging to use a realistic result for this without practical experiments. The effect of the COF on the fatigue life of the wire is given in Figure 91.

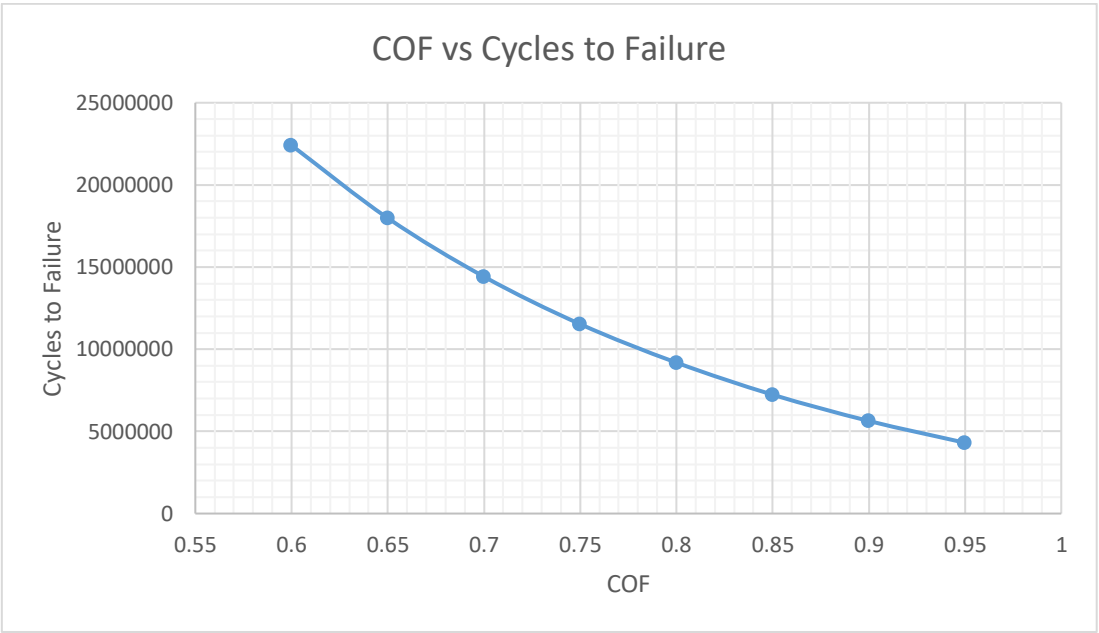

Figure 91: COF vs Cycle to Failure

This demonstrates that when the COF increases, the fatigue life of the wire decreases. It decreases with roughly a linear relationship with an average decrease in fatigue life of 18.6%

with each increment of 0.05. This relationship is to be expected as increasing the COF will naturally induce more damage on the contact surfaces and increase the rate of crack initiation.

The maximum wear depth results are also provided in Figure 92.

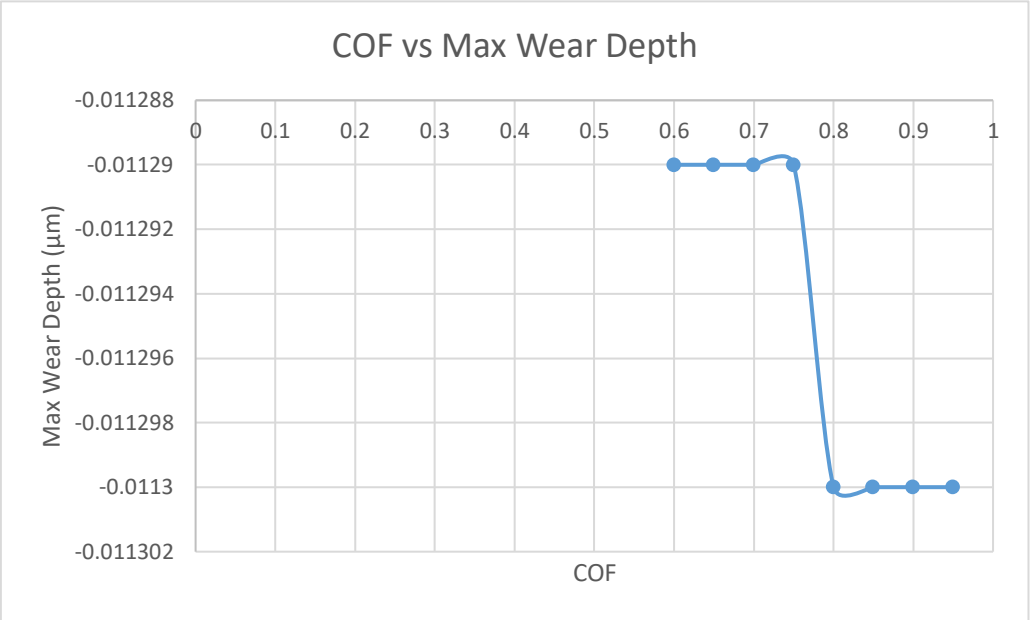

Figure 92: COF vs Max Wear Depth

This graph shows there is not much of a relationship between the maximum wear depth and the COF as the change in negligible. This is better demonstrated if all the maximum wear depth results are plotted on the same graph. This combined results plot is given in Figure 93 below.

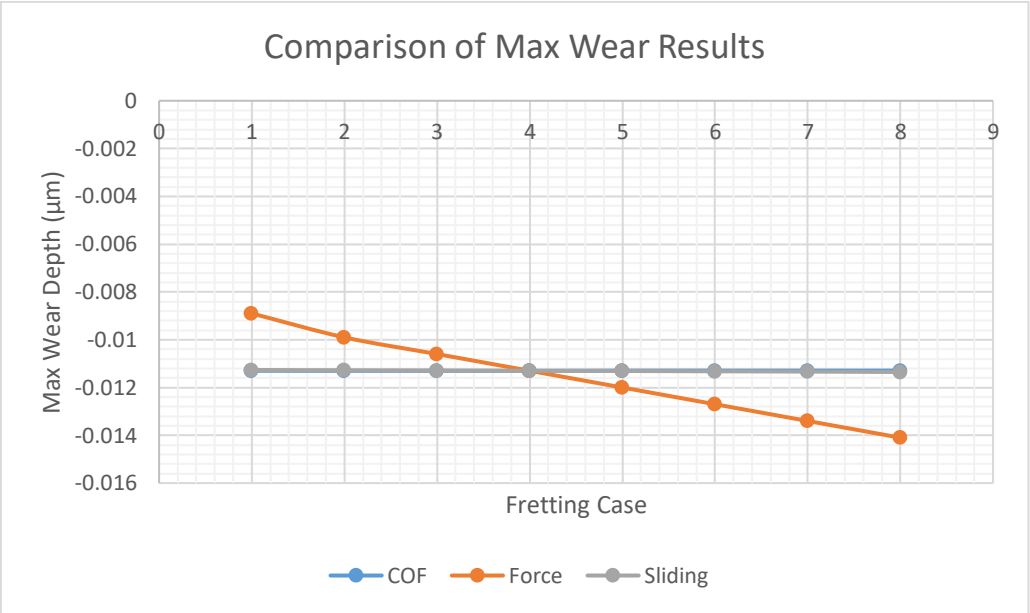

Figure 93: Comparison of Max Wear Results

This demonstrates that the variation of loading force has a much bigger influence on the maximum wear depth than either the sliding distance or COF for this model.

A comparison of the fatigue life results is also given in Figure 94.

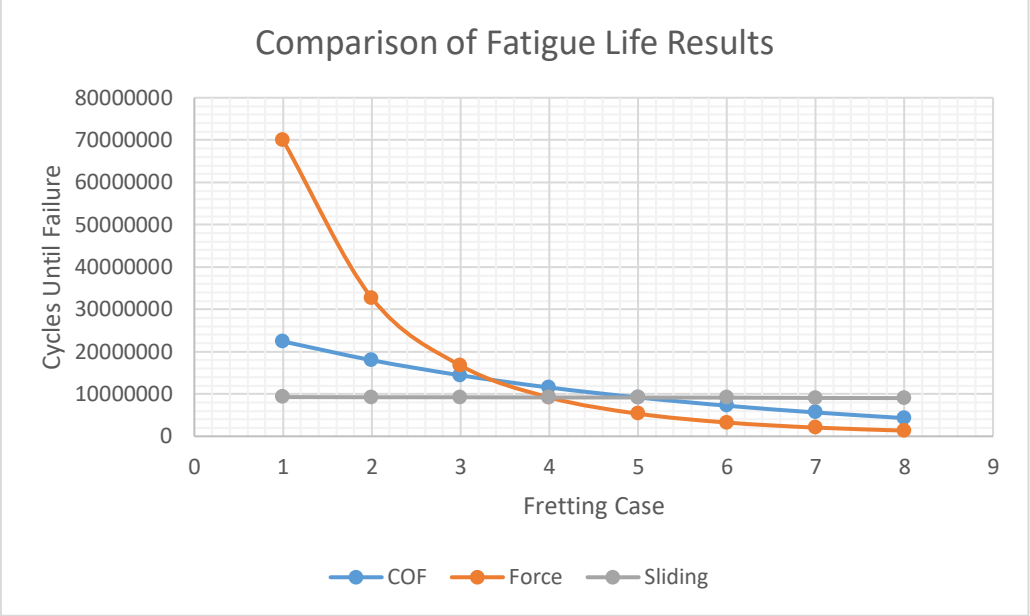

Figure 94: Comparison of Fatigue Life Results

This further demonstrates that the loading force has the biggest impact on the interwire fretting problem. When compared to the other values, it also shows that the sliding distance has very little effect on the number of cycles until failure.

4.2.5 Material Comparison Results

As the loading force has been identified as the most influential parameter in this study on the fatigue life of the cable, its effect was studied again on different conductor materials. Although copper is the most common conductor material, alternatives could provide more favourable mechanical or electrical properties.

Two other possible conductor materials, chosen for this study, are silver and stainless steel 302. The relevant mechanical properties for these are given in Table 22.

Table 22: Fretting Material Mechanical Properties

Material	Young's Modulus (GPa)	Poison Ratio	Vickers Hardness (MPa)	Wear Coefficient (MPa^{-1})
Copper	97	0.34	50	$2x10^{-7}$
Silver	71.5	0.38	251	$5.5x10^{-6}$
Stainless steel 302	193	0.25	139	$3x10^{-8}$

These materials were put under the same conditions as before for the loading cases.

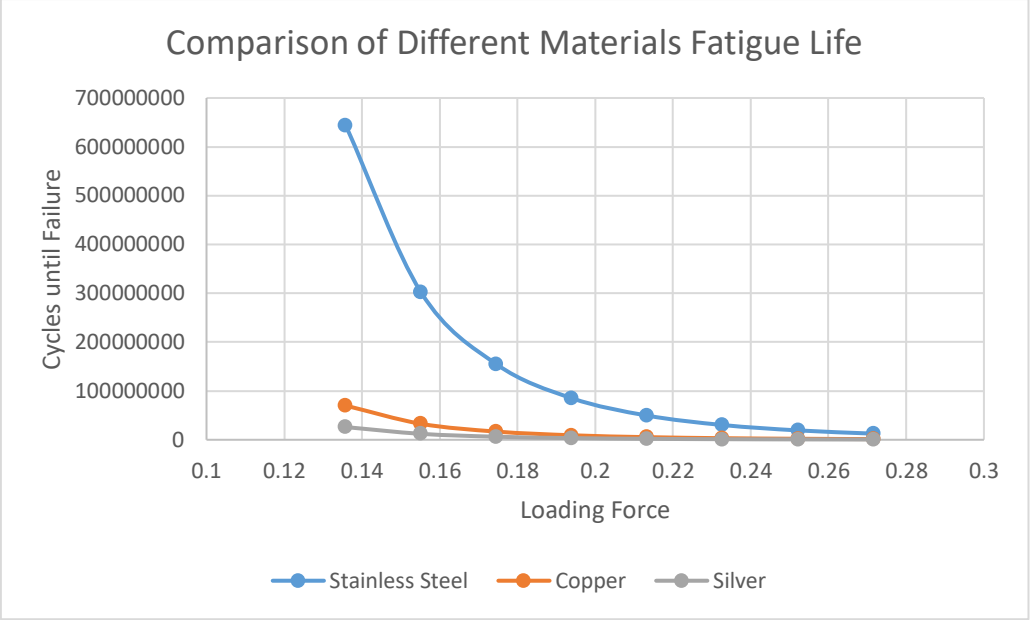

Figure 95: Comparison of Loading Force of Material Fatigue Life

Figure 95 shows that the stainless-steel conductor has a significantly higher fatigue life than the other two materials. This is due to its superior material properties, mainly the high Young's modulus. Silver has the highest hardness and a lower wear coefficient than copper, however, still has a lower fatigue life. This implies that it is the Young's modulus that has the greatest impact on fatigue life.

A similar conclusion can be drawn from the maximum wear depth results shown in Figure 96.

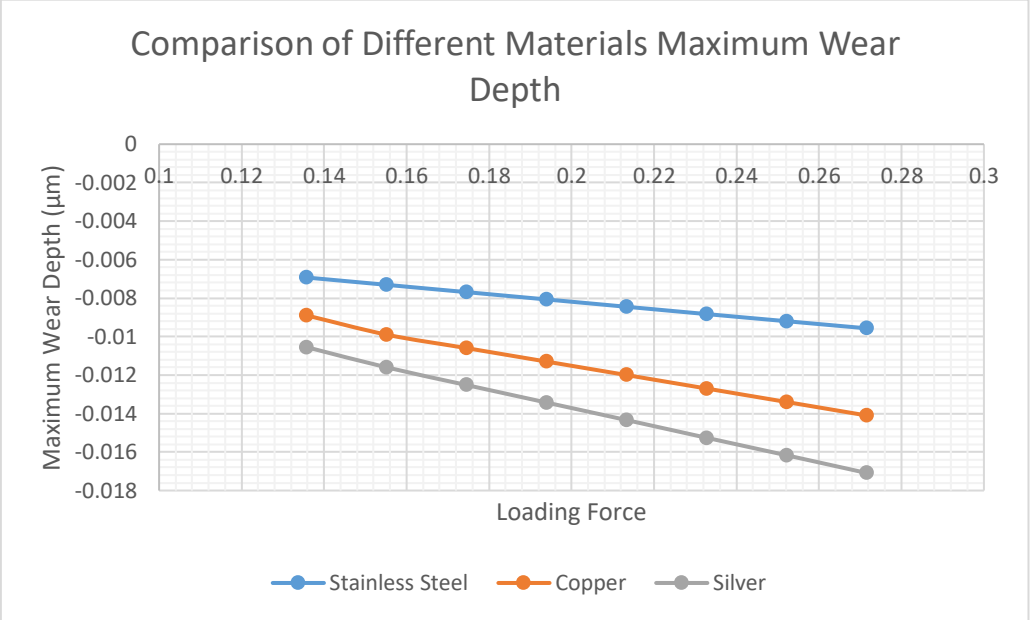

Figure 96: Comparison of Loading Force of Maximum Wear Depth

This highlights that steel again has the most desirable mechanical properties as it results in the smallest wear scar. However, as these materials are used in a conductor, their electrical properties must also be considered.

Table 23: Material Electrical Conductivity

Material	Electrical Conductivity (S/m)
Copper	$5.96x10^7$
Stainless Steel	$1.45x10^6$
Silver	$6.30x10^7$

As shown in Table 23, stainless steel has a significantly lower electrical conductivity that the other two materials. It is for this reason that it is not often used as an electrical conductor. However, if the induced stresses for this conductor are remarkably high, such as that in MDC's, a material with higher mechanical properties but lower electrical benefits could be considered to improve fatigue life.

4.2.6 Discussion of Fretting Results

These results seem to be valid when comparing them to results from relevant literature. In a paper written by T. Liskiewicz *et al* [69], the impact of different loading conditions was analysed on a titanium carbide. This study used displacement amplitudes to study the loading conditions rather than applied force and also utilised an energy dissipation technique to predict the lifetime of the part. Despite these differences the results are similar:

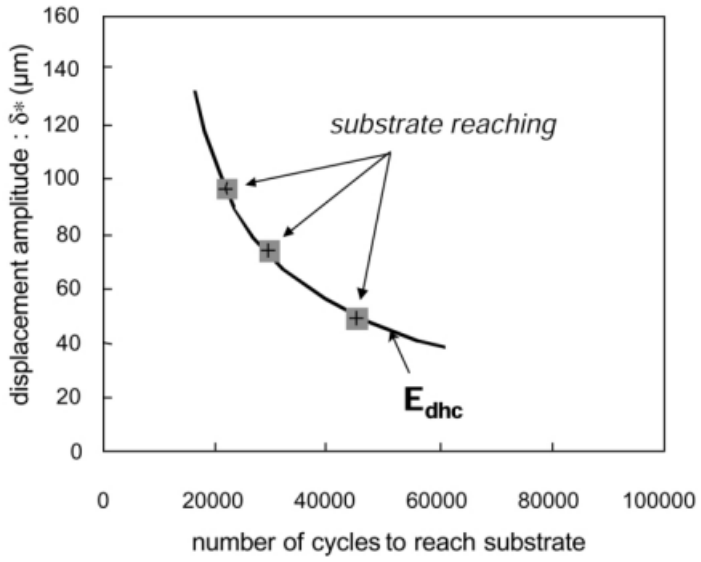

Figure 97: Energy Wohler wear chart (illustration of the accumulated energy wear damage approach) [69]

The numerical results differ due to the difference of material properties, loading and fretting conditions. However, the shape of the graph, provided in Figure 97, is very similar to that found in this study.

The results of the sliding amplitude can also be verified with literature. In another paper, by S.R. Pearson *et al* [70], the wear volume is compared with the variation of slip amplitude:

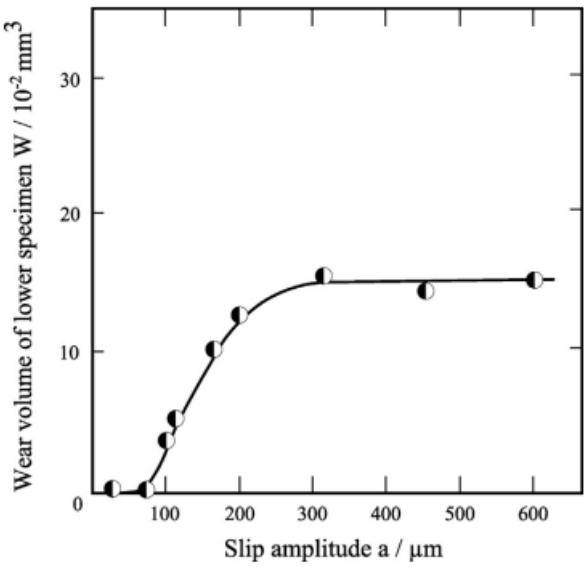

Figure 98: Wear volume as a function of slip amplitude [70]

Figure 98 shows that after a certain sliding distance is reached, the amount of wear volume or maximum wear depth plateaus and no longer increases with the slip amplitude. This behaviour can also be found in the results of this study.

Another fretting study, conducted by Andrés Úsuga *et al*[71], analyses the effect of the coefficient of friction on the crack nucleation behaviour. This paper also utilises Abaqus to study this phenomenon and shows good similarity to the results of this paper.

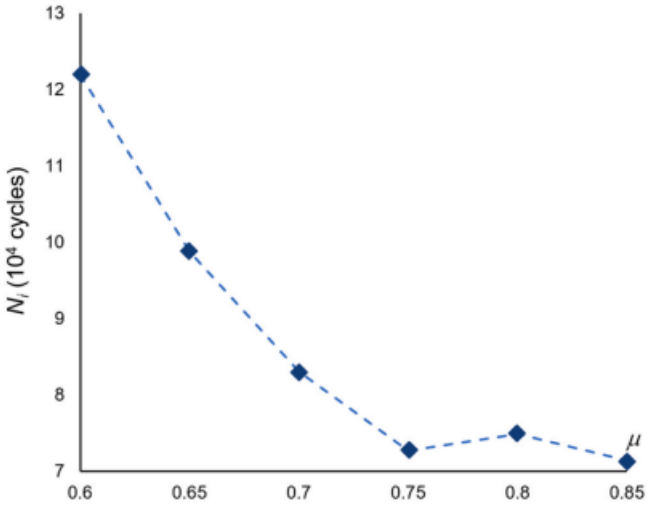

Figure 99: Crack nucleation life as a function of CoF [33]

In Figure 99 a decrease in the fatigue life of the specimen occurs as the COF increases. There is excellent similarity between the results between COF of 0.6 and 0.75 as both result in a decrease in the number of cycles of roughly 41%. There is some discrepancy after this point as the results from the literature shows the fatigue life plateaus as the COF continues to increase. Although the results from this study do show a slight decrease in gradient as the COF continues to grow, it is not as evident as in the literature.

4.3 Mechanical Stress Results

This section outlines the effect mechanical stress has on the propagation of water tree cracks within the XLPE insulation layer of the marine dynamic cable. Determining the fatigue life due to mechanical stresses is a multifaceted process that first relies on the results from the Global SIMA model. From SIMA the fatigue damage accumulation was calculated for varying sea states. The importance of these results in not just determining the fatigue damage accumulation, but additionally where such damage is taking place with respect to the length of the cable. Therefore, the fatigue damage accumulation was taken at the most critical location along the cable. Once this location was identified the global displacements could be employed from this location and inputted into the local model on ANSYS. Implementing the global displacements in ANSYS allows for the determination of local axial stresses present within the XLPE insulation layer. Moving forward, this section attempts to provide a fatigue life utilising the local insulation stresses.

4.3.1 Sea State Occurrences

Utilising the MATLAB fatigue analysis post-processing code, time series histograms of total stress at the maximum fatigue damage can be plotted for all three sea states. For the purpose of this thesis, the stress ranges are being taken from the location along the cable with the greatest fatigue damage accumulation. These locations are highlighted in Section 4.1.2.

Table 24 illustrates a tabulated format of the time series histogram of the total stress at the maximum fatigue damage location for Case 1.

Table 24: Case 1 Time Series Histogram Total Stress Max FDA

Case 1 1200s - Time series histogram of total stress at the maximum fatigue damage	
Stress Range [MPa]	Number of Occurrences
0.05	357
0.15	154
0.25	1

For case 1, a calm sea state, it is evident that there is a low maximum stress range and very few occurrences. For the 1200s period, the greatest stress range of 0.25 MPa was only recorded once throughout the 1200s simulation.

Table 25 illustrates a tabulated format of the time series histogram of the total stress at the maximum fatigue damage location for Case 2.

Table 25: Case 2 Time Series Histogram Total Stress Max FDA

Case 2 1200s - Time series histogram of total stress at the maximum fatigue damage	
Stress Range [MPa]	Number of Occurrences
0.2	255
0.6	78
1	12
1.4	0
1.8	1
2.2	1
2.6	0
3	1
3.4	1

For case 2, it can be found that the greatest stress range recorded increased significantly to approximately 3.4 MPa and this was also only found once throughout the 1200s simulation.

Table 26 illustrates a tabulated format of the time series histogram of the total stress at the maximum fatigue damage location for Case 3.

Table 26: Case 3 Time Series Histogram Total Stress Max FDA

Case 3 1200s - Time series histogram of total stress at the maximum fatigue damage	
Stress Range [MPa]	Number of Occurrences
0.3	234
0.9	79
1.5	32
2.1	8
2.7	1
3.3	2
3.9	0
4.5	0
5.1	0
5.7	1

For case 3, a harsh sea state, the greatest stress range recoded has further increased to 5.7 MPa and again located once throughout the 1200s period. It can be found for all three cases, that the lower stress ranges dominate the cyclic loading. This thesis focuses on the greatest strange ranges. The reason for this is greater stress ranges would grow the crack faster than reduced stress ranges. Therefore, for fatigue life predictions the greatest stress ranges for each case were taken to incur conservative but reliable service life predictions.

4.3.2 Axial Tensile Stress within XLPE Insulation

This section highlights the results calculated for the axial tensile stresses existent within the XLPE insulation. In ANSYS the normal stress in the z-direction, see Figure 56 for co-ordinate system, was computed. Such stress replicates the axial tensile stress. It is important to note the any compressive, negative, stresses evaluated were ignored. In Section 4.3.3 these axial stresses were used to determine a fatigue life due to mechanically stressed water trees.

Initially, Sea State 1 was simulated with the extrapolated global displacements in Tables 13 and 14. Both displacements for Nodes 1 and 4 and Nodes 91 and 94 were simulated. Following simulation on ANSYS the axial stresses present in the XLPE insulation layer from Sea State 1 Nodes 4 and Nodes 91 and 94 respectively are depicted in Figures 100 and 101.

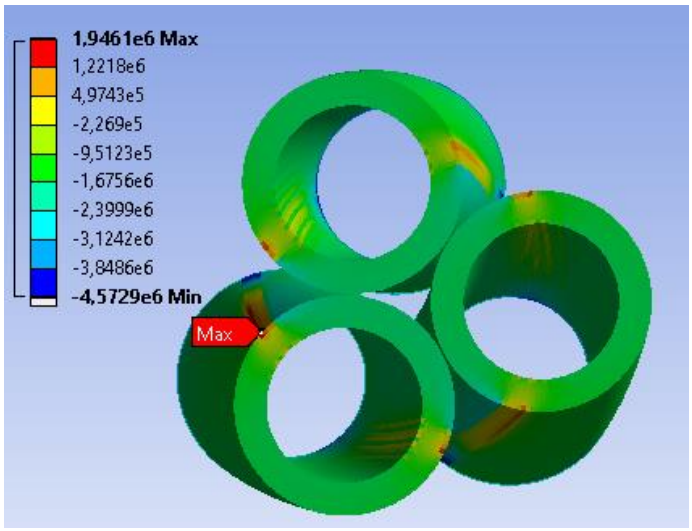

Figure 100: Sea State 1 - Normal Stress in XLPE Insulation (Nodes 1 & 4)

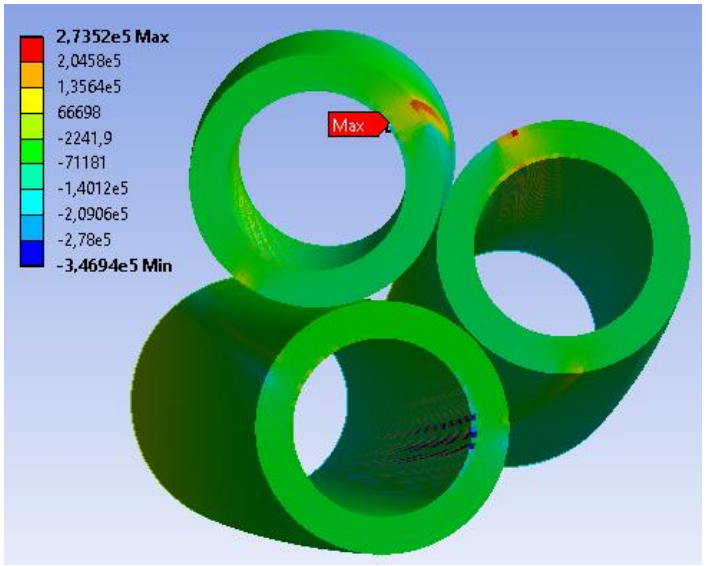

Figure 101: Sea State 1 - Normal Stress in XLPE Insulation (Nodes 91 & 94)

The axial tensile stress arising from Nodes 1 and 4 are greater than Nodes 91 and 94 for Sea State 1. As illustrated in Figures 100 and 101 the maximum stress occurs at the outer boundary of the insulation layer for both node conditions, highlighting the Kevlar ropes may have a great impact on the structural integrity of the insulation layer. Below are the maximum axial tensile stresses for Nodes 1 and 4 and Nodes 91 and 94.

$$\sigma_{axial,1-4} = 1.94\ MPa$$

$$\sigma_{axial,91-94} = 0.27\ MPa$$

In accordance with Table 8 in Section 3.3.6 the displacements created from Sea State 1 for both nodal conditions do not generate axial stress magnitudes sufficient to propagate the crack. Therefore, Sea State 1 was not included in fatigue life calculations for the cable.

Moving forward, Sea State 2 was simulated with the extrapolated global displacements in Tables 15 and 16. Both displacements for Nodes 1 and 4 and Nodes 91 and 94 were

simulated. Following simulation on ANSYS the axial stresses present in the XLPE insulation layer from Sea State 2 Nodes 1 and 4 and Nodes 91 and 94 respectively are depicted in Figures 102 and 103.

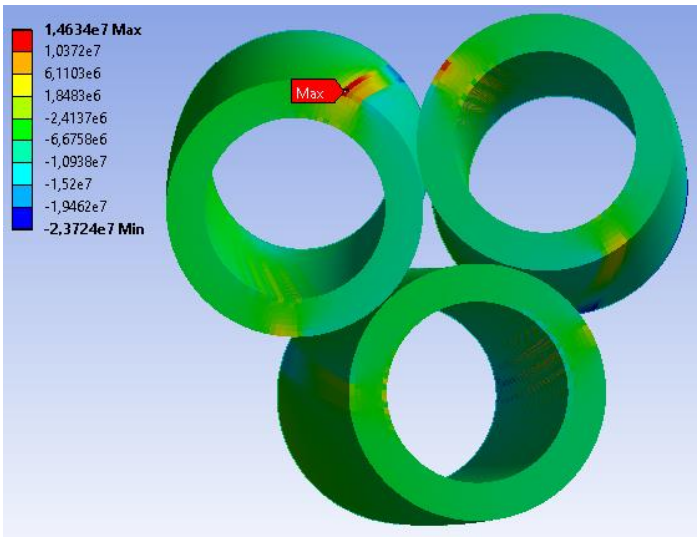

Figure 102: Sea State 2 - Normal Stress in XLPE Insulation (Nodes 1 & 4)

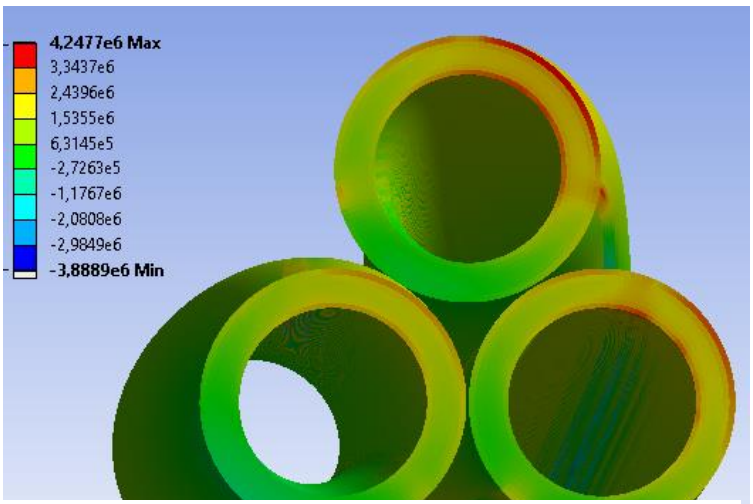

Figure 103: Sea State 2 - Normal Stress in XLPE Insulation (Nodes 91 & 94)

Like Sea State 1, the axial stress magnitudes for Nodes 1 and 4 are greater than that of Nodes 91 and 94. However, contrary to Sea State 1, the different nodal conditions for Sea State 2 establish different regions of maximum stress. For Nodes 1 and 4 the maximum stress is severely localised at a region on the outer boundary layer of the insulator. Whereas the displacements from Nodes 91 and 94 create a domain where the XLPE insulator is affected by the Kevlar ropes as well as the copper conductor wires. Below are the maximum axial tensile stresses for Nodes 1 and 4 and Nodes 91 and 94.

$$\sigma_{axial,1-4} = 14.63\ MPa$$

$$\sigma_{axial,91-94} = 4.24\ MPa$$

In accordance with Section 3.3.6, the displacements created from Sea State 2 for both nodal conditions produce large enough stress values to propagate the water tree crack. Using Equations 37 and 38 in Section 3.3, Table 27 highlights the initial crack length for the stress to have an impact on the fatigue damage of the cable for an edge and thumbnail crack with respect to Sea State 2.

Table 27: Sea State 2 - Initial Crack Length for Paris Law Initiation

Crack Geometry	Initial Crack Length Nodes 1 & 4 [mm]	Initial Crack Length Nodes 91 & 94 [mm]
Edge Crack	0.32	0.94
Thumbnail Crack	0.58	1.19

Table 27 demonstrates the importance of nodal selection along Segment 8 of the cable. For both crack geometries Nodes 91 and 94 yield initial crack lengths corresponding to 78% and 99% of the insulators critical 60% thickness criteria. Beyond this point the cable short circuits.

Finally, Sea State 3, the most severe scenario, was simulated with the extrapolated global displacements in Tables 17 and 18. Both displacements for Nodes 1 and 4 and Nodes 91 and 94 were simulated. Following simulation on ANSYS the axial stresses present in the XLPE insulation layer from Sea State 3 Nodes 1 and 4 and Nodes 91 and 94 respectively are depicted in Figures 104 and 105.

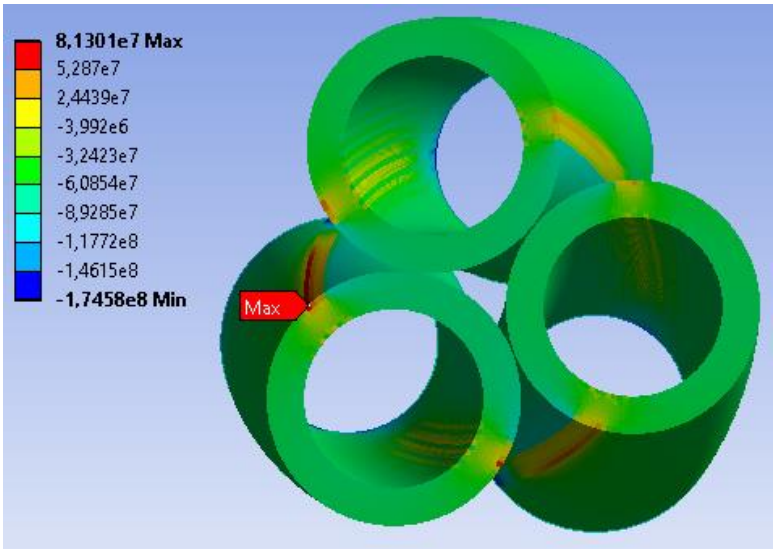

Figure 104: Sea State 3 - Normal Stress in XLPE Insulation (Nodes 1 & 4)

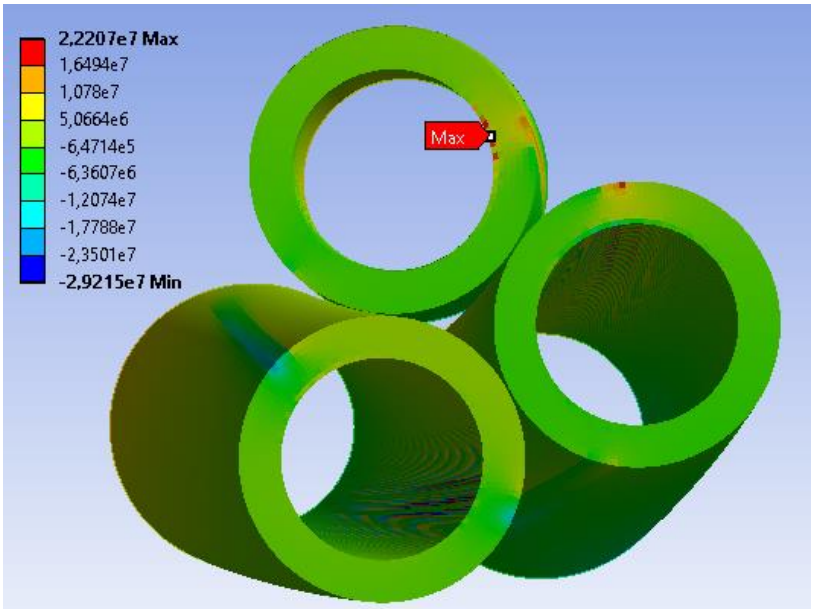

Figure 105: Sea State 3 - Normal Stress in XLPE Insulation (Nodes 91 & 94)

Sea State 3 results in immense stress values for both nodal conditions. Below are the maximum axial tensile stresses for Nodes 1 and 4 and Nodes 91 and 94.

$$\sigma_{axial,1-4} = 81.30\ MPa$$

$$\sigma_{axial,91-94} = 22.20\ MPa$$

Both stress values are large enough to cause crack propagation. Using Equations 37 and 38 in Section 3.3, Table 28 highlights the initial crack length for the stress to have an impact on the fatigue damage of the cable for an edge and thumbnail crack with respect to Sea State 3.

Table 28: Sea State 2 - Initial Crack Length for Paris Law Initiation

Crack Geometry	Initial Crack Length Nodes 1 & 4 [mm]	Initial Crack Length Nodes 91 & 94 [mm]
Edge Crack	N/A	0.17
Thumbnail Crack	0.04	0.37

Table 28 shows Sea State 3 produces extreme results. For the edge crack model, the stress within the XLPE insulator from Nodes 1 and 4 displacements generates a stress intensity factor that correlates to a smaller crack length than the initial crack length in the incremental study of 0.01 mm, hence no crack length for when the Paris Law is valid can be defined. Sea State 3 is a severe case and will not be used for fatigue life estimations due to mechanically stressed water tree cracks.

4.3.3 Determination & Discussion of Fatigue Life Predictions

This section aims to predict a fatigue life due to mechanical stresses. Referring to section 5.3.4, and as previously discussed, Sea State 1 and Sea State 3 will not be used to predict a fatigue life. Sea State 1 does not produce great enough stress to cause crack propagation, whereas Sea State 3 is an extreme sea state condition that harvests unreliable axial stress results. Considering such factors, the very probable case of Sea State 2 was used to determine a fatigue life prediction.

From the results calculated in Section 4.3.2, fatigue lives corresponding to Sea State 2 were calculated by applying the developed in-house MATLAB code and COMSOL Multiphysics fracture mechanic's model. Using MATLAB and COMSOL the fatigue life was calculated within the Paris Law domain, specifying an initial crack length and final crack length. For both nodal conditions and crack case models, the initial crack length relates to the lengths estimated in Table 27 in Section 4.3.2 whilst the final crack length was equal to 60% of insulator thickness, 1.2mm. The final crack length reflecting when the Paris Law is no longer valid, and the fatigue life can no longer be calculated since LEFM is no longer applicable. Employing the wave frequency from Section 4.3.1, Table 25 highlights the fatigue lives for an edge crack in a finitely extended plate and a thumbnail crack in a solid cylinder for both nodal situations.

Table 29: Edge & Thumbnail Crack Fatigue Lives for Sea State 2 (Both Nodal Conditions)

Crack Geometry	Wave Frequency [Hz]	Initial Crack Length Nodes 1 & 4 [mm]	Initial Crack Length Nodes 91 & 94 [mm]	Fatigue Life Nodes 1 & 4 [Hours]	Fatigue Life Nodes 91 & 94 [Hours]
Edge Crack	0.0008	0.32	0.94	9.88	1.97
Thumbnail Crack	0.0008	0.58	1.19	12.88	2.41

Firstly, Table 29 reinforces the assumption that the edge crack model is more conservative than the thumbnail crack geometry. At first glance it would appear nodes 91 and 94 are in the domain of maximum structurally vulnerability as the fatigue life across both crack models is significantly less compared to Nodes 1 and 4. However, as previously stated in Section 4.3.2, for Nodes 91 and 94 the crack does not begin to propagate until a minimum length of 78% of the insulators critical 60% thickness criteria. Therefore, Nodes 91 and 94 do not render an accurate illustration of the cables fatigue life since the stresses present in the insulator only influence the crack propagate when a large initial water tree size is present.

Nevertheless, Table 29 also shows both crack case geometries have an extremely short fatigue life for Nodes 1 and 4. This suggests that mechanical stress has no intrinsic effect on the water tree propagation with most of the water tree growth spearheaded by maxwell stresses. However, when mechanical loading does take effect the water tree begins to grow unstably almost immediately and the XLPE insulator fails within hours.

Nonetheless, considering all the factors, the fatigue life of the cable was determined by an edge crack in a finitely extended plate subject to loads arising from Segment 8 Nodes 1 and 4. Thus, due to mechanical stresses the marine dynamic cable has a fatigue life of approximately 9.88 hours.

Ultimately, the fatigue life of the XLPE insulator is drastically correlated to the dependability of XLPE material data. There is enormous uncertainty in XLPE's material properties, e.g., Paris Law co-efficient, that considerably alters the fatigue life of a component built of XLPE.

4.4 Electrical Stress Results

This section outlines the effect electrical stress has on the propagation of water tree cracks within the XLPE insulation of the marine dynamic cable. The results shown in this section are achieved by analysing the COMSOL models developed which are discussed in Section 3.5.

4.4.1 2D & 3D Electrical Stress Model

The initial results shown in this section are from the 2D electrical model incremental study. Figure 106 illustrates one of the simulations conducted and how COMSOL determined the electric field strength at the tip of the water tree crack.

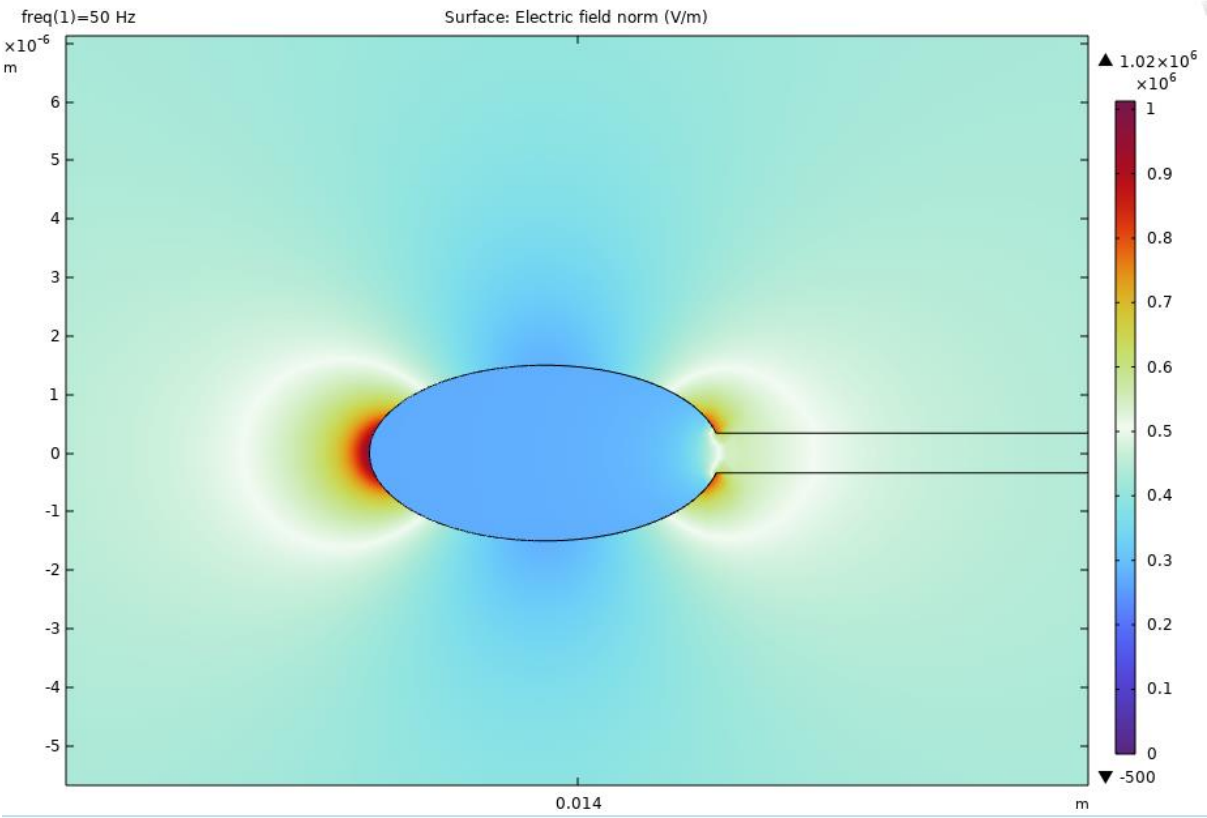

Figure 106: 2D Electrical COMSOL Model

Table 30 describes the results of the initial incremental study. The Maxwell stress values were calculated using Equation 14 as discussed in Section 2.7.2.

$$F = \frac{\varepsilon_0}{2}(\varepsilon_r - 1)E^2 \quad (14)$$

Table 30: 2D Incremental Study Results

Study No.	Crack Length (mm)	Electric Field (V/m)	Maxwell Stress (Pa)
1	0.01	1029834.0134103916	6.1009
2	0.055	1013574.7794632219	5.9097
3	0.1	1017671.7692889863	5.9576
4	0.145	1024488.9870203537	6.0377
5	0.19	1031632.4829547554	6.1222
6	0.235	1046357.8099068012	6.2982
7	0.28	1046337.4656903441	6.2980
8	0.325	1053632.9285768133	6.3861
9	0.37	1070503.8365616777	6.5922
10	0.415	1073920.6356275398	6.6344
11	0.46	1076653.4396333569	6.6682
12	0.505	1097307.0629276554	6.9265
13	0.55	1092960.1139104543	6.8717
14	0.595	1100692.6831621865	6.9693
15	0.64	1120476.569941442	7.2221
16	0.685	1117169.0357197537	7.1795
17	0.730	1132197.4630173484	7.3740
18	0.775	1134476.7762607415	7.4037
19	0.82	1147920.5937381652	7.5802
20	0.865	1152107.4166423266	7.6356
21	0.91	1160960.9266534238	7.7534
22	0.955	1180706.481909751	8.0194
23	1	1179673.902938778	8.0054
24	1.045	1196820.7632024225	8.2398
25	1.09	1203971.002437213	8.3385
26	1.135	1208460.5917807512	8.4008
27	1.18	1218349.6683063912	8.5389
28	1.225	1228625.624665427	8.6835

Using the results from this incremental study a fatigue life of 232.55 years was calculated using Equation 19 and the methodology described in Section 3.5.

$$0.5V_0\varepsilon_0(\varepsilon_r - 1)E^2 > \sigma_{yield}V_0 \quad (19)$$

The next set of results in this section are from the 3D electrical model incremental study. Figure 107 illustrates one of the simulations conducted using the 3D model and how COMSOL determined the electric field strength at the tip of the water tree crack.

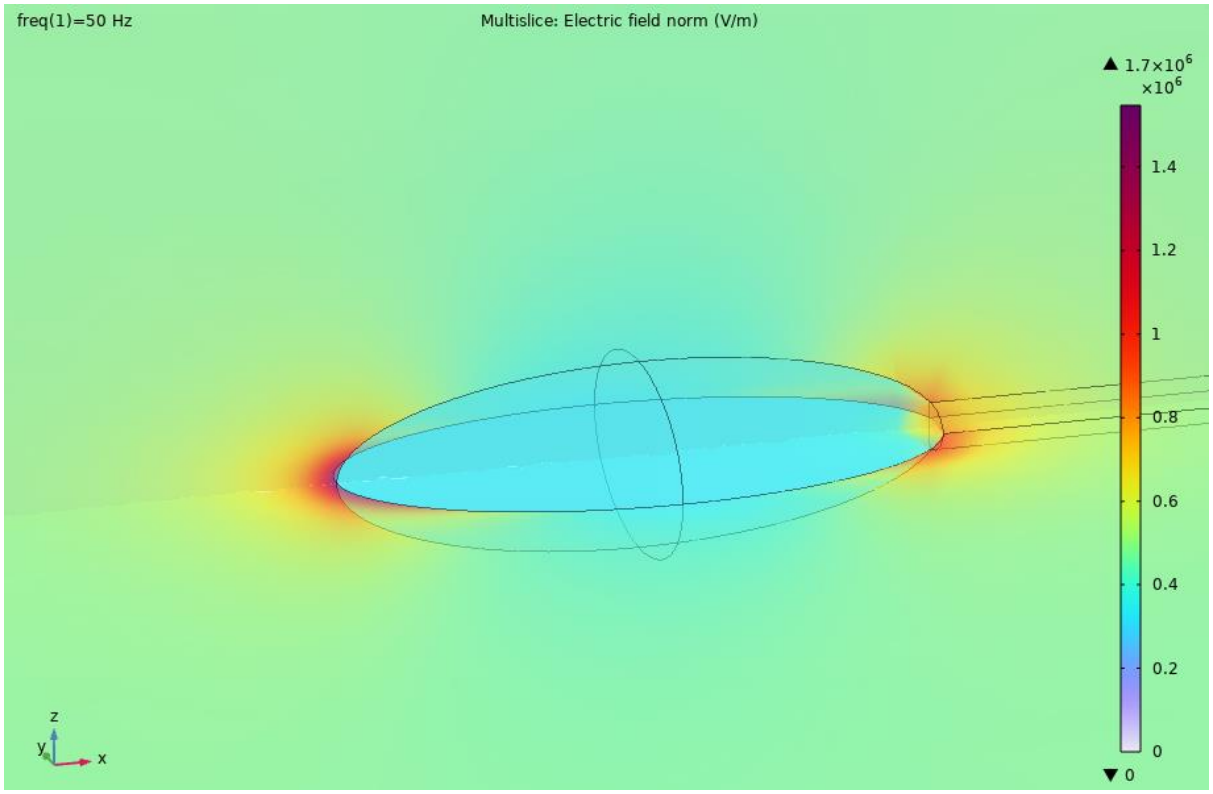

Figure 107: 3D Electrical COMSOL Model

Table 31 describes the results of the second incremental study. The Maxwell stress values were calculated using the same methodology as the previous study.

Table 31: 3D Incremental Study Results

Study No.	Crack Length (mm)	Electric Field (V/m)	Maxwell Stress (Pa)
1	0.01	1118194.545953899	7.1927
2	0.055	1141962.2070699253	7.5017
3	0.1	1146394.4231599846	7.5601
4	0.145	1184079.4185402272	8.0653
5	0.19	1197924.3696758377	8.2550
6	0.235	1196279.8520564672	8.2323
7	0.28	1215058.387613141	8.4928
8	0.325	1247321.7147577952	8.9498
9	0.37	1247165.98193527	8.9476
10	0.415	1271178.0139059892	9.2954
11	0.46	1284954.8151387128	9.4980
12	0.505	1317692.3822672546	9.9881
13	0.55	1322895.7184806743	10.0672
14	0.595	1377911.1104487604	10.9219
15	0.64	1421540.6105085143	11.6245
16	0.685	1466442.574212161	12.3705
17	0.730	1461963.3067519355	12.2950

18	0.775	1503729.5591063008	13.0076
19	0.82	1515180.7591691716	13.2064
20	0.865	1522750.2734176123	13.3387
21	0.91	1530448.3342949813	13.4739
22	0.955	1553442.4568087566	13.8818
23	1	1573283.1701440723	14.2387
24	1.045	1578317.0557908062	14.3300
25	1.09	1594922.9016646869	14.6331
26	1.135	1620770.272227576	15.1112
27	1.18	1678336.4432098363	16.2037
28	1.225	1693938.9135828689	16.5064

Using the results from this incremental study a fatigue life of 154.27 years was calculated using the same methodology as the previous study.

Figure 108 shows the comparison of both studies as the water tree crack propagates through the insulation.

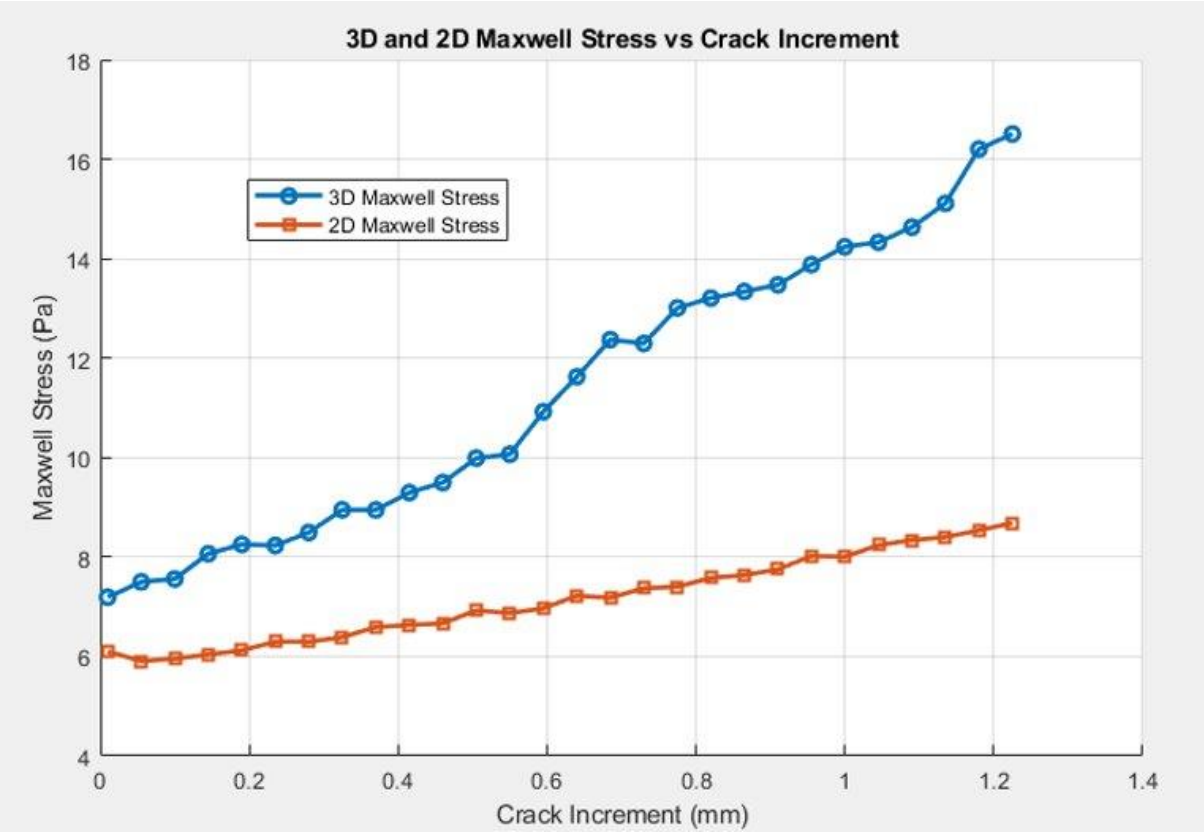

Figure 108: 2D vs 3D Maxwell Stress Against Crack Length

4.4.2 Multiphysics 3D Electrical Stress Model

Figure 109 illustrates one of the simulations conducted and how COMSOL determined the electric field strength at the tip of the water tree crack with the multi-physics model.

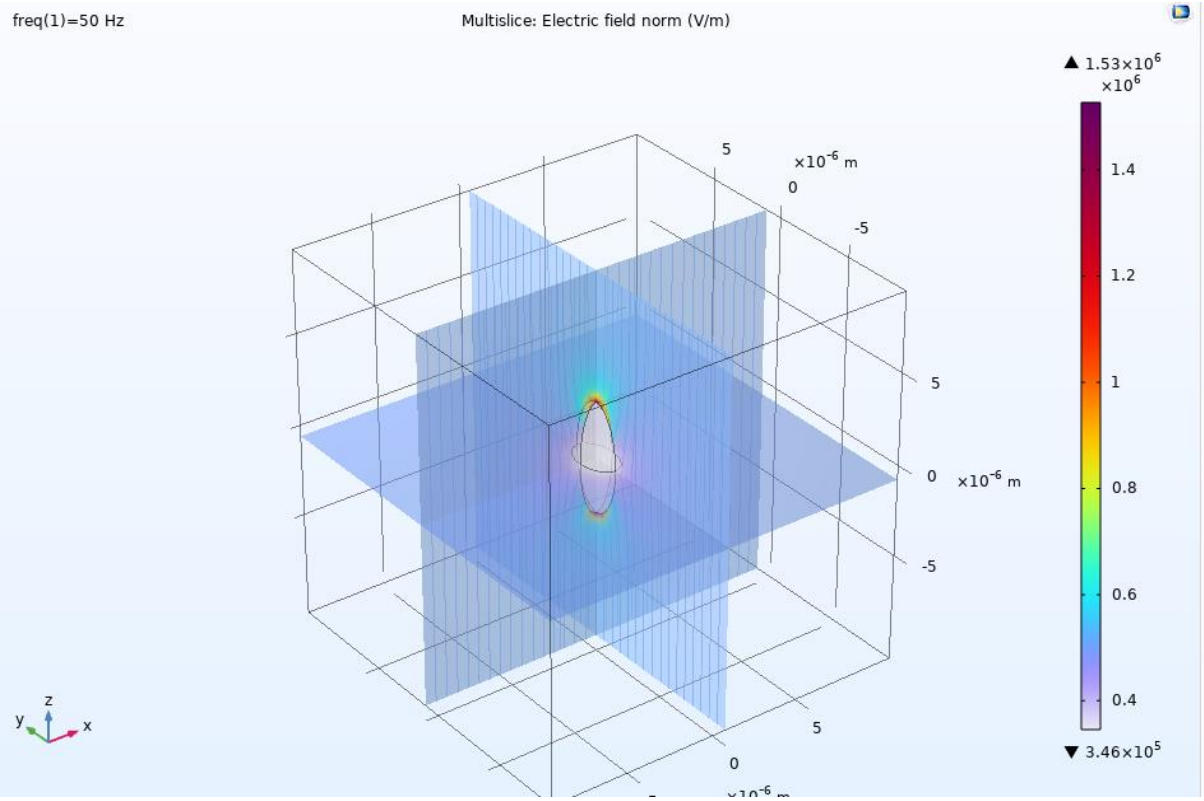

Figure 109: Electric Field Strength at Crack Tip (Multiphysics)

After analysing local model and mechanical stress results Table 32 describes the results of the initial incremental study. The Maxwell stress values were calculated using the same methodology as the previous study.

Table 32: Multiphysics Incremental Study Results

Study No.	Crack Length (mm)	Electric Field (V/m)	Maxwell Stress (Pa)
1	0.01	1545722.111	13.7442
2	0.055	1561521.228	14.0266
3	0.1	1578230.874	14.3284
4	0.145	1595833.34	14.6498
5	0.19	1614347.88	14.9917
6	0.235	1633780.726	15.3548
7	0.28	1654099.513	15.7391
8	0.325	1675355.016	16.1462

Using the results from this incremental study it was calculated that it would take 31.6 years of service until mechanical stress would impact the growth of the water tree. The same methodology was utilised as the previous studies.

The next set of results show the way in which the applied mechanical stress will impact the stress at the tip of the crack, the void was studied at 50% through the thickness of the insulator. First, the model was simulated with no multi-physics function in order to assess the stress at the void tip solely from electric field presence. Von Mises stress was analysed at the crack tip for both simulations so a comparison could be made. The first simulation gave a Von Mises

stress of 17.326 Pa at the tip. For the second simulation the multi-physics tool was activated and a stress of 14.6MPa was applied to the boundary layers simulating the axial stress determined from the local model. This simulation gave a Von Mises value of 1.1117×10^5 Pa at the tip of the void.

4.4.3 Discussion of Electrical Stress Results

The results produced from models developed correlate with the literature that has been produced on the subject, they illustrate the large impact that electric field strength and Maxwell stresses have on water tree propagation. Literature confirms the validity of the models as they demonstrate that Maxwell stress values at void tips will increase as the length of the water tree increases.

The voltage of the dynamic cable being investigated is the major factor in Maxwell stress generation. Taking the conservative 3D electrical model fatigue life of 154.27 years and comparing that to the fatigue life generated by [10] for a 66kV cable, which was found to be approximately 19 years. This illustrates the huge influence that voltage plays on water tree propagation.

As the manufacture's service life prediction of the cable is 25 to 30 years, if electrical stress was the on affecting factor acting on a water tree the dynamic cable should live up to this predicted service life.

The comparison between 2D and 3D electrical models on COMSOL show that the 3D model allows COMSOL to capture the physics, to a greater accuracy, that is taking place around the void. For this reason, 3D modes should be utilised for further research on this topic.

It is clear from the multi-physics model simulations that mechanical stress has a major effect on the stress that is developed at the void tip. However, since the Von Mises stress cannot be taken as crack propagation stress further work needs to be conducted on the model. This entails finding the principal stress values, in the correct direction, that propagate the water tree crack.

5 Conclusions

The structurally integrity of marine dynamic cables is essential for the effectiveness and safe operation of WEC's. The scope of this project was to emphasise multiple modes in which marine dynamic cables can be degraded due to their environment. Varying scales of analysis was incorporated to gain a broad understanding of different failure modes and how they impact the service life of the cable.

5.1 Global Analysis

The aim of the global analysis was to understand the failure mechanisms associated with dynamic power cables and the theories involved in calculating fatigue life. From here an understanding of SIMA was imperative in order to construct a 3D global model of the system under investigation. Through the implementation of multiple methodologies, post-processing could begin, critical regions, fatigue lives and relative nodal displacements were established.

The main findings that were achieve by implementing the describe methodologies was that fatigue damage, as expected, increases significantly as harsher conditions are introduced. As a result of this, the most conservative fatigue life for Case 1,2 and 3 were 6.05e+21 years, 7.096e+11 years and 3.858e+10 years respectively. Obtaining high fatigue lives through this model is expected as many phenomena are neglected *e.g.,* Water Trees, fretting and Biofouling. The importance of this model is based upon the determination of critical regions along the cable's length.

Following this, the second phase involved the calculation of relative displacements that could be integrated into the local FEA model to enable a more precise estimation of the stress found in the insulator layer of the cable. Displacements were found for all three cases and the two locations of importance. It was found for cases 1 and 2, the displacements were reasonable and were similar to previous literature. However, upon entering extreme conditions *i.e.,* Case 3, displacements began to become larger than expected reaching up to 18% of the element's length.

Overall, the results obtained from the global model were of great importance as it was the basis for the secondary phase of a smaller scale examination in the FEA model. The global analysis was useful as it allowed for the local models to investigate areas at a much smaller scale with confidence that these regions were of importance and where the greatest fatigue damage takes place on a global level. This allowed for fatigue lives on different scales to be predicted.

5.2 Local Fretting Analysis

The results provided in Section 4.2 give a clear indication of the impact the loading force, sliding distance and COF has on the fatigue life and maximum wear depth of the copper wires within MDC's. The results show that the loading force has a much greater effect than the sliding distance or COF on the fatigue life. However, these simulations use a constant force rather than a load which varies with time. Due to the nature of the cable's global movement, a time dependant load is perhaps a more likely loading case.

Another way the fretting fatigue model could be enhanced would be the additional study into crack propagation due to fretting. The model used assumes the cable fails once a crack initiates. This assumption is not often true in cases of low applied loads.

Currently, there is very little data on the interlayer and interwire forces and movements in subsea dynamic cables. Without this knowledge it is difficult to create a completely realistic model of the fretting problem. Despite this, the results appear reasonable as they predict failure before the classical S-N methodologies used in the global fatigue model. This premature failure also occurs in real MDCs.

5.3 Water Tree Fatigue Life

Comprehensive methodologies were established to determine the fatigue life of a marine dynamic cable due to the presence of water tree cracks. The objective was to calculate independent fatigue lives due to mechanical and electrical stress respectively. Once independent fatigue lives were predicted, a methodology was created to combine both stress states to define a combined and overall fatigue life. The fatigue life combining both stress states would be used as a service life prediction in a real-world application.

To determine a fatigue life due to purely mechanical stresses the water tree void was treated as a crack and linear elastic fracture mechanics was employed. Two crack case models were integrated, edge crack in finitely extended plate and thumbnail crack in a solid cylinder, to replicate the water growth through the XLPE insulation layer. To analyse the crack geometries and predict a fatigue life COMSOL Multiphysics and MATLAB was utilised. It was determined the edge crack in finitely extended plate was the most conservative case and would be used to predict a fatigue life of the cable. Furthermore, utilising the edge crack geometry and extrapolating the stress from Sea State 2 Nodes 1 and 4 the fatigue life of the marine dynamic cable as a result of mechanical stress was calculated to be 9.88 hours. Once mechanical stresses have an impact of the growth of the water tree stable crack growth occurs for a matter of hours before unstable crack growth occurs and the cable short circuits. The analyse highlights mechanical stresses have very little effect on the water tree expansion through the thickness of the insulator. Ultimately, the validity of mechanical stress analyse is extremely reliant of the reliability of the XLPE material properties. As previously mentioned, the uncertainty in XLPE material data makes it extremely difficult to predict an accurate and trustworthy fatigue life as a result of mechanical stresses.

Additionally, the fatigue life owing to electrical stresses is calculated by employing the kinetic theory of fatigue which determines the cyclic loading of Maxwell stress to break intermolecular bonds within the XLPE insulation. A 2D and 3D electrical model were developed and compared to analyse the electric field acting at a water tree void tip. It was concluded that for further research on the topic 3D models should be developed as they allow COMSOL to more efficiently capture the physics that is taking place around the void. It was also found that the voltage of a cable has the highest impact factor on water tree growth when analysing electrical stress, lower voltage cables will not propagate the crack as quickly as high voltage cable. A multi-physics model could be an effective way to analyse water tree crack growth as it can be concluded that mechanical stress does play a key role in generating stress at the void tip.

The objective was to determine a combined fatigue life owing to mechanical and electrical stresses. To do so an incremental case study was established, aiming to look at the water tree growth on a more granular level by inspecting water tree growth between a specified increment range for both mechanical and electrical stresses. Such practice was required to understand what stress is dominating at certain crack lengths. However, the incremental study became unnecessary after it was established once mechanical stresses effect water tree propagation, they cause cable failure within hours. Therefore, it was decided the combined fatigue life would be determined by simply summing the electrical and mechanical fatigue lives. The combined

fatigue life on the marine dynamic cable from mechanical and electrical stresses is 31.6 years. The electrical stress will propagate the water tree crack until such a water tree length where LEFM and the Paris Law can be applied. Once mechanical stresses influence crack propagation they dominate, and unstable crack growth occurs within half a day.

6 Future Work

Due to the short time period given and the novelty of the work for all members of the team, not all areas of work were explored as thoroughly as anticipated due to comprehensive literature reviews taking place and the learning new software. As a result of this, future work for each section of the thesis has been proposed.

6.1 Global Model

The first recommendation for the global model would be to increase the simulation times for each case study. This would ensure that the full JONSWAP-3 wave spectra is captured. It would be recommended to increase simulation times to at least 3600s however this will increase computational time. Following this, more sea states from the Runde wave scatter diagram should be introduced to draw better general conclusions in relation to the cable fatigue damage.

The second recommendation is to incorporate both wind and current into the simulations to create a more accurate depiction of the environmental conditions present in Runde.

Thirdly, for a continuation of this specific thesis, the W4P (Waves 4 Power) WEC should be integrated in the SIMA model. This was attempted however achieved convergence issues and also irregular movement of the WEC. This thesis uses the 'Runde' model.

The final recommendation would be to develop an improved version of the relative displacement methodology. Gaining accurate relative displacements for the neighbouring elements is difficult as SIMA outputs global positions instead of relative displacements. The difficulty arises as the cable doesn't always lie on plane during motion and causes issues when calculating the initial separation distance. The relative displacement method employed in this thesis is a rudimentary approach and stands as an area for potential improvement to increase the accuracy of the local FEA model findings.

6.2 Fretting

A recommendation for further work is to create a 3D model of the interwire fretting problem. This could more accurately capture the effects of fretting by allowing the inclusion of parameters such the lay angle and bending. A 3D Abaqus model was successfully developed for this project, however, it also required more in-depth subroutine and post processing codes. The model also took over 24 hours to run a simulation with only 4 fretting cycles. Due to the limited time available, and these previously stated issues, it was determined that there was not enough time to complete this model as part of this project.

Another area of future work is the development of an effective local interwire contact model. This could utilise the global movements of the cable to find accurate contact forces and sliding distances of the copper wires within the conductor. These could be used as more accurate inputs for the current fretting model.

6.3 Water Tree

Firstly, to calculate accurate and reliable fatigue lives fitting to water tree defects the material properties of XPLE must be further investigated. Currently, the material data for XLPE is extremely unknown hindering the fatigue life estimations, particularly predictions due to mechanical stresses.

Furthermore, to attempt to analyse the impact of mechanical stresses on water tree propagation elastic-plastic fracture mechanics could be employed. Currently, under LEFM the water tree is assumed not to grow until K_{th} is met. However, the crack may propagate at stress intensity values less than K_{th} as a result of plastic strains encompassing the crack tip. Utilising

plasticity may enable a more realistic depiction of how the crack grows at smaller crack lengths.

Finally, instead of calculating mechanical and electrical stresses independently a 3D COMSOL model could be developed incorporating both stress states. The model would replicate the 3D water tree void model in section 3.5.3 whilst including an applied axial tensile stress in the appropriate direction that fulfils the criteria of a mode I crack. This model would allow for the mechanical and electrical stresses to co-exist and propagate the crack simultaneously with the intention of calculating a more accurate fatigue life.

6.4 Local Model

To increase the accuracy of the local FEA model it would be appropriate to investigate the interaction between the components comprising the model. The current model assumes each component is fully bonded to one another with no slippage when the model is displaced. To increase the authenticity of the local model it would be applicable to include friction co-efficient between each component that reflects subsequent material of the component.

Lastly, the current model assumed isotropic elasticity, neglecting the influence of plasticity spreading through the insulator thickness. Though, the axial stress present in the XLPE insulator owing to Sea State 2 was notably higher than the yield strength of XLPE. For the purpose of this project, it was assumed the local model would not plastically collapse due to such stress magnitudes beyond the yield strength. However, to simulate the deformation characteristics of the XLPE insulation and calculate the local axial tensile stresses it would be beneficial to include a hardening material response to analyse how XLPE behaves beyond yield. Ultimately, the hope would be such alterations leads to more accurate fatigue life predictions.

7 References

[1] Z. Z. W. Q. Xin Li, “A fretting related damage parameter for fretting fatigue life prediction,” *International Journal of Fatigue,* vol. 73, pp. 110-118, 2015.

[2] ‘The Paris Agreement | UNFCCC’. Accessed: Jan. 04, 2024. [Online]. Available: https://unfccc.int/process-and-meetings/the-paris-agreement

[3] ‘Global Climate Agreements: Successes and Failures | Council on Foreign Relations’. Accessed: Jan. 05, 2024. [Online]. Available: https://www.cfr.org/backgrounder/paris-global-climate-change-agreements

[4] ‘WMO - Clean Energy Must Double By 2030 | UNFCCC’. Accessed: Jan. 05, 2024. [Online]. Available: https://unfccc.int/news/wmo-clean-energy-must-double-by-2030

[5] ‘What did the UK’s electricity generation mix look like in 2022? - edie’, *https://www.edie.net/*, Accessed: Jan. 05, 2024. [Online]. Available: https://www.edie.net/what-did-the-uks-electricity-generation-mix-look-like-in-2022/

[6] ‘Unlocking the potential of Ocean Energy: from megawatts to gigawatts - Energy Post’. Accessed: Jan. 05, 2024. [Online]. Available: https://energypost.eu/unlocking-the-potential-of-ocean-energy-from-megawatts-to-gigawatts/

[7] ‘Wave Energy Converters’. Accessed: Jan. 05, 2024. [Online]. Available: https://theliquidgrid.com/marine-clean-tech-briefs/wave-energy-converters/

[8] ‘Home - Waves4Power’. Accessed: Jan. 05, 2024. [Online]. Available: https://www.waves4power.com/

[9] Z. Li, J. W. Ringsberg, E. Johnson, and Y. Serdyuk, ‘CRACK PROPAGATION IN DYNAMIC POWER CABLES’, in *Proceedings of the International Conference on Offshore Mechanics and Arctic Engineering - OMAE*, 2022. doi: 10.1115/OMAE2022-79467.

[10] D. Glenn Young and C. Ng, ‘Predicting failure of dynamic oshore cables by insulation breakdown due to water treeing’, 2020.

[11] ‘8 Types of Wave Energy Converters and How Each Operates - Environment Go!’ Accessed: Dec. 23, 2023. [Online]. Available: https://environmentgo.com/types-of-wave-energy-converters/#google_vignette

[12] ‘High voltage dynamic subsea power cables for reliability | Engineer Live’. Accessed: Jan. 05, 2024. [Online]. Available: https://www.engineerlive.com/content/high-voltage-dynamic-subsea-power-cables-reliability

[13] P. R. Thies, L. Johanning, and G. H. Smith, ‘Assessing mechanical loading regimes and fatigue life of marine power cables in marine energy applications’, in *Proceedings of the Institution of Mechanical Engineers, Part O: Journal of Risk and Reliability*, 2012. doi: 10.1177/1748006X11413533.

[14] S. H. Yang, J. W. Ringsberg, E. Johnson, and Z. Hu, ‘Biofouling on mooring lines and power cables used in wave energy converter systems—Analysis of fatigue life and energy performance’, *Applied Ocean Research*, vol. 65, 2017, doi: 10.1016/j.apor.2017.04.002.

[15] ‘NKT | Cable Solutions – High, Medium, Low Voltage Cables & Accessories’. Accessed: Dec. 05, 2023. [Online]. Available: https://www.nkt.com/

[16] J. W. Ringsberg, L. Dieng, Z. Li, and I. Hagman, ‘Characterization of the Mechanical Properties of Low Stiffness Marine Power Cables through Tension, Bending, Torsion,

and Fatigue Testing', *J Mar Sci Eng*, vol. 11, no. 9, 2023, doi: 10.3390/jmse11091791.

[17] S.-H. Yang and Chalmers tekniska högskola, *Analysis of the fatigue characteristics of mooring lines and power cables for floating wave energy converters*.

[18] B. Bj¨ Bj¨orn, L. Simen, and S. Haukeland, 'Fatigue analysis of an umbilical cable designed for point absorbing wave energy converters A comparison of simulation models', 2017.

[19] T. A. Conway and G. A. Costello, 'BirdCaging in Wire Rope', *J Eng Mech*, vol. 116, no. 4, pp. 822–831, Apr. 1990, doi: 10.1061/(ASCE)0733-9399(1990)116:4(822).

[20] 'Runde - Google Maps'. Accessed: Jan. 07, 2024. [Online]. Available: https://www.google.com/maps/place/Runde/@62.8765327,0.9670498,5z/data=!4m10!1m2!2m1!1sgoogle+maps+runde!3m6!1s0x46173cce7b776317:0x7a60f85319e3e750!8m2!3d62.4006141!4d5.6241731!15sChFnb29nbGUgbWFwcyBydW5kZSIDiAEBWgciBXJ1bmRlkgEGaXNsYW5k4AEA!16zL20vMDhrZ3h2?entry=ttu

[21] S. H. Yang, J. W. Ringsberg, and E. Johnson, 'Parametric study of the dynamic motions and mechanical characteristics of power cables for wave energy converters', *Journal of Marine Science and Technology (Japan)*, vol. 23, no. 1, 2018, doi: 10.1007/s00773-017-0451-0.

[22] 'What is a SN-Curve?' Accessed: Oct. 10, 2023. [Online]. Available: https://community.sw.siemens.com/s/article/what-is-a-sn-curve

[23] 'Rainflow Counting'. Accessed: Oct. 11, 2023. [Online]. Available: https://community.sw.siemens.com/s/article/rainflow-counting

[24] 'Rainflow Counting - FEA-Solutions (UK) Ltd - Finite Element Analysis For Your Product Design'. Accessed: Oct. 13, 2023. [Online]. Available: https://fea-solutions.co.uk/rainflow-counting/

[25] 'Calculating Damage with Miner's Rule'. Accessed: Oct. 10, 2023. [Online]. Available: https://community.sw.siemens.com/s/article/calculating-damage-with-miner-s-rule

[26] 'EngArc - L - Mean Stress Equations'. Accessed: Jan. 07, 2024. [Online]. Available: https://www.engineeringarchives.com/les_fatigue_meanstressequations.html

[27] N. Santhosh, U. N. Kempaiah, G. Sajjan, and A. C. Gowda, 'Fatigue Behaviour of Silicon Carbide and Fly Ash Dispersion Strengthened High Performance Hybrid Al 5083 Metal Matrix Composites', *Journal of Minerals and Materials Characterization and Engineering*, vol. 05, no. 05, pp. 274–287, 2017, doi: 10.4236/jmmce.2017.55023.

[28] K. Pereira, T. Yue, and M. Abdel Wahab, 'Multiscale analysis of the effect of roughness on fretting wear', *Tribol Int*, vol. 110, 2017, doi: 10.1016/j.triboint.2017.02.024.

[29] 'Fretting Wear - About Tribology'. Accessed: Oct. 31, 2023. [Online]. Available: https://www.tribonet.org/wiki/fretting-wear/

[30] M. H. Zhu and Z. R. Zhou, 'On the mechanisms of various fretting wear modes', *Tribol Int*, vol. 44, no. 11, pp. 1378–1388, Oct. 2011, doi: 10.1016/J.TRIBOINT.2011.02.010.

[31] O. Vingsbo and S. Söderberg, 'On fretting maps', *Wear*, vol. 126, no. 2, pp. 131–147, Sep. 1988, doi: 10.1016/0043-1648(88)90134-2.

[32] E. Heitz, ‘ Fretting Corrosion. Von R. B. Waterhouse . 253 S. 306 Abb., 13 Tab. 1972, Pergamon Press, Oxford, New York, Toronto, Sydney, Braunschweig. Geb. £6.50 ’, *Materials and Corrosion*, vol. 26, no. 2, 1975, doi: 10.1002/maco.19750260224.

[33] ‘What is the Coulomb friction law? - Encyclopedia of the Environment’. Accessed: Jan. 05, 2024. [Online]. Available: https://www.encyclopedie-environnement.org/en/zoom/what-is-the-coulomb-friction-law/

[34] P. J. Blau, ‘The significance and use of the friction coefficient’, *Tribol Int*, vol. 34, no. 9, 2001, doi: 10.1016/S0301-679X(01)00050-0.

[35] I. R. McColl, J. Ding, and S. B. Leen, ‘Finite element simulation and experimental validation of fretting wear’, *Wear*, vol. 256, no. 11–12, 2004, doi: 10.1016/j.wear.2003.07.001.

[36] D. K. Zhang, S. R. Ge, and Y. H. Qiang, ‘Research on the fatigue and fracture behavior due to the fretting wear of steel wire in hoisting rope’, *Wear*, vol. 255, no. 7–12, 2003, doi: 10.1016/S0043-1648(03)00161-3.

[37] S. G. Y. Q. D.K. Zhang, “Research on the fatigue and fracture behavior due to the fretting wear of steel wire in hoisting rope,” *Wear,* vol. 25, no. 7-12, pp. 1233-137, 2003.

[38] J. J. Madge, ‘Numerical Modelling of the Effect of Fretting Wear on Fretting Fatigue’, *International Journal*, no. June, 2008.

[39] R. Weyler, J. Oliver, T. Sain, and J. C. Cante, ‘On the contact domain method: A comparison of penalty and Lagrange multiplier implementations’, *Comput Methods Appl Mech Eng*, vol. 205–208, no. 1, 2012, doi: 10.1016/j.cma.2011.01.011.

[40] J. Ding, I. R. McColl, S. B. Leen, and P. H. Shipway, ‘A finite element based approach to simulating the effects of debris on fretting wear’, *Wear*, vol. 263, no. 1-6 SPEC. ISS., 2007, doi: 10.1016/j.wear.2006.12.056.

[41] K. Li, K. Zhou, and G. Zhu, ‘Toward understanding the relationship between the microstructure and propagation behavior of water trees’, *IEEE Transactions on Dielectrics and Electrical Insulation*, vol. 26, no. 4, 2019, doi: 10.1109/TDEI.2019.007881.

[42] M. Alsharif, P. Wallace, D. Hepburn, and C. Zhou, ‘FEM Modeling of Electric Field and Potential Distributions of MV XLPE Cables Containing Void Defect’, *Excerpt from the Proceedings of the …*, no. 1, 2012.

[43] Q. Burkes, K. Makram, E. Hadidi, and R. Xu, ‘Capacitance of Water Tree Modeling in Underground Cables’, *Journal of Power and Energy Engineering*, vol. 2, pp. 9–18, 2014, doi: 10.4236/jpee.2014.211002.

[44] I. Radu, M. Acedo, P. Notingher, F. Frutos, and J. C. Filippini, ‘The danger of water trees in polymer insulated power cables evaluated from calculations of electric field in the presence of water trees of different shapes and permittivity distributions’, *J Electrostat*, vol. 40–41, pp. 343–348, Jun. 1997, doi: 10.1016/S0304-3886(97)00066-1.

[45] Z. Li, J. W. Ringsberg, Y. V. Serdyuk, D. Svensson, E. Johnson, and C. Andersson, ‘Predicting failure of dynamic subsea cables by electrical insulation breakdown due to water treeing’, in *Advances in the Analysis and Design of Marine Structures*, 2023. doi: 10.1201/9781003399759-53.

[46] D. H. Monssef, M. Sriharsha, N. Abhijit, C. Valter, and B. Pierre-Jean, ‘Numerical Simulation of Aging by Water-Trees of XPLE Insulator Used in a Single Hi-Voltage

Phase of Smart Composite Power Cables for Offshore Farms', *Energies (Basel)*, vol. 15, no. 5, 2022, doi: 10.3390/en15051844.

[47] J. C. Filippini and C. T. Meyer, 'Effect of Frequency on the Growth of Water Trees in Polyethylene', *IEEE Transactions on Electrical Insulation*, vol. EI-17, no. 6, 1982, doi: 10.1109/TEI.1982.298532.

[48] A. Abideen, F. Mauseth, Ø. L. Hestad, and H. Faremo, 'Review of Water Treeing in Polymeric Insulated Cables', *Proceedings of the Nordic Insulation Symposium*, vol. 27, no. 1, 2022, doi: 10.5324/nordis.v27i1.4732.

[49] S. Nordås and E. Ildstad, 'The influence of strain on water treeing in XLPE power cables', *Proceedings of the 2010 IEEE International Conference on Solid Dielectrics, ICSD 2010*, 2010, doi: 10.1109/ICSD.2010.5568215.

[50] E. Ildstad, H. Bardsen, H. Faremo, and B. Knutsen, 'Influence of mechanical stress and frequency on water treeing in XLPE cable insulation', *Conference Record of IEEE International Symposium on Electrical Insulation*, pp. 165–168, 1990, doi: 10.1109/ELINSL.1990.109732.

[51] M. Drissi-Habti, D. Raj-Jiyoti, S. Vijayaraghavan, and E. C. Fouad, 'Numerical simulation for void coalescence (water treeing) in XLPE insulation of submarine composite power cables', *Energies (Basel)*, vol. 13, no. 20, 2020, doi: 10.3390/en13205472.

[52] Z. P. Bažant, J.-L. Le, and M. Salviato, 'Fundamentals of Linear Elastic Fracture Mechanics', *Quasibrittle Fracture Mechanics and Size Effect*, pp. 11–52, Nov. 2021, doi: 10.1093/OSO/9780192846242.003.0002.

[53] J. J. Mecholsky, 'Fracture mechanics principles', *Dental Materials*, vol. 11, no. 2, pp. 111–112, Mar. 1995, doi: 10.1016/0109-5641(95)80044-1.

[54] '6: Three fundamental rupture modes are defined: Normal fracture (Mode... | Download Scientific Diagram'. Accessed: Jan. 06, 2024. [Online]. Available: https://www.researchgate.net/figure/Three-fundamental-rupture-modes-are-defined-Normal-fracture-Mode-I-in-plane-shear_fig8_283580678

[55] W. A. P. Paris, M. Gomez, P. C. Paris, M. P. Gomez, and W. E. P. Anderson, 'A Rational Analytic Theory of Fatigue', *The Trend in Engineering*, vol. 13, 1961.

[56] U. Zerbst, M. Madia, and D. Hellmann, 'An analytical fracture mechanics model for estimation of S–N curves of metallic alloys containing large second phase particles', *Eng Fract Mech*, vol. 82, pp. 115–134, Mar. 2012, doi: 10.1016/J.ENGFRACMECH.2011.12.001.

[57] 'Mechanical Behavior of Polymers | MATSE 81: Materials In Today's World'. Accessed: Jan. 06, 2024. [Online]. Available: https://www.e-education.psu.edu/matse81/node/2109

[58] J. R. Rice, 'A Path Independent Integral and the Approximate Analysis of Strain Concentration by Notches and Cracks', *J Appl Mech*, vol. 35, no. 2, pp. 379–386, Jun. 1968, doi: 10.1115/1.3601206.

[59] 'SIMA - SINTEF'. Accessed: Dec. 08, 2023. [Online]. Available: https://www.sintef.no/en/software/sima/

[60] J. Ding, S. B. Leen, and I. R. McColl, 'The effect of slip regime on fretting wear-induced stress evolution', *Int J Fatigue*, vol. 26, no. 5, 2004, doi: 10.1016/j.ijfatigue.2003.09.001.

[61] S. Kwofie, ‘An exponential stress function for predicting fatigue strength and life due to mean stresses’, *Int J Fatigue*, vol. 23, no. 9, 2001, doi: 10.1016/S0142-1123(01)00044-5.

[62] T. Łagoda, S. Vantadori, K. Głowacka, M. Kurek, and K. Kluger, ‘Using the Smith-Watson-Topper Parameter and Its Modifications to Calculate the Fatigue Life of Metals: The State-of-the-Art’, *Materials*, vol. 15, no. 10, May 2022, doi: 10.3390/MA15103481.

[63] Y. Wang and L. Susmel, ‘Critical plane approach to multiaxial variable amplitude fatigue loading’, *Frattura ed Integrita Strutturale*, vol. 9, no. 33, 2015, doi: 10.3221/IGF-ESIS.33.38.

[64] A. Cruzado, S. B. Leen, M. A. Urchegui, and X. Gómez, ‘Finite element simulation of fretting wear and fatigue in thin steel wires’, *Int J Fatigue*, vol. 55, 2013, doi: 10.1016/j.ijfatigue.2013.04.025.

[65] ‘Ansys Contact Types and Explanations - Mechead.com’. Accessed: Jan. 06, 2024. [Online]. Available: https://www.mechead.com/contact-types-and-behaviours-in-ansys/

[66] ‘Utilizing Remote Points Properly - Lesson 4 - ANSYS Innovation Courses’. Accessed: Jan. 06, 2024. [Online]. Available: https://courses.ansys.com/index.php/courses/connecting-parts-together/lessons/utilizing-remote-points-properly-lesson-4/

[67] J. Harikumar and R. Roux, ‘Crack propagation in dynamic power cables’, 2021.

[68] C. T. Poon, R. A. Barrett, and S. B. Leen, ‘Global and local modeling for inter-wire fretting in multi-wire copper conductors’, *Fatigue Fract Eng Mater Struct*, vol. 45, no. 6, 2022, doi: 10.1111/ffe.13683.

[69] T. Liskiewicz, S. Fouvry, and B. Wendler, ‘Impact of variable loading conditions on fretting wear’, *Surf Coat Technol*, vol. 163–164, 2003, doi: 10.1016/S0257-8972(02)00643-6.

[70] S. R. Pearson and P. H. Shipway, ‘Is the wear coefficient dependent upon slip amplitude in fretting? Vingsbo and Söderberg revisited’, *Wear*, vol. 330–331, 2015, doi: 10.1016/j.wear.2014.11.005.

[71] A. F. Hincapié Úsuga, L. V. Vanegas Useche, C. A. Mesa Montoya, C. Wang, and M. Abdel Wahab, ‘Effect of pad rotation angle and coefficient of friction on fretting fatigue crack nucleation behavior’, *Tribol Int*, vol. 189, p. 109012, Nov. 2023, doi: 10.1016/J.TRIBOINT.2023.109012.

[72] ‘Bend stiffeners’. Accessed: Oct. 16, 2023. [Online]. Available: https://www.balmoraloffshore.com/solutions/protection/bend-stiffeners

[73] ‘Rainflow Counting in SOLIDWORKS Simulation Explained | GoEngineer’. Accessed: Oct. 13, 2023. [Online]. Available: https://www.goengineer.com/blog/rainflow-counting-solidworks-simulation

[74] ‘Configuration Factor Solutions’. Accessed: Apr. 05, 2023. [Online]. Available: https://classes2022-2023.myplace.strath.ac.uk/mod/resource/view.php?id=824620&redirect=1

[75] ‘Stress Intensity Factor Solutions | MechaniCalc’. Accessed: Jan. 07, 2024. [Online]. Available: https://mechanicalc.com/reference/stress-intensity-factor-solutions

8 Appendices

Appendix A – Global Model Fatigue MATLAB Code

The Global Model Fatigue MATLAB Code utilises the elmfor.bin (force results) results file that is directly extracted from SIMA. The first script is where the main parameters are initialised and then calls in the other main program functions. The second script reads the raw force results file and extracts the results and places them in a matrix. The third script is where the main calculations take place *e.g.,* stress ranges, fatigue damage and fatigue life. The fourth script locates (along the cable and across cross-section) and quantifies the results acquired in the main calculation script. The final script plots these results in a more user friendly and useful manner which helps highlight trends and discrepancies.

Function – Parameter_input.m

```
clear all;
clc;
% If bin file is DeepC result, K=1; If bin file is sima result, K=1000;

addpath('C:/Users/fagan/Desktop/WAFO/WAFO/wafo_2017/wafo') %zl220915
initwafo


K=1000;
% Time Step(s)
T_s=0.005;
% Storege Step
S_s=20;
% Total Elements of the cable(store one of three elements)
t_e_c=106;
% Cable outer diameter(mm)
D=0.038;
% Analysis start and end time(s)
t_start = 0;
t_end = 1200;
% ramp duration/start up duration(s)
duration=300;
% Two ends of element at main segment of cable (close to WEC and Hub)(_)
E_W=23; % E stands for Element, W stands for WEC. 23 is the number of element of
the other 7 segments.
E_H=84;
% SN curve parameters(_)
SNm=6.238;
SNalpha=6.098E+19;
% Call main program function
main_program_read(K,T_s,S_s,t_e_c,t_start,t_end)
main_program_calculation(T_s,S_s,t_e_c,D,t_start,t_end,duration,E_W,E_H,SNm,SNalph
a)
main_program_output_save
main_program_figure
```

Function – main_program_read.m

```
%%
function[]=main_program_read(K,T_s,S_s,t_e_c,t_start,t_end)


mkdir('simulation')
% Read the dynamic result bin file, and give the different forces and bending
moments in the result file to the corresponding elements

% Opening the file
fileID = fopen('sima_elmfor_Case3_1200s.bin');
Forces = fread(fileID, 'single');
% Conversion of variable units
FORCES=K.*Forces;
% Removing the unused values
FORCES = FORCES(3:end-1);
% Opening the file
fclose(fileID);

% Number of time steps from DeepC or Sima(_)
t_n=(t_end-t_start)/(S_s*T_s);

% Initialisation
forces = ["Axial_force","Torsion_moment", "Mom_Y_end1", "Mom_Y_end2",
"Mom_Z_end1", "Mom_Z_end2"];
[Axial_force, Torsion_moment, Mom_Y_end1, Mom_Y_end2, Mom_Z_end1, Mom_Z_end2] =
deal(zeros(t_n,t_e_c));
t_inc = 0;

while ~isempty(FORCES)
    % Step increment
    t_inc = t_inc + 1;
    % The force quantity of the total elements on the cable
    f_q = 10.*t_e_c;
    % Extraction of the values
    column = transpose(FORCES(1 : f_q));
    for i = 1:length(forces)
        % The axial force, bending moment, torque, shear force and other values
are extracted and converted into strings and saved in the corresponding matrix.
        eval(sprintf('%s(t_inc,:) = column(%d:10:f_q);', forces(i), i))
    end
    % Check if the extraction is over or removing the unused values
    if length(FORCES) == f_q && t_n == t_inc
        FORCES = [];
        disp("The forces have been correctly extracted.")
    else
        % Removing the unused values.
        % The useless value consists of 4 time interval points and start and end
identifiers
        FORCES = FORCES(f_q+4:end);
    end
end

save('.\simulation\Axial_force', 'Axial_force')
```

```
save('.\simulation\Mom_Y_end1', 'Mom_Y_end1')
save('.\simulation\Mom_Z_end1', 'Mom_Z_end1')
save simulation_read.mat
```

Function – main_program_calculation.m

```
%%
function[]=main_program_calculation(T_s,S_s,t_e_c,D,t_start,t_end,duration,E_W,E_H
,SNm,SNalpha)

load simulation_read.mat

% calculate axial stress [MPa]
axialStress_1Kv = zeros(size(Axial_force));

for A = 1 : length(Axial_force(1, :))
    % Cross-sectional area
    CrossArea=pi*D^2/4;
    axialStress_1Kv(:, A) = Axial_force(:, A) ./ CrossArea ./ 1E6;
end
clear A
% claculate intermediate bending stress matrix [MPa]
bendingStressY_1Kv = zeros(size(Mom_Y_end1));
bendingStressZ_1Kv = zeros(size(Mom_Z_end1));

for B1 = 1 : length(Mom_Y_end1(1, :))
    % Moment of inertia
    I=pi*D^4/64;
    % Distance from the neutral layer
    y=D/2;
    % bending stress
    bendingStressY_1Kv(:, B1) = Mom_Y_end1(:, B1) .* y./ I ./ 1E6;
end
for B2 = 1 : length(Mom_Z_end1(1, :))
    % Moment of inertia
    I=pi*D^4/64;
    % Distance from the neutral layer
    y=D/2;
    % bending stress
    bendingStressZ_1Kv(:, B2) = Mom_Z_end1(:, B2) .* y./ I ./ 1E6;
end
clear B1 B2

save('.\simulation\axialStress_1Kv', 'axialStress_1Kv')
save('.\simulation\bendingStressY_1Kv', 'bendingStressY_1Kv')
save('.\simulation\bendingStressZ_1Kv', 'bendingStressZ_1Kv')
%%
%Select 12 hot spots on the section of 1kV cable and calculate the total stress at
the 12 hot spots.
%The stress range at each hot spot is calculated by calling the variables in wafo
toolkit.
%And the fatigue life of each hot spot is calculated by the average stress
correction.
```

```
% Interval to check different points in one cross section[deg]
angle=30;

for Angle = 0 : angle : (360 - angle)
    % calculate bending stress [MPa]
    bendingStressY_1Kv_deg = bendingStressY_1Kv.* sind(Angle);
    % Output bending stress in Y direction of different hotspots

eval(['bendingStressY_1Kv_deg',num2str(Angle),'=','bendingStressY_1Kv_deg',';']);
    bendingStressZ_1Kv_deg = - bendingStressZ_1Kv.* cosd(Angle);
    % Output bending stress in Z direction of different hotspots

eval(['bendingStressZ_1Kv_deg',num2str(Angle),'=','bendingStressZ_1Kv_deg',';']);
    % calculate total stress
    totalStress_1Kv_deg = axialStress_1Kv + bendingStressY_1Kv_deg +
bendingStressZ_1Kv_deg;
    % Output different hotspots total stress
    eval(['totalStress_1Kv_deg',num2str(Angle),'=','totalStress_1Kv_deg',';']);


    % timeSeries
    timeSeries = transpose(linspace(t_start,t_end,t_n));

    Stress_range=[];Stressrange_11=zeros(2000,t_e_c);
    for a = 1 : length(totalStress_1Kv_deg(1,:))
        % find turning point
        [tp ind] = dat2tp([timeSeries((duration/(T_s.*S_s)):t_n)
totalStress_1Kv_deg((duration/(T_s.*S_s)):t_n, a)]);
        % find rainflow cycle
        rFCycle = tp2rfc(tp);

        Stressrange_1=[];
        for k=1:length(rFCycle(:,1))
            % Stress range at each cycle
            stressrange=abs(rFCycle(k, 2) - rFCycle(k, 1));
            % Prevent data from being overwritten
            Stressrange_1=[Stressrange_1;stressrange];
        end

        % Damage after one cycle  % D = sum(S^m) / alpha
        totalDamage = (Stressrange_1 .^ SNm) ./ SNalpha;
        % Record number of cycle
        totalStressNumOfCycle_deg_no_stress(a, 1) = length(totalDamage);
        % calculate the fatigue damage along the entire line
        totalFatigueDamage_deg(a, 1) = sum(totalDamage);
        % Output different hotspots fatigue damage

eval(['totalFatigueDamage_deg',num2str(Angle),'=','totalFatigueDamage_deg',';']);
        % Find the maximum stress range on each element
        stressrange_m=max(max(Stressrange_1));
        % Prevent data from being overwritten
        Stress_range=[Stress_range; stressrange_m];
        % Output different hotspots Stress range
        eval(['Stress_range',num2str(Angle),'=','Stress_range',';']);
        % Assign the stress range of each column (each element) to a matrix
        Stressrange_11(1:length(Stressrange_1),a)=Stressrange_1;
    end
```

```
    Stress_range_goodman=[];Stressrange_22=zeros(2000,t_e_c);
    for a = 1 : length(totalStress_1Kv_deg(1,:))
        % find turning point
        [tp ind] = dat2tp([timeSeries((duration/(T_s.*S_s)):t_n)
totalStress_1Kv_deg((duration/(T_s.*S_s)):t_n, a)]);
        % find rainflow cycle
        rFCycle = tp2rfc(tp);

        Stressrange_2=[];
        for k=1:length(rFCycle(:,1))
            % Stress amplitude
            stress_a=abs(rFCycle(k, 2) - rFCycle(k, 1))/2;
            % Average stress
            stress_m=abs(rFCycle(k, 2) + rFCycle(k, 1))/2;
            % Tensile strength of 1kv cable
            stress_uts=395;
            % Equivalent stress
            stress_equivalent_goodman=stress_a./(1-stress_m./stress_uts);
            % Stress range
            stress_range_a=2*stress_equivalent_goodman;
            % Prevent data from being overwritten
            Stressrange_2=[Stressrange_2;stress_range_a];
        end

        % Damage after one cycle  % D = sum(S^m) / alpha
        totalDamage_goodman = (Stressrange_2 .^ SNm) ./ SNalpha;
        % Record number of cycle
        totalStressNumOfCycle_deg_goodman(a, 1) = length(totalDamage_goodman);
        % calculate the fatigue damage along the entire line
        totalFatigueDamage_deg_goodman(a, 1) = sum(totalDamage_goodman);
        % Output different hotspots fatigue damage

eval(['totalFatigueDamage_deg_goodman',num2str(Angle),'=','totalFatigueDamage_deg_
goodman',';']);
        % Find the maximum stress range on each element
        Stress_range=max(max( Stressrange_2));
        % Prevent data from being overwritten
        Stress_range_goodman=[Stress_range_goodman;Stress_range];
        % Output different hotspots Stress range

eval(['Stress_range_goodman',num2str(Angle),'=','Stress_range_goodman',';']);
        % Assign the stress range of each column (each element) to a matrix
        Stressrange_22(1:length(Stressrange_2),a)=Stressrange_2;

    end

    Stress_range_gerber=[];Stressrange_33=zeros(2000,t_e_c);
    for a = 1 : length(totalStress_1Kv_deg(1,:))
        % find turning point
        [tp ind] = dat2tp([timeSeries((duration/(T_s.*S_s)):t_n)
totalStress_1Kv_deg((duration/(T_s.*S_s)):t_n, a)]);
        % find rainflow cycle
        rFCycle = tp2rfc(tp);

        Stressrange_3=[];
        for k=1:length(rFCycle(:,1))
            % Stress amplitude
            stress_a=abs(rFCycle(k, 2) - rFCycle(k, 1))/2;
```

```
            % Average stress
            stress_m=abs(rFCycle(k, 2) + rFCycle(k, 1))/2;
            % Tensile strength of 1kv cable
            stress_uts=395;
            % Equivalent stress
            stress_equivalent_gerber=stress_a./(1-(stress_m./stress_uts)^2);
            % Stress range
            stress_range_a=2*stress_equivalent_gerber;
            % Prevent data from being overwritten
            Stressrange_3=[Stressrange_3;stress_range_a];
        end

        % Damage after one cycle  % D = sum(S^m) / alpha
        totalDamage_gerber = (Stressrange_3 .^ SNm) ./ SNalpha;
        % Record number of cycle
        totalStressNumOfCycle_deg_gerber(a, 1) = length(totalDamage_gerber);
        % calculate the fatigue damage along the entire line
        totalFatigueDamage_deg_gerber(a, 1) = sum(totalDamage_gerber);
        % Output different hotspots fatigue damage

eval(['totalFatigueDamage_deg_gerber',num2str(Angle),'=','totalFatigueDamage_deg_g
erber',';']);
        % Find the maximum stress range on each element
        Stress_range=max(max( Stressrange_3));
        % Prevent data from being overwritten
        Stress_range_gerber=[Stress_range_gerber;Stress_range];
        % Output different hotspots Stress range

eval(['Stress_range_gerber',num2str(Angle),'=','Stress_range_gerber',';']);
        % Assign the stress range of each column (each element) to a matrix
        Stressrange_33(1:length(Stressrange_3),a)=Stressrange_3;
    end

end
%%

% Fatigue damage of different hotspots is integrated into a matrix
Total_sum_fatiguedamage=[totalFatigueDamage_deg0,totalFatigueDamage_deg30,totalFat
igueDamage_deg60,totalFatigueDamage_deg90,...

totalFatigueDamage_deg120,totalFatigueDamage_deg150,totalFatigueDamage_deg180,tota
lFatigueDamage_deg210,...

totalFatigueDamage_deg240,totalFatigueDamage_deg270,totalFatigueDamage_deg300,tota
lFatigueDamage_deg330];
% FATIGUE
F=[];  L=[];s=[];
for e=1:length(Total_sum_fatiguedamage(:,1))
    % Fatigue_damage_max
    F_max=max(max(Total_sum_fatiguedamage(e,:)));
    % Minimum fatigue life
    s_min=(t_end-t_start)/F_max;
    % The fatigue life unit is converted to years
    s_min_year=s_min/(3600*24*365);
    % Prevent data from being overwritten
    s=[s;s_min_year];
    % Prevent data from being overwritten
    F=[F;F_max];
    % Location
```

```
    L0=find(Total_sum_fatiguedamage(e,:)==F_max);
    % Prevent data from being overwritten
    L=[L;L0];
end


% Fatigue damage of different hotspots is integrated into a matrix
Total_sum_fatiguedamage_goodman=[totalFatigueDamage_deg_goodman0,totalFatigueDamag
e_deg_goodman30,totalFatigueDamage_deg_goodman60,totalFatigueDamage_deg_goodman90,
...

totalFatigueDamage_deg_goodman120,totalFatigueDamage_deg_goodman150,totalFatigueDa
mage_deg_goodman180,totalFatigueDamage_deg_goodman210,...

totalFatigueDamage_deg_goodman240,totalFatigueDamage_deg_goodman270,totalFatigueDa
mage_deg_goodman300,totalFatigueDamage_deg_goodman330];
% FATIGUE
F_goodman=[];  L_goodman=[];s_goodman=[];
for f=1:length(Total_sum_fatiguedamage_goodman(:,1))
    % Fatigue_damage_max
    F_max=max(max(Total_sum_fatiguedamage_goodman(f,:)));
    % Minimum fatigue life
    s_min=(t_end-t_start)/F_max;
    % The fatigue life unit is converted to years
    s_min_year=s_min/(3600*24*365);
    % Prevent data from being overwritten
    s_goodman=[s_goodman;s_min_year];
    % Prevent data from being overwritten
    F_goodman=[F_goodman;F_max];
    % Location
    L0=find(Total_sum_fatiguedamage_goodman(f,:)==F_max);
    % Prevent data from being overwritten
    L_goodman=[L_goodman;L0];
end

% Fatigue damage of different hotspots is integrated into a matrix
Total_sum_fatiguedamage_gerber=[totalFatigueDamage_deg_gerber0,totalFatigueDamage_
deg_gerber30,totalFatigueDamage_deg_gerber60,totalFatigueDamage_deg_gerber90,...

totalFatigueDamage_deg_gerber120,totalFatigueDamage_deg_gerber150,totalFatigueDama
ge_deg_gerber180,totalFatigueDamage_deg_gerber210,...

totalFatigueDamage_deg_gerber240,totalFatigueDamage_deg_gerber270,totalFatigueDama
ge_deg_gerber300,totalFatigueDamage_deg_gerber330];
% FATIGUE
F_gerber=[];  L_gerber=[];s_gerber=[];
for g=1:length(Total_sum_fatiguedamage_gerber(:,1))
    % Fatigue_damage_max
    F_max=max(max(Total_sum_fatiguedamage_gerber(g,:)));
    % Minimum fatigue life
    s_min=(t_end-t_start)/F_max;
    % The fatigue life unit is converted to years
    s_min_year=s_min/(3600*24*365);
    % Prevent data from being overwritten
    s_gerber=[s_gerber;s_min_year];
    % Prevent data from being overwritten
    F_gerber=[F_gerber;F_max];
    % Location
    L0=find(Total_sum_fatiguedamage(g,:)==F_max);
```

```
    % Prevent data from being overwritten
    L_gerber=[L_gerber;L0];
end

%%
% Maximum stress range of all hotspots on the cable
Total_sum_stress_range=[Stress_range0,Stress_range30,Stress_range60,...
    Stress_range90,Stress_range120,Stress_range150,Stress_range180,...
    Stress_range210,Stress_range240,Stress_range270,Stress_range300,...
    Stress_range330];

stress_range2222=[];
for v=1:length(Total_sum_stress_range(:,1))
    stress_range_222=max(max(Total_sum_stress_range(v,:)));
    stress_range2222=[stress_range2222;stress_range_222];
end
% Maximum total stress of all hotspots on the cable
total_s_0=[];
for r=E_W:E_H
    total_s_m_0=max(max(abs(totalStress_1Kv_deg0(:,r))));
    total_s_0=[total_s_0;total_s_m_0];
end

total_s_30=[];
for r=E_W:E_H
    total_s_m_30=max(max(abs(totalStress_1Kv_deg30(:,r))));
    total_s_30=[total_s_30;total_s_m_30];
end

total_s_60=[];
for r=E_W:E_H
    total_s_m_60=max(max(abs(totalStress_1Kv_deg60(:,r))));
    total_s_60=[total_s_60;total_s_m_60];
end

total_s_90=[];
for r=E_W:E_H
    total_s_m_90=max(max(abs(totalStress_1Kv_deg90(:,r))));
    total_s_90=[total_s_90;total_s_m_90];
end

total_s_120=[];
for r=E_W:E_H
    total_s_m_120=max(max(abs(totalStress_1Kv_deg120(:,r))));
    total_s_120=[total_s_120;total_s_m_120];
end

total_s_150=[];
for r=E_W:E_H
    total_s_m_150=max(max(abs(totalStress_1Kv_deg150(:,r))));
    total_s_150=[total_s_150;total_s_m_150];
end

total_s_180=[];
for r=E_W:E_H
    total_s_m_180=max(max(abs(totalStress_1Kv_deg180(:,r))));
    total_s_180=[total_s_180;total_s_m_180];
end
```

```
total_s_210=[];
for r=E_W:E_H
    total_s_m_210=max(max(abs(totalStress_1Kv_deg210(:,r))));
    total_s_210=[total_s_210;total_s_m_210];
end

total_s_240=[];
for r=E_W:E_H
    total_s_m_240=max(max(abs(totalStress_1Kv_deg240(:,r))));
    total_s_240=[total_s_240;total_s_m_240];
end

total_s_270=[];
for r=E_W:E_H
    total_s_m_270=max(max(abs(totalStress_1Kv_deg270(:,r))));
    total_s_270=[total_s_270;total_s_m_270];
end

total_s_300=[];
for r=E_W:E_H
    total_s_m_300=max(max(abs(totalStress_1Kv_deg300(:,r))));
    total_s_300=[total_s_300;total_s_m_300];
end

total_s_330=[];
for r=E_W:E_H
    total_s_m_330=max(max(abs(totalStress_1Kv_deg330(:,r))));
    total_s_330=[total_s_330;total_s_m_330];
end

Total_sum_stress=[total_s_0,total_s_30,total_s_60,total_s_90,total_s_120,total_s_1
50,total_s_180,total_s_210,total_s_240,total_s_270,total_s_300,total_s_330];

totalstress3333=[];

for w=1:length(Total_sum_stress(:,1))
    stress_range_333=max(max(Total_sum_stress(w,:)));
    totalstress3333=[totalstress3333;stress_range_333];
end
save simulation_calculation.mat
```

Function – main_program_output_save.m

```
function[]=main_program_output_save

load simulation_calculation.mat

%%
% X is the position of the maximum stress range of cable section under stress free
correction (Element)
X1=find(max(Stress_range0(E_W:E_H,1))==Stress_range0(E_W:E_H,1));
X2=find(max(Stress_range30(E_W:E_H,1))==Stress_range30(E_W:E_H,1));
X3=find(max(Stress_range60(E_W:E_H,1))==Stress_range60(E_W:E_H,1));
X4=find(max(Stress_range90(E_W:E_H,1))==Stress_range90(E_W:E_H,1));
X5=find(max(Stress_range120(E_W:E_H,1))==Stress_range120(E_W:E_H,1));
X6=find(max(Stress_range150(E_W:E_H,1))==Stress_range150(E_W:E_H,1));
```

```
X7=find(max(Stress_range180(E_W:E_H,1))==Stress_range180(E_W:E_H,1));
X8=find(max(Stress_range210(E_W:E_H,1))==Stress_range210(E_W:E_H,1));
X9=find(max(Stress_range240(E_W:E_H,1))==Stress_range240(E_W:E_H,1));
X10=find(max(Stress_range270(E_W:E_H,1))==Stress_range270(E_W:E_H,1));
X11=find(max(Stress_range300(E_W:E_H,1))==Stress_range300(E_W:E_H,1));
X12=find(max(Stress_range330(E_W:E_H,1))==Stress_range330(E_W:E_H,1));

XX=[X1,X2,X3,X4,X5,X6,X7,X8,X9,X10,X11,X12];
% X (element) corresponding to the maximum stress range of cable cable section
XX1=Stress_range0(X1+E_W-1,1);
XX2=Stress_range30(X2+E_W-1,1);
XX3=Stress_range60(X3+E_W-1,1);
XX4=Stress_range90(X4+E_W-1,1);
XX5=Stress_range120(X5+E_W-1,1);
XX6=Stress_range150(X6+E_W-1,1);
XX7=Stress_range180(X7+E_W-1,1);
XX8=Stress_range210(X8+E_W-1,1);
XX9=Stress_range240(X9+E_W-1,1);
XX10=Stress_range270(X10+E_W-1,1);
XX11=Stress_range300(X11+E_W-1,1);
XX12=Stress_range330(X12+E_W-1,1);

XXX=[XX1,XX2,XX3,XX4,XX5,XX6,XX7,XX8,XX9,XX10,XX11,XX12];
% Find out the Hotspot where the maximum stress range is located
[xx1,yy1]=find(max(XXX)==XXX);
% The location, hotspot and value of the maximum stress range without stress
correction
M1=XX(1,yy1);
N1=(yy1-1)*30;
P1=XXX(1,yy1);
% The corresponding value is output to the command line
disp(['Location of maximum stress range M1=',num2str(M1)]);
disp(['Hotspot at the place with maximum stress range N1=',num2str(N1)]);
disp(['Value of maximum stress range P1=',num2str(P1)]);


% Y is the position of the maximum stress range of cable section under Goodman
(Element)
Y1=find(max(Stress_range_goodman0(E_W:E_H,1))==Stress_range_goodman0(E_W:E_H,1));
Y2=find(max(Stress_range_goodman30(E_W:E_H,1))==Stress_range_goodman30(E_W:E_H,1))
;
Y3=find(max(Stress_range_goodman60(E_W:E_H,1))==Stress_range_goodman60(E_W:E_H,1))
;
Y4=find(max(Stress_range_goodman90(E_W:E_H,1))==Stress_range_goodman90(E_W:E_H,1))
;
Y5=find(max(Stress_range_goodman120(E_W:E_H,1))==Stress_range_goodman120(E_W:E_H,1
));
Y6=find(max(Stress_range_goodman150(E_W:E_H,1))==Stress_range_goodman150(E_W:E_H,1
));
Y7=find(max(Stress_range_goodman180(E_W:E_H,1))==Stress_range_goodman180(E_W:E_H,1
));
Y8=find(max(Stress_range_goodman210(E_W:E_H,1))==Stress_range_goodman210(E_W:E_H,1
));
Y9=find(max(Stress_range_goodman240(E_W:E_H,1))==Stress_range_goodman240(E_W:E_H,1
));
Y10=find(max(Stress_range_goodman270(E_W:E_H,1))==Stress_range_goodman270(E_W:E_H,
1));
Y11=find(max(Stress_range_goodman300(E_W:E_H,1))==Stress_range_goodman300(E_W:E_H,
1));
```

```
Y12=find(max(Stress_range_goodman330(E_W:E_H,1))==Stress_range_goodman330(E_W:E_H,
1));

YY=[Y1,Y2,Y3,Y4,Y5,Y6,Y7,Y8,Y9,Y10,Y11,Y12];
% Y (element) corresponding to the maximum stress range of cable cable section
YY1=Stress_range_goodman0(Y1+E_W-1,1);
YY2=Stress_range_goodman30(Y2+E_W-1,1);
YY3=Stress_range_goodman60(Y3+E_W-1,1);
YY4=Stress_range_goodman90(Y4+E_W-1,1);
YY5=Stress_range_goodman120(Y5+E_W-1,1);
YY6=Stress_range_goodman150(Y6+E_W-1,1);
YY7=Stress_range_goodman180(Y7+E_W-1,1);
YY8=Stress_range_goodman210(Y8+E_W-1,1);
YY9=Stress_range_goodman240(Y9+E_W-1,1);
YY10=Stress_range_goodman270(Y10+E_W-1,1);
YY11=Stress_range_goodman300(Y11+E_W-1,1);
YY12=Stress_range_goodman330(Y12+E_W-1,1);

YYY=[YY1,YY2,YY3,YY4,YY5,YY6,YY7,YY8,YY9,YY10,YY11,YY12];
% Find out the Hotspot where the maximum stress range is located
[xx2,yy2]=find(max(YYY)==YYY);
% The location, hotspot and value of the maximum stress range with goodman
M2=XX(1,yy2);
N2=(yy2-1)*30;
P2=XXX(1,yy2);
% The corresponding value is output to the command line
disp(['Location of maximum stress range(goodman) M2=',num2str(M2)]);
disp(['Hotspot at the place with maximum stress range(goodman) N2=',num2str(N2)]);
disp(['Value of maximum stress range(goodman) P2=',num2str(P2)]);

% Z is the position of the maximum stress range of cable section under Gerber
(Element)
Z1=find(max(Stress_range_gerber0(E_W:E_H,1))==Stress_range_gerber0(E_W:E_H,1));
Z2=find(max(Stress_range_gerber30(E_W:E_H,1))==Stress_range_gerber30(E_W:E_H,1));
Z3=find(max(Stress_range_gerber60(E_W:E_H,1))==Stress_range_gerber60(E_W:E_H,1));
Z4=find(max(Stress_range_gerber90(E_W:E_H,1))==Stress_range_gerber90(E_W:E_H,1));
Z5=find(max(Stress_range_gerber120(E_W:E_H,1))==Stress_range_gerber120(E_W:E_H,1))
;
Z6=find(max(Stress_range_gerber150(E_W:E_H,1))==Stress_range_gerber150(E_W:E_H,1))
;
Z7=find(max(Stress_range_gerber180(E_W:E_H,1))==Stress_range_gerber180(E_W:E_H,1))
;
Z8=find(max(Stress_range_gerber210(E_W:E_H,1))==Stress_range_gerber210(E_W:E_H,1))
;
Z9=find(max(Stress_range_gerber240(E_W:E_H,1))==Stress_range_gerber240(E_W:E_H,1))
;
Z10=find(max(Stress_range_gerber270(E_W:E_H,1))==Stress_range_gerber270(E_W:E_H,1)
);
Z11=find(max(Stress_range_gerber300(E_W:E_H,1))==Stress_range_gerber300(E_W:E_H,1)
);
Z12=find(max(Stress_range_gerber330(E_W:E_H,1))==Stress_range_gerber330(E_W:E_H,1)
);

ZZ=[Z1,Z2,Z3,Z4,Z5,Z6,Z7,Z8,Z9,Z10,Z11,Z12];
% Z (element) corresponding to the maximum stress range of cable cable section
ZZ1=Stress_range_gerber0(Z1+E_W-1,1);
ZZ2=Stress_range_gerber30(Z2+E_W-1,1);
ZZ3=Stress_range_gerber60(Z3+E_W-1,1);
ZZ4=Stress_range_gerber90(Z4+E_W-1,1);
```

```
ZZ5=Stress_range_gerber120(Z5+E_W-1,1);
ZZ6=Stress_range_gerber150(Z6+E_W-1,1);
ZZ7=Stress_range_gerber180(Z7+E_W-1,1);
ZZ8=Stress_range_gerber210(Z8+E_W-1,1);
ZZ9=Stress_range_gerber240(Z9+E_W-1,1);
ZZ10=Stress_range_gerber270(Z10+E_W-1,1);
ZZ11=Stress_range_gerber300(Z11+E_W-1,1);
ZZ12=Stress_range_gerber330(Z12+E_W-1,1);

ZZZ=[ZZ1,ZZ2,ZZ3,ZZ4,ZZ5,ZZ6,ZZ7,ZZ8,ZZ9,ZZ10,ZZ11,ZZ12];
% Find out the Hotspot where the maximum stress range is located
[xx3,yy3]=find(max(ZZZ)==ZZZ);
% The location, hotspot and value of the maximum stress range with goodman
M3=ZZ(1,yy3);
N3=(yy3-1)*30;
P3=ZZZ(1,yy3);
% The corresponding value is output to the command line
disp(['Location of maximum stress range(gerber) M3=',num2str(M3)]);
disp(['Hotspot at the place with maximum stress range(gerber) N3=',num2str(N3)]);
disp(['Value of maximum stress range(gerber) P3=',num2str(P3)]);


Total_sun_stress_max=max(max(Total_sum_stress));

[M4,n4]=find(Total_sum_stress==max(max(Total_sum_stress)));
N4=(n4-1)*30;
P4=Total_sum_stress(M4,n4);

disp(['Location of maximum stress amplitude M4=',num2str(M4)]);
disp(['Hotspot at the place with maximum stress amplitude N4=',num2str(N4)]);
disp(['Value of maximum stress amplitude P4=',num2str(P4)]);

% 30 is the degree difference!
Angle=(n4-1)*30;
% The maximum stress range is located on the whole cable
MM1=M4+E_W-1;
bendingStressY_1Kv_deg = bendingStressY_1Kv.* sind(Angle);
bendingStressZ_1Kv_deg = - bendingStressZ_1Kv.* cosd(Angle);
totalStress_1Kv_deg = axialStress_1Kv + bendingStressY_1Kv_deg +
bendingStressZ_1Kv_deg;

[Element,time]=find(P4==totalStress_1Kv_deg);

Time=time.*(t_end-t_start)./t_n;

disp(['Time of maximum stress amplitude Time=',num2str(Time)]);

% find turning point
[tp ind] = dat2tp([timeSeries(1:t_n) totalStress_1Kv_deg(1:t_n, MM1)]);
% find rainflow cycle
RFCycle = tp2rfc(tp);

S_r=[];
for k=1:length(RFCycle(:,1))
    % Stress range at each cycle
    s_r=abs(RFCycle(k, 2) - RFCycle(k, 1));
    % Prevent data from being overwritten
    S_r=[S_r;s_r];
end
```

```
% Find out the maximum and minimum values of the stress range
S_r_max=max(max(S_r));
% Integer up the maximum value
S_n=ceil(S_r_max);
% Divide into 10 intervals
aa1=linspace(0,S_n,10);
% Quantity in corresponding interval
[nn1,xout_1]=hist(S_r,aa1);
% Histogram abscissa
bb1=(1/20*S_n:1/10*S_n:(S_n-1/20*S_n));



Total_sum_fatiguedamage_gerber_cable=[totalFatigueDamage_deg_gerber0(E_W:E_H,1),to
talFatigueDamage_deg_gerber30(E_W:E_H,1),totalFatigueDamage_deg_gerber60(E_W:E_H,1
),totalFatigueDamage_deg_gerber90(E_W:E_H,1),...

totalFatigueDamage_deg_gerber120(E_W:E_H,1),totalFatigueDamage_deg_gerber150(E_W:E
_H,1),totalFatigueDamage_deg_gerber180(E_W:E_H,1),totalFatigueDamage_deg_gerber210
(E_W:E_H,1),...

totalFatigueDamage_deg_gerber240(E_W:E_H,1),totalFatigueDamage_deg_gerber270(E_W:E
_H,1),totalFatigueDamage_deg_gerber300(E_W:E_H,1),totalFatigueDamage_deg_gerber330
(E_W:E_H,1)];


[M5,n5]=find(Total_sum_fatiguedamage_gerber_cable==max(max(Total_sum_fatiguedamage
_gerber_cable)));
N5=(n5-1)*30;
P5=Total_sum_fatiguedamage_gerber_cable(M5,n5);

disp(['Location of Maximum fatigue damage(Gerber) M5=',num2str(M5)]);
disp(['Hotspot at the place with Maximum fatigue damage(gerber)
N5=',num2str(N5)]);
disp(['Maximum fatigue damage value(gerber) P5=',num2str(P5)]);
% 30 is the degree difference!
Angle=(n5-1)*30;

% The maximum stress range is located on the whole cable
MM2=M5+E_W-1;

bendingStressY_1Kv_deg = bendingStressY_1Kv.* sind(Angle);
bendingStressZ_1Kv_deg = - bendingStressZ_1Kv.* cosd(Angle);
totalStress_1Kv_deg = axialStress_1Kv + bendingStressY_1Kv_deg +
bendingStressZ_1Kv_deg;


% find turning point
[tp ind] = dat2tp([timeSeries(1:t_n) totalStress_1Kv_deg(1:t_n, MM2)]);
% find rainflow cycle
RFCycle = tp2rfc(tp);

S_r=[];
for k=1:length(RFCycle(:,1))
    % Stress range at each cycle
    s_r=abs(RFCycle(k, 2) - RFCycle(k, 1));
    % Prevent data from being overwritten
    S_r=[S_r;s_r];
```

```
end

% Find out the maximum and minimum values of the stress range
S_r_max=max(max(S_r));
% Integer up the maximum value
S_n=ceil(S_r_max);
% Divide into 10 intervals
aa2=linspace(0,S_n,10);
% Quantity in corresponding interval
[nn2,xout_2]=hist(S_r,aa2);
% Histogram abscissa
bb2=(1/20*S_n:1/10*S_n:(S_n-1/20*S_n));


Total_sum_fatiguedamage_goodman_cable=[totalFatigueDamage_deg_goodman0(E_W:E_H,1),
totalFatigueDamage_deg_goodman30(E_W:E_H,1),totalFatigueDamage_deg_goodman60(E_W:E
_H,1),totalFatigueDamage_deg_goodman90(E_W:E_H,1),...

totalFatigueDamage_deg_goodman120(E_W:E_H,1),totalFatigueDamage_deg_goodman150(E_W
:E_H,1),totalFatigueDamage_deg_goodman180(E_W:E_H,1),totalFatigueDamage_deg_goodma
n210(E_W:E_H,1),...

totalFatigueDamage_deg_goodman240(E_W:E_H,1),totalFatigueDamage_deg_goodman270(E_W
:E_H,1),totalFatigueDamage_deg_goodman300(E_W:E_H,1),totalFatigueDamage_deg_goodma
n330(E_W:E_H,1)];

[M6,n6]=find(Total_sum_fatiguedamage_goodman_cable==max(max(Total_sum_fatiguedamag
e_goodman_cable)));
N6=(n6-1)*30;
P6=Total_sum_fatiguedamage_goodman_cable(M6,n6);

disp(['Location of Maximum fatigue damage(goodman) M6=',num2str(M6)]);
disp(['Hotspot at the place with Maximum fatigue damage(goodman)
N6=',num2str(N6)]);
disp(['Maximum fatigue damage value(goodman) P6=',num2str(P6)]);


Total_sum_fatiguedamage_cable=[totalFatigueDamage_deg0(E_W:E_H,1),totalFatigueDama
ge_deg30(E_W:E_H,1),totalFatigueDamage_deg60(E_W:E_H,1),totalFatigueDamage_deg90(E
_W:E_H,1),...

totalFatigueDamage_deg120(E_W:E_H,1),totalFatigueDamage_deg150(E_W:E_H,1),totalFat
igueDamage_deg180(E_W:E_H,1),totalFatigueDamage_deg210(E_W:E_H,1),...

totalFatigueDamage_deg240(E_W:E_H,1),totalFatigueDamage_deg270(E_W:E_H,1),totalFat
igueDamage_deg300(E_W:E_H,1),totalFatigueDamage_deg330(E_W:E_H,1)];

[M7,n7]=find(Total_sum_fatiguedamage_cable==max(max(Total_sum_fatiguedamage_cable)
));
N7=(n7-1)*30;
P7=Total_sum_fatiguedamage_cable(M7,n7);

disp(['Location of Maximum fatigue damage(no_stress) M7=',num2str(M7)]);
disp(['Hotspot at the place with Maximum fatigue damage(no_stress)
N7=',num2str(N7)]);
disp(['Maximum fatigue damage value(no_stress) P7=',num2str(P7)]);
%%
save('.\simulation\totalStress_1Kv_deg0', 'totalStress_1Kv_deg0')
save('.\simulation\totalStress_1Kv_deg30', 'totalStress_1Kv_deg30')
```

```
save('.\simulation\totalStress_1Kv_deg60', 'totalStress_1Kv_deg60')
save('.\simulation\totalStress_1Kv_deg90', 'totalStress_1Kv_deg90')
save('.\simulation\totalStress_1Kv_deg120', 'totalStress_1Kv_deg120')
save('.\simulation\totalStress_1Kv_deg150', 'totalStress_1Kv_deg150')
save('.\simulation\totalStress_1Kv_deg180', 'totalStress_1Kv_deg180')
save('.\simulation\totalStress_1Kv_deg210', 'totalStress_1Kv_deg210')
save('.\simulation\totalStress_1Kv_deg240', 'totalStress_1Kv_deg240')
save('.\simulation\totalStress_1Kv_deg270', 'totalStress_1Kv_deg270')
save('.\simulation\totalStress_1Kv_deg300', 'totalStress_1Kv_deg300')
save('.\simulation\totalStress_1Kv_deg330', 'totalStress_1Kv_deg330')

save('.\simulation\Stress_range0', 'Stress_range0')
save('.\simulation\Stress_range30', 'Stress_range30')
save('.\simulation\Stress_range60', 'Stress_range60')
save('.\simulation\Stress_range90', 'Stress_range90')
save('.\simulation\Stress_range120', 'Stress_range120')
save('.\simulation\Stress_range150', 'Stress_range150')
save('.\simulation\Stress_range180', 'Stress_range180')
save('.\simulation\Stress_range210', 'Stress_range210')
save('.\simulation\Stress_range240', 'Stress_range240')
save('.\simulation\Stress_range270', 'Stress_range270')
save('.\simulation\Stress_range300', 'Stress_range300')
save('.\simulation\Stress_range330', 'Stress_range330')

save('.\simulation\Stress_range_goodman0', 'Stress_range_goodman0')
save('.\simulation\Stress_range_goodman30', 'Stress_range_goodman30')
save('.\simulation\Stress_range_goodman60', 'Stress_range_goodman60')
save('.\simulation\Stress_range_goodman90', 'Stress_range_goodman90')
save('.\simulation\Stress_range_goodman120', 'Stress_range_goodman120')
save('.\simulation\Stress_range_goodman150', 'Stress_range_goodman150')
save('.\simulation\Stress_range_goodman180', 'Stress_range_goodman180')
save('.\simulation\Stress_range_goodman210', 'Stress_range_goodman210')
save('.\simulation\Stress_range_goodman240', 'Stress_range_goodman240')
save('.\simulation\Stress_range_goodman270', 'Stress_range_goodman270')
save('.\simulation\Stress_range_goodman300', 'Stress_range_goodman300')
save('.\simulation\Stress_range_goodman330', 'Stress_range_goodman330')

save('.\simulation\Stress_range_gerber0', 'Stress_range_gerber0')
save('.\simulation\Stress_range_gerber30', 'Stress_range_gerber30')
save('.\simulation\Stress_range_gerber60', 'Stress_range_gerber60')
save('.\simulation\Stress_range_gerber90', 'Stress_range_gerber90')
save('.\simulation\Stress_range_gerber120', 'Stress_range_gerber120')
save('.\simulation\Stress_range_gerber150', 'Stress_range_gerber150')
save('.\simulation\Stress_range_gerber180', 'Stress_range_gerber180')
save('.\simulation\Stress_range_gerber210', 'Stress_range_gerber210')
save('.\simulation\Stress_range_gerber240', 'Stress_range_gerber240')
save('.\simulation\Stress_range_gerber270', 'Stress_range_gerber270')
save('.\simulation\Stress_range_gerber300', 'Stress_range_gerber300')
save('.\simulation\Stress_range_gerber330', 'Stress_range_gerber330')

save('.\simulation\totalFatigueDamage_deg0', 'totalFatigueDamage_deg0')
save('.\simulation\totalFatigueDamage_deg30', 'totalFatigueDamage_deg30')
save('.\simulation\totalFatigueDamage_deg60', 'totalFatigueDamage_deg60')
save('.\simulation\totalFatigueDamage_deg90', 'totalFatigueDamage_deg90')
save('.\simulation\totalFatigueDamage_deg120', 'totalFatigueDamage_deg120')
save('.\simulation\totalFatigueDamage_deg150', 'totalFatigueDamage_deg150')
save('.\simulation\totalFatigueDamage_deg180', 'totalFatigueDamage_deg180')
save('.\simulation\totalFatigueDamage_deg210', 'totalFatigueDamage_deg210')
save('.\simulation\totalFatigueDamage_deg240', 'totalFatigueDamage_deg240')
```

```
save('.\simulation\totalFatigueDamage_deg270', 'totalFatigueDamage_deg270')
save('.\simulation\totalFatigueDamage_deg300', 'totalFatigueDamage_deg300')
save('.\simulation\totalFatigueDamage_deg330', 'totalFatigueDamage_deg330')

save('.\simulation\totalFatigueDamage_deg_goodman0',
'totalFatigueDamage_deg_goodman0')
save('.\simulation\totalFatigueDamage_deg_goodman30',
'totalFatigueDamage_deg_goodman30')
save('.\simulation\totalFatigueDamage_deg_goodman60',
'totalFatigueDamage_deg_goodman60')
save('.\simulation\totalFatigueDamage_deg_goodmans90',
'totalFatigueDamage_deg_goodman90')
save('.\simulation\totalFatigueDamage_deg_goodman120',
'totalFatigueDamage_deg_goodman120')
save('.\simulation\totalFatigueDamage_deg_goodman150',
'totalFatigueDamage_deg_goodman150')
save('.\simulation\totalFatigueDamage_deg_goodman180',
'totalFatigueDamage_deg_goodman180')
save('.\simulation\totalFatigueDamage_deg_goodman210',
'totalFatigueDamage_deg_goodman210')
save('.\simulation\totalFatigueDamage_deg_goodman240',
'totalFatigueDamage_deg_goodman240')
save('.\simulation\totalFatigueDamage_deg_goodman270',
'totalFatigueDamage_deg_goodman270')
save('.\simulation\totalFatigueDamage_deg_goodman300',
'totalFatigueDamage_deg_goodman300')
save('.\simulation\totalFatigueDamage_deg_goodman330',
'totalFatigueDamage_deg_goodman330')

save('.\simulation\totalFatigueDamage_deg_gerber0',
'totalFatigueDamage_deg_gerber0')
save('.\simulation\totalFatigueDamage_deg_gerber30',
'totalFatigueDamage_deg_gerber30')
save('.\simulation\totalFatigueDamage_deg_gerber60',
'totalFatigueDamage_deg_gerber60')
save('.\simulation\totalFatigueDamage_deg_gerber90',
'totalFatigueDamage_deg_gerber90')
save('.\simulation\totalFatigueDamage_deg_gerber120',
'totalFatigueDamage_deg_gerber120')
save('.\simulation\totalFatigueDamage_deg_gerber150',
'totalFatigueDamage_deg_gerber150')
save('.\simulation\totalFatigueDamage_deg_gerber180',
'totalFatigueDamage_deg_gerber180')
save('.\simulation\totalFatigueDamage_deg_gerber210',
'totalFatigueDamage_deg_gerber210')
save('.\simulation\totalFatigueDamage_deg_gerber240',
'totalFatigueDamage_deg_gerber240')
save('.\simulation\totalFatigueDamage_deg_gerber270',
'totalFatigueDamage_deg_gerber270')
save('.\simulation\totalFatigueDamage_deg_gerber300',
'totalFatigueDamage_deg_gerber300')
save('.\simulation\totalFatigueDamage_deg_gerber330',
'totalFatigueDamage_deg_gerber330')

save('.\simulation\M1', 'M1')
save('.\simulation\N1', 'N1')
save('.\simulation\P1', 'P1')

save('.\simulation\M2', 'M2')
```

```
save('.\simulation\N2', 'N2')
save('.\simulation\P2', 'P2')

save('.\simulation\M3', 'M3')
save('.\simulation\N3', 'N3')
save('.\simulation\P3', 'P3')

save('.\simulation\M4', 'M4')
save('.\simulation\N4', 'N4')
save('.\simulation\P4', 'P4')

save('.\simulation\M5', 'M5')
save('.\simulation\N5', 'N5')
save('.\simulation\P5', 'P5')

save('.\simulation\M6', 'M6')
save('.\simulation\N6', 'N6')
save('.\simulation\P6', 'P6')

save('.\simulation\M7', 'M7')
save('.\simulation\N7', 'N7')
save('.\simulation\P7', 'P7')

save result.mat M1 N1 P1 M2 N2 P2 M3 N3 P3 M4 N4 P4 Time M5 N5 P5 M6 N6 P6 M7 N7
P7
save simulation_output_save.mat
```

Function – main_program_figure.m

```
function[]=main_program_figure

load simulation_output_save.mat

%%
% Stress range of different hot spots of 1kV cable section at corresponding
element (without stress correction)
figure(1)
plot(Stress_range30(E_W:E_H,1),'-or')
hold on
plot(Stress_range90(E_W:E_H,1),'-+g')
plot(Stress_range150(E_W:E_H,1),'-*c')
plot(Stress_range210(E_W:E_H,1),'-sy')
plot(Stress_range270(E_W:E_H,1),'->m')
plot(Stress_range330(E_W:E_H,1),'-pb')
% X coordinate description
xlabel('Elements','fontsize',20);
% Y coordinate description
ylabel('Stressrange(MPa)','fontsize',20);
% Legend description
legend('30','90','150','210','270','330');
title('Stressrange ');
set(gca,'FontSize',20);
mkdir figure-png
mkdir figure-fig
saveas(gcf,'figure-png\figure-stressrange.png')
savefig(gcf,'figure-fig\figure-stressrange.fig')
```

```
% Stress range of different hot spots in cable section of 1kV cable at
corresponding element (corrected by Goodman formula)
figure(2)
plot(Stress_range_goodman30(E_W:E_H,1),'-or')
hold on
plot(Stress_range_goodman90(E_W:E_H,1),'-+g')
plot(Stress_range_goodman150(E_W:E_H,1),'-*c')
plot(Stress_range_goodman210(E_W:E_H,1),'-sy')
plot(Stress_range_goodman270(E_W:E_H,1),'->m')
plot(Stress_range_goodman330(E_W:E_H,1),'-pb')
% X coordinate description
xlabel('Elements','fontsize',20);
% Y coordinate description
ylabel('Stressrange(MPa)','fontsize',20);
% Legend description
legend('30','90','150','210','270','330');
title('Stressrange goodman')
set(gca,'FontSize',20);
saveas(gcf,'figure-png\figure-stressrange-goodman.png')
savefig(gcf,'figure-fig\figure-stressrange-goodman.fig')

figure(3)
plot(Stress_range_gerber30(E_W:E_H,1),'-or')
hold on
plot(Stress_range_gerber90(E_W:E_H,1),'-+g')
plot(Stress_range_gerber150(E_W:E_H,1),'-*c')
plot(Stress_range_gerber210(E_W:E_H,1),'-sy')
plot(Stress_range_gerber270(E_W:E_H,1),'->m')
plot(Stress_range_gerber330(E_W:E_H,1),'-pb')
% X coordinate description
xlabel('Elements','fontsize',20);
% Y coordinate description
ylabel('Stressrange(MPa)','fontsize',20);
% Legend description
legend('30','90','150','210','270','330');
title('Stressrange gerber')
set(gca,'FontSize',20);
saveas(gcf,'figure-png\figure-stressrange-gerber.png')
savefig(gcf,'figure-fig\figure-stressrange-gerber.fig')

figure(4)
plot(stress_range2222(E_W:E_H,1),'-or')
% X coordinate description
xlabel('Elements','fontsize',20);
% Y coordinate description
ylabel('Stressrange(MPa)','fontsize',20);
title('Stressrange');
set(gca,'FontSize',20);
saveas(gcf,'figure-png\figure-stressrange-max.png')
savefig(gcf,'figure-fig\figure-stressrange-max.fig')

% Fatigue damage distribution of different hot spots at corresponding elements of
1kV cable section
figure(5)
plot(totalFatigueDamage_deg30(E_W:E_H,1),'-or')
hold on
plot(totalFatigueDamage_deg90(E_W:E_H,1),'-+g')
plot(totalFatigueDamage_deg150(E_W:E_H,1),'-*c')
```

```
plot(totalFatigueDamage_deg210(E_W:E_H,1),'-sy')
plot(totalFatigueDamage_deg270(E_W:E_H,1),'->m')
plot(totalFatigueDamage_deg330(E_W:E_H,1),'-pb')
% X coordinate description
xlabel('Elements','fontsize',20);
% Y coordinate description
ylabel('Fatiguedamage','fontsize',20);
% Legend description
legend('30','90','150','210','270','330');
title('totalFatigueDamage')
set(gca,'FontSize',20);
saveas(gcf,'figure-png\figure-totalFatigueDamage.png')
savefig(gcf,'figure-fig\figure-totalFatigueDamage.fig')

figure(6)
plot(totalFatigueDamage_deg_goodman30(E_W:E_H,1),'-or')
hold on
plot(totalFatigueDamage_deg_goodman90(E_W:E_H,1),'-+g')
plot(totalFatigueDamage_deg_goodman150(E_W:E_H,1),'-*c')
plot(totalFatigueDamage_deg_goodman210(E_W:E_H,1),'-sy')
plot(totalFatigueDamage_deg_goodman270(E_W:E_H,1),'->m')
plot(totalFatigueDamage_deg_goodman330(E_W:E_H,1),'-pb')
% X coordinate description
xlabel('Elements','fontsize',20);
% Y coordinate description
ylabel('Fatiguedamage','fontsize',20);
% Legend description
legend('30','90','150','210','270','330');
title('totalFatigueDamage goodman')
set(gca,'FontSize',20);
saveas(gcf,'figure-png\figure-totalFatigueDamage-goodman.png')
savefig(gcf,'figure-fig\figure-totalFatigueDamage-goodman.fig')

figure(7)
plot(totalFatigueDamage_deg_gerber30(E_W:E_H,1),'-or')
hold on
plot(totalFatigueDamage_deg_gerber90(E_W:E_H,1),'-+g')
plot(totalFatigueDamage_deg_gerber150(E_W:E_H,1),'-*c')
plot(totalFatigueDamage_deg_gerber210(E_W:E_H,1),'-sy')
plot(totalFatigueDamage_deg_gerber270(E_W:E_H,1),'->m')
plot(totalFatigueDamage_deg_gerber330(E_W:E_H,1),'-pb')
% X coordinate description
xlabel('Elements','fontsize',20);
% Y coordinate description
ylabel('Fatiguedamage','fontsize',20);
% Legend description
legend('30','90','150','210','270','330');
title('totalFatigueDamage gerber')
set(gca,'FontSize',20);
saveas(gcf,'figure-png\figure-totalFatigueDamage-gerber.png')
savefig(gcf,'figure-fig\figure-totalFatigueDamage-gerber.fig')


%% Fatigue life distribution diagram
figure(8)
plot(s(E_W:E_H,1),'-ob','linewidth',2)
% hold on
% plot(s_goodman(E_W:E_H,1),'-og','linewidth',2)
% plot(s_gerber(E_W:E_H,1),'-or','linewidth',2)
```

```
% X coordinate description
xlabel('Elements','fontsize',20);
% Y coordinate description
ylabel('Fatiguelife(year)','fontsize',20);
% Legend description
% legend('s no stress','s goodman','s gerber');
legend('s');
set(gca,'FontSize',20);
saveas(gcf,'figure-png\figure-Fatiguelife.png')
savefig(gcf,'figure-fig\figure-Fatiguelife.fig')

figure(9)
plot(totalstress3333(1:62,1),'-ok')
% X coordinate description
xlabel('Elements','fontsize',20);
% Y coordinate description
ylabel('TotalStress(MPa)','fontsize',20);
title('TotalStress');
set(gca,'FontSize',20);
saveas(gcf,'figure-png\figure-totalstress-max.png')
savefig(gcf,'figure-fig\figure-totalstress-max.fig')


% Time series histogram of total stress at maximum amplitude
figure(10)
bar(bb1,nn1,1)
xlabel('Normal stress range/MPa')
ylabel('Number of occurances[-]')
set(gca,'FontSize',20);
saveas(gcf,'figure-png\figure-histogram-stressrange(1).png')
savefig(gcf,'figure-fig\figure-histogram-stressrange(1).fig')

% Time series histogram of total stress at the maximum fatigue damage
figure(11)
bar(bb2,nn2,1)
xlabel('Normal stress range/MPa')
ylabel('Number of occurances[-]')
set(gca,'FontSize',20);
saveas(gcf,'figure-png\figure-histogram-stressrange(2).png')
savefig(gcf,'figure-fig\figure-histogram-stressrange(2).fig')

%%
% histogram

% total stress
xxx1=(0:30:180);
W1=Total_sum_stress(2,1:7);
w1=Total_sum_stress(34,1:7);
yyy1=[W1(1,1),w1(1,1);W1(1,2),w1(1,2);W1(1,3),w1(1,3);W1(1,4),w1(1,4);W1(1,5),w1(1
,5);W1(1,6),w1(1,6);W1(1,7),w1(1,7)];
figure(12)
bar(xxx1,yyy1)
xlabel('Hotspots/deg')
ylabel('Totalstress/Mpa')
% title('Hs1d5Tp5d5-totalstress');
% title('Hs2d5Tp6d5-totalstress');
title('Hs3d5Tp7d5-totalstress');
legend('Element4','Element100');
set(gca,'FontSize',20);
```

```
saveas(gcf,'figure-png\figure-histogram-totalstress.png')
savefig(gcf,'figure-fig\figure-histogram-totalstress.fig')

% stress range
xxx2=(0:30:180);
V1=Total_sum_stress_range(24,1:7);
v1=Total_sum_stress_range(56,1:7);
yyy2=[V1(1,1),v1(1,1);V1(1,2),v1(1,2);V1(1,3),v1(1,3);V1(1,4),v1(1,4);V1(1,5),v1(1
,5);V1(1,6),v1(1,6);V1(1,7),v1(1,7)];
figure(13)
bar(xxx2,yyy2)
xlabel('Hotspots/deg')
ylabel('Stressrange/Mpa')
% title('Hs1d5Tp5d5-stressrange');
% title('Hs2d5Tp6d5-stressrange');
title('Hs3d5Tp7d5-stressrange');
legend('Element4','Element100');
saveas(gcf,'figure-png\figure-histogram-stressrange-compare.png')
savefig(gcf,'figure-fig\figure-histogram-stressrange-compare.fig')


% fatigue life
cable_fatigue_life=(t_end-t_start)./Total_sum_fatiguedamage_cable/(3600*24*365);

xxx3=(0:30:180);
W2=cable_fatigue_life(2,1:7);
w2=cable_fatigue_life(34,1:7);
yyy3=[W2(1,1),w2(1,1);W2(1,2),w2(1,2);W2(1,3),w2(1,3);W2(1,4),w2(1,4);W2(1,5),w2(1
,5);W2(1,6),w2(1,6);W2(1,7),w2(1,7)];
figure(14)
bar(xxx3,yyy3)
xlabel('Hotspots/deg')
ylabel('Fatigue-life/year')
% title('Hs1d5Tp5d5-fatigue life');
% title('Hs2d5Tp6d5-fatigue life');
title('Hs3d5Tp7d5-fatigue life');
legend('Element4','Element100');
set(gca,'FontSize',20);
saveas(gcf,'figure-png\figure-histogram-fatigue-life.png')
savefig(gcf,'figure-fig\figure-histogram-fatigue-life.fig')

xxx4=(0:30:180);
W3=Total_sum_fatiguedamage_cable(2,1:7);
w3=Total_sum_fatiguedamage_cable(34,1:7);
yyy4=[W3(1,1),w3(1,1);W3(1,2),w3(1,2);W3(1,3),w3(1,3);W3(1,4),w3(1,4);W3(1,5),w3(1
,5);W3(1,6),w3(1,6);W3(1,7),w3(1,7)];
figure(15)
bar(xxx4,yyy4)
xlabel('Hotspots/deg')
ylabel('total-fatiguedamage')
% title('Hs1d5Tp5d5-fatiguedamage');
% title('Hs2d5Tp6d5-fatiguedamage');
title('Hs3d5Tp7d5-fatiguedamage');
legend('Element4','Element100');
set(gca,'FontSize',20);
% imwrite(gcf,'figure\figure-histogram-fatiguedamage.png')
saveas(gcf,'figure-png\figure-histogram-fatiguedamage.png')
savefig(gcf,'figure-fig\figure-histogram-fatiguedamage.fig')
```

```
%%
% Save the results in mat format
save simulation.mat
```

Appendix B – Global Model Relative Displacement MATLAB Code

This MATLAB code reads the extracted global positional displacements from the SIMA simulations and calculates relative displacements for a set of neighbouring nodes along the power cable. For the example shown below, the global positional displacements were read from Case 2 nodes 1 and 4 for all x,y and z-axis direction from SIMA. These displacements are stored in an array in a separate script and are called in to increase efficiency. The code calculates relative displacements while taking into account the initial distance the nodes are separated by. The MATLAB code outputs a total displacement, relative displacements in the x,y and z-axis directions and also the overall strain.

Function – NewDisplacementCode.m

```
clc
clear all
clf
%Call in displacement array after being extracted from SIMA
Case2_Node1_and_Node4

%Taking transpose of called in matrices
Node1x = A';

Node4x = B';

Node1y = C';

Node4y = D';

Node1z = E';

Node4z = F';


%Plotting Node1z vs Node4z for verification
figure(21), clf
plot(Node1z,'b-'), hold on
plot(Node4z,'r-')
title('Node1z vs Node4z')
legend('Node1z','Node4z')
ylabel('Global Displacement z-direction [m]')
xlabel('Time Step')

%Factoring in that the nodes are already at a set distance away from each
%other and then calculating the relative x,y and z-displacement
startcondx=Node1x(1,1)-Node4x(1,1);
Node4x_new=Node4x+startcondx;
Diffx_test=Node1x-Node4x_new;

startcondy=Node1y(1,1)-Node4y(1,1);
Node4y_new=Node4y+startcondy;
Diffy_test=Node1y-Node4y_new;

startcondz=Node1z(1,1)-Node4z(1,1);
Node4z_new=Node4z+startcondz;
Diffz_test=Node1z-Node4z_new;
```

```
%Plotting the relative x,y and z-displacement on same graph
figure(22), clf
plot(Diffx_test,'k-'), hold on
plot(Diffy_test,'r-')
plot(Diffz_test,'b-')
legend('Relative x-displacement','Relative y-displacement','Relative z-
displacement')
xlabel('Time Step')
ylabel('Relative Displacement [m]')
title('Relative x,y and z-displacements')
%Calculating the Total Displacment, this allows for important time steps to
%be identified
TotalDisplacement_test = sqrt((Diffx_test).^2+(Diffy_test).^2+(Diffz_test).^2);


%Plotting TotalDisplacement
figure(23), clf
plot(TotalDisplacement_test,'k-'), hold on
title('Case 2 Nodes 91 and 94')
xlabel('Time Step')
ylabel('Total Displacement [m]')
mean_y = mean(TotalDisplacement_test), hold on
line([0, 12000], [mean_y, mean_y], 'Color', 'red', 'LineStyle', '--', 'LineWidth',
1);
legend('Total Displacement','Mean Total Displacement')

%calcualting the mean total displacement (this can also be found within the
%figure properties
mean_y = mean(TotalDisplacement_test);
disp(mean_y); % Display the mean value

%Calculating and plotting the overall strain, this helps give a clear
%representation of how much the cable is displacing
figure(24), clf
plot(TotalDisplacement_test/2.1*100,'k-'), hold on
xlabel('Time Step')
ylabel('Strain [%]')
title('Total Strain')
```

Appendix C – MatLab Code Edge Crack in Finitely Extended Plate

```
% Crack Case #1
% Edge Crack in Finitely Extended Plate

% XLPE Threshold SIF
Kth = 0.6; % MPA*m^.5
w = 0.002; % Plate width in [m]

% Crack Dimensions
ai = 0.01; %mm
af = 1.20; %mm (0.6*2)

%%%% Crack Case 1 - Edge crack in finitely extended plate %%%%
disp ('***')
disp ('Crack Case 1 - Edgecrack in finitely extended plate')
disp ('***')

f = zeros(length(0.01e-3:0.1322e-3:1.2e-3),1);
A = zeros(length(0.06e-3:0.1322e-3:1.2e-3),1);

ind = 1;
for i = 0.01e-3:0.1322e-3:1.2e-3
    A(ind) = pi*i / (2*w);

    f(ind) = sqrt( (1 / A(ind)) * tan(A(ind)) ) /  cos(A(ind)) * ...
        (0.752 + 2.02 * (i / w) + 0.37 * (1 - sin(A(ind)))^3);

    SGMA(ind) = Kth / (f(ind)*sqrt(pi*i));

    ind = ind + 1;
end

disp ('Minimum axial tensile stress required to cause propagation [MPa]')
disp (SGMA(:))
```

Appendix D – MATLAB Code Centre Through Crack in Plate

```
% Case 2
% Center Through Crack in Plate

% Initialsing variables
%b = 7.83e-4; %[m] % Set b to 45% of the thickness
b = (2.00-3 / 100)*10;
Kth = 0.60; %MPa*m^.5

% Storing Yt and Yb as an array over the crack length
Yt = zeros(length(0.01e-3:0.1322e-3:1.20e-3),1);
Yb = zeros(length(0.01e-3:0.1322e-3:1.20e-3),1);

% Calculating axial tensile stress

ind = 1;
for i = 0.01e-3:0.1322e-3:1.20e-3
    Yt(ind) = sqrt(sec(pi*i / 2*b));

    ind = ind + 1;
end

% With a small 'b' value i.e. 1-10% of insultator thickness, values of Yt
% are virtually the same.
% With a greater 'b' value the equilbrium conditions of the insulator i.e
% 60% will be breached even if the initial crack size is not at 60%
% thickness
%disp (Yt);

ind = 1;
for i = 0.01e-3:0.1322e-3:1.20e-3
    SGMA_TEN(ind) = Kth/(sqrt(pi*i)*Yt(ind));

    ind = ind + 1;
end
disp('Minimum axial stress required to cause crack propagation [MPa]')
disp (SGMA_TEN(:))

ind = 1;
for i = 0.01e-3:0.1322e-3:1.20e-3
    Yb(ind) = Yt(ind) / 2;

    ind = ind + 1;
end

ind = 1;
for i = 0.06e-3:0.126e-3:1.20e-3
    SGMA_BND(ind) = Kth/(sqrt(pi*i)*Yb(ind));

    ind = ind + 1;
end
disp('Minimum bending stress required to cause crack propagation [MPa]')
disp(SGMA_BND(:))
```

Appendix E – MATLAB Code Edge Through Crack in Plate

```
% Crack Case 3
% Edge Through Crack in Plate

% XLPE Threshold SIF
Kth = 0.6; % MPA*m^.5
b = 0.002; % Plate width in [m]

% Crack Dimensions
ai = 0.01; %mm
af = 1.20; %mm (0.6*2)

%%%% Crack Case 2 - Edge through crack in plate %%%%
disp ('***')
disp ('Crack Case 1 - Edge through crack in plate')
disp ('***')

% Storing Yt, Yb and alpha as an array over the crack length
Yt = zeros(length(0.01e-3:0.1322e-3:1.20e-3),1);
Yb = zeros(length(0.01e-3:0.1322e-3:1.20e-3),1);
alpha = zeros(length(0.01e-3:0.1322e-3:1.20e-3),1);

% Determing alpha
ind = 1;
for i = 0.01e-3:0.1322e-3:1.20e-3
    alpha(ind) = i / b;
    Yt(ind) = 0.265*(1-alpha(ind))^4+(0.857+0.265*alpha(ind))/(1-
alpha(ind))^(3/2);

    ind = ind + 1;
end

% Calculating axial tensile stress
ind = 1;
for i = 0.01e-3:0.1322e-3:1.20e-3
    SGMA_TEN(ind) = Kth/(sqrt(pi*i)*Yt(ind));

    ind = ind + 1;
end

disp ('Minimum axial tensile stress required to cause propagtaion in [MPa]')
disp(SGMA_TEN(:))

% Calculating bending stress
ind = 1;
for i = 0.01e-3:0.1322e-3:1.20e-3
    alpha(ind) = i / b;
    Yb_tmp = sqrt((2/(pi*alpha(ind)))*tan((pi*alpha(ind))/2))*((0.923+0.199*(1-
sin((pi*alpha(ind))/2))^4)/(cos(pi*alpha(ind))/2));
    Yb(ind) = Yb_tmp;
    ind = ind + 1;
end

ind = 1;
for i = 0.01e-3:0.1322e-3:1.20e-3
    SGMA_BND(ind) = Kth/(sqrt(pi*i)*Yb(ind));
```

```
    ind = ind + 1;
end

disp ('Minimum bending stress required to cause propagation in [MPa]')
disp(SGMA_BND(:))
```

Appendix F – MATLAB Code Edge Ellipitical Surface Crack In Plate

```
% Crack Case 4
% Elliptical Surface Crack in Plate

% Initialsing Variables
Kth = 0.6; % MPA*m^.5
t = 0.002; % Plate width in [m]
b = 100e-3;

% Creating vectors, for axial stress, that change every loop
Yt = zeros(length(0.01e-3:0.1322e-3:1.20e-3),1);
F = zeros(length(0.01e-3:0.1322e-3:1.20e-3),1);
H = zeros(length(0.01e-3:0.1322e-3:1.20e-3),1);

% The determination of the stress is heavily dependent on the relationship
% between 'c' - the crack length, and 'a' - the crack length
% crack width '2c' can grow without limitations, it is not bounded by final crack
length (60%)
c = 0.4e-3;

% Calculating axial tensile stress

%fi = 90 at a-crack tip @ full depth
%fi = 0 at c-tip
fi = 0;

ind = 1;
for i = 0.01e-3:0.1322e-3:1.20e-3 % i = a
    if i <= c
        Q=1+1.464*(i/c)^1.65;
        M1=1.13-0.09*(i/c);
        M2=-0.54+0.89/(0.2+(i/c));
        M3=0.5-1/(0.65+(i/c))+14*(1-(i/c))^24;
        f1=((i/c)^2*(cos(fi))^2+(sin(fi))^2)^0.25;
        f2=(sec(pi*c/2/i*sqrt((i/t))))^0.5;
        g=1+(0.1+0.35*(i/t)^2)*(1-sin(fi))^2;
        p=0.2+(i/c)+0.6*(i/t);
        G11=-1.22-0.12*(i/c);
        G21=0.55-1.05*(i/c)^(3/4)+0.47*(i/c)^(3/2);
        H1=1-0.34*(i/t)-0.11*(i/c)*(i/t);
        H2=1+G11*(i/t)+G21*(i/t)^2;

    else
        Q=1+1.464*(c/i)^1.65;
        M1=sqrt(c/i)*(1+0.04*(c/i));
        M2=0.2*(c/i)^4;
        M3=-0.11*(c/i)^4;
        f1=((c/i)^2*(sin(fi))^2+(cos(fi))^2)^0.25;
        f2=(sec(pi*c/2/b*sqrt((i/t))))^.5;
        g=1+(0.1+0.35*(c/i)*(i/t)^2)*(1-sin(fi))^2;
        p=0.2+(c/i)+0.6*(i/t);
        G11=-0.04-0.41*(c/i);
        G12=0.55-1.93*(c/i)^(3/4)+1.38*(c/i)^(3/2);
        G21=-2.11-0.77*(c/i);
        G22=0.55-0.72*(c/i)^(3/4)+0.14*(c/i)^(3/2);
        H1=1+G11*(i/t)+G12*(i/t)^2;
        H2=1+G21*(i/t)+G22*(i/t)^2;
```

```
    end

    F(ind) = (M1+M2*(i/t)^2+M3*(i/t)^4)*f1*f2*g;
    H(ind) = H1+(H2-H1)*(sin(fi))^p;
    Yt = F*sqrt(1/Q);
    Yb = H.*Yt;

    ind = ind + 1;

end

ind = 1;
for i = 0.01e-3:0.1322e-3:1.20e-3 % where i = a
    SGMA_TEN(ind) = Kth / sqrt(pi*i)*Yt(ind);

    ind = ind + 1;
end

disp('Minimum axial stress to propagate the crack when fi = 90 [MPa]')
disp(SGMA_TEN(:))

% Calculating bending stress

ind = 1;
for i = 0.01e-3:0.1322e-3:1.20e-3 % where i = a
    SGMA_BND(ind) = Kth / sqrt(pi*i)*Yb(ind);

    ind = ind + 1;
end

disp('Minimum bending stress to propagate the crack when fi = 90 [MPa]')
disp(SGMA_BND(:))
```

Appendix G – MATLAB Code Thumbnail Crack in Solid Cylinder

```
% Crack Case 5
% Thumbnail crack in solid cylinder

% XLPE Threshold SIF
Kth = 0.6; % MPA*m^.5
b = 0.002; % Plate width in [m]

% Crack Dimensions
ai = 0.01; %mm
af = 1.20; %mm (0.6*2)
% Dimensional paramters
%b = 0.01442; %diameter of solid cylinder [m]

disp ('***')
disp ('Crack Case 5 - Thumbnail crack in a solid cylinder  ')
disp ('***')

% Storing Yt, Yb and alpha as an array over the crack length
Yt = zeros(length(0.01e-3:0.1322e-3:1.20e-3),1);
Yb = zeros(length(0.01e-3:0.1322e-3:1.20e-3),1);
beta = zeros(length(0.01e-3:0.1322e-3:1.20e-3),1);

% Calculate Yt and beta for 10 independent points
ind = 1;
for i = 0.01e-3:0.1322e-3:1.20e-3
    beta(ind) = (pi/2)*(i/b);
    H = 1 - sin(beta(ind));
    G = 0.92*(2/pi)*(sec(beta(ind)).*sqrt(tan(beta(ind))/beta(ind)));
    Yt(ind) = G*(0.752 + 1.286*beta(ind) + 0.37*H^3);

    ind = ind+1;
end

% Calculating axial tensile stress
ind = 1;
for i = 0.01e-3:0.1322e-3:1.20e-3
    SGMA_TEN(ind) = Kth/(sqrt(pi*i)*Yt(ind));
    ind = ind + 1;
end

disp ('Minimum axial tensile stress required to cause propagation in [MPa]')
disp (SGMA_TEN(:))

% Calcualting bending stress
ind = 1;
for i = 0.01e-3:0.1322e-3:1.20e-3 %inital crack length increments [m]
    beta(ind) = (pi/2)*(i/b);
    H = 1 - sin(beta(ind));
    G = 0.92*(2/pi)*(sec(beta(ind)).*sqrt(tan(beta(ind))/beta(ind)));
    Yb(ind) = G*(0.923 + 0.199*H^4);

    ind = ind + 1;
end

ind = 1;
for i = 0.01e-3:0.1322e-3:1.20e-3
```

```
    SGMA_BND(ind) = Kth/(sqrt(pi*i)*Yb(ind));
    ind = ind + 1;
end

disp ('Minimum bending stress required to cause propagtaion in [MPa]')
disp(SGMA_BND(:))
```

Appendix H – MATLAB Code Y vs YCor

```
%%%Variables
Kth = 0.69;
w = 0.002; % Plate width in [m]

%%%%%%%%% Y = 1.12 Stress %%%%%%%%%

ind = 1;
for i = 0.01e-3:0.000005:1.2e-3
    SGMA_Y(ind) = Kth / (1.12*sqrt(pi*i));

    ind = ind + 1;
end

%%%%%%%%% Correction Stress %%%%%%%%
f = zeros(length(0.01e-3:0.000005:1.2e-3),1);
K = zeros(length(0.01e-3:0.000005:1.2e-3),1);
i_values = zeros(length(0.01e-3:0.000005:1.2e-3),1);
A = zeros(length(0.01e-3:0.000005:1.2e-3),1);

ind = 1;
for i = 0.01e-3:0.000005:1.2e-3
    A(ind) = pi*i / (2*w);

    f(ind) = sqrt( (1 / A(ind)) * tan(A(ind)) ) /  cos(A(ind)) * ...
        (0.752 + 2.02 * (i / w) + 0.37 * (1 - sin(A(ind)))^3);

    SGMA_cor(ind) = Kth / (f(ind)*sqrt(pi*i));

    i_values(ind) = i;

    ind = ind + 1;
end

disp(SGMA_Y)
disp(SGMA_cor)

figure;
plot(i_values, SGMA_Y, 'b', 'LineWidth', 2);
hold on
plot(i_values, SGMA_cor, 'r', 'LineWidth', 2);
xlabel('Crack Length [m]');
ylabel('Min. Axial Tensile Stress to Cause Propagation [MPa]');
legend('Y = 1.12', 'Y = f(a/w)');
title('Y = 1.12 vs. Y = f(a/w)');
grid on;
```

Appendix I – MATLAB Code Edge Crack Number of Cycles

```
%% SEA STATE 2 - NODES 1 AND 4 - NUMBER OF CYCLES - EDGE CRACK
clear all; close all; clc;
SeaState2_EdgeCrack_ConFigMatrix_yy
%constants
w = 0.002; %define w here, if it is constant. Else it has to be a function
argument
sigma = 10;
C = 1.71e-4;
m = 9.07;
a0 = 0.000135; % Initial crack length
af = 0.00105; % final crack length

%quick fitting of the width w from your data
    %done by example: https://de.mathworks.com/help/optim/ug/nonlinear-data-
fitting-example.html
    x = linspace(a0,af,184); % This value changes as with respect to the y matrix

    f = @(w,a)
sqrt(2.*w./(pi.*a).*tan(pi.*a./(2.*w))).*(0.752+2.02.*(a./w)+0.37*(1-
sin(pi.*a./(2.*w))).^3)./(cos(pi*a/(2.*w)));
    figure()
    plot(x,yy,'ro',"LineWidth",1.3)
    xlabel("crack length a");
    ylabel("function value f(a,w)")
    grid on
    [w,resnorm,~,exitflag,output] = lsqcurvefit(f,w,x,yy);
    hold on
    plot(x,f(-0.0019,x),"LineWidth",1.3);
    hold off
    title("Fitting w")
    legend("DataPoints","Fitted Curve")
    disp("Found w = "+num2str(w));
%% Version 1: using the actual function f(a)

f = @(a) sqrt(2.*w./(pi.*a).*tan(pi.*a./(2.*w))).*(0.752+2.02.*(a./w)+0.37*(1-
sin(pi.*a./(2.*w))).^3)./(cos(pi*a/(2.*w)));


K = @(a)f(a).*sigma.*sqrt(pi.*a);

%calculate the integral
no_of_cycles =@(a) 1./(C.*K(a).^m);
N_f = integral(no_of_cycles,a0,af);

disp("Version 1: Using constant values of f(a)")
disp(N_f)


%% Version 2: use constant values for each block
fvec = yy; %Calling in geomerty config. matrix
avec = linspace(a0,af,length(fvec)+1);


%now, split integral into as many pieces as you have chosen values for f
N_f = 0;
no_of_cycles_const_vals = zeros(1,length(fvec)+1);
for l = 1:length(fvec)
    fval = fvec(l);
```

```
    K = @(a)fval.*sigma.*sqrt(pi.*a);
    no_of_cycles_const =@(a) 1./(C.*K(a).^m);
    no_of_cycles_const_vals(l) =no_of_cycles_const(avec(l));
    N_f = N_f +integral(no_of_cycles_const,avec(l),avec(l+1));
end
    no_of_cycles_const_vals(end) =no_of_cycles_const(avec(end));
disp("Version 2: Splitting integral into as many peices as of f(a)")
disp(N_f)

%% Version 3: interpolate a function between the chosen values of f and use that
fvec = yy; %Calling in geometry config. matrix
avec = linspace(a0,af,length(fvec));
f_interpolated = pchip(avec,fvec); %Piecewise Cubic Hermite Interpolating
Polynomial function of x y

K = @(a)ppval(f_interpolated,a).*sigma.*sqrt(pi.*a);
%calculate the integral
no_of_cycles_interpolated =@(a) 1./(C.*K(a).^m);
N_f = integral(no_of_cycles_interpolated,a0,af);

disp("Version 3: Interpolating function between f(a) values")
disp(N_f)

%% Plots

%functions f(a) in the three versions
figure()
plot(avec,f(avec),"LineWidth",1.3);
hold on
stairs(avec,fvec,"LineWidth",1.3);
plot(avec,ppval(f_interpolated,avec),"LineWidth",1.3);
hold off
grid on
xlabel("crack width a");
ylabel("f(a)")
legend("Complete function f(a)","Constant values f(a)","Interpolated version of
f(a)")
title("Function f(a) of the three versions")

%number of cycles (function under the integral) in the three versions
xvec = linspace(a0,af,1000);
figure()
plot(xvec,no_of_cycles(xvec),"LineWidth",1.3);
hold on
plot(linspace(a0,af,length(no_of_cycles_const_vals)),no_of_cycles_const_vals,"ro",
"LineWidth",1.3);
%I've interpolated version 2 points, this may not be completely accurate
plot(xvec,no_of_cycles_interpolated(xvec),"LineWidth",1.3);
hold off
grid on
xlabel("crack width a");
ylabel("Number of Cycles")
legend("Version 1","Version 2","Version 3")
title("Number of cycles of the three versions")
```

Appendix J – MATLAB Code Thumbnail Crack Number of Cycles

```
close all; clear all; clc;
% This script takes on the whole process
% Section 1 - Determining SIF for each crack increment
% Section 2 - Finding when Paris Law starts
% Section 3 - Determing Yt values for LEFM (Paris Law)
% Section 4 - Version 1 - No. of Cycles
% Section 5 - Version 2 - No. of Cycles
% Section 6 - Version 3 - No. of Cycles

% Apllied load
SGMA = 14.63;

% Plate width in [m]
b = 0.002;
% Crack Dimensions
ai = 0.01; %mm
af = 1.20; %mm (0.6*2)

% Storing as an array over the crack length
Yt = zeros(length(0.01e-3:0.000005:1.20e-3),1);
Yb = zeros(length(0.01e-3:0.000005:1.20e-3),1);
beta = zeros(length(0.01e-3:0.000005:1.20e-3),1);
i_values = zeros(length(0.01e-3:0.000005:1.2e-3),1);

% Calculate Yt and beta for 10 independent points
ind = 1;
for i = 0.01e-3:0.000005:1.20e-3
    beta(ind) = (pi/2)*(i/b);
    H = 1 - sin(beta(ind));
    G = 0.92*(2/pi)*(sec(beta(ind)).*sqrt(tan(beta(ind))/beta(ind)));
    Yt(ind) = G*(0.752 + 1.286*beta(ind) + 0.37*H^3);

    ind = ind+1;
end

% Calculating Stress Inetnsity Factor
ind = 1;
for i = 0.01e-3:0.000005:1.20e-3
    K(ind) = Yt(ind) * SGMA * sqrt(pi*i);

    i_values(ind) = i;

    ind = ind + 1;
end

disp ('Stress Intensity Factor')
disp (K(:))

%% Finding value of i for K = 0.60

tol = 1e-2;
Kth = 0.60;
index = find(abs(K - Kth) < tol, 1, 'first');
corresponding_1 = i_values(index);

disp(['For K =', num2str(Kth), ', i = ', num2str(corresponding_1)]);
```

```
% The Paris Law begins at a crack length = 0.00032 m

%% Extracting Yt values from Kth length to KIc length

% SIF never = KIc
b = 0.002;
ParisLaw_CrackLength = 0.00058:0.000005:0.0012;

Yt_2 = zeros(size(ParisLaw_CrackLength));

for ind = 1:length(ParisLaw_CrackLength)
    i = ParisLaw_CrackLength(ind);

    beta(ind) = (pi/2)*(i/b);
    H = 1 - sin(beta(ind));
    G = 0.92*(2/pi)*(sec(beta(ind)).*sqrt(tan(beta(ind))/beta(ind)));
    Yt_2(ind) = G*(0.752 + 1.286*beta(ind) + 0.37*H^3);
end

disp(Yt_2(:))

%% Version 1: using the actual function f(a)
% Variables
a0 = 0.00058; %value will be determined from section 2
af = 0.0012;
%C = 1.71e-4;
C = 3.8874e-7;
m = 9.07;
SGMA = 14.63;

f = @(a) G*(0.752 + 1.286*beta(ind) + 0.37*H^3);


K = @(a)f(a).*SGMA.*sqrt(pi.*a);

%calculate the integral
no_of_cycles =@(a) 1./(C.*K(a).^m);
N_f = integral(no_of_cycles,a0,af);

disp("Version 1:")
disp(N_f)


%% Version 2: use constant values for each block

fvec = Yt_2;

avec = linspace(a0,af,length(fvec)+1);


%now, split integral into as many pieces as you have chosen values for f
N_f = 0;
no_of_cycles_const_vals = zeros(1,length(fvec)+1);
for l = 1:length(fvec)
    fval = fvec(l);

    K = @(a)fval.*SGMA.*sqrt(pi.*a);
    no_of_cycles_const =@(a) 1./(C.*K(a).^m);
```

```
    no_of_cycles_const_vals(l) =no_of_cycles_const(avec(l));
    N_f = N_f +integral(no_of_cycles_const,avec(l),avec(l+1));
end
    no_of_cycles_const_vals(end) =no_of_cycles_const(avec(end));
disp("Version 2:")
disp(N_f)

%% Version 3: interpolate a function between the chosen values of f and use that

fvec = Yt_2;
avec = linspace(a0,af,length(fvec));
f_interpolated = pchip(avec,fvec); %Piecewise Cubic Hermite Interpolating
Polynomial function of x y

K = @(a)ppval(f_interpolated,a).*SGMA.*sqrt(pi.*a);
%calculate the integral
no_of_cycles_interpolated =@(a) 1./(C.*K(a).^m);
N_f = integral(no_of_cycles_interpolated,a0,af);

disp("Version 3:")
disp(N_f)
```

Appendix K – Project Flowchart

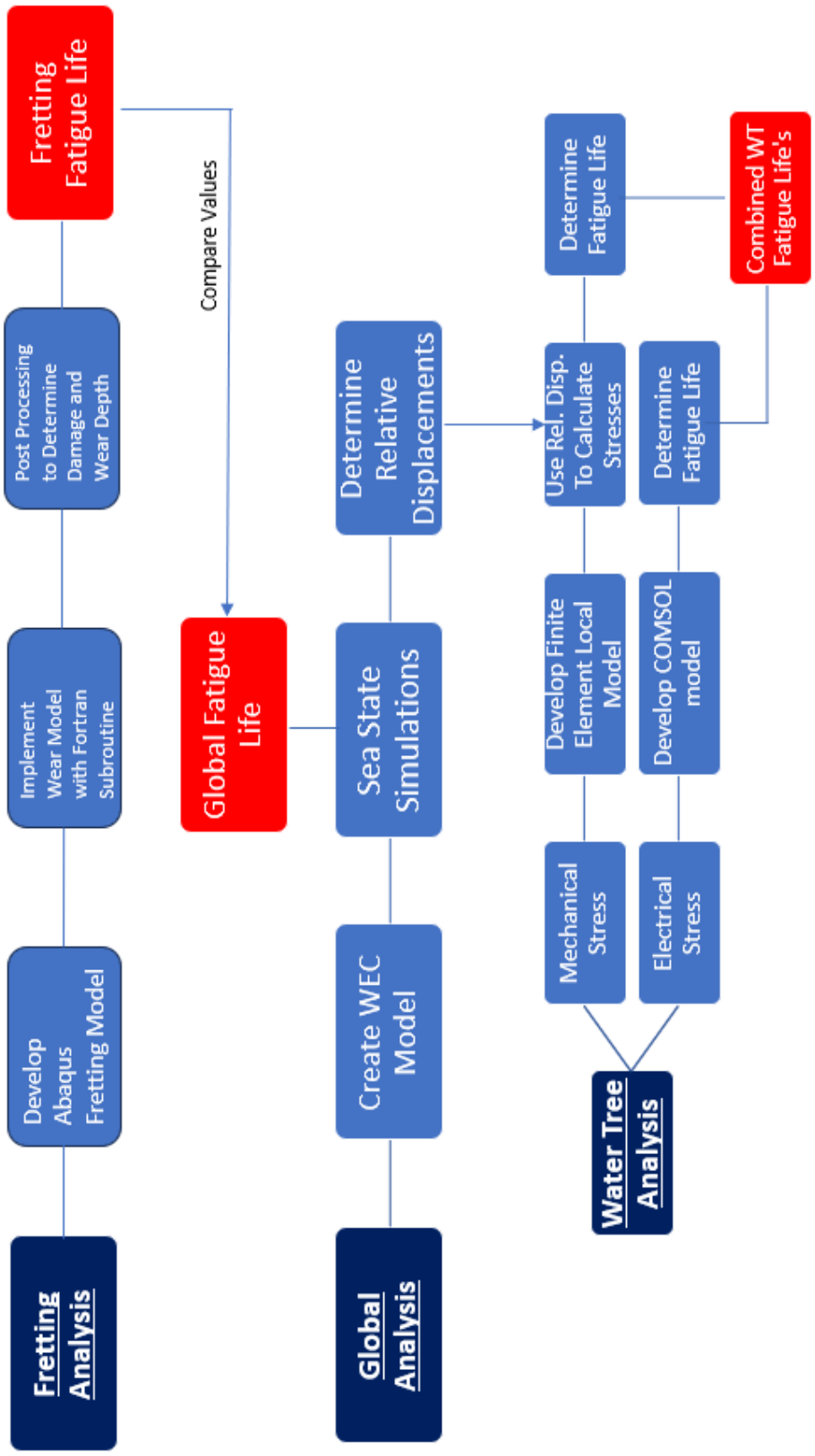

Appendix L – Reflection Report

Reflection Report

Nicholas Fagan - 201924476

Robbie McCormick - 201914748

Tom Marwood - 201917152

Greg Stewart - 201919528

Supervisor: Dr. Zhiyuan Li

zhiyuan.li@chamlers.se

Project Advisor: Dr. Jonas Ringsberg

jonas.ringsberg@chalmers.se

A report submitted in partial fulfilment of the requirements of the MEng in Aero / Mechanical Engineering

Contents

Figures

Introduction

This report outlines the steps taken to successfully manage the project for the duration of the exchange period. Details are given on the initial stages of the project, such as selecting a supervisor and developing a scope. It will also cover the techniques used to manage the project and mitigate potential risks. A summary of the group's reflection on the project is also provided.

Many project management tools were utilised during this project such as a Gannt Chart, a risk assessment matrix and regular meetings to provide updates to the supervisor. These methods assisted in the initiation and progress of the project ultimately leading to its successful completion.

Getting Started

Before travelling to Sweden, the team initially introduced themselves to one another in an informal setting to establish good communication and an effective working relationship. The group thought that it would be a good idea to share accommodation for the exchange period to help with project communication and the sharing of ideas.

Selecting a Project and Supervisor

The next step was to select a project and supervisor by Chalmers' May 12th deadline. After reviewing past projects conducted by Strathclyde students at Chalmers, two potential supervisors were contacted. After various communications, the group decided to work with Dr. Zhiyuan Li on the project "Structural Integrity Analyses of Marine Dynamic Cables". Although the group members did not have much experience in this field, it was agreed that it was a very interesting topic and would allow for the team to collectively expand and apply knowledge in a different sector. Dr. Zhiyuan Li was also enthusiastic to work with Strathclyde students again.

Developing Project Scope

The initial meeting with Dr. Zhiyuan Li, on September 5th, involved confirming the groups meeting schedule, sharing contact information and establishing the team's working environment with PC's and necessary software.

Furthermore, Dr. Zhiyuan Li introduced the team to Dr. Jonas Ringsberg, the Head of Division of Marine Technology, who served as a project advisor and regularly participated in meetings. Initial meetings involved discussion around the concept of Wave Energy Convertors (WECs), and the issues related to the assembly and lifetime of marine dynamic power cables.

The main scope of the project was to continue the research into the structural integrity of subsea dynamic cables. This involved further investigation into subjects covered by the previous year, such as fretting, and analysis of other damage phenomena such as global fatigue and water trees.

The group would initially work individually on specific areas of the fatigue and later compare and combine their results on the estimated lifetime of the cable.

Project Management

The management of this project was key to its success as it ensured work was completed on time and to a high standard. Due to the limited timeframe available, it was essential to establish a realistic timeline and constantly monitor risks and progress to make sure the deadlines were met.

Team Structure

From the beginning of the project, it was decided that each team member would work on their own specific area. These areas were outlined by Dr. Li and were as follows:

- Global Cable Fatigue – Nicholas Fagan
- Fretting Wear – Tom Marwood
- Water Tree Crack Propagation due to Mechanical Stresses – Greg Stewart
- Water Tree Crack Propagation due to Electrical Stresses – Robbie McCormick

After discussion within the group and with the supervisor, the team allocated their roles due to personal interest and experience. Nicholas and Greg both had previous MATLAB experience, so it was decided that they would take on these roles as it required the use of it. The Global model also heavily involved the use of a new software – SIMA – in which Nicholas was keen to learn and utilise. The subjects chosen by Robbie and Tom both involved new topics and software packages, such as COMSOL and Abaqus. Both students had no experience with these programmes but were excited for the opportunity to learn.

Each group member was also responsible for the literature review and discussion of results for their allocated topic. For the sections that did not directly fall under these topics, each group member was assigned equal sections to write up for deliverables such as the interim report and final report.

The delegation of the work at the initial stage of the project was essential as there was not enough time available for each student to read literature and learn software relevant to all topics. Having one specialised subject each, allowed each team member to focus their time appropriately and produce high quality work within the given timeframe.

Other roles were also assigned to improve with the efficiency of the project. It was decided that Nicholas would be appointed as the project manager as he had been successful in this role in previous group projects. Having a project manager helped when it came to important decisions within the group such as the assignment of the other work that did not fall into one of the previous subjects. It was also decided that Greg would take meeting minutes to ensure that key information was not missed or forgotten. This ensured that if a team member was absent, they would have the ability to catch up and understand the topics that were discussed during the meetings.

Flow Chart

A flow chart was produced to help the team visual how all the different components of the project would come together to complete the project. This chart was continually reviewed and updated to match the current goals of the project and was a useful tool for the management of the project. (See Appendix A).

Developing Timeline

After the project scope had been decided upon, the team spent time reviewing literature for their relevant sections. This allowed them to gain a better understanding of the topics and decide on specific aims and objectives. It was decided that a project Gantt Chart would be created to ensure that all deliverables were met within the time constraints.

The Gantt Chart allowed the members to break down their chosen topic into more manageable tasks. It allowed a better visualisation of the project, as a whole, by dividing it into specific deliverables all with their own due date. (See Appendix B and C)

The key deadline for this project was the final report which was due on the 8th of January. Also, as all the students had planned on travelling home for the Christmas and New Year's period,

the work required on generating the results had to be completed beforehand. With this in mind, the team and supervisor decided on a final presentation date at Chalmers on the 14th of December. By this time, the team had carried out their respective methodologies to generate results and discussed them in detail. These findings were then presented to the supervisors and the final report was mostly completed. Over the holiday period the team made final adjustments to the report and worked on creating the showcase video required before the final presentation at Strathclyde.

Other key dates included the statement of purpose, which was required two weeks after arrival at Chalmers. The interim report was a major milestone that allowed the team to reflect on the work done to date and how to manage the project going forward.

Project Progression

To allow the group and supervisor to see how the project was progressing, a shared OneDrive and Teams folder was created. This made the sharing of documents easy and allowed the team to work on shared files, such as the final report, simultaneously.

The group also had a designated office space within the University where they were all assigned their own personal computers. Being able to work in close proximity to each other was extremely helpful in allowing the group to share ideas and address issues when they occurred.

It was also decided, by the team and supervisor, that weekly meetings would be an effective way to monitor progress and ask questions. At these meetings each team member gave a short presentation on the work they had completed in that week and what they planned to do for the next one. This was a great help as it gave the supervisor the opportunity to suggest possible alternatives to our focus. This advice was especially helpful in the initial stages of the project when our knowledge of the area was more limited.

In the later stages of the project, once the team had a clear understanding of the work required, the number of meetings were reduced and were held upon request of the team. This allowed the group to dedicate more time to generating results and meeting the aims and objectives of the project.

Each team member also produced a weekly report covering past and future work. This helped when it came to completing the interim and final report as most of the work was already written up.

The team also continuously revised the Gantt Chart to account for slight changes in scope or timelines of specific aims. Updating the Gantt Chart ensured that despite the changes to the work, enough time was being left to complete each of the tasks.

Risk Management

Risk management is a key stage in any project as it important to highlight what could likely go wrong and the impact this would have on the success of the project. It is also essential to identify ways to mitigate these issues and carry out these methods to avoid the negative impact.

A risk matrix was created to highlight the likelihood and servery of the risks involved with this project.

Chalemers Maters Thesis 2023 - Group Risk Assessment								
Risk	Effect on team	Probability	Severity	Rating	Mitigation	Revised Probability	Revised Severity	Revised Rating
Team member unable to work due to an unforseen circumstance.	An increased workload for the rest of the team, and could lead to incomplete aims/objectives.	2	4	8	Ensure all team members are familiar with various aspects of the project.	2	3	6
Software issues	Licensing issues / corrupt files could reuslt in the inability to complete simulations.	3	5	15	Having access to the Chalmers Remote Desktop. This will allow for simuations to be conducted anywhere.	3	2	6
Inexperiecne of subject field and related software	The inexperience of the group in the Marine engineering field and unfamiliar software.	4	3	12	Initally, a period was chosen to complete backround research on the field and software related tutorials.	2	2	4
Long simulation times	Long simulation times can result in incomplete work and/or a lack of exploration via other routes. The main softwares of conecern in this thesis are SIMA and Abaqus.	5	3	15	The intensity of simulations are initially reduced to ensure the correct output is achieved. After achieving this, the simulation parameters can be altered to represent a more accurate model. The simulations could also be left to run overnight.	4	1	4
Loss of digital files	Loss of work could severely setback the team in respect to deadlines.	2	5	10	Store all files via cloud storage *e.g.*, onedrive or microsoft teams.	1	5	5
Failing to adhere to deadlines and project schedule	Could result in aims not being met and hence a reduced grade.	4	5	20	An inital and revised Gantt chart are implemented and are followed closely to ensure all deadlines are met.	2	5	10
Scope creep	An uncontrolled expansion to the project scope may result in confusion and/or incomplete work.	3	4	12	At the beginning, a statement of purpose was created in which was agreed upon by the supervisors. This is followed by regular meetings to ensure the group were on track with the predetermined objectives.	2	4	8

Figure 110: Risk Assessment Matrix

Risk Assessment Scoring System	**Probability**				
Severity	Almost impossible **(1)**	Not likely to occur **(2)**	Could occur **(3)**	Known to occur **(4)**	Common occurance **(5)**
Catastrophic **(5)**	5	10	15	20	25
Major **(4)**	4	8	12	16	20
Moderate **(3)**	3	6	9	12	15
Minor **(2)**	2	4	6	8	10
Insignificant **(1)**	1	2	3	4	5

Figure 111: Risk Matrix Scoring System

Using this method and through effective communication, the majority of the risks were avoided. The main issue faced by the group was scope creep. This was particularly apparent in the fretting area as the initial scope was to develop a 3D fretting model. However, as time progressed it was realised that this was too large a task to be completed by one person in such a short time frame. The previous 2D model had been completed by two students, one focused on the Abaqus element and one on the subroutine and post processing codes. A 3D fretting model was completed on Abaqus, however, it required a more complex subroutine and post processing script to be developed. Also, the model took many hours to run even for just four fretting cycles, the post processing typically takes even longer. For these reasons it was decided that there was not sufficient time to develop these new codes or run the much larger simulations. The scope then changed to producing a parameter sensitivity analysis on the existing model and creating a more realistic model.

Reflection of Groupwork

The opportunity to studying in Gothenburg on their master's thesis has allowed the team to learn and improve upon many important skills. This thesis allowed the group to gain experience of working as a team on a large project with set deadlines and deliverables. This

led to the development of skills such as teamwork, communication and time management to meet these deadlines. The members all agreed that many of these skills are transferable and will play an important role in their future careers.

One of the key factors that helped with the running of this project was the fact the team all worked in close proximity. This meant that is any issues arose during the working day, they were able to discuss them instantly. The group also shared accommodation with one another which allowed them to develop a good working relationship and share ideas they had regarding the project. These factors meant that no time had to be spent organising meetings between the team or waiting on replies via email.

The group also shared a similar working routine which was generally 9-5 Monday-Friday. The team worked longer hours and sometimes during the weekend when it came to meeting important deadlines such as the interim and final report. As the whole team followed the same schedule it allowed for more fluid communication as they were all working similar hours. The team's effort and commitment to this project also played a major role in its success.

Having two advisors on this project came with its pros and cons. It allows for different perspectives due the range of expertise of both advisors. However, this also sometimes led to issues as the team sometimes received contradictory advice on how to proceed with the project. This would lead to delays and confusion which could hinder the progress of the project. For example, if one advisor was not present for a meeting, a team member could spend an entire week completing certain tasks which were later identified as incorrect by the other advisor.

Another factor which was a major consideration of the project management was the fact the team members would be returning home for the Christmas and New Years period. As the deadline for the final report was at the beginning of January, this meant all results had to be completed before the students left Gothenburg in December. To ensure that these would be completed, the team set their own deadline for the 14th of December where they would have finalised results and present them to the supervisors. After returning to Scotland, the team were required to work remotely with one-another to finalise the report and create the showcase video. All members had prior experience of online group work during the COVID-19 pandemic so were quite comfortable with this. It required more use of file sharing and video calls using Microsoft teams and some more informal methods of communication like text messages. Using these techniques, the group was able to keep up strong communication which greatly assisted in the completion of these tasks.

The team was also keen to explore Gothenburg and other areas of Sweden while on their exchange. Leaving the weekends free to enjoy this time in a new country and meet new people resulted in a healthy work-life balance and led to an enjoyable experience for all. This also helped in the completion of the project as the students were well rested and able to be more focused on the task at hand.

Conclusions

In conclusion, the team worked as an effective unit for the duration of the project and were able to handle issues which arose due to effective project and time management. Each member has come away from this experience with improved soft skills in areas such as team management, communication and managing client expectations. They have also learnt new technical skills like learning how to use new software packages such as COMSOL, Abaqus and SIMA. These skills will be taken forward and utilised in future university group projects and throughout the members engineering careers. Finally, the project was condensed into a

conference paper, with the help of the supervisors, and will feature at the OMAE conference in June 2024. This highlights the success of the project and the continuous effective management implemented by the team.

Appendices

Appendix A

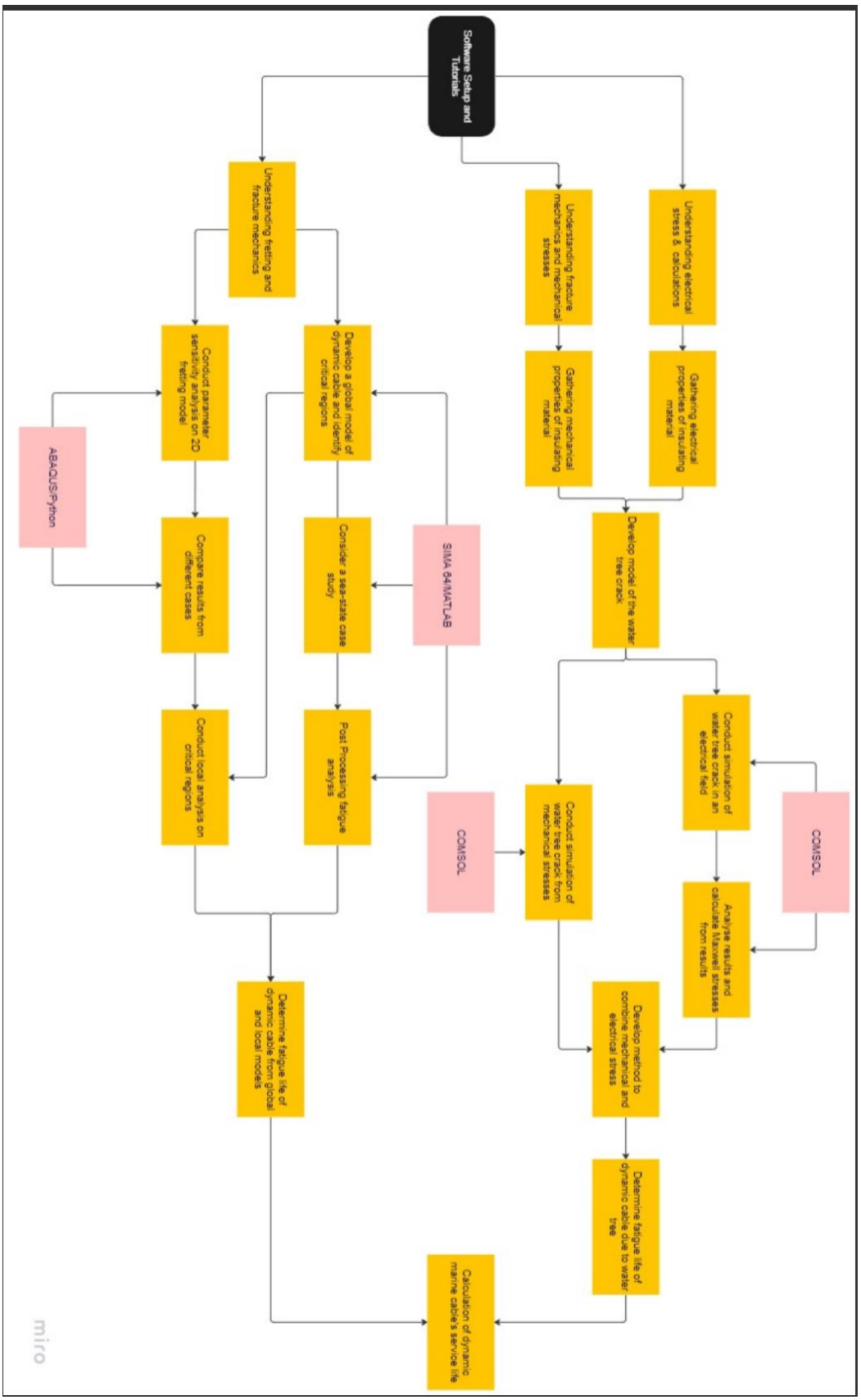

Figure 112: Project Flow Chart

Appendix B

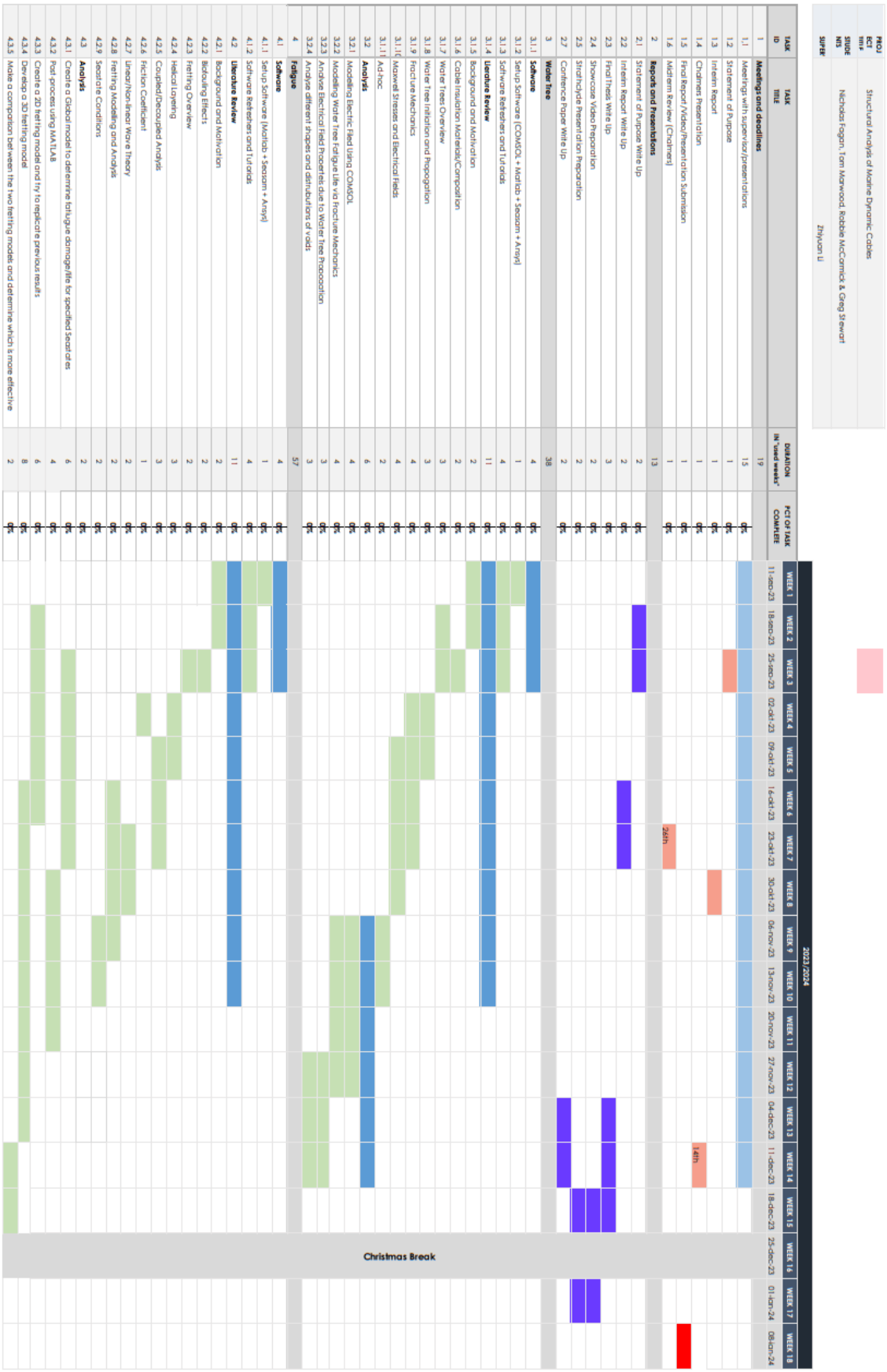

Figure 113: Initial Project Gantt Chart

Appendix C

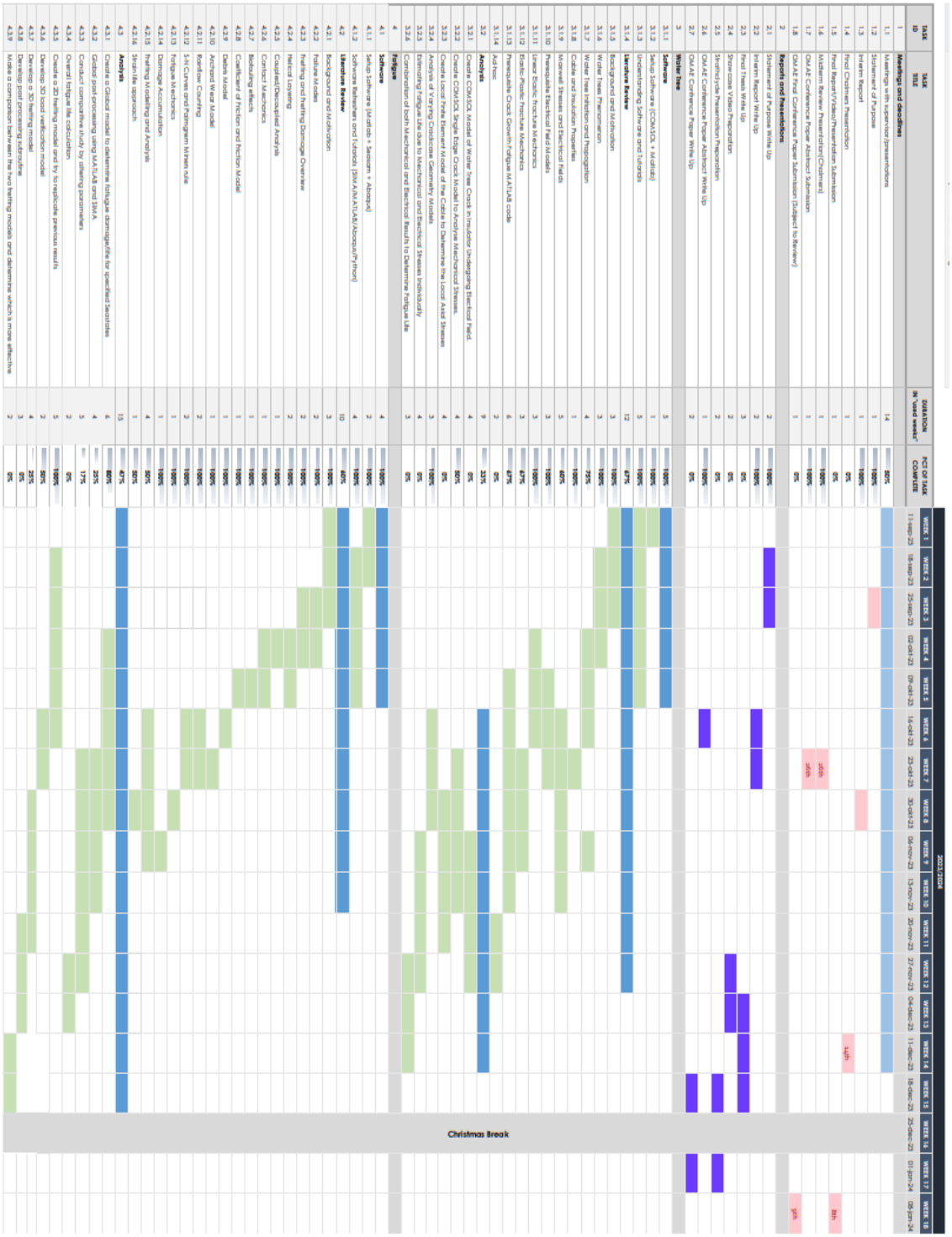

Figure 114: Revised Gantt Chart